Terarylene-based molecular switches : towards tunable photocyclization quantum yield and dual photo- and redox-responsive behavior

Nicolò Baggi

THESE DE DOCTORAT

NNT : 2022UPASF036

université PARIS-SACLAY

Terarylene-based molecular switches: towards tunable photocyclization quantum yield and dual photo- and redox-responsive behavior

Commutateurs moléculaires à base de terarylène : vers un rendement quantique de photocyclisation modulable et un comportement photo- et électro-actif

Thèse de doctorat de l'université Paris-Saclay

École doctorale n° 571 - Sciences Chimiques : Molécules, Matériaux, Instrumentation et Biosystèmes (2MIB)
Spécialité de doctorat : Chimie
Graduate School : Chimie. Référent : Faculté des sciences d'Orsay

Thèse préparée à l'**Institut de chimie moléculaire et des matériaux d'Orsay (Université Paris-Saclay, CNRS)**, sous la direction de **Pei Yu**, Chargé de Recherche, et le co-encadrement d'**Anne Léaustic**, Maître de Conférences

Thèse soutenue à Paris-Saclay, le 24 mai 2022, par

Nicolò BAGGI

Composition du Jury

Keitaro NAKATANI Professeur, ENS Paris-Saclay	Président
Eléna ISHOW Professeure, Université de Nantes	Rapporteure & Examinatrice
Guy ROYAL Professeur, Université Grenoble Alpes	Rapporteur & Examinateur
Jean-Christophe LACROIX Professeur, Université de Paris	Examinateur
Pei YU Chargé de Recherche, CNRS, Université Paris-Saclay	Directeur de thèse

université PARIS-SACLAY

ÉCOLE DOCTORALE
Sciences Chimiques : Molécules, Matériaux, Instrumentation et Biosystèmes (2MIB)

Titre : Commutateurs moléculaires à base de terarylène : vers un rendement quantique de photocyclisation modulable et un comportement photo- et électro-actif

Mots clés : Photochromisme – Teraryléne – Photocommutateur – Rendement quantique – Électrocommutateur - DFT

Résumé : Au cours des dernierès années, de nombreuses molécules photo-chromiques ont été largement étudiées en tant que commutateurs moléculaires en vue d'une large gamme d'applications potentielles.
Dans cette perspective il est important de contrôler des paramètres liés à la photoisomérisation (i.e. les spectres d'absorption des isomères, les rendements quantiques, la stabilité thermique, la résistance à la fatigue).
Les diaryléthènes (DAEs) représentent une famille très connue de photocommutateurs car ils peuvent être commutés de manière réversible entre deux isomères, une forme ouverte moins conjuguée et une forme fermée plus conjuguée, tous les deux photorésistants et thermiquement stables. Néanmoins, la modulation de l'efficacité de cette isomérisation reste un défi.
Le premier objectif de cette thèse était de développer un modèle permettant d'ajuster le rendement quantique de la photocyclisation dans une famille homogène de terarylènes grâce au caractère de transfert de charge généré par l'introduction de divers groupes donneurs et/ou accepteurs d'électrons.
La possibilité de moduler le rendement quantique de la photocyclisation en suivant ce modèle a été exploitée pour synthétiser un dérivé approprié pour le second objectif de cette thèse, la préparation d'un système multichromophore photocommutateur présentant une hystérésis de fluorescence induite par la lumière. Dans un projet conjoint avec l'ENS Paris-Saclay, des architectures moléculaires composées de multiples unités fluorescentes et photochromiques et le terarylène synthétisé ont été combinés en vue de permettre d'induire des processus de transfert d'énergie entre eux.
Des études préliminaires ont confirmé que la différence entre la cinétique de photoisomérisation de notre photochrome et celle de l'autre unité fluorescente photo-active conduit à une hystérésis de fluorescence sous irradiation UV ou visible.
Une autre caractéristique intéressante des diaryléthènes est la possibilité de développer un comportement à double réponse par une fonctionnalisation appropriée (un autre stimulus en plus des photons peut induire l'isomérisation)
En particulier, dans le cadre de ce projet de thèse, une étude a été menée sur les terarylènes présentant une isomérisation induite par réduction ou oxydation.
Afin d'obtenir ce comportement, plusieurs molécules fonctionnalisées ont été synthétisées, caractérisées et étudiées.
Les terarylènes portant des groupes N-méthylpyridinium ont montré la possibilité de la fermeture de cycle par réduction. De plus, ces dérivés montrent également la possibilité d'une cycloréversion oxydative, ce qui en fait les premiers terarylènes caractérisés par une commutation photo- et redox- bidirectionnelle.
D'autre part, les terarylènes développés pour la cyclisation oxydative ont montré un comportement électrochimique différent de celui rapporté dans la littérature pour les diaryléthènes avec des ponts cyclopentène ou perfluorocyclopentène : l'oxydation a conduit à la forme fermée dicationique, mais la réduction ultérieure, au lieu de donner la forme fermée neutre comme dans les DAEs cités, a conduit au retour vers la forme ouverte neutre. Sur la base de plusieurs données spectroscopiques, un nouveau mécanisme a été proposé pour expliquer cette isomérisation induite par oxydation et réduction.

université PARIS-SACLAY

ÉCOLE DOCTORALE
Sciences Chimiques : Molécules, Matériaux, Instrumentation et Biosystèmes (2MIB)

Title : Terarylene-based molecular switches: towards tunable photocyclization quantum yield and dual photo- and redox-responsive behavior

Keywords : Photochromism – Terarylene – Photoswitch – Quantum yield – Redoxswitch - DFT

Abstract : Plenty of photochromic molecules have been extensively studied over the years as molecular switches for a broad range of potential applications. In this perspective, a control over the parameters related to the photoisomerization (i.e. absorption spectra of the isomers, quantum yields, thermal stability, fatigue resistance) is highly desired.

One popular family of photoswitches is represented by diarylethenes (DAEs), since they can be reversibly switched between two photo-resistant, thermally-stable isomers, a less conjugated open form and a more conjugated closed form. Nonetheless, the modulation of the efficiency of this isomerization remains challenging.

As first objective of this thesis, a model to tune the photocyclization quantum yield in a homogeneous family of terarylenes through the charge transfer character generated by introducing various electron-donating and/or electron-withdrawing groups has been developed.

The possibility of tuning the photocyclization quantum yield by following this model has been exploited to synthesize a suitable derivative for the second objective of this thesis, the preparation of a photoswitchable multichromophoric system showing a light-induced fluorescence hysteresis. In a joint project with ENS Paris-Saclay, molecular architectures composed of multiple fluorescent and photochromic units and the synthesized terarylene have been combined to allow energy transfer processes between them.

Notably, preliminary studies have confirmed that the difference between the photoisomerization kinetics of our photochrome and those of the other photo-active fluorescent unit leads to a fluorescence hysteresis when illuminated by UV or visible light.

Another appealing feature of diarylethenes is the possibility of developing a dual-responsive behavior (another input in addition to photons can induce the isomerization) through proper functionalization.

In particular, as last focus of this thesis project, an investigation has been conducted on terarylenes showing a redox-driven isomerization.

In order to achieve these behavior, several adequately functionalized molecules have been synthesized, characterized and studied.

The terarylenes bearing N-methylpyridinium groups have shown the occurrence of the reductive ring-closure. Moreover, these derivatives were found to undergo also the oxidative cycloreversion, making them the first terarylenes characterized by bi-directional photo- and redox-switching.

On the other hand, the terarylene-based derivatives designed for the oxidative cyclization have shown a different electrochemical behavior compared to that reported in the literature for diarylethenes with cyclopentene or perfluorocyclopentene bridges: the oxidation led to the dicationic closed form, but the subsequent reduction, instead of affording the neutral closed form as in reported DAEs, restored the neutral open form. Based on various spectroscopic data, a novel mechanism to explain this redox-driven isomerization has been proposed.

Acknowledgments

I'm deeply thankful for the support that I have received by many people throughout these years of PhD in ICMMO and this certainly contributed to make this period of my life so nice and unforgettable.

First and foremost, I thank Yu and Anne, who welcomed me as a Master student back in 2018 for an Erasmus internship and then gave me the opportunity to join the group as a PhD candidate. Thank you Yu because I personally felt that you haven't been only a supervisor, but also a teacher to me, in many theoretical and practical aspects of chemistry. Thank you Anne for all your explanations and help in several characterizations techniques, for your support when dealing with French bureaucracy and all the corrections of my French orthography.

Then I want to thank the members of the Jury: Pr. Eléna Ishow and Pr. Guy Royal, who have kindly accepted to be *rapporteurs* of this manuscript, Pr. Keitaro Nakatani and Pr. Jean-Christophe Lacroix. Thank you for the time that you have dedicated to my thesis.

I would also like to acknowledge Dr. Rémi Métivier, coordinator of the ANR project which financed my PhD, for his help and teaching about the measurements of the quantum yields at ENS Cachan during my first year and then at ENS Paris-Saclay, Pr. François Maurel for the collaboration over these years and the extensive theoretical modelling and Dr. Clémence Allain for all the advices as *comité de suivi*.

Moving to the permanents of LCI, I want to thank Talal Mallah and Ally Aukauloo, former and current directors of the lab, respectively, as well as all the other members who I have met in these years. Special mentions go to Laure for the amazing and comfy apartment, to Zak for all the (mean) jokes and talks about basketball, and to Jean-No for the songs suggestions, the help in some stopped-flow experiments attempts and the fun while having beers together.

I also want to thank all the non-permanent members of LCI, past and present: Linh, for inviting me for a beer in Paris on the first day that I got to the lab, making me feel included in the group immediately, Khaled and Antoine (I have beautiful memories of your *pot de thèse*); Amanda, for being kind since day one, with plenty of help in the redaction of mails; Eva and Juan for the friendship and all the fun time outside the lab; Adelais, for being always there for chemistry talks, advices in electrochemistry and in general for your constant support. There are so many others to thank, like Sophie, Axel, Laura, Asma, Elvin, Alberto, Marìa, Adama, Aman (you're at CEA, but I'll make an exception) and so on, but the paragraph would become endless and I would very much like to thank you in person.

Concerning other non-permanent students working outside of ICMMO, I want to thank two students at ENS Paris-Saclay: Yang, for all the work that we shared during our PhDs and the nice kayaking, and Céline, for the fruitful collaboration and my first-ever ramen.

I want to give a special thank you to Christian, not only for the EPR experiments, but also for being always available to provide assistance even if I was a nuisance, double-checking my drafts and motivation letters, removing most of the fancy (?) adverbs that I wanted to use and

for the last two years of uninterrupted lunches together.

I would like to thank all my friends. In particular, a sincere thank you to Carolina, for all these years of friendship and the delicious meals whenever I have spent some time back in Italy.

Last, I would also like to express my gratitude to my family, who always supported and believed in me.

Table of Contents

List of Abbreviations

A, B, C

A and Abs: absorbance
ACQ: aggregation-caused quenching
AIE: aggregation-induced effect
AIEE: aggregation-induced enhanced emission
ASE: aromatic stabilization energy
bisDMDPI-BN: (2,2′-dimethoxydiphenylimidazole)-1,1′-binaphthyl
c: concentration
CASSCF: combination of active space self-consistent field
CF: closed form
CHD: cyclohexadiene
CI: conical intersection
CPD: cyclophanediene
CT: charge transfer
CV: cyclic voltammetry / cyclovoltammogram

D, E, F

DAE: diarylethene
DASA: donor-acceptor Stenhouse adduct
$d_{C\text{-}C}$: carbon-carbon distance
DCM: dicyanomethylene or dichloromethane
DFT: density functional theory
DHP: dihydropyrene
DMF: dimethylformamide
DTE: dithienylethene
$E_{1/2}$: half-wave potential
E_a: activation energy
E_p: peak potential (for irreversible waves)
ESIPT: excited state intramolecular proton transfer
Fc: ferrocene
FC: Franck-Condon
Fc^+: ferrocenium
FRET: Förster resonance energy transfer

G, H, I, J

HABI: hexaarylbiimidazole
HD: halogen-dance
HI: hemiindigo
HOMO: highest occupied molecular orbital
HPLC: high-performance liquid chromatography
HT: hexatriene
HTI: hemithioindigo

I: photon flux
IEFPCM: integral equation formalism variant of the polarizable continuum model
ITO: indium tin oxide

K, L, M

k: rate constant
LDA: lithium diisopropylamide
LUMO: lowest unoccupied molecular orbital
M: molarity
MMVB: molecular mechanics-valence bond
MO: molecular orbital
MOF: metal organic framework

N, O, P

N_A: Avogadro's number
NBS: N-bromosuccinimide
OF: open form
OTf: triflate
PALM: photo-activated localization microscopy
PES: potential energy surface
Ph: phenyl
PivOH: pivalic acid
PMMA: poly(methyl methacrylate)
PSS: photo-stationary state

Q, R, S

Q*: amount of transferred charge
RESOLFT: reversible saturable opticaL fluorescence transitions
RT: room temperature
S_0: ground state
S_1: first excited state (singlet)
SCE: saturated calomel electrode

T, U, V, W, X, Y, Z

$TBAPF_6$: tetrabutylammonium hexafluorophosphate
TD-DFT: Time Dependent-Density Functional Theory
THF: tetrahydrofuran
TICT: twisted intramolecular charge transfer
TS: transition state
UV: Ultraviolet
V: volume

Symbols

α_{CF}: closed form percentage
β: fraction of absorbed photons
ΔE: peak-to-peak potential difference (for reversible waves)
Δr: transfer distance
ε: molar absorption coefficient
λ: wavelength
μ: dipole moment
ν: scan rate
$\tau_{1/2}$: half-lifetime
$\Phi_{C\text{-}O}$: cycloreversion quantum yield
Φ_F: fluorescence quantum yield
Φ_{FRET}: FRET efficiency
$\Phi_{O\text{-}C}$: cyclization quantum yield

Nicolò Baggi

Chapter 1: Organic photochromism

Nicolò Baggi

1.1 Discovery of the phenomenon and its definition

The reversible color variation of organic molecules induced by light was reported for the first time towards the end of the 19th century by Fritzsche, who observed that an orange-colored solution of tetracene became colorless if exposed to sunlight and that the initial color could be recovered in the dark [1], and by ter Meer, who studied a dinitroethane potassium salt showing a color change in its solid state under irradiation. [2] This phenomenon was initially called "phototropy" (from *phototropie* in German) by Markwald [3] and it was studied in terms of descriptive means. In 1950, with the exploitation of spectroscopic techniques that allowed a more scientific study of the molecules showing this behavior, the name "photochromism" was finally proposed by Hirshberg. [4]

Photochromism is described as the reversible conversion of a chemical species induced by light in at least one direction between two isomers A and B, characterized by different absorption spectra. [5] In most of the cases, the passage from a colorless species to a colored one is observed and the phenomenon has been defined as "positive photochromism". A simplified representation is depicted in Figure 1.

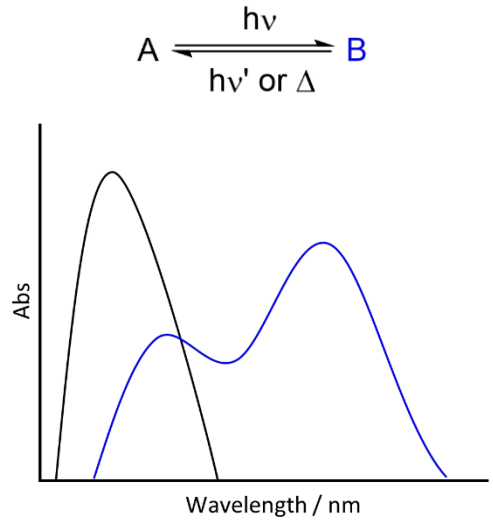

Figure 1: Schematic representation of photochromism.

However, also the opposite "negative photochromism", consisting in a light-induced bleaching as a consequence of the isomerization, is documented. [6,7]

The optical contrast (i.e. the difference in the UV-vis spectra of the two isomers) is actually only one manifestation of the isomerization. In fact, the structural change triggered by the photochemical reaction affects many other properties associated to the two isomers, such as their fluorescence, their redox potentials, their chiral properties, etc. [8]

Moreover, this impact of the photoisomerization at the molecular level can be exploited macroscopically if the photochromic derivative is included in supramolecular system or matrixes. An extensive review by Hecht and Boelke summarizes the design of several examples

of photochromes for smart, soft materials such as liquid crystals, hydrogels and flexible transistors. [9]

As it is stated in the definition, light isn't necessarily involved in both the isomerizations. In fact, if A and B are separated by a small potential barrier then B is metastable and it can revert back to A spontaneously. Molecules in which this thermal back reaction occurs are defined as T-type photochromes. On the contrary, if the two isomers are separated by a high energy barrier, the system is bistable and only photons are able to cause the back reaction. P-type photochromes belong to this class.

Whatever the type of photochromic system, the efficiencies of the photon-induced isomerization processes are reported in terms of quantum yields, that is the ratio of the number of reacted molecules of A to afford B to the number of absorbed photons. Other important properties to be considered are:

- The fatigue resistance, that is the ability of the photochrome to undergo many isomerization cycles without significant degradation.
- The thermal stability, that is the half-life of the photogenerated isomer at a specific temperature.
- The degree of photoconversion, that is the percentage of photogenerated isomer at the photostationary state reached for a specific irradiation wavelength.

1.2 Examples of organic photochromes

This section aims to provide an overview of some of the most important families of organic photochromes. In particular, the first part will be dedicated to azobenzenes, spiropyranes and spirooxazines, chromenes, fulgides and dihydropyrenes, that will be classified according to their isomerization mechanisms. The second part will briefly introduce some more recent photochromes such as donor-acceptor Stenhouse adducts (DASAs), hemi- and hemithioindigoes and binaphthyl-bridged imidazole dimers. Diarylethenes and their sub-class terarylenes, objects of this thesis, will be described more in depth separately (Section 1.3).

1.2.1 E/Z isomerization

The main family of organic photochromes whose isomerization is based on *E/Z* isomerization is represented by azobenzenes. Discovered in the 19th century, azobenzene's photochromism was reported in 1937 by Hartley who observed a change in its absorption spectrum induced by light due to a *trans*/*cis* isomerization (Figure 2). [10]

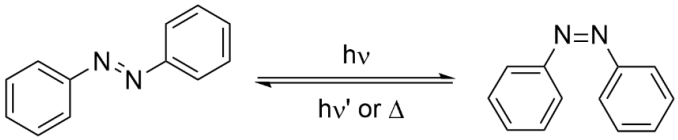

Figure 2: Photochromic reaction of azobenzene.

By switching the thermodynamically stable *trans* isomer to the *cis* one, the optical contrast is generally small, but the spatial structural change is important. Moreover, azobenzene is a T-type photochrome, since this species can spontaneously revert back to the initial configuration in the dark.

These derivatives have been studied for various applications ranging from switches in polymers and molecular machines [11] to photopharmacology, that is a branch of pharmacology that aims to use light to modulate the activity of drugs so to improve their efficacy and safety. Extensive reviews on the subject have been published by Feringa and co-workers [12,13] by Pianowski [14] and by Jerca et *al.* [15]

In particular, in this latter field, recent studies carried out by Gorostiza's group showed the possibility of exploiting the *E/Z* isomerization of these photochromes in the development of azobenzene-based analogues of tricyclic drugs (Figure 3) and adrenergic drugs. [16,17]

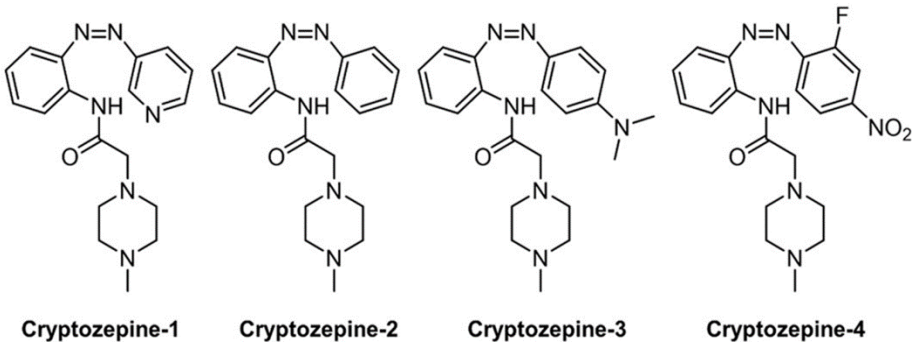

Figure 3: Structures of azobenzene-based tricyclic drugs analogues described in ref. [16]

Interestingly, these molecules show negligible activity in the *trans* configuration and antagonism in the *cis* one, thus indicating the possibility of developing novel photoswitchable drugs.

In 2021, in the perspective of developing azobenzene-based data storage devices, Staubitz and co-workers developed the macrocycle shown in Figure 4, that shows unusual properties for this photochromic family, since it is thermally stable at 20°C, the absorption bands for the two isomers are separated by ~100 nm and its photochromism is observed also in the solid state, an unexpected phenomenon when the isomerization causes big structural changes. [18]

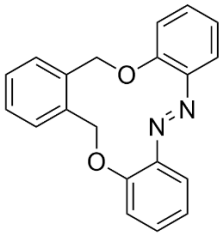

Figure 4: Structures of the azobenzene macrocycle described in ref. [18]

1.2.2 Bond cleavage

1.2.2.1 Spiropyranes, spirooxazines and chromenes

Spiro-compounds and chromenes are derivatives whose photochromic reaction involves the cleavage of a C-O bond.

As mentioned in Section 1.1, the research by Hirshberg in the 50s marked a turning point in the field of photochromism, with the synthesis and the study of spiropyrans. [19–23] These molecules, consisting in a pyran that shares the carbon atom in the position 2 with a second ring system, show an isomerization between a colorless spiropyran form and a merocyanine colored one (Figure 5).

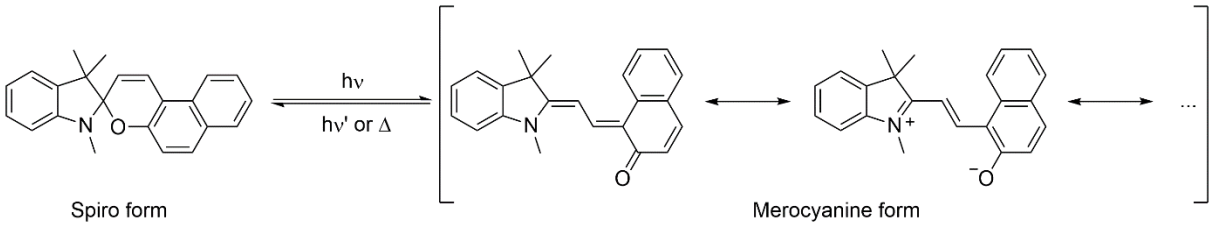

Figure 5: Photochromic reaction of 1,3,3-trimethylindoline-2-spiro-6'-(2',3'-β-naphthopyran), described in ref. [19]

The photochromic reaction is based on a photoinduced heterolytic cleavage of the quaternary carbon-oxygen bond to generate the conjugated open form, for which multiple quinonic or zwitterionic resonance structures exist. As it can be observed, the isomerization induces an important structural change when passing from the spiro form to the merocyanine isomer.

The spiropyran form is colorless because the quaternary spiro carbon atom prevents delocalization over the two condensed rings and the molecule consequently absorbs only in the UV region. On the contrary, the merocyanine isomer shows absorption bands in the visible because of the conjugation in the planar open form.

Photochromes belonging to this family are generally T-type, but more stable open forms can be achieved with the introduction of stabilizing functionalities such as nitro groups. [24,25] Moreover, even if rarer, cases of negative photochromism in which the open, colored form is the thermodynamically stable species have also been reported. [6,7,26,27]

However, as stated by Bertelson in his "Reminiscence about organic photochromes", spiropyrans, even if largely studied, couldn't be successfully exploited in commercial applications because of their poor photoresistance. [28]

In the attempt to solve these limitations, spirooxazines were synthesized and they ended up taking more interest than spiropyrans because of their better performances.

This improved resistance towards photodegradation is due to the stability of the 2*H*-[1,4]oxazine that replaced the 2*H*-pyran ring. The first example of spirooxazine was reported in the 70s, with the synthesis of 1,3,3-trimethylspiro[indoline-2,3'-[3*H*]naphth[2,1-β][1,4]oxazine] (Figure 6). [29]

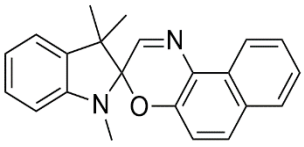

Figure 6: 1,3,3-trimethylspiro[indoline-2,3'-[3H]naphth[2,1-β][1,4]oxazine].

A part from the commercial application in photochromic lenses, spiro-photochromes have been investigated to be used for data storage or fluorescence modulation by combining them to fluorophores. [30]

Chromenes represent a family of molecules that have seen large use in the development of photochromic lenses because of their complementary nature to spiro-compounds. In fact, in these molecules, the photochromic isomerization (reported for the first time by Becker and Michl in 1966 [31]) doesn't induce an optical contrast as large as that of spirooxazines and the obtainable colors are consequently different. The photoinduced reaction of these derivatives is depicted in Figure 7. [32]

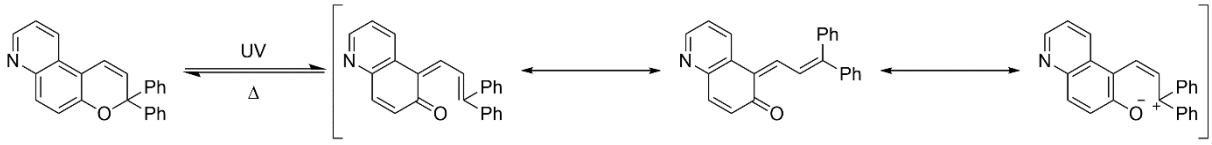

Figure 7: Photochromic reaction of a chromene derivative.

Again, the photo-induced reaction causes a C-O bond cleavage. The generated species can exist in solution in *E*- or *Z*-quinoidal forms or as zwitterion with the phenolate group. The structure of the colored open form depends on the functionalization of the investigated derivative. [32]

In addition to the industrial application in ophthalmic eyewear, chromenes have been used as potential photoswitchable receptors. [33,34]

1.2.2.2 Dihydropyrenes

Dihydropyrenes (DHPs) are negative photochromes since the thermally stable form is the colored DHP isomer. Visible light irradiation causes the cleavage of the central C-C bond, thus forming the colorless cyclophanediene (CPD) (Figure 8). [35] However, depending on the functionalization, it is possible to have the cyclophanediene as the thermodynamically stable species. [36] The back-reaction restoring the DHP isomer can occur thermally or with UV light.

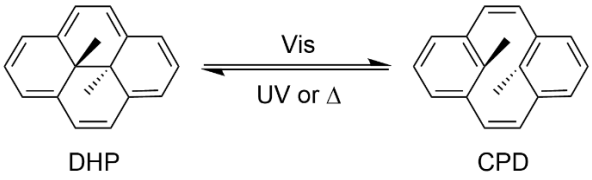

Figure 8: General photochromic reaction of a DHP.

DHPs have been studied in fundamental research about aromaticity [37] and they have found potential application in smart molecular devices for optoelectronics [38] and in photopharmacology. [39]

Concerning their exploitation in the biomedical field, Royal and co-workers showed in 2015 the possibility of using the dihydropyrene in Figure 9 as oxygen carrier and singlet oxygen ($^1O_2$) producer. [40]

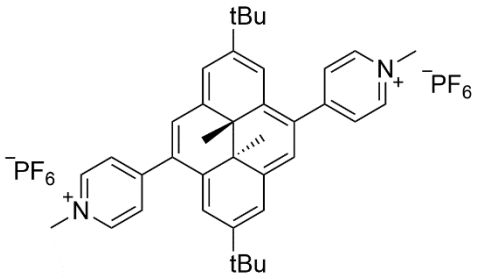

Figure 9: DHP acting as oxygen carrier and singlet oxygen producer investigated in ref. [40]

This molecule is capable of trapping molecular oxygen when switched to the CPD isomer. By heating the obtained adduct, singlet oxygen is released and the DHP isomer is restored. This controlled generation of $^1O_2$ is clearly appealing for photodynamic therapy. Moreover, the authors have shown that the phenomenon can be observed if the molecule is grafted on a surface, too. [41]

1.2.3 Electrocyclization

Even if the photochromes described in the previous section could have been included in this one since the back reaction from the photogenerated isomer is an electrocyclization, the focus here will be on systems whose thermodynamically stable species is the one undergoing the photoinduced cyclization reaction, as in the case of fulgides.

These compounds have been discovered by Stobbe at the beginning of the 20th century. [42] Initially they were thermally reversible photochromes, but proper functionalization allowed to make the cycloreversion photochemically driven. Fulgides can be consequently considered as P-type systems. As described in detail in the review published by Yokoyama in 2000, the photochromic reaction of fulgides occurs through 6π-electrocyclization of the 1,3,5-hexatriene core unit in the E-isomer, while the Z-one is inactive (Figure 10). [43]

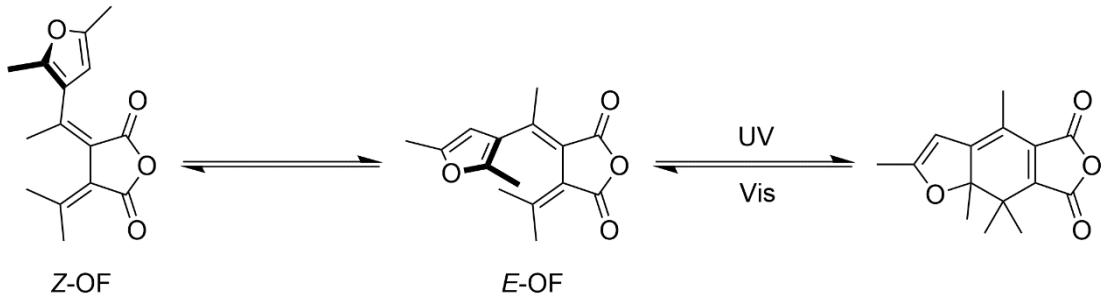

Figure 10: Photochromic reaction of a fulgide derivative described in ref. [43]

These photochromes have been employed in many applications: for data storage since the photogenerated species is thermally irreversible, as perturbing factors in liquid crystals by exploiting the structure change with the isomerization, in non-linear optics. [43] As an example of optical memory system, Schwartz and co-workers have recently proposed a fulgide@MOF adduct based on the photochrome in Figure 11 as promising hybrid material for the development of a data storage device. [44]

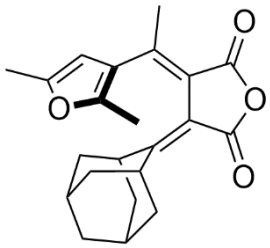

Figure 11: Fulgide derivative used in ref. [44] for the preparation of a fulgide@MOF hybrid material.

The same isomerization mechanism occurs in diarylethenes, more successful systems thanks to their better fatigue resistance and the neglected *cis*/*trans* isomerization that is detrimental to the photocyclization [45], which will be described in detail in Section 1.3.

1.2.4 Recent photochromic derivatives

Some of the most recent photochromic families, whose investigations started in the 21th century, will be briefly described in this Section to complete the overview of the most important organic photochromes that have been studied over the years.

1.2.4.1 Donor-acceptor Stenhouse adducts (DASAs)

Donor-acceptor Stenhouse adducts (DASAs) have been designed as novel negative photochromes by Read de Alaniz and co-workers in 2014 [46], by developing push-pulls systems based on the adducts named after the chemist that discovered them in 1850. [47]

By visible light irradiation, a DASA isomerizes from a conjugated, colored and hydrophobic open form to a colorless, closed and hydrophilic (since zwitterionic) one, as shown in Figure 12.

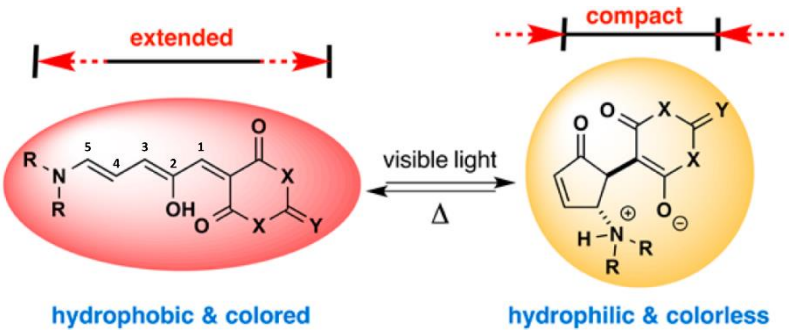

Figure 12: General scheme of DASA's photochromic reaction, adapted from ref. [46]

As it can be observed, the isomerization is also accompanied by one of the largest structural variation among those observed for the photochromes that will be briefly described in this Section. The closed form (CF) reverts back to the open form (OF) thermally and repetitive cycles can be performed with high fatigue resistance. The reaction mechanism has been in-depth investigated by Feringa and co-workers and consists in an initial *Z*/*E* isomerization around the double bond bearing the –OH group (i.e. C_2=C_3) followed by a rotation around the single bond

C_3-C_4 so to obtain the right conformer undergoing the conrotatory 4π-cyclization to afford the closed form. [48]

After the first paper, a second and a third generation of DASAs have been developed to optimize the usable visible light wavelengths and the solvent compatibility (i.e. the solvents in which the reversible photochromic behavior can be observed). [49,50] In particular, the third generation, based on aromatic amines and strong carbon acids, as in the example provided in Figure 13, have shown the best properties.

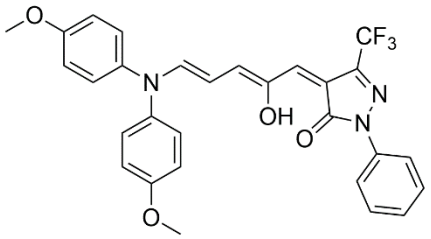

Figure 13: Example of 3rd gen DASA derivative investigated in ref. [50]

The impact of the donor and the acceptor strengths have been largely studied experimentally, with the support of theoretical modelling. [51–53]

Since their discovery, the interest around DASAs has risen significantly thanks to their potential application as actuators for renewable energy or in medicine delivery through photopharmacology (since visible light is used to induce the isomerization instead of the harmful UV one) as well as amines detectors or colorimetric detectors of nerve agent mimics. [54]

1.2.4.2 Hemi- and hemithioindigos

Known since 1883, hemiindigo (HI) is a chromophore based on an indigo unit (a natural blue dye) linked to a stilbene moiety by a shared double bond. [55] However, its potential use as photoswitch has remained unexplored till 2017, year in which Dube et *al*. showed the highly interesting performances of this derivative as P-type photochrome operative in the visible region of the spectrum. [56]

The photochromic reaction is a based the *Z*/*E* isomerization around the double bond (Figure 14).

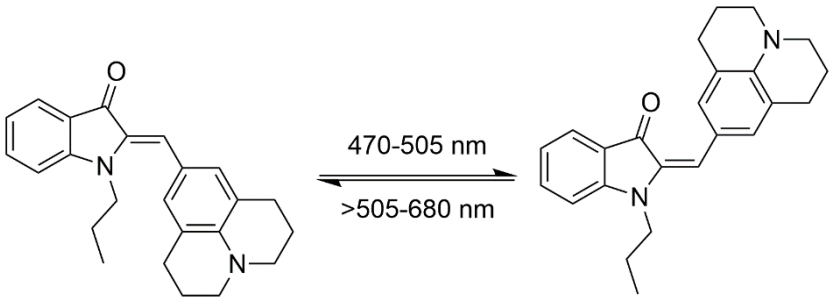

Figure 14: Z/E photo-induced isomerization of one of the hemiindigos investigated in ref. [56]

Almost quantitative switching is achieved by using visible and near infrared lights, an appealing aspect to take into account for potential applications in pharmaceutical and medical fields.

Similar biologically compatible wavelengths can be used to irradiate hemithioindigo (HTI) derivatives, molecules studied as possible photochromes always by Dube's group in which the indigo moiety has been replaced by a thioindigo one (Figure 15). [57]

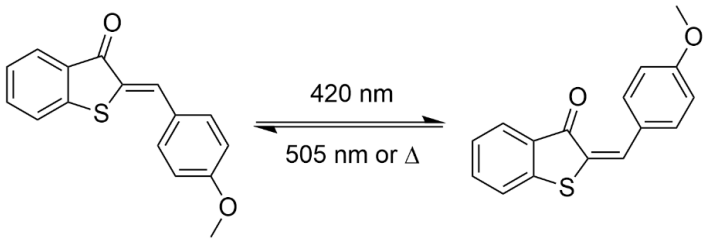

Figure 15: Example of hemithioindigo investigated in ref. [57]

Once again, visible light induces the isomerization around the double bond of the thermodynamically stable *Z*-isomer to afford the *E*-one.

Bistability can be achieved by introducing electron-donating groups such as $–NMe_2$ in *para* position to the sulfur atom on the phenyl ring of the thioindigo unit. [58]

Synthetically easy to obtain as the hemiindigo analogues, HTIs are interesting switches for photopharmacological applications: in 2021, Thorn-Seshold and co-workers have in fact shown that a pyrrole hemithioindigo derivative could allow visible-light imaging and photoswitching in live cells. This behavior led to modulation of microtubule dynamics with cell-precision and guaranteed control over cell life and death. [59]

1.2.4.3 Binaphthyl-bridged imidazole dimers

Relatively recent example of negative photochrome, (2,2′-dimethoxydiphenylimidazole)-1,1′-binaphthyl (bisDMDPI-BN, Figure 16) was described for the first time by Abe and co-workers in 2013. [60]

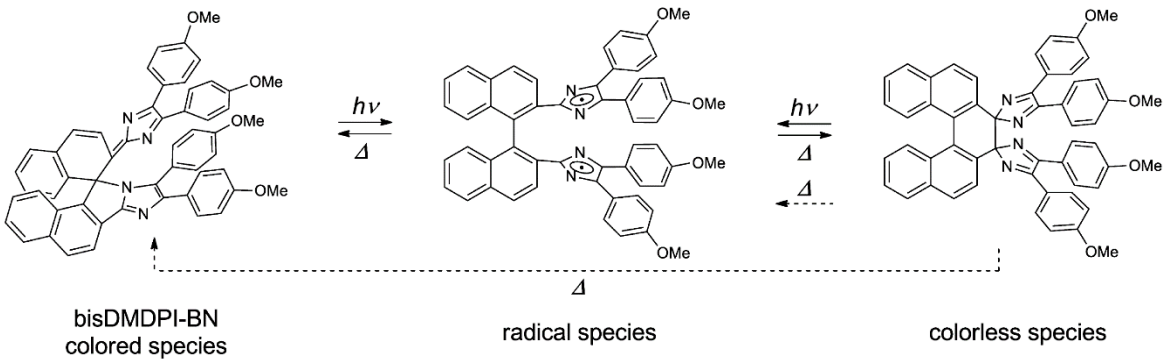

Figure 16: Isomerization of bisDMDPI-BN, novel negative photochrome discovered by Abe and co-workers; adapted from ref. [60]

This derivative is an evolution of hexaarylbiimidazole (HABI), a system developed in the 60s by Hayashi and Maeda [61] and largely characterized over the years by Abe's group [62], that shows positive photochromism (Figure 17).

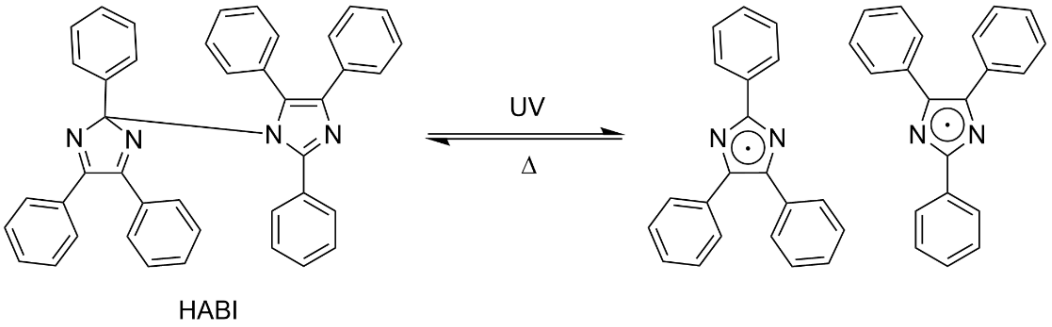

Figure 17: Photochromic reaction of hexaarylbiimidazole (HABI).

As shown in the Figure 16, the thermally stable colored species can be reversibly switched to a colorless one by visible light irradiation. The obtained isomer is thermally unstable and spontaneously reverts to the colored one in the dark at room temperature.

The photo-bleaching occurs *via* a biradical intermediate that is generated through homolytic cleavage of the C-N bond. Radical coupling eventually leads to the formation of the new C-C bond between the two imidazole units, thus affording the colorless isomer. The lifetime of this metastable species can be modulated from minutes to seconds to milliseconds through substitution. [60,63,64]

After this pioneering work, binaphtyl-bridged imidazole dimers have been investigated to achieve turn-on fluorescence by exploitation of the negative photochromic behavior [65] or to develop red/near infrared light photochromic systems suitable for biological applications. [66] Moreover, it has been possible to obtain a real-time dynamic 3D hologram by using the imidazole dimers shown in Figure 18. [67]

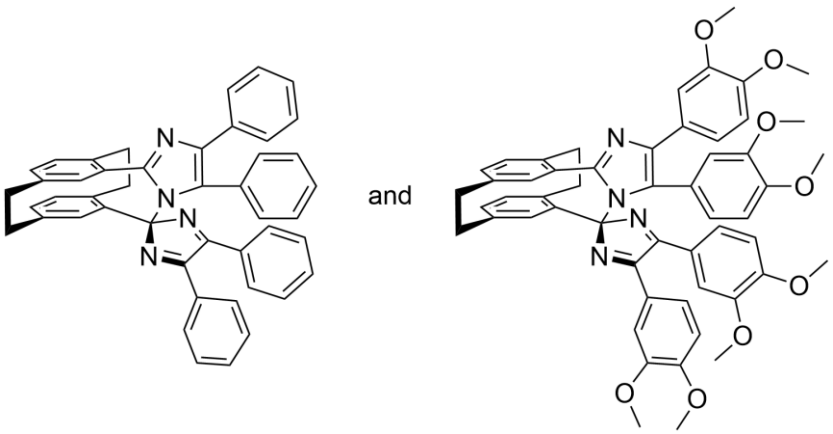

Figure 18: Bridged imidazole dimers used to obtain a real-time dynamic hologram of a 3D object in ref. [67]

1.3 Diarylethenes

As stated by Irie in the first paper that was published about these molecules in 1988, diarylethenes (DAEs) represent a class of "thermally irreversible photochromic systems". [68]

Since that report came out, interest around diarylethenes grew exponentially thanks to their properties and possible applications, as it can be observed in Figure 19, where the number of publications per year (available on Scopus) containing the words "Diarylethene" or "Dithienylethene" (i.e. an alternative name for thiophene-based diarylethenes) between 1988 and September 2021 is provided.

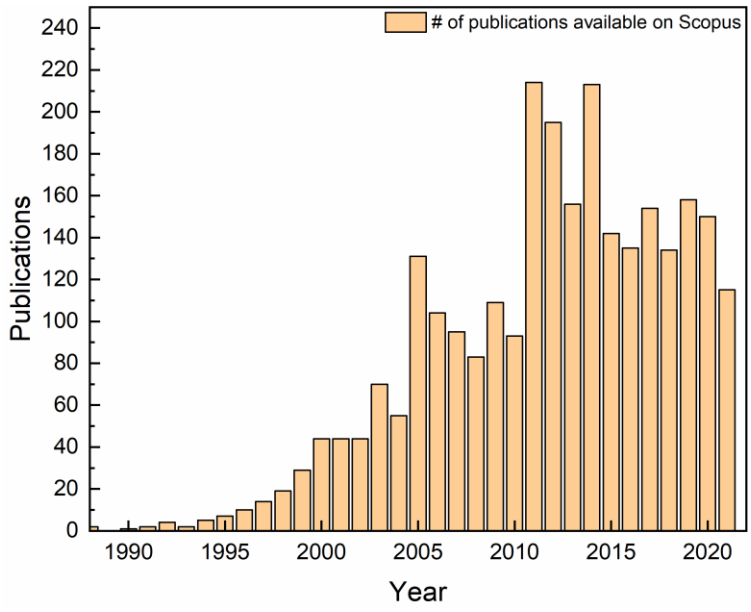

Figure 19: Number of publications per year containing the words "Diarylethene" or "Dithienylethene". Research on Scopus, covering the period between 1988 and September 2021.

Even if these derivatives are generally taken as examples of P-type photochromes in which the isomer that is generated by light irradiation is thermally stable and the back reaction isn't observed in the dark at room temperature, T-type DAEs exist too, since the thermal stability can be modulated by properly designing the molecules. In fact, examples of photo-generated isomers characterized by half-life times ranging from minutes to seconds to milliseconds have been reported. [69–72]

Stilbene is often taken as the simplest example to explain the isomerization of this family of photochromic compounds. [73] A photoinduced cyclization can occur on its *Z*-isomer with the consequent formation of dihydrophenantrene. This species can revert thermally to the initial state unless oxygen causes the irreversible formation of phenantrene by dehydrogenation. All these reactions are depicted in Figure 20, where the actual photochromic ring-closing reaction is circled in prune.

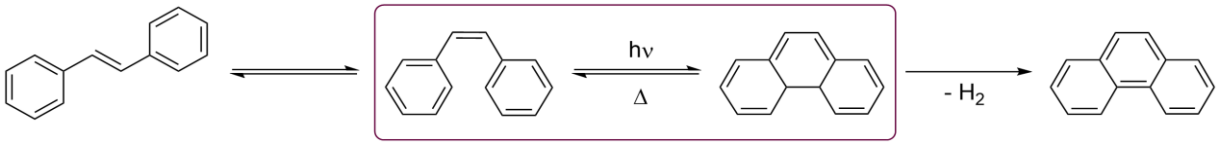

Figure 20: Photochromic reaction of Z-stilbene to dihydrophenantrene and irreversible dehydrogenation to phenanthrene.

Diarylethenes are a thermally stable and reversible evolution of this simple system. First of all, the ethene bridge was replaced with five-membered rings such as maleic anhydride, maleimide, cyclopentene or hexafluorocyclopentene to inhibit the *Z*/*E* isomerization, a competitive detrimental process, since the *trans* isomer can't undergo the cyclization reaction. Secondly, the replacement of the aryl rings with heterocycles such as thiophene, thiazole or oxazole led to more stable cyclized forms. [45,74] Finally, the substitution of the hydrogen atoms on the reactive carbons (i.e. the carbon atoms involved in the formation of the new C-C bond) with methyl groups – or others – prevented the dehydrogenation by oxidation (Figure 21).

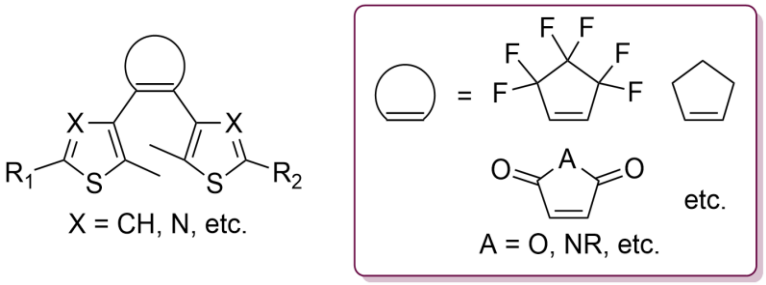

Figure 21: General structure of a DAE.

If the central moiety is instead a (hetero)aryl group, the derivative is named "terarylene". [75–77] Terarylenes represent an interesting sub-class of DAEs because the presence of an additional central aryl group offers an extra site for eventual functionalization, as highlighted in prune in Figure 22 for clarity.

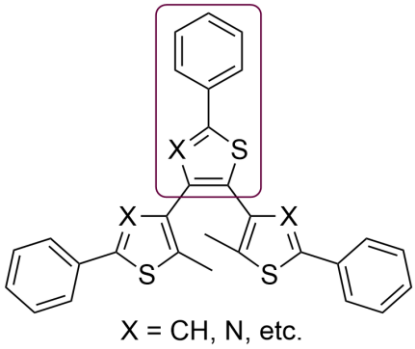

Figure 22: General structure of a terarylene.

However, it is worth noting that the closed forms of these systems are less stable than those of diarylethenes. In fact, the overall aromatic stabilization energy (ASE) is higher in terarylenes and the loss of aromaticity concerns three rings during the cyclization. [77]

As summarized by Irie, Fukaminato, Matsuda and Kobatake in their review of 2014 [5], all these measures allowed to obtain DAEs with highly desired performances. In addition to the already cited tunable thermal stability, these molecules are generally characterized by a large optical contrast between the two isomeric forms since the colorless open form (OF) absorbs in the UV region while the conjugated closed form (CF) shows absorption bands in the visible. They also possess excellent fatigue resistance and their photoinduced cyclization and cycloreversion can occur with high efficiencies, or quantum yields.

Moreover, the photochromic reaction has been observed also in crystals (Figure 23), a behavior that is not common for systems undergoing isomerizations, since large geometric change is not allowed in a crystalline phase. However, it can be observed in some DAEs thanks to the fact that the photoinduced reaction doesn't cause a structure change as big as in other photochromic derivatives such as azobenzenes or DASAs. [78,79]

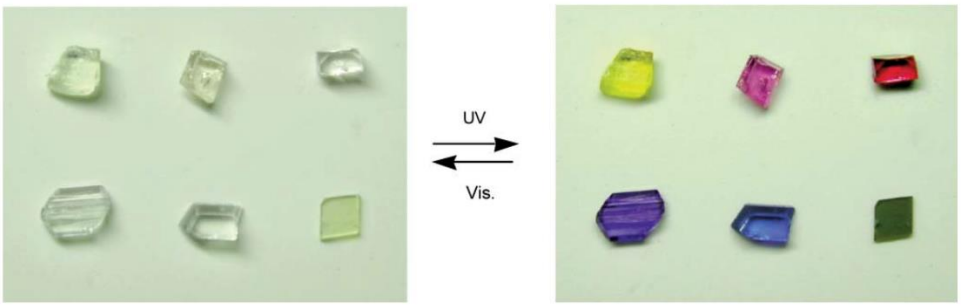

Figure 23: Photochromism in DAEs single crystals. Adapted from ref. [79]

An important aspect that must be remembered is the fact that many properties in addition to the absorption spectra can be affected by having control on the conversion between the open form and the closed form of a diarylethene, thus making them "multifunctional" switches.

This allowed to employ DAEs in applications with paramount importance: as light-driven crystal actuators for micro- and nanomechanics (Figure 24) [80], as fluorescent cellular markers in living cells [81,82], in optically switchable transistors [83,84], in flexible cognitive nanodevices [85], in miniaturized molecular junctions [86] and many others. [87]

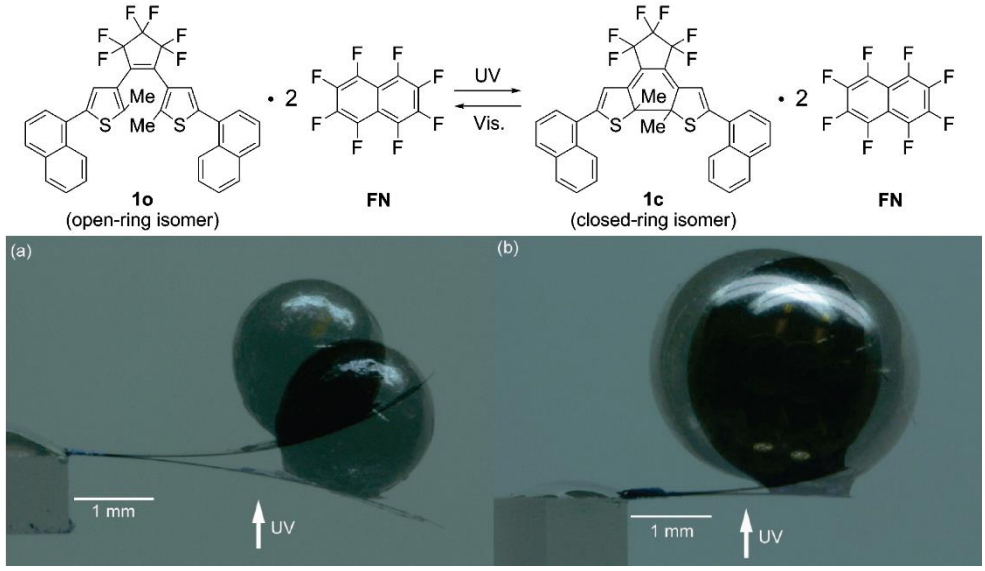

Figure 24: (top) Photochromic reaction of the cocrystal investigated in ref. [80]; bottom) photomechanical work of the cocrystal under UV irradiation, lifting a) a lead ball or b) a steel ball, adapted from ref. [80]

1.3.1 Diarylethenes' 6π-electrocyclization

Going more into detail about the photochromic reaction of these derivatives, the light induced isomerization consists in a 6π-electrocyclization of the central 1,3,5-hexatriene unit to cyclohexadiene, that occurs with a conrotatory mechanism (Figure 25), according to the Woodward-Hoffman rules about the conservation of π orbitals symmetry. [88]

Figure 25: Light-induced conrotatory cyclization of 1,3,5-hexatriene to cyclohexadiene

In the case of diarylethenes, the free rotation around the single bonds of the hexatriene core allows the existence of two conformers in solution, an antiparallel and a parallel one. [68,89] The two aryl rings are in C_2 symmetry in the antiparallel conformation and they are in mirror in the parallel one. While the former geometry can undergo the cyclization respecting the Woodward-Hoffman rules, the latter remains photo-inactive, as indicated in Figure 26.

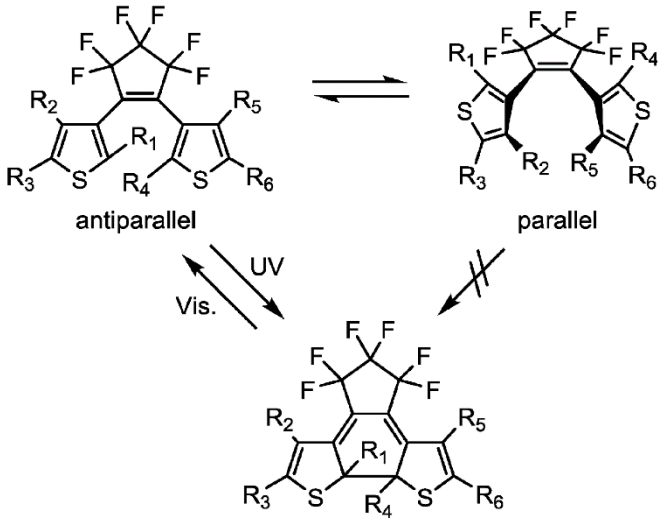

Figure 26: Possible conformations for a DAE derivative and consequent photochromic activity, described in ref. [5]

Spectroscopic time-resolved techniques have been useful to elucidate this electrocyclization ruling the photochromic reaction. A first study by Miyasaka and Irie published in 1994, based on picosecond laser photolysis and transient absorption spectroscopy in solution of 1,2-bis(2,4,5-trimethyl-3-thienyl)maleic anhydride, allowed to understand that the isomerization occurs in a picosecond timescale. [90] Similar analyses were performed again by Miyasaka, Irie and Tamai on other diarylethenes or DAE-based oligomers extending the study also to the crystalline phase and confirmed the very fast kinetics of the events. [91,92]

In 2020, the same molecule (Figure 27) has been reinvestigated by Hamdi et *al*. to study more in depth the dynamics of the process. It has been observed that the kinetics of the reactions are actually much faster, occurring in a femtosecond timescale. [93]

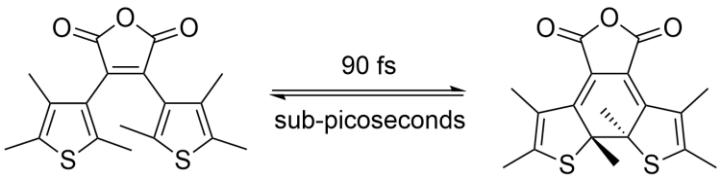

Figure 27: Time constant for the photocyclization of 1,2-bis(2,4,5-trimethyl-3-thienyl)maleic anhydride, determined in ref. [93]

1.3.1.1 Theoretical modelling of the cyclization

In addition to the cited studies based on transient absorption techniques, theoretical modelling has been carried out to rationalize the ring-closing reaction. Boggio-Pasqua et *al*. showed in 2003 that the ultrafast cyclization of diarylethenes occurs in the first excited state S_1 from the Franck–Condon (FC) region through a conical intersection (CI) that was identified and characterized through a combination of active space self-consistent field (CASSCF) study of the potential energy surfaces (PESs) and a molecular mechanics-valence bond (MMVB) computation of the dynamics. [94]

Conical intersections are defined as the regions where two or more potential energy surfaces intersect thus allowing non-adiabatic processes (such as the achievement of the ground state closed form isomer after the cyclization reaction in the excited state) to occur, thanks to the possibility of crossing between surfaces without radiative transitions.

As observed by Boggio-Pasqua, by initially building the S_0 and S_1 PESs through CASSCF, it was possible to identify four minima, two for each state, i.e. ground state OF (or HT, from "hexatriene" and CF (or CHD, from "cyclohexadiene") and first excited state OF* (or HT*) and CF* (or CHD*). In addition to the transition states TS_0 and TS_1, several conical intersections were characterized. Among them, the intersection named CI_3 appeared to be a "door" to reach both the open form and the closed form geometries in the ground state (Figure 28). MMVB dynamic computation also showed that almost half of the trajectories decayed at geometries near this conical intersection confirming its involvement in the cyclization process (and in the cycloreversion, too).

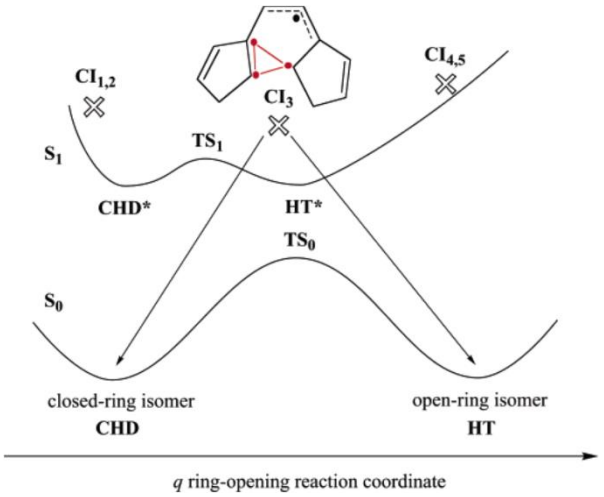

Figure 28: Approximation of the S_1 reaction pathway, as published in ref. [94]

TD-DFT (Time Dependent-Density Functional Theory) calculations, even if they have limitations in the characterization of conical intersections [95], represent a valuable alternative to the computationally expensive CASSCF method to gain some insight into the photoreactivity of DAEs, as demonstrated by Fihey and Maurel. [96] In fact, TD-DTF allows to compute the topology of the molecular orbitals involved into molecular transitions. For example, the authors have reported that the HOMO of the open form isomer of a reference dithienylethene resembles the LUMO of its closed form isomer, and vice versa (Figure 29). Moreover, the OF's LUMO shows the right symmetry for the bonding interaction between the reactive carbon atoms involved into the 6π-electrocyclization.

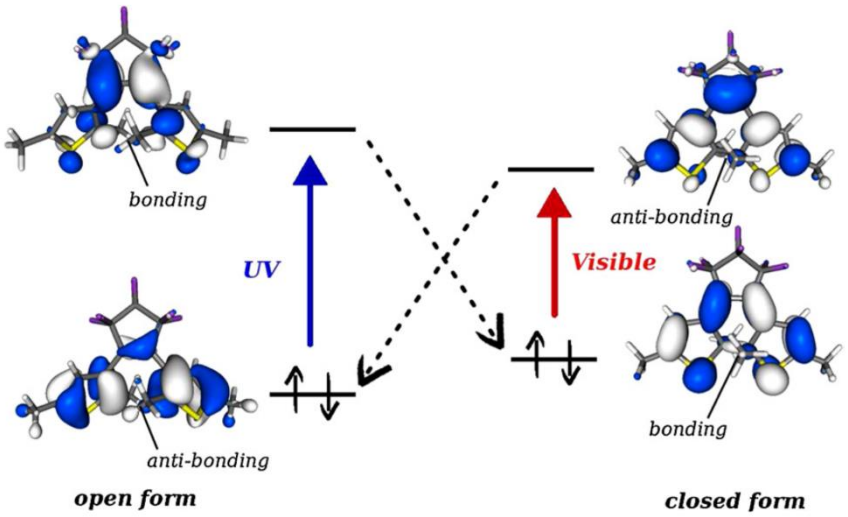

Figure 29: Frontier orbitals of the reference DTE in its open and closed forms, as published in ref. [96]

1.3.2 Cyclization quantum yield

As previously stated, the efficiencies of the two isomerization reactions of a DAE are indicated in terms of cyclization and cycloreversion quantum yields ($\Phi_{O\text{-}C}$ and $\Phi_{C\text{-}O}$), i.e. the ratios of the number of molecules undergoing the photoinduced reaction to afford the closed form or the open form to the number of absorbed photons, with values ranging between 0 and 1.

While the thermal stability and the absorption spectra can be finely tuned by functionalizing the diarylethenes as desired, quantum yields are the most difficult parameters to modulate. [45]

In the case of the open form isomer, two conformations, a parallel photoinactive and an antiparallel photoactive one, are coexisting in solution (Section 1.3.1, Figure 26). If their ratio is 50:50 and only half of the species are capable to cyclize under UV light irradiation, the theoretical maximum value for the cyclization reaction is 0.5.

Many efforts have been carried out to improve the efficiency of this process by increasing the percentage of the antiparallel conformer. Enhanced photocyclization quantum yields were obtained in 1999 by taking advantage of **steric hindrance**. [97]

Fifteen years later, Zhu's group exploited steric effects to obtain a photocyclization quantum yield of ~0.91 for the molecule shown in Figure 30. [98]

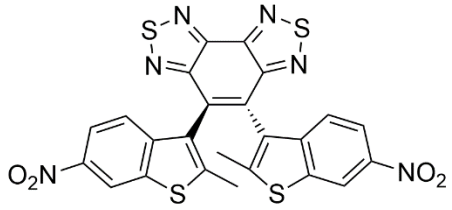

Figure 30: Sterically hindered benzobisthiadiazole-bridged diarylethene showing extremely high photocyclization quantum yield, investigated in ref. [98]

In fact, the authors had already highlighted in a previous work how sterically hindered diarylethenes could offer the possibility of separating the pure photoactive conformer from the parallel one by column chromatography. [99] Similarly, the authors isolated the antiparallel open form of the molecule depicted above to reach such a high $\Phi_{O\text{-}C}$.

In 2009, Yokoyama showed that the percentage of the antiparallel conformer could also be increased through **intramolecular interactions** with the description of the bisarylindenone and its acetal derivative depicted in Figure 31. [100]

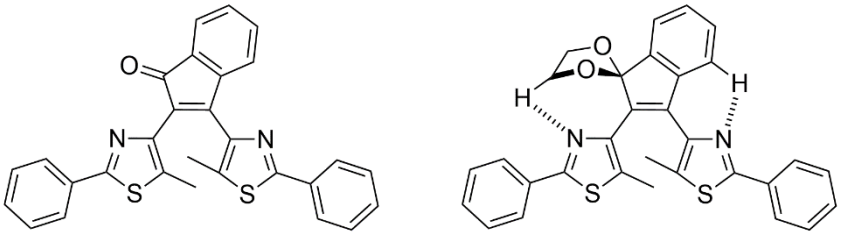

Figure 31: Photochromic reactions of the bisarylindeone (left) and its acetal derivative (right) investigated in ref. [100]

While the photocyclization quantum yield for the indenone-based precursor appeared to be 0.10 in acetonitrile, the introduction of the acetal moiety improved it to 0.63 in the same solvent. In an apolar solvent such as hexane, $\Phi_{O\text{-}C}$ was even higher (0.81). At the time, this value was the highest ever reported for DAEs derivatives in solution. The authors attributed the possible origin of such an enhancement to the presence of intramolecular N---H interactions between the nitrogen atoms the thiazoles and the hydrogen atoms of the indenone's phenyl and acetal groups. These interactions would in fact force the open form to assume the reactive antiparallel conformation. Moreover, the fact that the quantum yield was smaller in a polar solvent capable to diminish the hydrogen bonding was coherent with this proposition.

Two years later, Kawai and co-workers reported an almost quantitative isomerization for another terarylene derivative by exploiting similar intramolecular interactions. [101] The authors synthesized and characterized the dithiazolylbenzothiophene depicted in Figure 32, in which S---N interaction and hydrogen bonding blocked the open form in the photoactive antiparallel conformation.

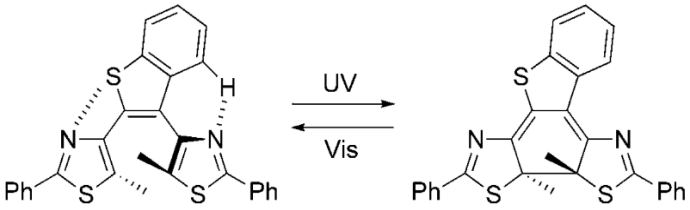

Figure 32: Photochromic reaction of the dithiazolylbenzothiophene showing intramolecular interactions that enhance the photocyclization quantum yield, as published in ref. [101]

In hexane, the investigated photochrome showed a photocyclization quantum yield equal to 0.98. By switching to a protic solvent such as methanol, capable to affect the H-bond that was locking the open form in the C_2 symmetry, the value decreased to 0.54. Furthermore, the antiparallel conformation was maintained in the single crystal too, thus allowing solid-state photochromism. The same authors have also shown that photon-quantitative $\Phi_{O\text{-}C}$ could be achieved also in MeOH, with an analogue molecule having a thienyl ring instead of a thiazyl one (Figure 33). [102]

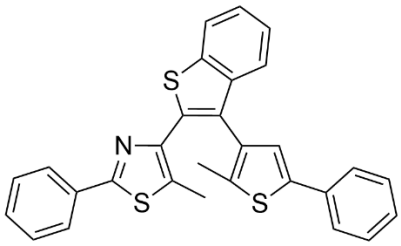

Figure 33: Terarylene showing photon-quantitative photocyclization quantum yield in MeOH, investigated in ref. [102]

Another possible way to increase the percentage of open form in the photoactive conformation is the **inclusion in a confined space**: either in cavities such as cyclodextrine (as summarized by Irie [45] and cucurbit[n]uril [103] or in polymers, as demonstrated in 1999 by Stellacci and co-workers with the synthesis of a DTE-based polymer whose $\Phi_{O\text{-}C}$ had been measured as up to 0.86 thanks to the fact that the only viable conformation in the polymer backbone was the antiparallel one. [104]

1.3.2.1 Impact of donor and acceptor groups

On the contrary, it has been observed that electron donating and/or electron withdrawing groups, whose introduction could be appealing to promote a solvatochromic behavior [105,106] or to modulate the fluorescence [107,108], is generally unfavorable because of the development of a charge transfer character.

For example, Kawai reported that the ring-closure quantum yield drastically diminished to 0.0083 by including a thienothiophene-imidazole fluorescent unit into a terarylene photochrome (Figure 34). [109]

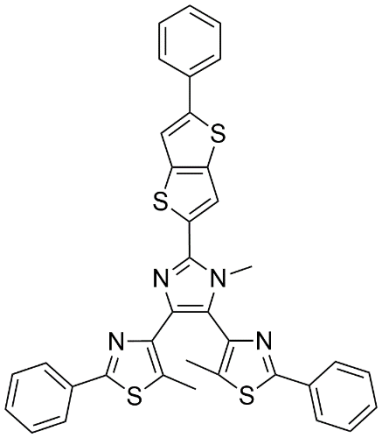

Figure 34: Investigated thienothiophene-imidazole-containing terarylene in ref. [109]

The generated push−pull system is in fact characterized by charge transfer states that are in competition with the cyclization. This was supported by TD-DFT calculations which showed that the S_1 excited state consisted in a HOMO → LUMO transition with a CT character. No distribution on the reactive carbons was observed in the LUMO, suggesting little (or absent) contribution to the photocyclization process.

Dithienylethene-based donor-π-acceptor photochromic dyes have been extensively investigated by Li and co-workers. [110–113] These systems showed a marked solvent-dependent photochromic behavior, due to their intramolecular charge transfer character affecting the photocyclization quantum yields. As an example, a decrease of $\Phi_{O\text{-}C}$ from 0.55 to 0.063 was registered for the carbazole−dithienylethene−difluoroboron β-diketonate system investigated in ref. [112] and depicted in Figure 35, when passing from a toluene to an acetone solution.

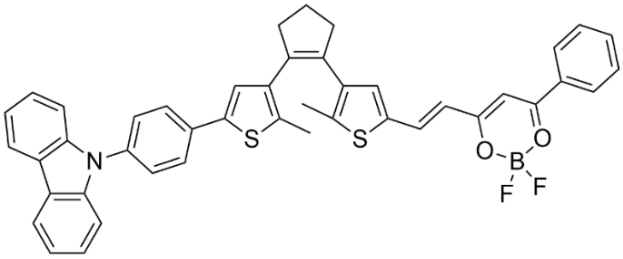

Figure 35: Investigated carbazole−dithienylethene−difluoroboron β-diketonate system in ref. [112]

TD-DFT calculations were carried out again to gain more insights into this behavior. As for the previously described case, an evident charge transfer was characterizing the lowest energy transition, with the HOMO on the arm containing the carbazole and the LUMO only on the other one, because of the electron-withdrawing effect of boron atom. This CT state is favored in polar solvents, thus affecting the efficiency of the photochromic reaction.

Similarly, Zhou and co-workers have proposed a study on donor-acceptor switches whose poor photochromic properties have been explained in terms of decreased Mulliken charge on the reactive carbons involved in the electrocyclization as a consequence of the charge transfer character. [114] Likewise, Jaung and co-workers have investigated diarylethenes bearing electron-

donating and electron-withdrawing groups, stating that the decrease of electron density on the reactive carbons was responsible for the low quantum yields. [115]

The presence of a CT character can also lead to a suppression of the photochromic activity in polar solvents, because of twisted intramolecular charge transfer (TICT). [116] The photochromic behavior of 1,2-bis(2,4,5-trimethylthiophene-3-yl)maleic anhydride depicted in Figure 36 has been described by Irie and Sayo. [117] The authors highlighted how the ring-closing quantum yield was decreased from 0.13 to 0.003 by passing from *n*-hexane to acetonitrile. The investigation about the impact of the solvent polarity on the isomerization (and on the fluorescence) of this derivative led to the identification of a TICT state. The stabilization of this state is favored in polar solvents (Figure 36).

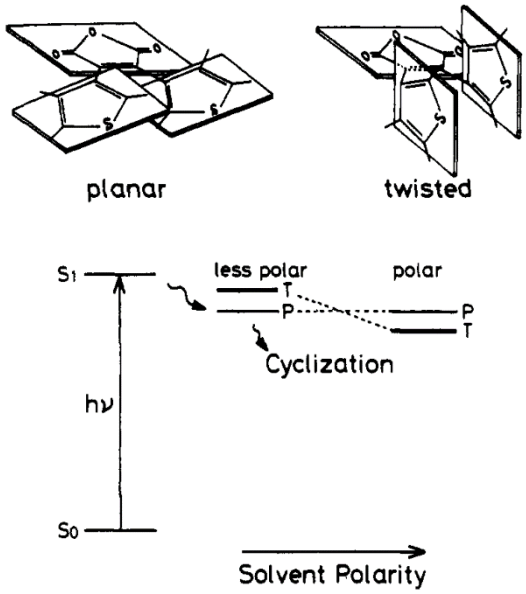

Figure 36: (top) Investigated 1,2-bis(2,4,5-trimethylthiophene-3-yl)maleic anhydride in the planar (P) and the twisted (T) geometries; (bottom) excited states' stability depending on the solvent polarity, as published in ref. [117]

The rotation around the single bonds of the central unit can lead to different conformations in the excited state. The planar conformation, being less polar than the twisted one, is favored in an apolar solvent such as hexane. The opposite occurs in the polar acetonitrile, where the twisted geometry is energetically more stable. This is detrimental towards the cyclization because the photochrome can't undergo the isomerization in this state and an energy barrier blocks the conversion to the reactive planar one. The molecule would consequently return to the ground state without forming the closed form isomer. The impact of TICT to explain a possible lack of reactivity has been invoked in other studies, too. [118]

1.3.2.2 Additional factors influencing $\Phi_{O\text{-}C}$

In 1998, Krischy and Martin reported a reduction of the efficiency of the ring-closing reaction with the increase of the delocalization over the π-conjugated chains in carotenoid-like diarylethenes. [119] The observed lowering of the photocyclization quantum yield in toluene (from 0.76 to 0.0053) was correlated to a decrease of the excitation density at the hexatriene unit involved in the photochromic reaction and to the shorter carotenoids' excited state lifetimes with the extension of the polyene chain.

Another possible functionalization capable to affect the quantum yield, but whose impact isn't always foreseeable, is the introduction of positive charges by pyridine N-methylation. [120,121] Irie reported in 2003 the synthesis and the characterization of two diarylethenes having a N-methylpyridinium cation only on one or on both the thiophene arms. The symmetric dicationic photochrome showed a surprisingly high photocyclization quantum yield, equal to 0.71, that was attributed to the Coulombic electrostatic repulsion between the arms favoring the adoption of the photoactive antiparallel conformation. On the contrary, the monocationic derivative showed a ring-closing quantum yield of 0.20, that was correlated to possible π-interactions between the phenyl ring of one arm and the pyridinium ring of the other one that would stabilize the inactive parallel conformer.

However, the effect of the quaternization of pyridines can't be easily predicted. In fact, our group has described the behavior of a similar diarylethene (Figure 37, where the photochromes investigated in ref. [120] are shown for comparison) whose photocyclization quantum yield was dramatically lowered by methylating the two pyridine rings, with a decrease from 0.77 to 0.08 in acetonitrile. [121]

.

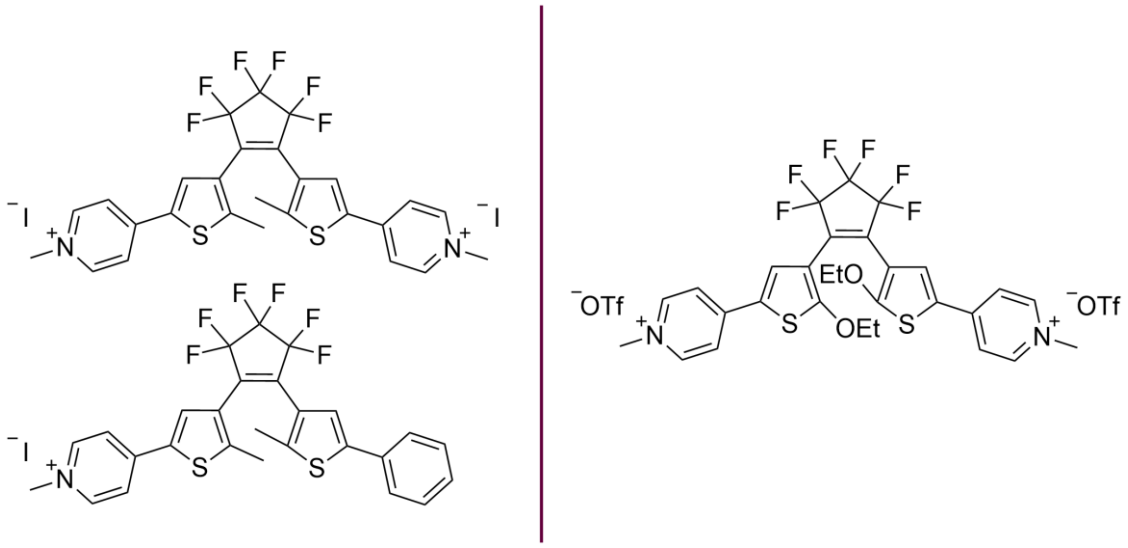

Figure 37: Comparison between (left) monocationic and dicationic DAEs investigated in ref. [120] and (right) dicationic DAE investigated by our group in ref. [121]

1.3.3 Cycloreversion quantum yield

Concerning the cycloreversion quantum yield, the values are generally smaller than those for $\Phi_{O\text{-}C}$ by two orders of magnitude, even if exceptions have been reported, depending on the functionalization of the investigated DAEs. [5,45] To rationalize this trend, the delocalization in the CF is generally invoked as cause, since it leads to a decrease of the anti-bonding nature in S_1 of the single C-C bond formed with the cyclization. [119,122]

The lower efficiency of the back-reaction is also correlated to the existence of an energy barrier in the excited state that must be overcome to reach the conical intersection allowing the return to the ground state following the ring-opening. Irie and co-workers provided a proof about this energy barrier by showing that the cycloreversion quantum yield is wavelength-dependent. [123] In fact, the authors observed that excitations at shorter wavelengths (i.e. at higher energies) could impart an excess of vibrational energy to the molecules, thus enhancing the exceeding of the barrier.

Moreover, the cycloreversion quantum yield is temperature-dependent as demonstrated by Ishibashi and Irie by femtosecond laser photolysis. [124] A rise in temperature is in fact accompanied by an increase of the efficiency of the ring-opening process. This study was repeated in 2020 by Bragg and co-workers, who analyzed the three photochromes depicted in Figure 38, where the linear relation correlating $\Phi_{C\text{-}O}$ and temperature is also provided. [125]

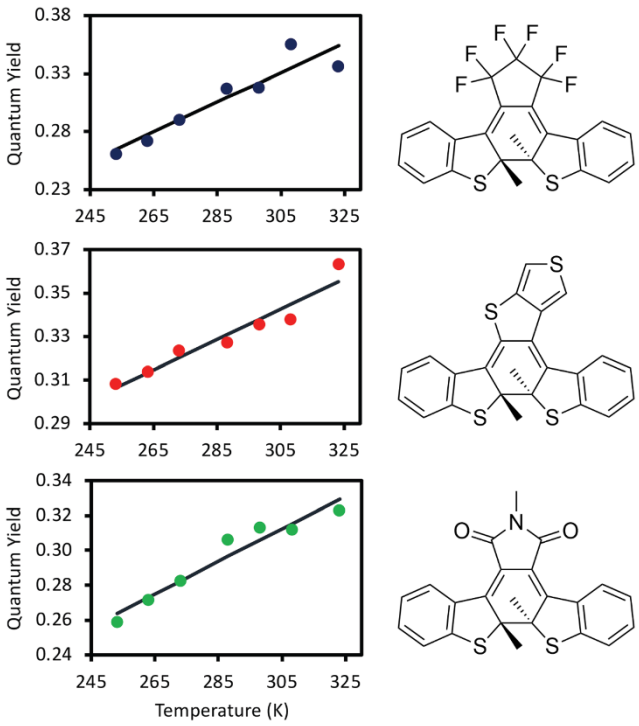

Figure 38: (left) $\Phi_{C\text{-}O}$ variation with temperature rising from 253 to 323 K in acetonitrile, as shown in ref. [125]; (right) structures of the analyzed CF isomers.

1.4 Dual-mode diarylethenes

This section aims to describe DAEs showing *"dual-mode-responsive"* behavior, meaning that the cyclization and/or the cycloreversion can be induced with a stimulus different from light.

For example, acid/base photochromism has been reported for the first time by Liebeskind and Deng in 2001: the authors showed that the ring-closing reaction could be induced by strong Lewis acid or protic ones in quinone-bridged photochromes. [126] Extensive study on this subject have been carried out by Kawai's group [127,128] and several examples have been summarized by Pu and co-workers in their review published in 2016. [129]

However, the focus here will be on redox-active diarylethenes and their isomerization.

1.4.1 Electrochromism of redox-active diarylethenes

Switchable units such as diarylethenes are appealing in the perspective of developing multifunctional materials, whose macroscopic behavior is controlled by the isomerization of the molecular unit under an external input. An interesting characteristic of these photochromic derivatives is that an electrochemical stimulus can be used in place of the photochemical one, thus allowing the isomerization from the OF to the CF (or vice versa), but through a different mechanism from the photoinduced 6π-electrocyclization. The majority of the works available in the literature is based on molecules showing either oxidative ring-opening or oxidative ring-closing reactions, but reductive cyclization has been reported too.

1.4.1.1 Oxidative cycloreversion

The first example of a DAE system showing redox switching in addition to the photoinduced one was reported by Kawai and co-workers in 1995. By investigating the *cis*-1,2-dicyano-1,2-bis(2,4,5-trimethyl-3-thienyl)ethene shown in Figure 39, the authors observed that the cycloreversion could be achieved by oxidizing the CF. [130]

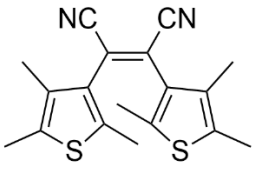

Figure 39: *cis*-1,2-dicyano-1,2-bis(2,4,5-trimethyl-3-thienyl)ethane described in ref. [130]

The authors proposed a chain reaction mechanism to explain this phenomenon: the oxidation of the neutral CF led to an instable radical, $CF^{+\cdot}$, that would spontaneously re-open to afford the open form radical $OF^{+\cdot}$. If this radical is an oxidant strong enough to oxidize the neutral closed form, a radical that can undergo the same reaction again would be generated while obtaining the neutral OF.

A similar effect was reported by Peters and Branda on the photochrome depicted in Figure 40 [131] and by Irie and co-workers [132] on a benzothiophene- and 1-methylindole-containing dissymmetric DAE.

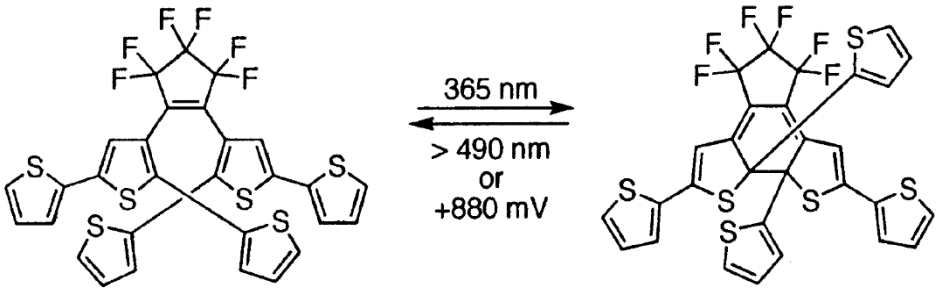

Figure 40: 1,2-bis(5′,2′-di(thiophen-2-yl)thien-3′-yl)perfluorocyclopentene photochromic and redox-active behavior described in ref. [131]

A total conversion to the open form as a consequence of the oxidation of the closed form was detected. Moreover, the process appeared to be catalytic and the oxidation of a small fraction of CF was enough to start the chain reaction that led to the cycloreversion.

In Irie's work, the cycloreversion could also be induced with 0.1 eq of $FeCl_3$. The possibility of not respecting the stoichiometry between substrate and oxidant was in accordance with the process being catalytic.

In a similar fashion, Kawai et *al*. showed that the catalytic ring-opening occurs also on the terarylene in Figure 41 and in-depth investigated the mechanism by combining cyclic voltammetry, stopped-flow measurements, spectroelectrochemistry and theoretical modelling. [133]

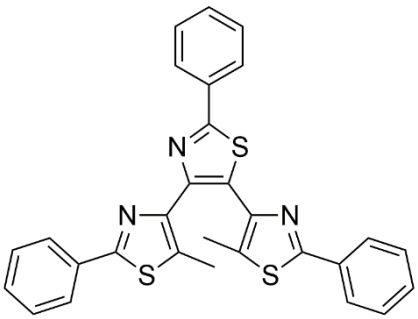

Figure 41: Terarylene undergoing oxidative cycloreversion investigated in ref. [133]

The catalytic nature of the process was clearly recognized by comparing the moles of converted CF and the quantity of used electricity. In fact, 6.7×10^{-8} mol of substrate needed only 7.4×10^{-9} mol·electron to complete the cycloreversion. The authors proposed the cascade reaction in Figure 42 as possible reaction mechanism. Moreover, the same efficient cycloreversion could be achieved by using a sufficiently strong chemical oxidant.

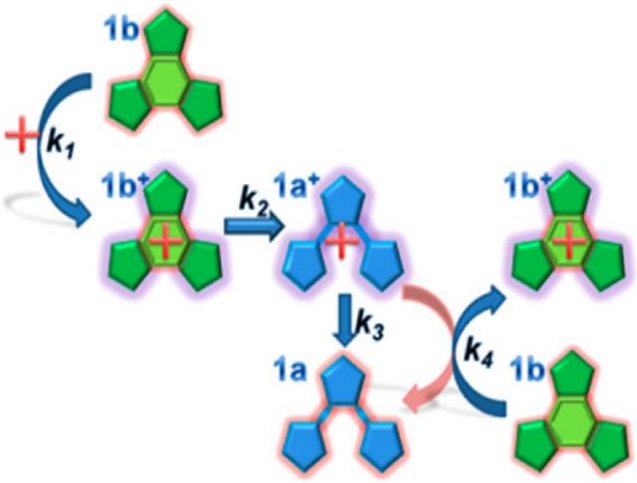

Figure 42: Chain reaction model proposed and published in ref. [133], where 1b: CF; $1b^+$: CF^+; 1a: OF and $1a^+$: OF^+.

This oxidation-induced cycloreversion was further investigated by the same group and a study showing a remarkable improvement was published in 2016. [134] In particular, by replacing the methyl groups on the reactive carbons of the molecule previously shown in Figure 41 with two phenyl rings, the net ring-opening rate was increased by up to 1300-fold and the efficiency appeared to be 100000% with respect to the oxidant. This improvement was due to the enhanced stabilization of $OF^{+\cdot}$ thanks to the presence of the phenyl groups with consequent acceleration of the isomerization of $CF^{+\cdot}$.

1.4.1.2 Oxidative cyclization

Several groups have reported the possibility of inducing the cyclization of the open form by oxidizing it. For example, Branda' group published in 2003 a study about the dithienylethene presented in Figure 43, whose ring-closing reaction could be performed electrochemically. [135]

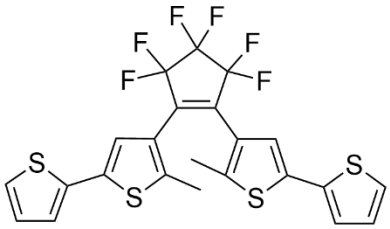

Figure 43: Investigated DAE in ref. [135], whose cyclization is also oxidation-induced.

The authors observed by cyclic voltammetry that the oxidation of the closed form couldn't cause the cycloreversion. The redox wave for the CF appeared to be actually reversible. The oxidation of the OF was instead an irreversible process that interestingly led to the appearance of a reduction wave coincident with that for the CF radical. Multiple CV cycles on the open form showed that this wave was exactly that of the closed-ring isomer. It was consequently concluded that the oxidation of the OF could induce the cyclization. The voltammograms are shown in Figure 44 for clarity.

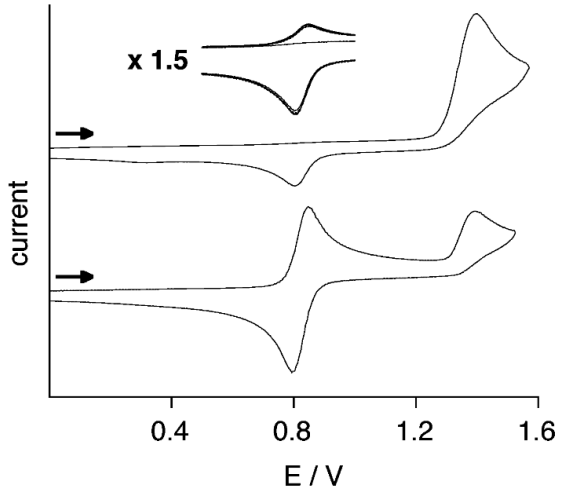

Figure 44: (top) CV of the OF in CH_3CN / 0.1 M NBu_4PF_6. The inset shows the effect of 5 cycles; (bottom) CV of the CF. ν = 200 mV/s. As published in ref. [135]

Two years later, extensive studies on the oxidative cyclization of DAEs functionalized either with electron-donating or electron-withdrawing groups have been published by Coudret, Launay et *al.* [136] and by Feringa and co-workers. [137,138] Both the contributions showed that the presence of electron donors favored the ring-closure of the switches.

Furthermore, the investigation conducted by Feringa's group on the molecules depicted in Figure 45 highlighted that the nature of the central core unit had a significant impact on the redox properties of the photochromes.

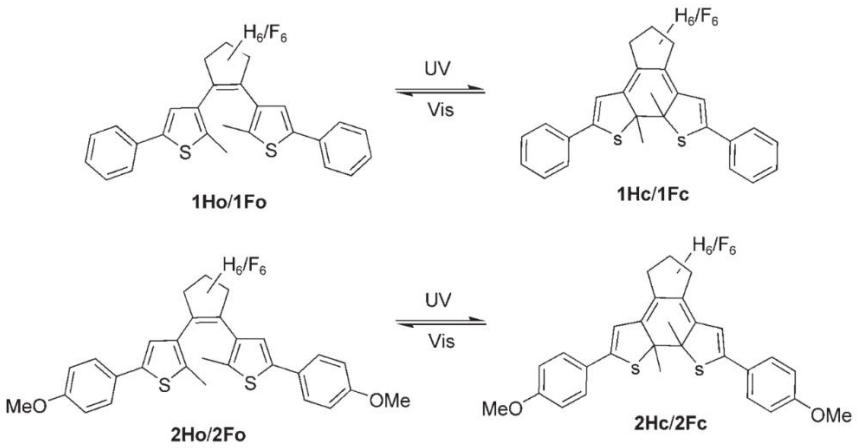

Figure 45: Dithienylethenes investigated in ref. [137], reproduced from the publication.

The cyclopentene and the hexafluoropentene bridges have in fact opposite electronic properties, being the former electron-donating and the latter electron-withdrawing. This structural modification was enough to neglect the oxidative cyclization of 1F, contrarily to what observed for its analogue 1H.

Similar trends about the redox-active behavior of a large family of dithienylethenes bearing donor or acceptor groups have been reported also by Hecht and co-workers. [139] Interestingly,

in the case of the dissymmetric derivative depicted in Figure 46, the two arms were oxidized at different potentials and the ring-closure couldn't be observed if the oxidation was stopped at the first wave, thus suggesting a cyclization in the dicationic state. When electron-withdrawing groups were introduced, no oxidative ring-closing reaction happened. Last, hexafluorocyclopentene-based molecules could show the redox-driven process only if bearing strong donors.

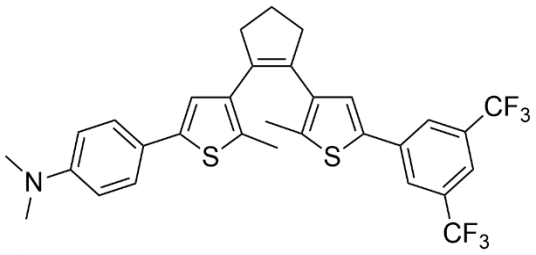

Figure 46: Dissymmetric redox-active DTE investigated in ref. [139]

All the described studies have been carried out exclusively on dithienylethenes. Only one paper reports the possibility of oxidatively ring-close a thiazole-based switch. [118] The difficulty in observing this redox-driven phenomenon when thiophene rings are replaced by thiazoles can be ascribed to the electron-poorer nature of the nitrogen-containing heterocycle. The N atom attracts the electron density from the double bonds, thus making the ring electron-deficient. Very strong electron-donating groups such as morpholine are then needed (Figure 47).

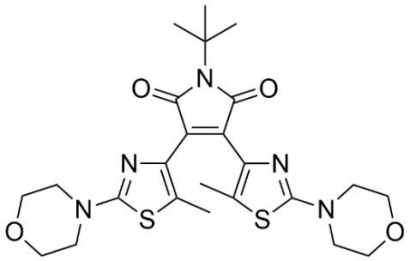

Figure 47: Morpholino-containing dithiazolylethene investigated in ref. [118]

Furthermore, the presence of the electron-withdrawing maleimide bridge inhibits the photochemical cyclization (the authors consider the possibility of TICT – described in Section 1.3.1.3 – preventing the ring-closure), thus making the formation of the CF possible only by electrochemical input. On the contrary, the ring-opening occurs only by light irradiation.

As it can be noticed, the behavior of these derivatives has been extensively studied in solution. However, several works are available in the literature to illustrate applications of this oxidative cyclization in solid state, involving redox active polymers [140] or modified electrodes for information storage. [141] Functionalized electrodes with a DTE-based layer can also be used in molecular junctions, but in this case light is used to switch the molecules and modulate the passage of current. [142–144]

1.4.1.3 Reductive cyclization

Even if it is more scarcely reported than the oxidative cyclization, also the reductive ring-closing reaction is feasible in certain diarylethene derivatives.

Proper functionalization with strong electron-withdrawing groups is needed to observe this phenomenon, so to have the reduction of the OF at accessible potentials in the electrochemical windows that are generally available with commonly used combinations of solvents and electrolytes. Not all the electron acceptor groups are capable of inducing the ring-closure reaction [145], but it has been reported in presence of N-methylated pyridines [121,146,147] and benzonitriles. [148] Interestingly, also open forms having an extended π system can show this type of redox-active behavior. [148]

The first example of a photochromic DTE capable to undergo reductive ring-closing has been published by Branda and co-workers in 2004. [146] The bis-N-methylpyridinium-containing molecule shown on the left in Figure 48, whose synthesis had already been carried out by Lehn's group previously [149], could be irreversibly reduced consuming one electron. As a consequence of this reduction, the generated radical $OF^{+\cdot}$ spontaneously isomerized to $CF^{+\cdot}$, that was finally oxidized to the dication CF (i.e. the same species that could be photochemically generated).

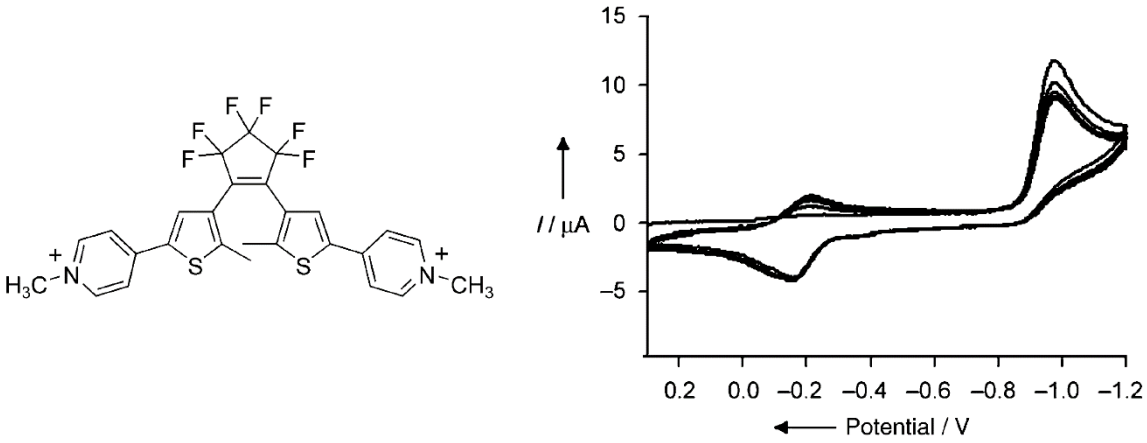

Figure 48: (left) dicationic DTE undergoing reductive cyclization, (right) cyclic voltammograms in DMF / 0.1 M tetrabutylammonium perchlorate; ν = 200 mV/s. Adapted from ref. [146]

Our group has studied an analogue dicationic dithiazolylethene, which could show the reductive cyclization, but, interestingly occurring through a different, bielectronic mechanism. [121]

By exploiting the presence of N-methylpyridinium units appended to the thiophene rings, Royal and co-workers have recently shown that this redox-active behavior can be observed even in a dithienylethene derivative having a phenantrene bridging unit. [150]

However, this kind of redox-driven isomerization has been reported also for systems that do not contain this functionalization. In fact, Hecht and co-workers have shown that the stiff DAE in Figure 49 (as well as a similarly functionalized "classical" DAE with a cyclopentene bridge [138]) could be reductively ring-closed thanks to the presence of the -CN groups. [148] The so-called stiff diarylethenes are a sub-class of this photochromic family in which the bridging cyclic ring has been replaced by an exocyclic double bond. The presence of this unit adds an *E/Z* isomerization to the OF/CF one.

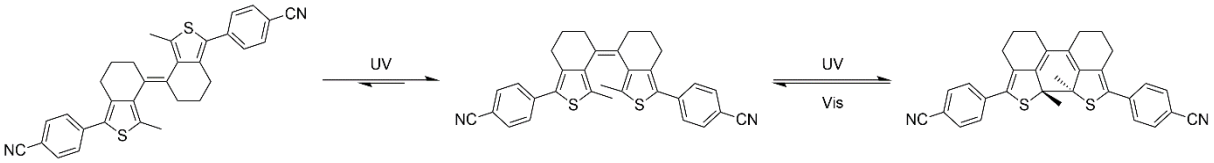

Figure 49: Stiff DAE investigated in ref. [148], showing a *E/Z* isomerization around the exocyclic double bond and the typical OF/CF isomerization for diarylethene derivatives.

Remarkably, while the reduction of the *Z*-isomer was irreversible and induced the reductive cyclization, it was reversible in the *E*-isomer and no ring-closure was detected. On the contrary, the oxidative cyclization that could also occur on the open form worked for both the isomers.

The authors have shown that the introduction of groups allowing large delocalization could allow the reductive ring-closing reaction, too.

1.4.1.4 Electrofluorochromism

As previously put in evidence for the photochromic reaction (Section 1.1), also the redox-active behavior allows to modulate properties such as the fluorescence emission. The tuning of fluorescence exerted through redox stimuli is defined as "electrofluorochromism" and it is an appealing phenomenon for applications in devices like sensors and in optoelectronics. [151–153]

For example, Rigaut, Norel and co-workers described in 2019 a multifunctional system that offered dual control (light-based and redox-based) over the luminescence of an ytterbium ion thanks to the co-existence of a photoswitchable DAE unit and a redox-active ruthenium-containing moiety, as depicted in Figure 50. [154]

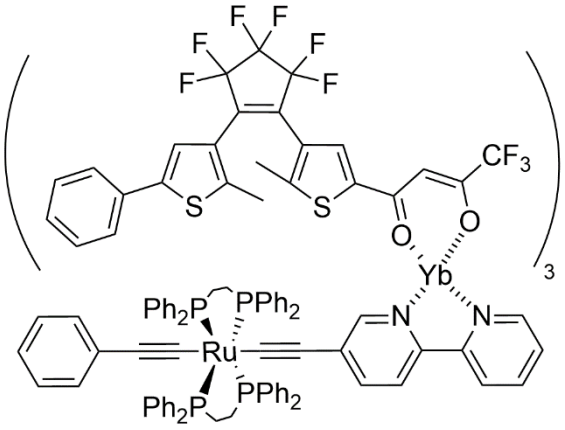

Figure 50: Multifunctional hybrid system investigated in ref. [154]

The emission of the lanthanide ion could be quenched not only by switching the DTE to its closed form thanks to UV irradiation, but also by oxidizing the ruthenium center.

Such a dual-mode control makes electrofluorochromism an appealing phenomenon to be investigated in intrinsically fluorescent redox-active photochromes.

Nicolò Baggi

Chapter 2: Modulation of the photocyclization quantum yield

Nicolò Baggi

2.1 Aim of the study

As introduced in Chapter 1, Section 1.3.1.3, quantum yield is one of the most important parameters to take into account when looking at the performances of a photochrome. Consequently, the ability to know how to control it is highly desired.

Plenty of works have been carried out over the years to understand the parameters affecting the ring-closing quantum yield so to be able to tune it. Most of these studies have been dedicated to increase the antiparallel conformer percentage through intramolecular interactions or steric hindrance in order to improve the $\Phi_{O\text{-}C}$. In fact, it is reasonable to expect an increment of the quantum yield if the percentage of species that can undergo the photoreaction is increased.

By introducing donor and acceptor groups, a detrimental effect has been generally observed instead. Nevertheless, the impact of the presence of these groups and the consequent charge-transfer character on $\Phi_{O\text{-}C}$ has not been rationalized in the studies available in the literature, to the best of our knowledge. This means that a model suggesting how to tune the photocyclization quantum by introduction of electron-donating and electron-withdrawing groups is yet to be proposed.

A family of eight terthiazoles having the same terphenylthiazole skeleton to make the comparison meaningful has been synthesized and fully investigated (Figure 51) in the perspective of developing a method permitting to correlate the photocyclization quantum yield to the CT character, so to have a modulation guideline on the expectable photochromic performances of functionalized diarylethenes and terarylenes.

In addition to the known unsubstituted switch **1** [77] and the anisole-containing photochrome **2** [155], six novel appropriately functionalized molecules have been included to cover a wide range of charge transfer character, expecting to achieve progressively smaller ring-closing quantum yields.

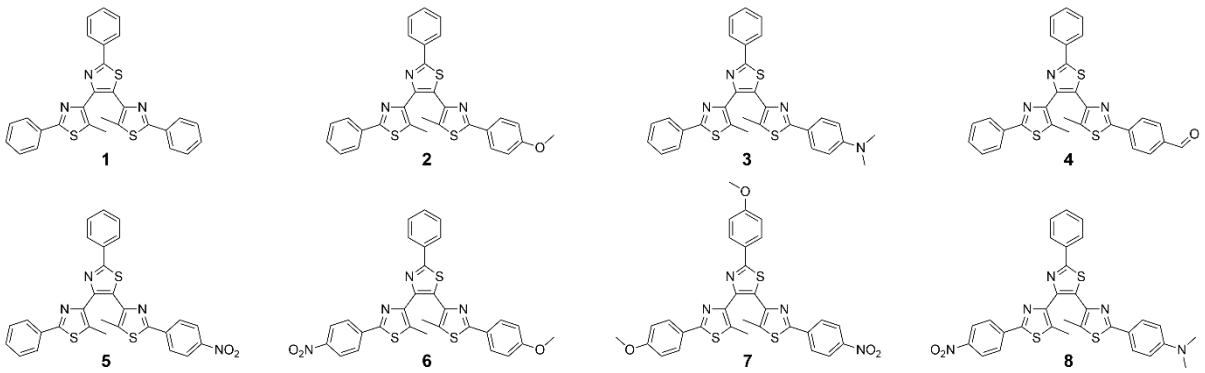

Figure 51: Investigated family of terarylenes showing progressively increasing charge transfer character.

2.2 Synthesis and characterizations

2.2.1 Synthesis route

The eight derivatives could be obtained through a multi-step synthesis that offers large flexibility. Thiazoles have been chosen as heterocycles to build the switches because of their easy synthetic access, as shown in the first steps depicted in Figure 52.

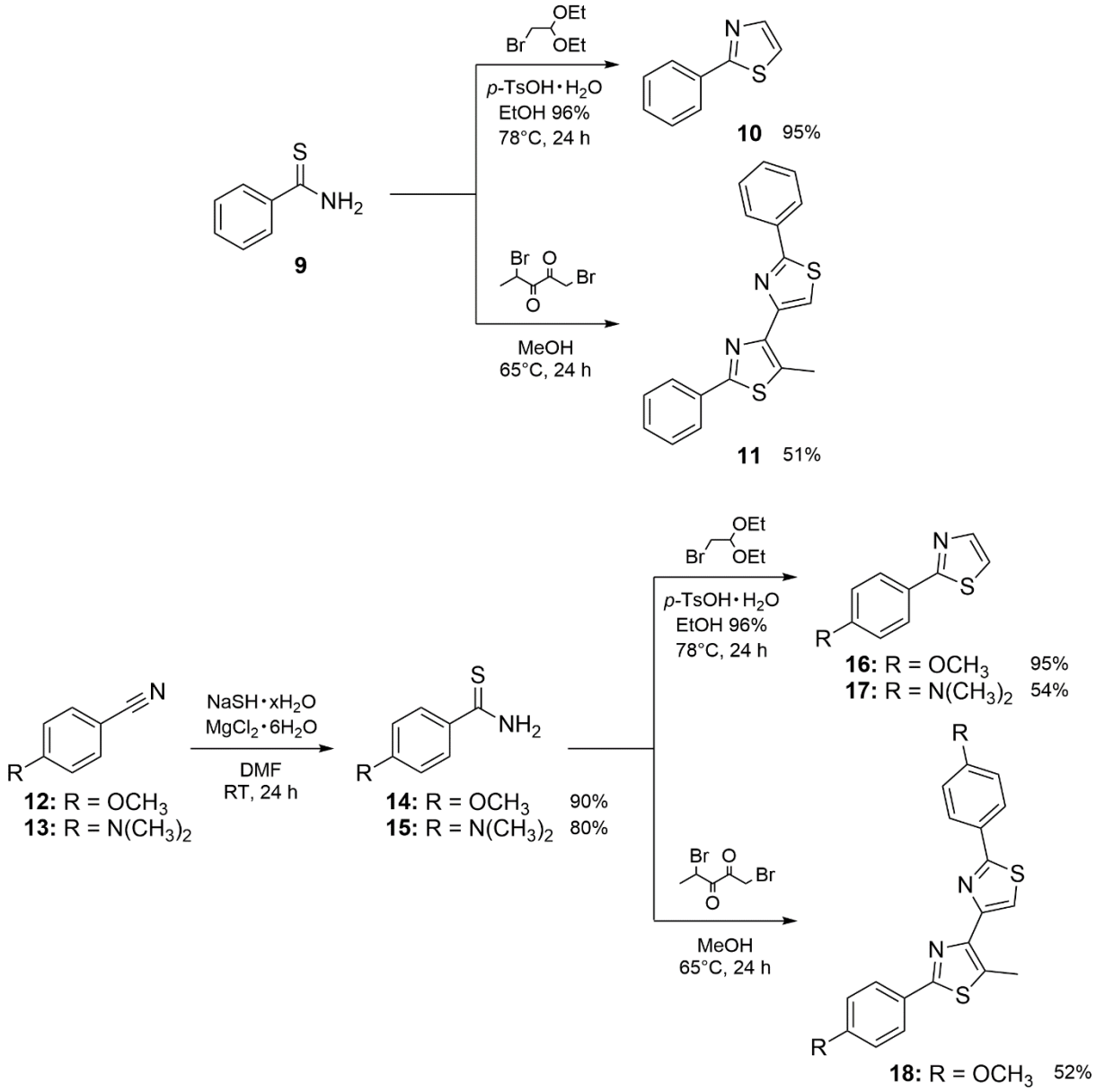

Figure 52: Synthesis route to intermediates **10**, **11**, **16**, **17** and **18**.

Thiazole **10** and bithiazole **11** have been obtained from the commercially available benzothioamide (**9**) by Hantzsch reaction. [156,157] In the cases of 2-(4-functionalized-phenyl)-thiazoles **16** and **17** and bithiazole **18**, the needed thioamides have been prepared from the respective benzonitriles by following the procedure proposed by Manaka and Sato. [158]

The heterocycles **10**, **16** and **17** have been brominated with N-bromosuccinimide (NBS) in DMF before being used in Halogen Dance reactions [159] to afford the last intermediates **22**, **23** and **24**, required for the synthesis of terthiazoles **1**,**2** and **3** (Figure 53).

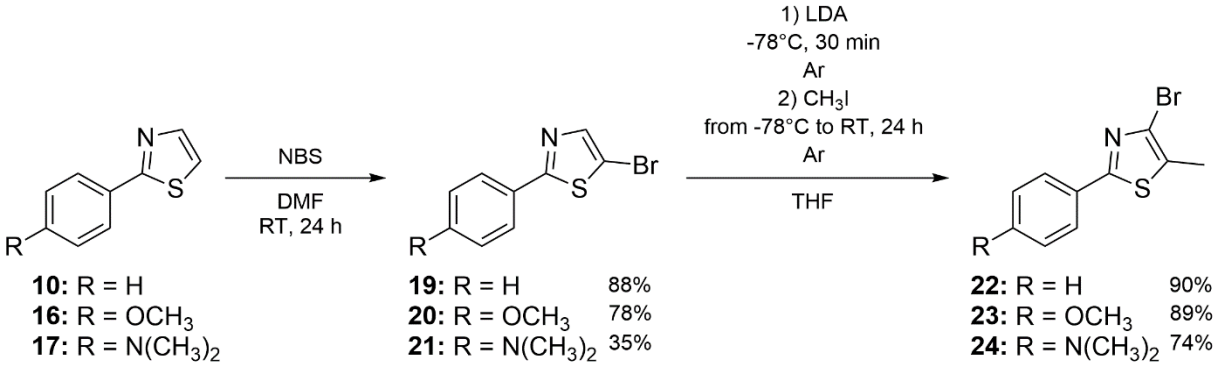

Figure 53: Synthesis route to intermediates **10** and **11**.

Halogen Dance reaction is an intermolecular reaction that allows to "move" the Br atom from C_5 to C_4 in the used thiazoles in presence of a strong base such as lithium diisopropylamide (LDA) and to introduce an electrophile (as $–CH_3$ from iodomethane) in the newly available position 5.

Photochromes **1**,**2** and **3** have been finally obtained by C-H direct arylation [160–163] of bithiazole **11** with **22**, **23** and **24** (Figure 54). This cross-coupling reaction allowed to skip additional steps like the preparation of the organoboron derivatives of the 2-(4-functionalized-phenyl)-4-bromo-5-methyl-thiazoles and the synthesis of the brominated bithiazole, substrates that could have been used in a Suzuki-Miyaura coupling to afford the desired terarylenes (procedure used for the synthesis of **2** in ref. [155] described this route).

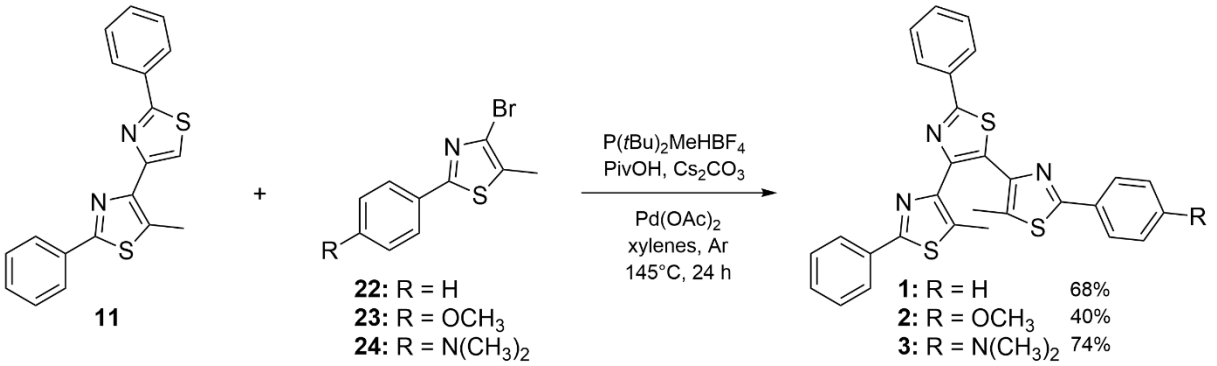

Figure 54: Synthesis route to terarylenes **1**, **2** and **3**.

As it can be seen, this cross-coupling reaction is Pd-catalyzed in the presence of a phosphine as di-tert-butyl(methyl)phosphonium tetrafluoroborate, a base as cesium carbonate (Cs_2CO_3) and pivalic acid (PivOH). [163,164]

In order to obtain the photochrome **4**, 2-(4-formyl-phenyl)-4-bromo-5-methyl-thiazole (**25**) has been synthesized through the Suzuki-Miyaura reaction in Strotman conditions [165] shown in Figure 55 and then used with **11** in the C-H direct arylation coupling.

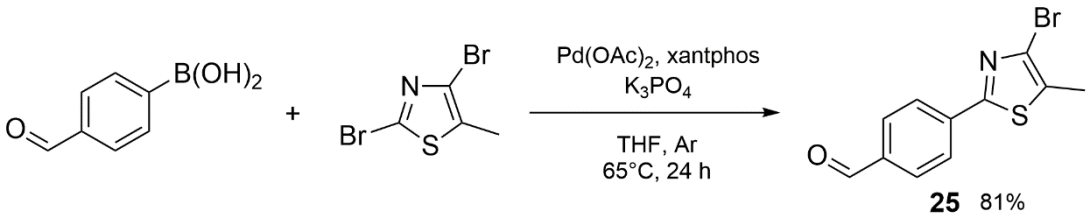

Figure 55: Synthesis of the intermediate **25**.

To prepare the remaining four terthiazoles, 2-(4-nitro-phenyl)-4-bromo-5-methyl-thiazole (**26**) was the required intermediate. It has been obtained by treating the substrate **22** with potassium nitrate (KNO_3) in sulfuric acid (H_2SO_4), as depicted in Figure 56.

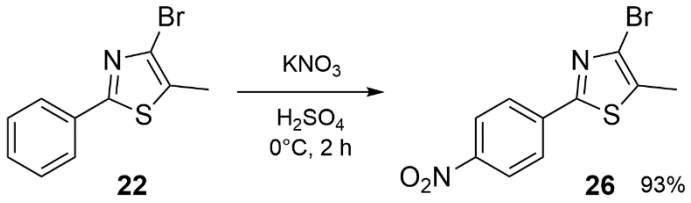

Figure 56: Synthesis of the intermediate **26**.

Again, direct arylation of **11** and **18** with **26** allowed to synthesize terarylenes **5** and **7**, respectively.

The route to obtain the two remaining photochromes (i.e. **6** and **8**) required additional steps for the preparation of 5-methyl-2-(4-nitrophenyl)-2'-phenyl-4,4'-bithiazole (**29**) to be finally reacted with **23** and **24**.

Halogen dance has been carried out on **19** but with MeOH as source of the electrophile, so to have Br in C_4 and a proton in C_5 of the thiazyl ring. The obtained substrate (**27**) has been used to prepare the boronic acid pinacol ester **28** that eventually afforded the desired bithiazole (**29**) through Suzuki-Miyaura cross-coupling with **26**. All the reactions are depicted in Figure 57.

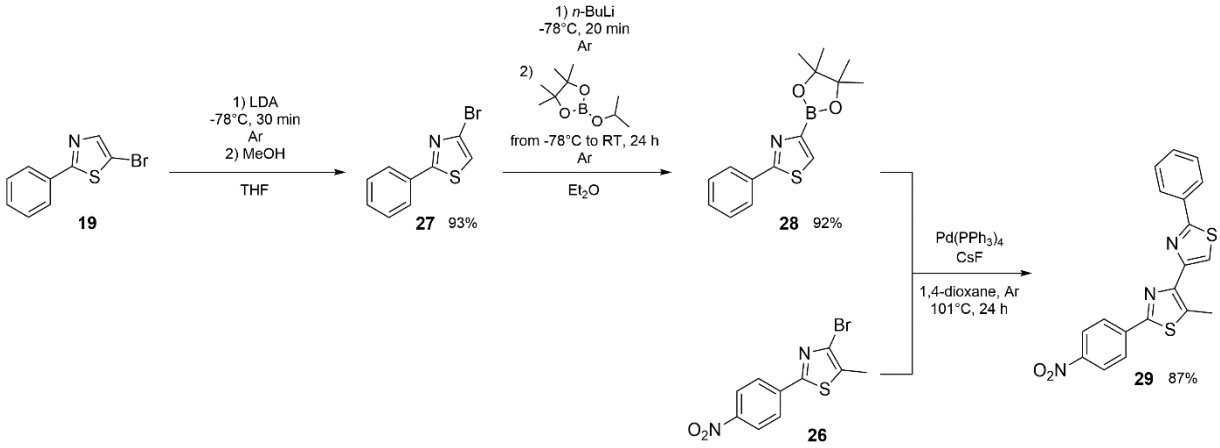

Figure 57: Synthesis route to intermediate **29**.

2.2.2 Photochemical behavior

2.2.2.1 Stationary UV-vis spectroscopy

The eight switches have been investigated in acetonitrile at room temperature. The solutions haven't been degassed unless stated otherwise. The spectra of the OFs are indicated with black solid lines while the photostationary states reached under UV light irradiation (320 nm for compounds **1**-**7** and 340 nm for **8**) are in blue (Figure 58).

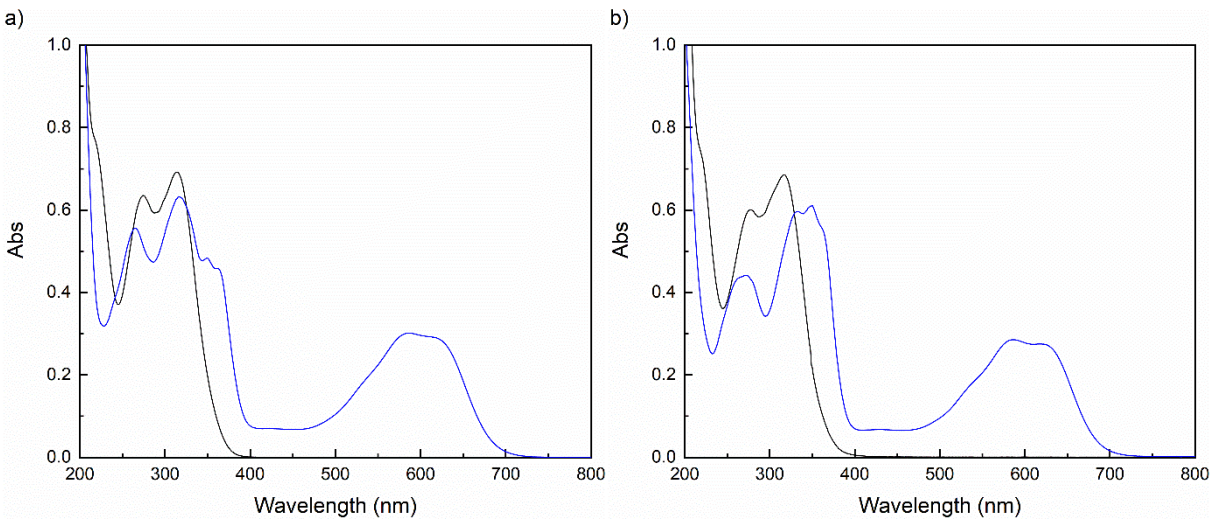

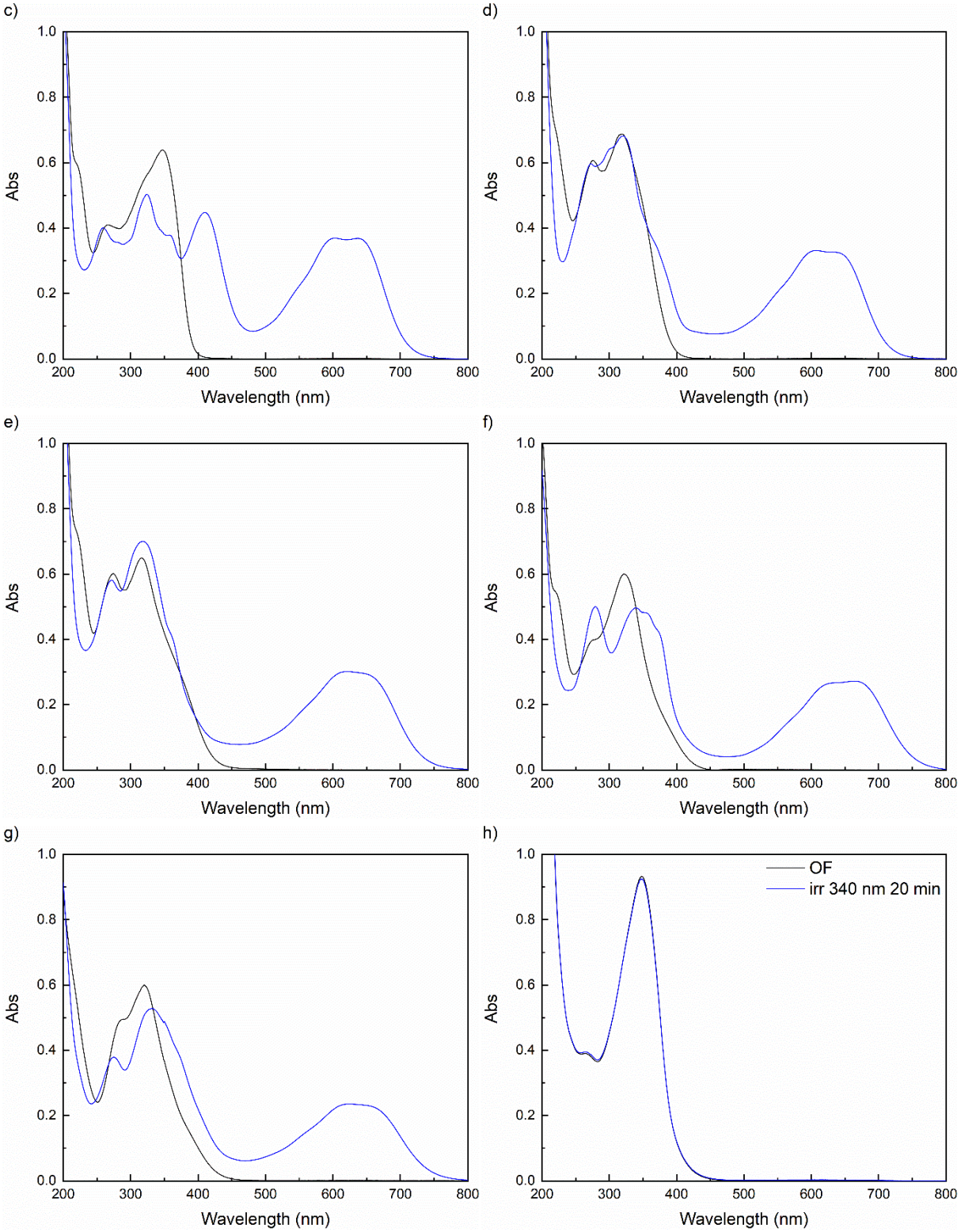

Figure 58: Absorption spectra in acetonitrile of (a) **1** (2.39 x 10^{-5} M), (b) **2** (1.85 x 10^{-5} M), (c) **3** (1.76 x 10^{-5} M), (d) **4** (2.13 x 10^{-5} M), (e) **5** (2.41 x 10^{-5} M), (f) **6** (1.60 x 10^{-5} M), (g) **7** (1.70 x 10^{-5} M) and (h) **8** (2.15 x 10^{-5} M), showing the evolution under UV light irradiation (at 320 nm for **1**-**7**, at 340 nm for **8**) from the black lines for the OFs to the blue lines to indicate the respective photostationary states. Optical path of the cuvette: 1 cm.

As it can be observed in the figure above, all the terthiazoles in their open forms absorb in the UV region, with intense absorption bands between 300 and 350 nm. By irradiating the

colorless solutions in acetonitrile with UV light, the closed form isomers (that are thermally stable at room temperature) are generated, as it is confirmed by the growth of broad absorption bands with maxima between 600 and 700 nm. This is not observed for **8**, that is the molecule bearing nitro and dimethylamino groups and consequently possessing the most pronounced charge transfer character among the considered terarylenes. The fact that this molecule isn't photochromic in a polar solvent such as acetonitrile is not unexpected and less polar solvents are needed to investigate its switching behavior, like toluene (Figure 59). In fact, similar behavior has been reported for a D-A type dithienylethene showing solvatochromism and gated photochromism. [111] Nevertheless, the molecule remains poorly photochromic and long irradiation times are needed to reach the PSS. This became a limitation that hindered the determination of the photocyclization quantum yield in this solvent.

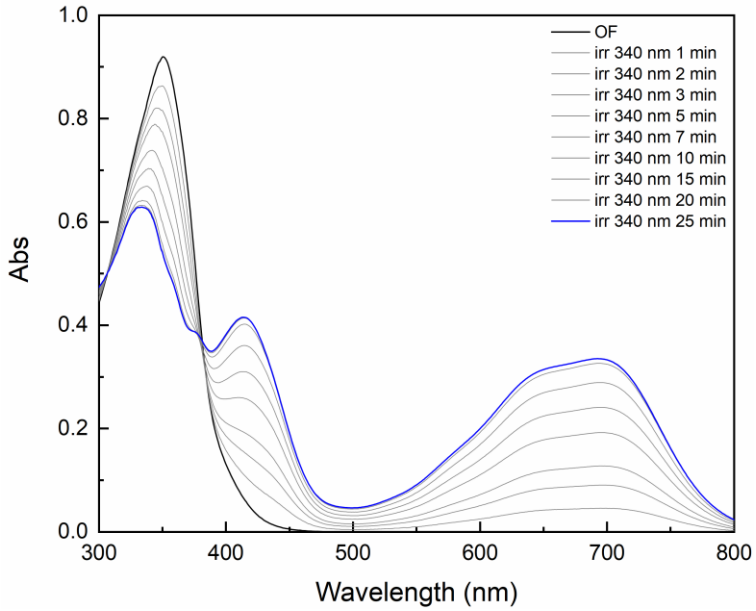

Figure 59: Photochromic behavior of **8** (2.04 x 10^{-5} M) in toluene. The spectrum of the OF is shown with a black solid line while the PSS is indicated in blue. The solution has been irradiated at 340 nm. Optical path of the cuvette: 1 cm.

2.2.2.2 Determination of the photocyclization quantum yields

A continuous photolysis experiment has been conducted at ENS Paris-Saclay on the seven derivatives that have shown the isomerization in acetonitrile to determine the values of their photocyclization quantum yields. For each photochrome, a solution in CH_3CN has been irradiated at 335 nm to promote the ring-closing reaction until the obtainment of the photostationary state. By plotting the absorption variation against the time of the experiment, it is possible to observe the kinetic profile of the photocyclization in the applied conditions at the chosen observation wavelength. The kinetic profile for the UV light-induced isomerization of terarylene **5** is provided as example in Figure 60, with the fit to the experimental data shown with a red solid line. The other profiles are provided in the Annexes (Page 245).

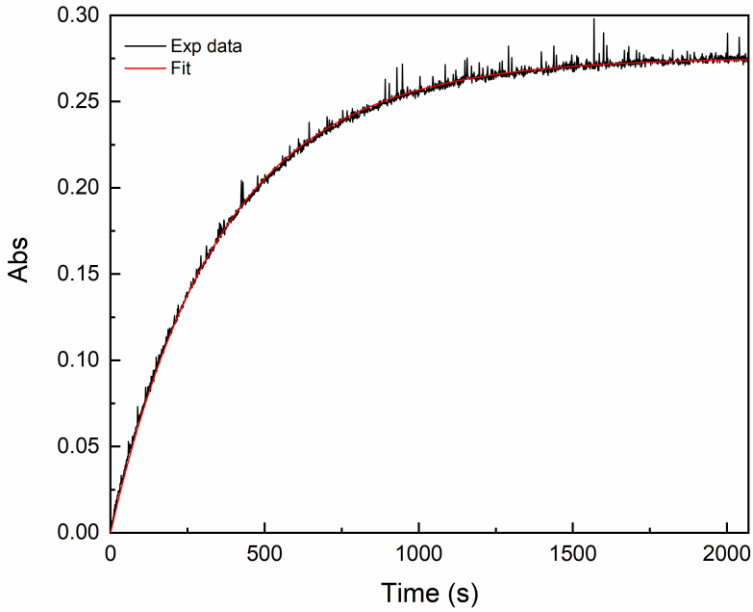

Figure 60: Kinetic profile for the photocyclization of **5** in acetonitrile under irradiation at 335 nm. Observation wavelength: 625 nm. Red line: fit.

To actually obtain the value of the constant describing the efficiency of the process, it is necessary to fit the experimental data taking into account several parameters, such as the power of the lamp used for the irradiation, the number of moles of photochrome in the irradiated solution and the molar absorption coefficients (ε) of the derivative in its OF and CF.

While ε_{OF} is easily accessible, the determination of the molar absorption coefficient for the closed-ring isomer requires either the separation of the pure species (e.g. by HPLC) or the application of extrapolation methods based on the combination of stationary UV-vis and ^{1}H-NMR spectroscopies.

The latter route has been employed to determine ε_{CF}. A solution of the analyzed photochrome in deuterated acetonitrile (CD_3CN) has been irradiated with UV light to obtain a state containing at least more the 20% of CF. The percentage of closed form isomer has been determined by doing the ratio of the integrals of the signals for the OF and the CF in the proton NMR spectrum (α_{CF} should be >20% to have reliable integrations). Then, the solution has been diluted to record the corresponding absorption spectrum. By irradiating the solution with visible light, the open form has been completely restored and since ε_{OF} was known, the total concentration has been calculated by applying the Beer-Lambert law.

Once the concentration has been determined, ε_{OF} and ε_{PSS} at every wavelength could be obtained and used in the following formula to finally extrapolate the molar absorption coefficient of the pure closed form:

$$\varepsilon_{CF} = \frac{\varepsilon_{PSS} - (1 - \alpha_{CF})\varepsilon_{OF}}{\alpha_{CF}}$$

Where ε_{CF}, ε_{OF} and ε_{PSS} are the molar absorption coefficients of the CF, the OF and the specific state reached under UV light irradiation, respectively. α_{CF} is the percentage of closed form in that photogenerated state and, as said, it is determined by NMR spectroscopy.

Eventually, the absorption spectra below have been obtained for photochrome **5** (Figure 61).

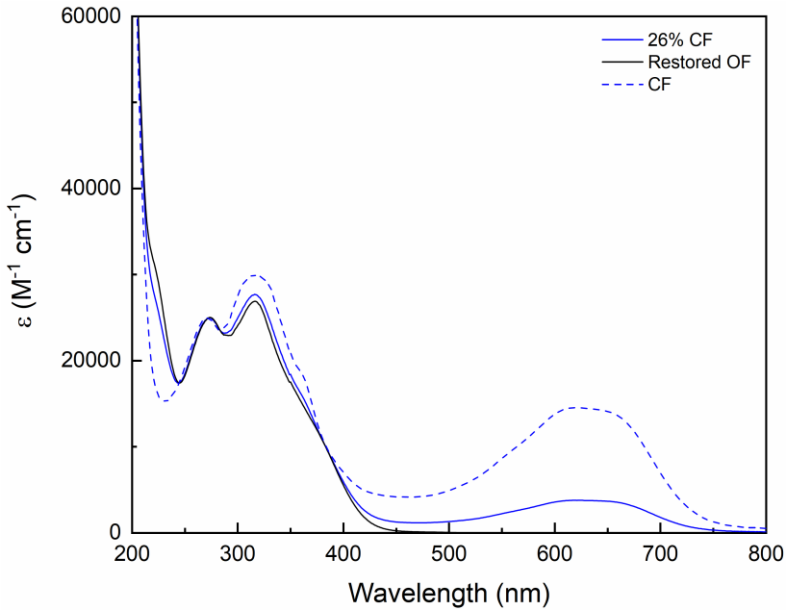

Figure 61: Extrapolation of the absorption spectrum of the pure CF (blue dashed line) of **5** in acetonitrile by combination of UV-vis and NMR spectroscopy. Restored OF's spectrum in black solid line; PPS spectrum for α_{CF} = 26% in solid blue line. Optical path of the cuvette: 1 mm.

All these parameters finally allowed to determine the value of $\Phi_{O\text{-}C}$ (and $\Phi_{C\text{-}O}$, too) for **5** thanks to the fit of the kinetic profile, based on the following formula that takes into account also the absorption of the CF at the chosen irradiation wavelength:

$$\frac{d[\mathbf{5}_{OF}]}{dt} = -\frac{\Phi_{O-C} \cdot I \cdot \beta_{\mathbf{5}_{OF}}(t)}{N_A \cdot V} + \frac{\Phi_{C-O} \cdot I \cdot \beta_{\mathbf{5}_{CF}}(t)}{N_A \cdot V}$$

Where $\Phi_{O\text{-}C}$ and $\Phi_{C\text{-}O}$ are photochrome **5**'s photocyclization and cycloreversion quantum yields; I is the photon flux, which depends on the power of the irradiation lamp; $\beta_{\mathbf{5}_{OF}}$ and $\beta_{\mathbf{5}_{CF}}$ are the fractions of photons absorbed by the OF and the CF during the irradiation time (this are the factors taking into account ε_{OF} and ε_{CF}); N_A is Avogadro's number and V is the volume of the sample.

The formula has been adapted from that presented by Stranius and Börjesson in their study about the determination of quantum yields of photochromes either in solution or in the solid state. [166]

The same analysis has been conducted on the other derivatives and the spectroscopic data for the whole family of terthiazoles are listed in Table 1.

Table 1: Main photochromic data in acetonitrile of the investigated pool of terarylenes.

	λ_{max} [nm] (ε [M^{-1} cm^{-1}])				
	OF	CF	Φ_{O-C} (335 nm)	Φ_{C-O} (575 nm)	α_{CF} (335 nm)
1	274 (26700) 314 (29000)	265 (23000) 317 (26400) 349 (20500) 587 (13000)	0.40	0.025	96%
2	279 (31150) 317 (37000)	272 (24500) 348 (33800) 586 (16000)	0.32	0.023	97%
3	348 (36400)	324 (28140) 410 (28000) 603 (23000)	0.23	0.006	90%
4	317 (32300)	319 (32360) 606 (17450)	0.27	0.007	89%
5	274 (25000) 317 (27000)	272 (25000) 319 (30000) 622 (14550)	0.10	0.009	96%
6	276 (26000) 322 (37600)	280 (33000) 342 (31800) 355 (31000) 664 (18150)	0.04	0.003	90%
7	286 (30800) 320 (35300)	275 (23500) 333 (33400) 624 (18200)	0.05	0.007	83%
8	348 (43400)	/	/	/	/

A clear decreasing trend can be observed for the photocyclization quantum yield which passes from 0.40 for the reference unsubstituted terthiazole in acetonitrile to 0 for the switch **8**, thus confirming the detrimental impact of the CT character on the photocyclization quantum yield. The same conclusion can't be drawn for the cycloreversion quantum yield that seems to be independent from it.

To establish if the charge transfer was the main cause of the decrease of $\Phi_{O\text{-}C}$, other factors potentially affecting it have been taken into account. First, the possibility that this lowering was related to an increase of the percentage of unreactive parallel conformer in acetonitrile has been verified by ^{1}H-NMR spectroscopy, to check the observable sets of signals for the OF at room temperature. For all the eight compounds, only one set of signals (e.g. only two singlets for the methyl groups on the reactive carbon atoms) has been observed, a proof that the interconversion between the two conformations could occur freely at RT, making their ratio 50:50. The proton NMR of **5** in CD_3CN is provided in Figure 62 as example.

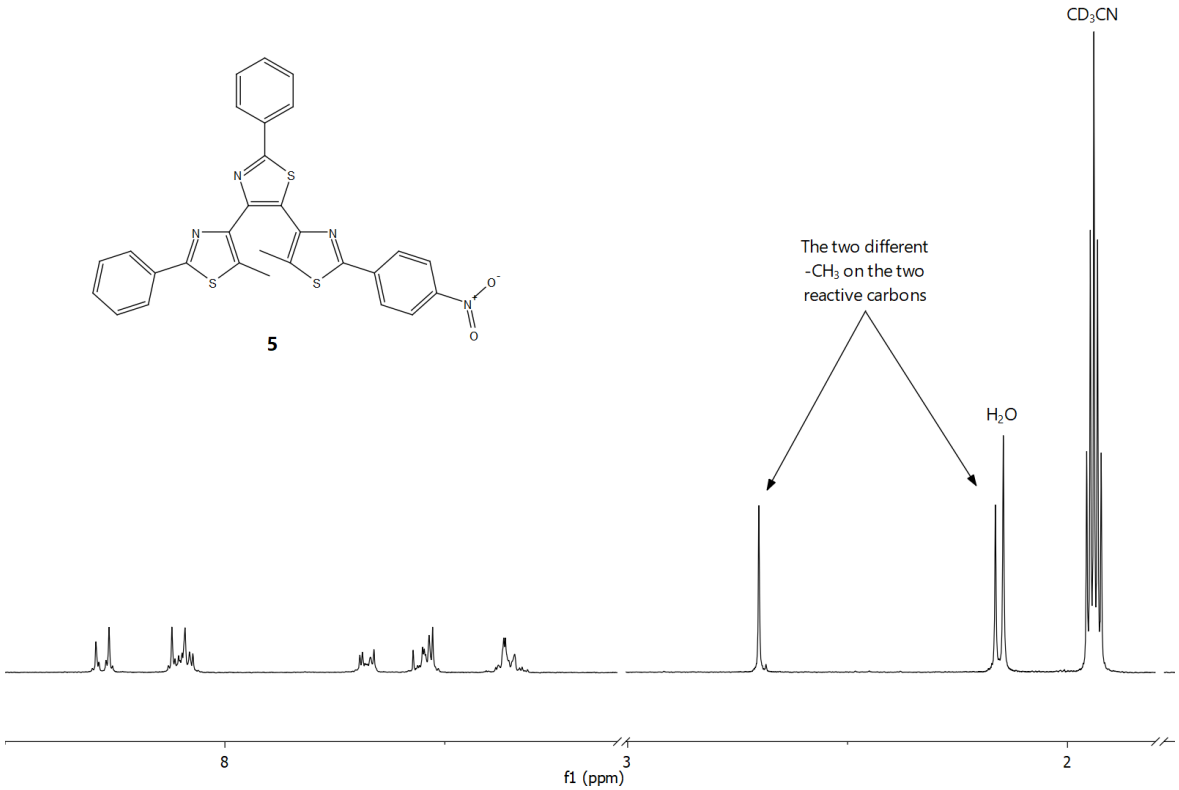

Figure 62: ^{1}H-NMR of **5** (OF) in CD_3CN at RT showing only one set of signals.

Secondly, the effect of the strong electron-withdrawing $–NO_2$ group has been studied. In fact, by looking at the experimentally observed variation of the photocyclization quantum yield, its introduction marked the most significant decrease of $\Phi_{O\text{-}C}$, which diminished from 0.40 for **1** to 0.10 for **5**. This functional group is known to provide the possibility of populating triplet states through intersystem crossing. [167–169] This process would have a negative impact on the photochromic reaction efficiency if T_1 relaxes to the ground state without ring-closing reaction occurring in it. Since triplet states can be efficiently quenched by oxygen [170], the photochromic behavior of **5** in aerated and degassed solutions has been compared. An acetonitrile solution of **5** has been irradiated with UV light before and after degassing with Ar to evaluate the extent of the triplet population and the consequences on the photochromic activity (Figure 63).

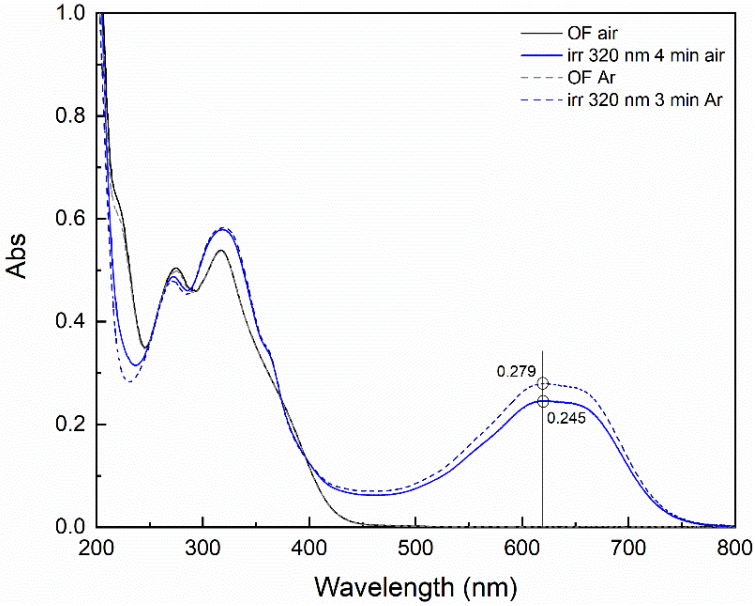

Figure 63: Absorption spectra of **5** (2.00 x 10^{-5} M) in acetonitrile. OF in aerated solution in black solid line: OF in degassed solution in black dashed line; PPS in aerated solution by irradiating at 320 nm in blue solid line; PSS in degassed solution by irradiating at 320 nm in dashed blue line. Optical path of the cuvette: 1 cm.

The absorption spectra show that the conversion in the degassed solutions improved by 10% ca., thus indicating that the impact of this triplet state is not significant on the reactivity of these derivatives and the main study can be focused on the singlet excited state reactivity. An identical analysis has been performed on photochrome **7** and the same 10%-improvement has been observed (Figure 64).

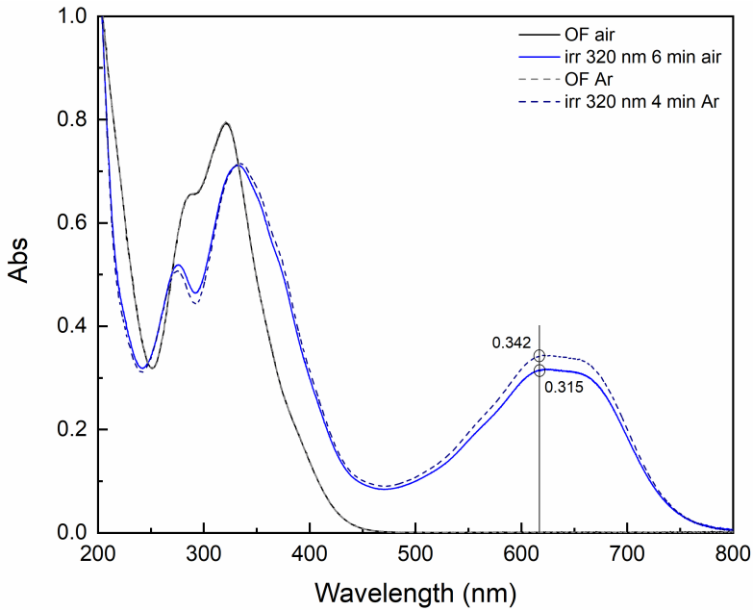

Figure 64: Absorption spectra of **7** (2.24 x 10^{-5} M) in acetonitrile. OF in aerated solution in black solid line: OF in degassed solution in black dashed line; PPS in aerated solution by irradiating at 320 nm in blue solid line; PSS in degassed solution by irradiating at 320 nm in dashed blue line. Optical path of the cuvette: 1 cm.

2.3 Theoretical modelling

To gain a better insight on this detrimental effect of CT character towards the photochromic behavior of the investigated family of terarylenes, a theoretical investigation has been conducted not only on the ground state, but also on the first singlet excited state in collaboration with Pr. Maurel (ITODYS – Université de Paris).

First, the eight structures have been optimized at the DFT level with CAM-B3LYP/6-311G(d,p) and wB97XD/6-311G(d,p) in acetonitrile, that has been taken into account by applying the Integral Equation Formalism variant of the Polarizable Continuum Model (IEFPCM). The conformations in these optimized geometries were antiparallel for all the eight investigated derivatives and the distances between the reactive carbons resulted below the upper limit of 4.2 Å to observe the photoinduced cyclization. This suggests that the diminishing trend of the photoactivity in solution is not due to an increase of the parallel conformer percentage when passing from **1** to **8**.

Then, TD-DFT calculations with CAM-B3LYP/6-311G(d,p) have been carried out to calculate the UV-vis spectra for switches **1**-**8** (in their open form, indicated with **o**, and their closed form, indicated with **c**) and a comparison with the experimental ones is given in Table 2, where f is the oscillator strength of the assigned transitions.

Table 2: Comparison between the calculated and the experimental optical properties of the eight investigated terthiazoles.

	Theoretical λ (nm)	Experimental λ (nm)	f	Assigned transition
1o	311 299 295	314 274 /	0.643 1.353 0.034	HOMO → LUMO HOMO → LUMO+1 HOMO → LUMO+2
1c	552 361 315	587 349 317	0.617 0.819 0.447	HOMO → LUMO HOMO → LUMO+1 HOMO-1 → LUMO
2o	313 305 294	317 / 279	0.515 1.323 0.378	HOMO → LUMO HOMO → LUMO+2 HOMO-1 → LUMO+1
2c	527 348 312	586 348 272	0.526 0.553 0.355	HOMO → LUMO HOMO → LUMO+1 HOMO → LUMO+2
3o	330 314 295	348 322 (sh[a]) /	1.063 0.803 0.508	HOMO → LUMO+2 HOMO-1 → LUMO HOMO-1 → LUMO+1

3c	563 369 336	603 410 324	0.818 1.199 0.167	HOMO → LUMO HOMO → LUMO+1 HOMO-1 → LUMO
4o	324 307 291	317 / 274	0.934 0.775 0.531	HOMO → LUMO HOMO → LUMO+1 HOMO → LUMO+2
4c	569 384 322	606 364 (sh[a]) 319	0.664 0.706 0.003	HOMO → LUMO HOMO → LUMO+1 HOMO-8 → LUMO
5o	335 307 291	317 / 274	0.814 0.779 0.556	HOMO → LUMO HOMO → LUMO+1 HOMO → LUMO+2
5c	576 397 319	622 360 (sh[a]) 319	0.651 0.599 0.613	HOMO → LUMO HOMO → LUMO+1 HOMO-1 → LUMO
6o	336 309 303	322 / 276	0.854 0.402 1.092	HOMO → LUMO HOMO → LUMO+1 HOMO → LUMO+2
6c	587 372 345	664 355 342	0.750 0.533 0.484	HOMO → LUMO HOMO → LUMO+1 HOMO → LUMO+2
7o	344 309 394	322 / 286	0.669 0.721 0.691	HOMO → LUMO HOMO → LUMO+1 HOMO → LUMO+2
7c	559 401 327	624 / 333	0.608 0.406 0.685	HOMO → LUMO HOMO → LUMO+1 HOMO-1 → LUMO
8o	340 331 315	348 / /	1.139 0.450 0.813	HOMO → LUMO HOMO → LUMO+2 HOMO-1 → LUMO+1
8c	604 383 361	/ / /	0.899 0.789 0.553	HOMO → LUMO HOMO → LUMO+1 HOMO-1 → LUMO+1

[a] sh: shoulder.

For all the eight switches in their OFs, the lowest energy transition ($S_0 \rightarrow S_1$) is HOMO → LUMO. An apparent exception is observed for **3o**, whose transition is HOMO → LUMO+2. However, the computations show that also HOMO → LUMO contributes to it.

Overall, the fit between the experimental data and the theoretical ones is satisfying, especially for the OFs. In fact, the maxima of the UV bands are reproduced with an error between 3 nm (for **1o**) and 22 nm (for **7o**). Concerning the visible band of the CFs, the energies of the corresponding transitions (that are HOMO → LUMO for all the investigated compounds) are slightly overestimated, with and error ranging from 40 nm to 60 nm ca. Nevertheless, the experimentally observed red-shift of the λ_{max} for the characteristic band of the ring-closed isomers is reproduced by the calculations.

The localization of the frontier orbitals in the investigated compounds clearly indicated the CT character of the transition as it can be observed by the isocontour plots (Figure 65).

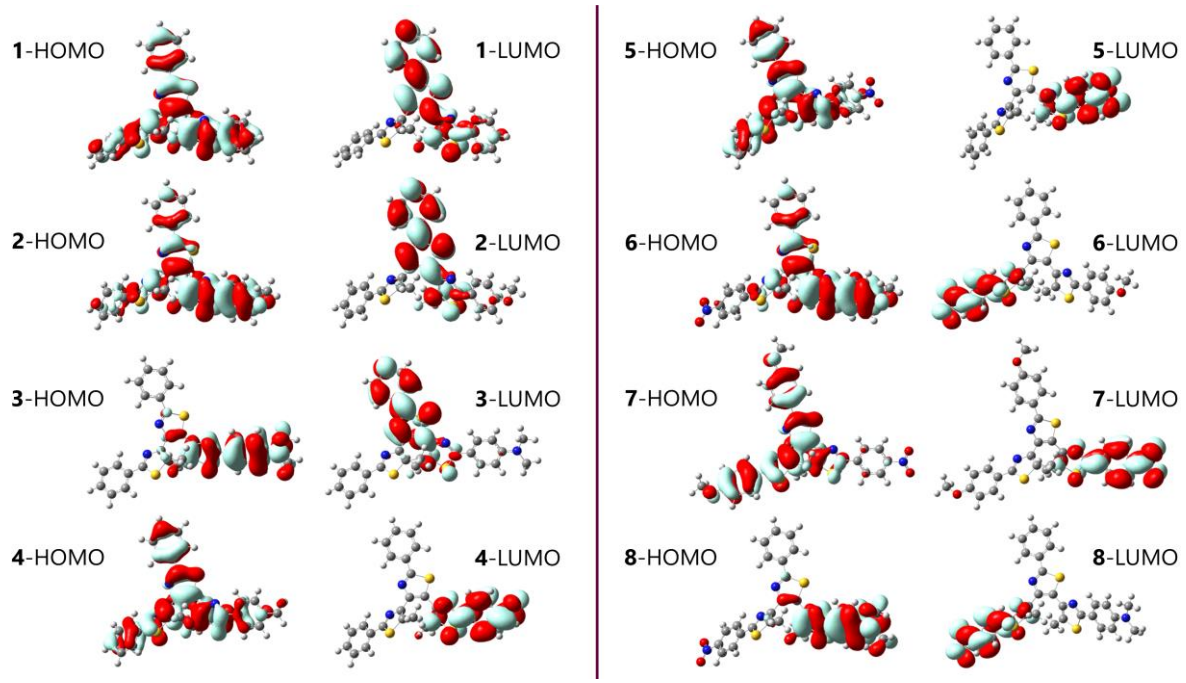

Figure 65: CAM-B3LYP/6-311G(d,p) modelling of HOMOs and LUMOs for the eight investigated terarylenes.

For non-functionalized photochrome **1**, the charge transfer character appears to be due to the electron-deficient nature of thiazoles. The additional presence of the methoxy group leads to a partial major distribution of the HOMO on the anisole-containing arm and a more localized LUMO on the central phenyl-thiazole bridge for **2**. Unambiguous charge transfer is observed for switch **3**, whose HOMO is fully localized on the arm bearing the $–N(CH_3)_2$ group and LUMO is exclusively on the central core. In the case of acceptor-containing switches, HOMOs are limited on the electron-richer part of the molecules while LUMOs are always restricted on the thiazole arm bearing the electron withdrawing group, either –CHO or $–NO_2$.

Moreover, it has been possible to estimate the amount of transferred charge (Q*) accompanying the transition from the ground state (S_0) to the first excited one (S_1), the transfer

distance (Δr) and the dipole moment (μ) at the excited state through the calculations. A graphical explanation of Q* and Δr is provided in Figure 66, with the results of the modelling on **8**.

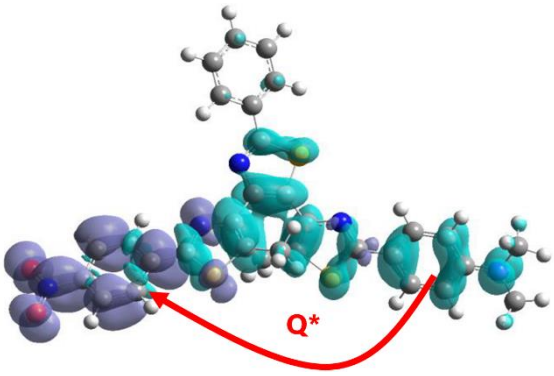

Figure 66: Electron density variation (Q*) with the $S_0 \rightarrow S_1$ transition (electron loss in aqua green, electron gain in purple) for terthiazole **8**. The red arrow indicates the transfer distance (Δr).

Visually, the side of the molecule that lost electron density with the HOMO → LUMO transition (i.e. the hexatriene core unit and the dimethylamino-containing arm) is shown in aqua green, while the side that gained it is in purple.

The values of these three parameters for all the eight derivatives are reported in Table 3.

Table 3: Charge transfer parameters of the investigated terarylenes determined at the CAM-B3LYP/6-311G(d,p)//wB97XD/6-311G(d,p) level of theory.

	Q*	Δr (Å)	μ (D)
1	0.47	1.874	4.3
2	0.47	1.958	4.4
3	0.562	2.332	6.294
4	0.611	3.466	10.171
5	0.7	4.188	14
6	0.71	4.399	15.9
7	0.73	4.527	15
8	0.76	5.467	20

As previously stated, **1** is characterized by CT even if it doesn't contain donor or acceptor functional groups because of the presence of electron-poor thiazoles. Furthermore, the

identified parameters for this reference compound and **2** are the same, thus confirming the scarce electron-donating strength of the methoxy substituent, whose introduction doesn't generate a more important dipole moment compared to that of the non-functionalized photochrome. The presence of a stronger donor group such as the dimethylamino leads instead to an increase of Q*, as corroborated by the determined value for **3**. The two examined electron withdrawing groups, i.e. formyl and nitro groups, enhanced the charge transfer character of switches **4** and **5**, respectively. Terthiazole **6** is the first example of D-A photochrome within the investigated family and it shows a 1.5 times bigger amount of transferred charge because of the functionalization with $–OCH_3$ and $–NO_2$, compared to the reference unsubstituted molecule. Slightly increased CT characteristics are determined for the trisubstituted species **7**. Finally, compound **8**, which isn't experimentally reactive in acetonitrile, is coherently characterized by the biggest Q*.

Again, also the computations show that the introduction of the nitro group is accompanied by the most evident impact on the charge transfer character of the investigated derivatives.

2.3.1 $\Phi_{O\text{-}C}$ – Q correlation as predictive model of the photochromic behavior*

By looking at the available data, the photcyclization quantum yield and the electron density variation due to the $S_0 \rightarrow S_1$ transition appear to be inversely proportional, with a decrease of the former if the latter increases. Interestingly, by correlating the two parameters, an almost linear dependence has been observed (Figure 67).

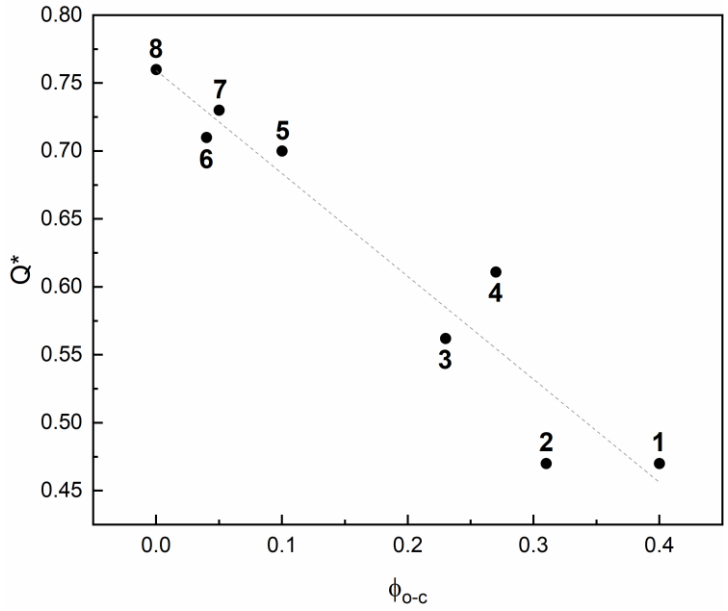

Figure 67: Correlation between the amount of transferred charge between S_0 and S_1 (Q*) and the ring-closing quantum yield (Φo-c).

This almost linear relation linking Q* and $\Phi_{O\text{-}C}$ may be appealing as predictive model to estimate the photocyclization quantum yield of terthiazoles, a parameter related to a complex

excited state phenomenon, through easily accessible data, thanks to proper theoretical modelling.

The validity of this correlation for other photochromic compounds has been extended to molecules already known in the literature to check its possible generalization. In particular, the same investigation has been performed on the derivatives studied by Jaung and co-workers, which showed "horizontal" or "vertical" charge transfer character depending on the position of the donor and acceptor substituents (Figures 68a and 68b). [115] The application of the proposed correlation is shown below the structures of the considered molecules.

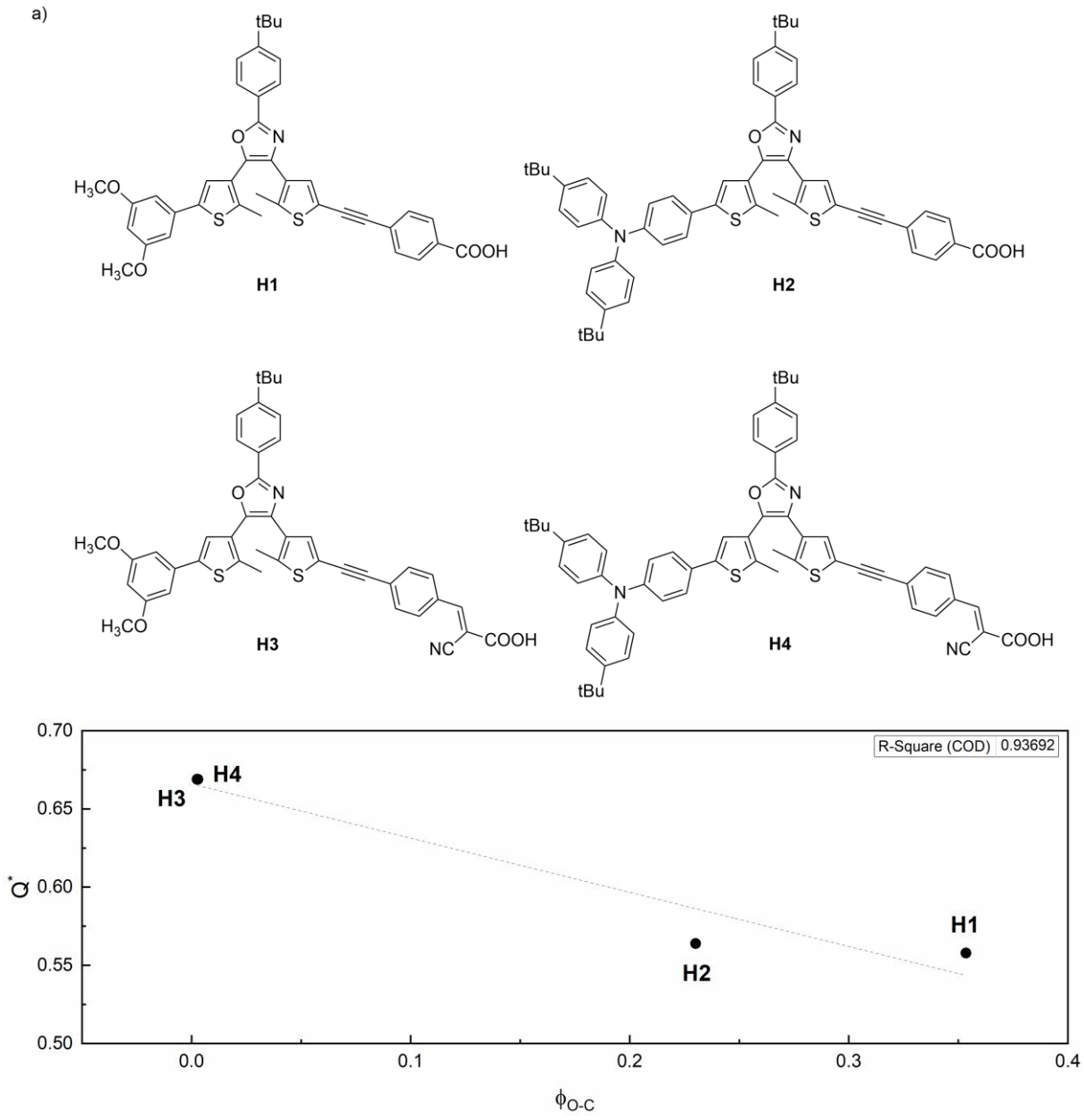

Figure 68a: top) Structures of the four photochromes showing "horizontal" CT investigated in ref. [115]; bottom) Application of the correlation between the amount of transferred charge between S_0 and S_1 (Q*) and the ring-closing quantum yield (Φo-c).

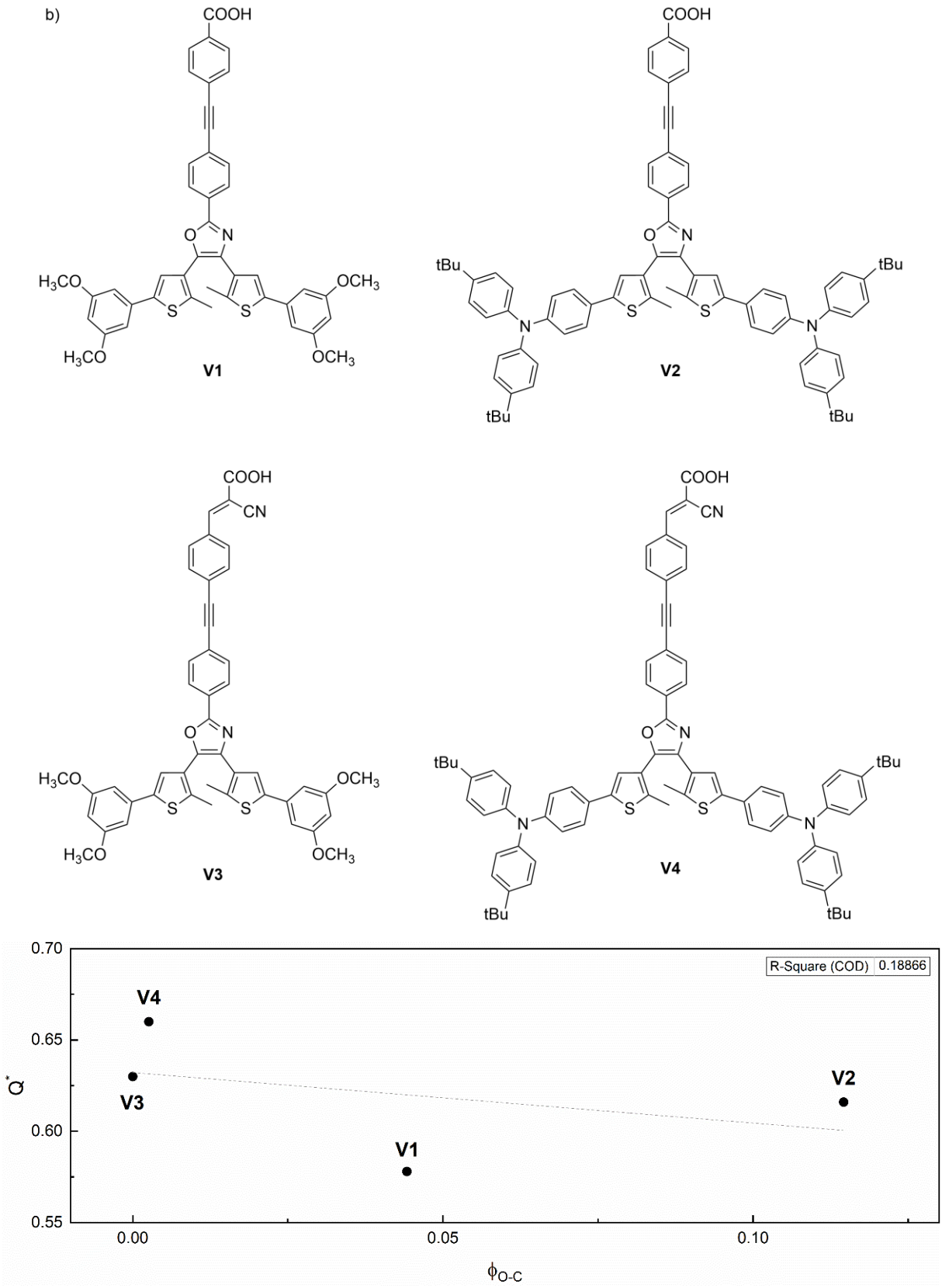

Figure 68b: top) Structures of the four photochromes showing "vertical" CT investigated in ref. [115]; bottom) Application of the correlation between the amount of transferred charge between S_0 and S_1 (Q*) and the ring-closing quantum yield (Φo-c).

The correlation appears to be satisfyingly extendable to the four switches bearing the electron-donating and electron-withdrawing groups on the two thienyl-based arms, thus consequently showing the same kind of "horizontal" charge transfer character as the eight terthiazoles presented in this Chapter. The same can't be said when applying the method to the "vertical" series. In this case, LUMOs get localized on the central *para*-substituted phenyl(ethynyl)phenyl unit, far from the central hexatriene core undergoing the electrocyclization. Since the electron density isn't on at least one of the arms bearing the carbon atoms involved in the new C-C bond formation, it may be supposed that CT is always detrimental to the photocyclization quantum yield (this is also supported by the lower Φo-c values for the V-compounds compared to H-switches' ones), but the correlation can't be applied because the electronic systems for the $S_0 \rightarrow S_1$ transition are not comparable passing from an "horizontal" charge transfer character to a "vertical" one.

Other "horizontal-CT" photochromes have then been considered, such as the DAEs synthesized and characterized by Pu's groups that are depicted in Figure 69. [171]

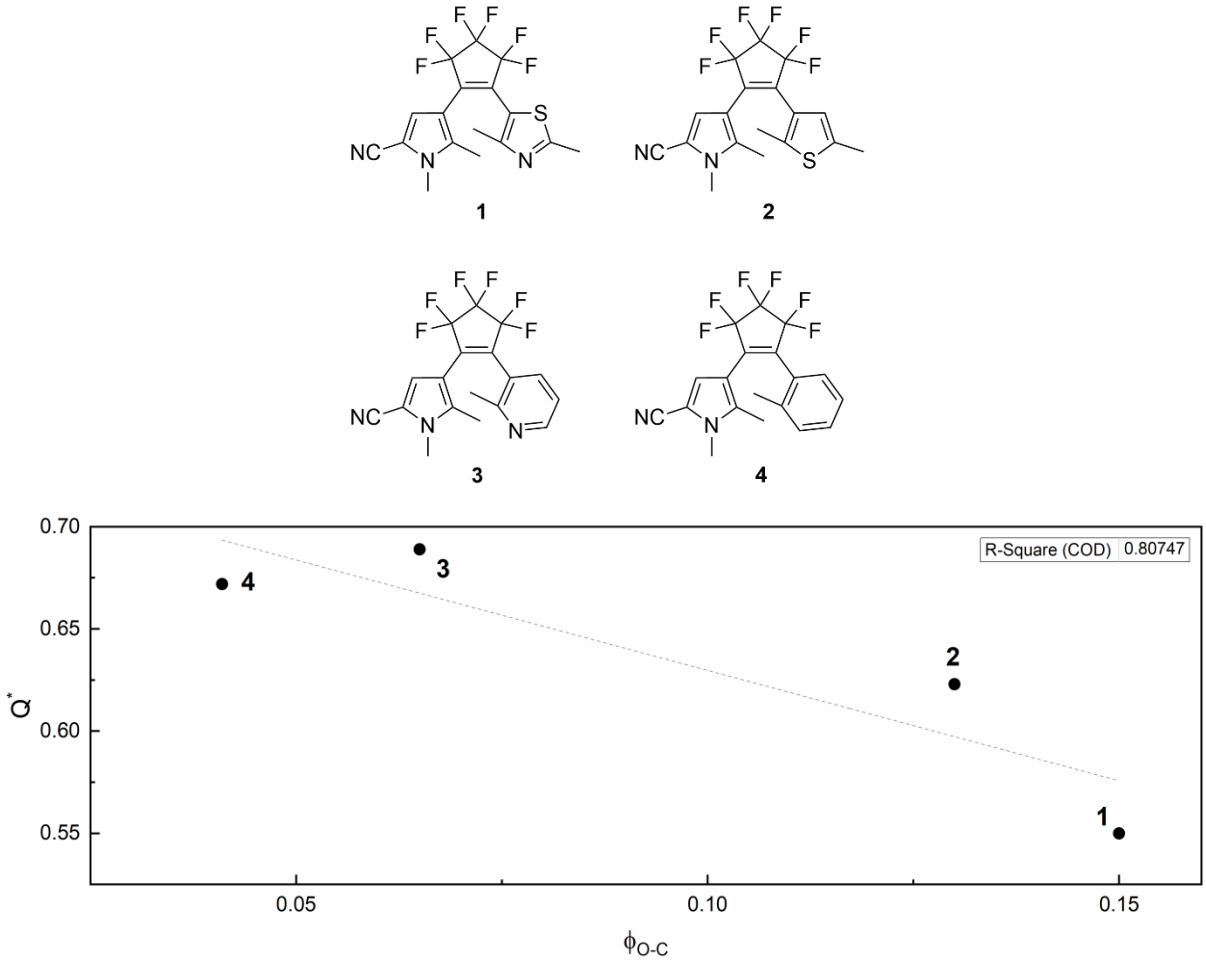

Figure 69: top) Structures of the four photochromes investigated in ref. [171]; bottom) Application of the correlation between the amount of transferred charge between S_0 and S_1 (Q*) and the ring-closing quantum yield (Φo-c).

The almost linear correlation appears to be fitting again in this case. Clearly, charge transfer can't be the only parameter affecting a complex phenomenon occurring at the excited state

such as the cyclization. In fact, the authors of this cited work highlighted the impact of the aromatic stabilization energy (ASE), that varied in a non-negligible fashion when passing from thienyl and thiazyl groups to pyridyl and phenyl ones and led to smaller Φo-c values.

2.4 "Early" and "late" photochromes

To further investigate the $S_0 \rightarrow S_1$ transition and its impact on the photochromic behavior, the reaction pathway for the ring-closure at the ground state has been built for all the eight molecules by progressively diminishing the distance between the reactive carbons ($d_{C\text{-}C}$) and by optimizing all the geometries for each point while keeping $d_{C\text{-}C}$ constant during the computation.

Then, TD-DFT calculations on every ground-state geometry allowed to obtain an approximation of the energy surface of the first excited state. In fact, all the obtained geometries haven't been optimized since it would have been a complicated and computationally expensive modelling. However, it may be interesting to optimize at least the first geometry and the transition state (TS) in the S_1 to calculate the energy barrier for the cyclization reaction. The obtained values are reported in Table 4.

Table 4: Activation energy (E_a) in kJ/mol for the ring-closing reaction of the eight investigated terthiazoles and distance between the reactive carbons in the transition state, TS.

	E_a (kJ/mol)	$d_{C\text{-}C}$ (Å)
1	2.22	3.054
2	1.81	3.064
3	2.32	3.071
4	10.99	3.075
5	23.98	2.760
6	17.38	2.767
7	21.41	2.741
8	12.67	2.729

From the obtained values of the activation energies, a remarkable dependence from the structure can be noticed, with values passing from 2.22 kJ/mol for the non-substituted photochrome **1** to 23.98 for **5**. Nevertheless, a correlation between the variation of the energy barrier and the variation of the photocyclization quantum yields isn't observed. In fact, terarylenes **3** and **4** have close quantum yields (0.23 and 0.27), but significantly different E_a

(2.32 kJ/mol and 10.99 kJ/mol) and **8**, which isn't photoactive in acetonitrile because of the CT character developed by introducing $–NO_2$ and $–N(CH_3)_2$ groups, shows a smaller energy barrier for the ring-closing reaction in S_1 than switches **5**,**6** and **7**.

The theoretical modelling of the activation energy for the cyclization reaction of terarylene **8** has been conducted also in toluene and, interestingly, a much smaller Ea has been determined (i.e. 4.6 kJ/mol), in line with the experimentally observed solvent polarity-dependent photochromic behavior.

The decreasing trend of the distance between the reactive carbons in the TS geometry is instead in accordance with the lowering of Φo-c.

By looking at the whole energy curves approximating the S_1 reaction pathway of the eight photochromes, two limiting cases can be observed when evaluating the delocalization of the LUMO at different reactive carbons distances, as shown by compounds **1** and **5** (Figure 70).

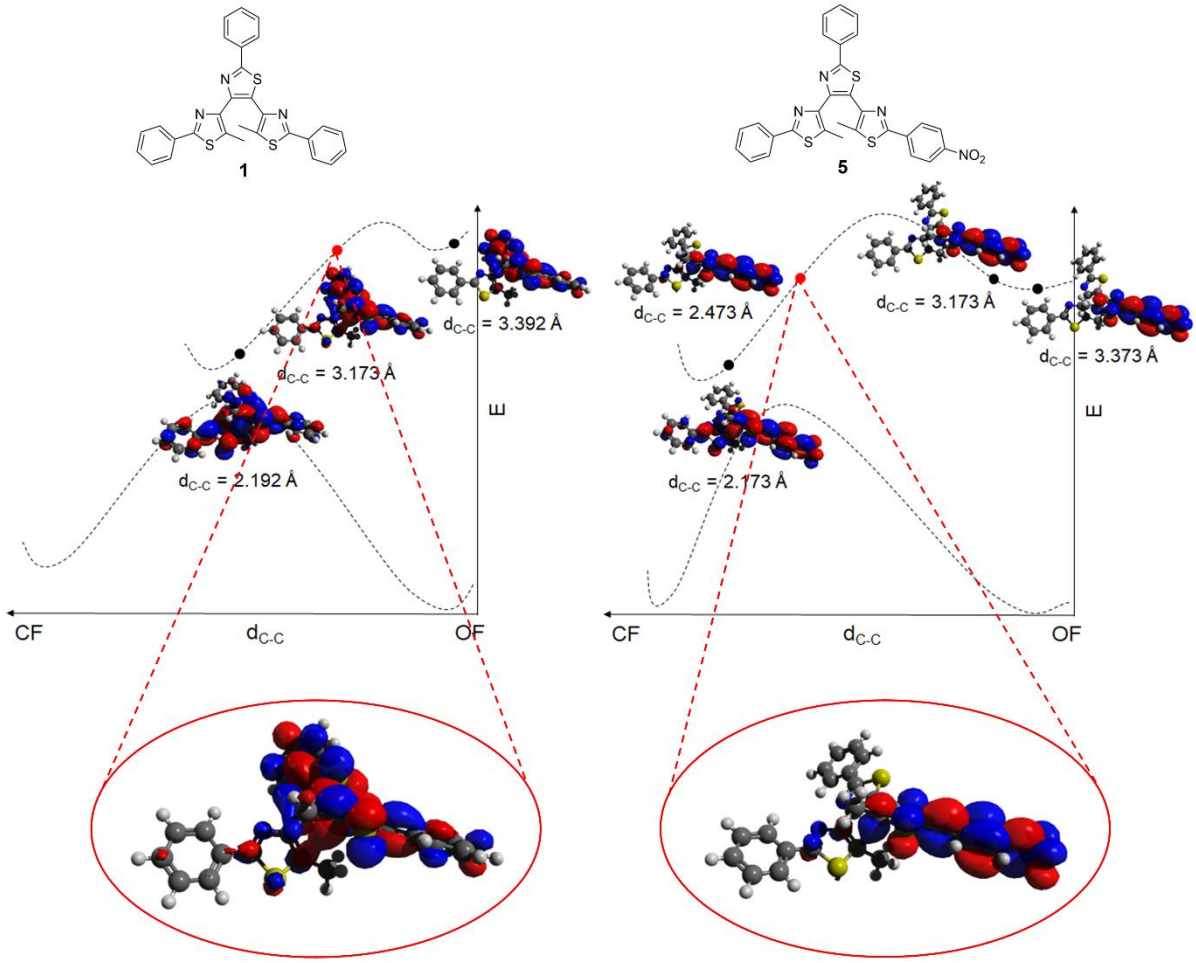

Figure 70: Approximation of the S_0 and S_1 reaction pathways of (left) **1** and (right) **5**. The red dots indicate the geometries in which the bonding interaction in the LUMO is occurring, as confirmed by the isocontour plots, that are zoomed in the red circle.

Molecular orbitals with adequate symmetry must be on both the reactive carbons involved in the conrotatory cyclization reaction to have the ring-closure. In the case of compound **1**, the bonding interaction leading to the closed form appears to start at a distance between the reactive carbons slightly below 3.2 Å. A significantly smaller distance (< 2.5 Å) is required to have the same interaction for terthiazole **5**. This different development of the bonding interaction leads to a distinction between an "early" photochrome in which the formation of the new C-C bond can occur at longer $d_{C\text{-}C}$ and a "late" switch whose ring-closing reaction needs a geometry in which the C-C are much closer to each other to have the proper orbital delocalization. Coherently, the photocyclization quantum yield of the former is four times bigger than that of the latter. It can be said that charge transfer is detrimental towards the cyclization because the LUMO remains strongly localized on one of the arms, thus hindering the needed delocalization to achieve the ring-closure.

The study was extended to the remaining switches of the homogeneous family and the resulting HOMO and LUMO relative evolution with the variation of the distance between the reactive carbons is provided in Figure 71.

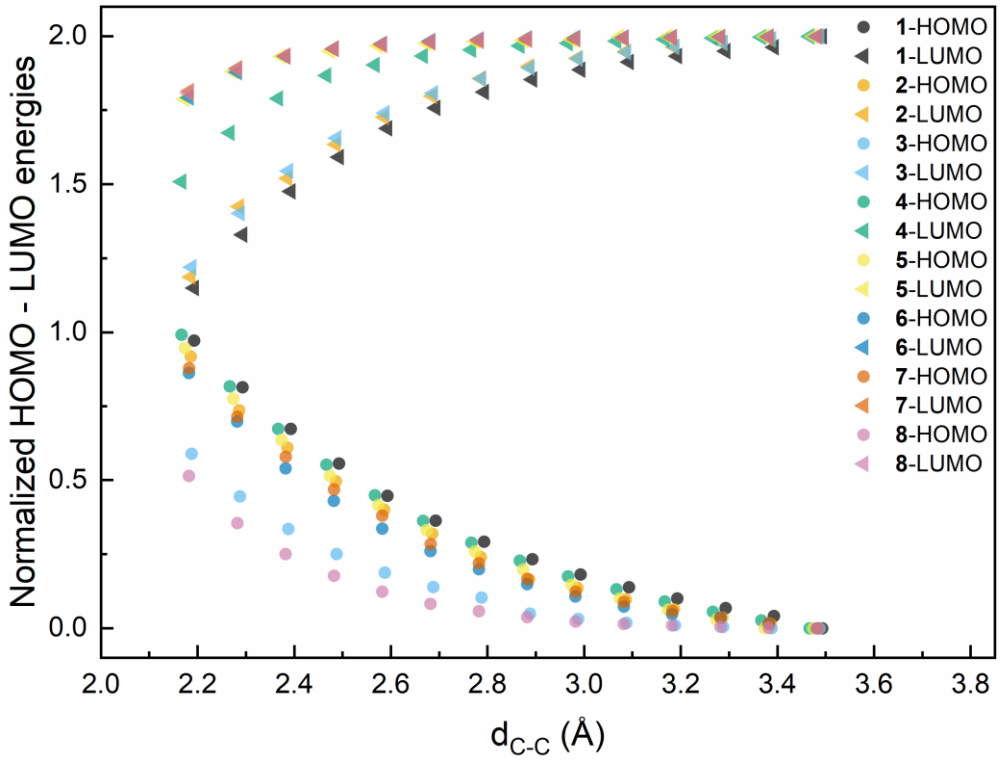

Figure 71: Relative evolution of HOMOs (circles) and LUMOs (triangles) of the eight investigated terarylenes with the variation of $d_{C\text{-}C}$.

To obtain every curve, the geometries of the eight open forms have been taken as references and their HOMOs and LUMOs have been set to 0 and 2, respectively. Then, all the energy values for the frontier orbitals at progressively shorter carbon-carbon distances have been calculated in relation to these normalized values.

As it can be observed, a significant energy variation in the LUMO starts early (3.2 Å) for compounds **1** and **2**, in accordance with the experimentally observed reactivity. While terthiazoles **3** and **4** show an intermediate character (energy variation at ~3 Å and ~2.8 Å, respectively), **6**, **7** and **8** join derivative **5** in the "late" class of photochromes. In fact, the energy of the LUMOs for smaller distances between the reactive carbons remains almost constant until the very short distance of ~2.5 Å.

2.5 Conclusions

A homogeneous family of eight terthiazoles showing progressively increasing charge transfer character has been synthesized and fully characterized to rationalize the impact of electron-donating and electron-withdrawing functional groups on the photocyclization quantum yield.

By combining the experimentally determined $\Phi_{O\text{-}C}$ with the theoretical modelling of the ground state and the first singlet excited state, it has been confirmed that the charge transfer character is detrimental to the photochromic behavior. Moreover, the impact of CT on the efficiency of the ring-closing reaction has been rationalized: the stronger the charge transfer, the shorter the required reactive C-C distance to have a bonding interaction in the LUMO, thus leading to a distinction between more reactive, or "early", and less reactive, or "late", photochromes.

By comparison with the "early" switches, "late" ones have lower $\Phi_{O\text{-}C}$ values because they require geometries characterized by significantly smaller $d_{C\text{-}C}$ to have the proper delocalization of the LUMO on the reactive carbon atoms to achieve the ring-closure. The molecular orbital would be otherwise restricted on the electron-poor arm of the molecule, thus hindering the photocyclization.

Interestingly, an almost linear correlation between the photocyclization quantum yield and the charge transferred during the S_0 to S_1 transition (Q*) has been observed. This suggests that by determining such a parameter through DFT and TD-DFT calculations, it is possible to obtain indications about the expectable photochromic properties of a terarylene derivative.

Extension of this correlation to other diarylethenes and terarylenes known in the literature has shown a satisfying validity if the charge transfer is "horizontal", which means that it involves the two arms bearing the reactive carbons participating in the formation of the new C-C bond with the photoreaction.

Nicolò Baggi

Chapter 3: Design of photochromic-fluorescent molecular architectures showing switchable light-induced fluorescence hysteresis

Nicolò Baggi

3.1 Fluorescence modulation by diarylethenes

Among the multifunctional switches, those capable to exert control on the fluorescence response through the isomerization are appealing in the perspective of developing memories or fluorescent probes. Clearly, multiple examples of photochromic fluorescent systems exist and several reviews are available in the literature to take into account the various families of photochromes [172,173], but here the focus will be on diarylethene-based derivatives.

3.1.1 Photomodulation of fluorescence

As proposed by Fukaminato, Ishida and Métivier [174], the systems showing both photochromism and fluorescent properties can be classified in three main categories:

- Type 1: Inherently fluorescent photoswitchable molecules.
- Type 2: Covalently linked photochromic-fluorescent dyads.
- Type 3: Hybrid materials merging fluorescent molecules with photochromic ones.

While a Type 1 system allows the modulation of its own fluorescence through the photochromic reaction, in the cases of Type 2 and 3 derivatives, the control over the emission is exerted by the photochromic unit through energy or electron transfer.

Classic examples of inherently fluorescent photochromes are those systems where the open form is emissive while the closed form quenches the fluorescence. This is the case of the molecule depicted in Figure 72 (top), whose emission in hexane solution diminished with the photocyclization achieved by irradiating the sample at 313 nm, as it can be observed in the provided spectra (bottom). The residual fluorescence intensity (indicated with a dashed line) is related to the remaining OF in the photostationary state. [175]

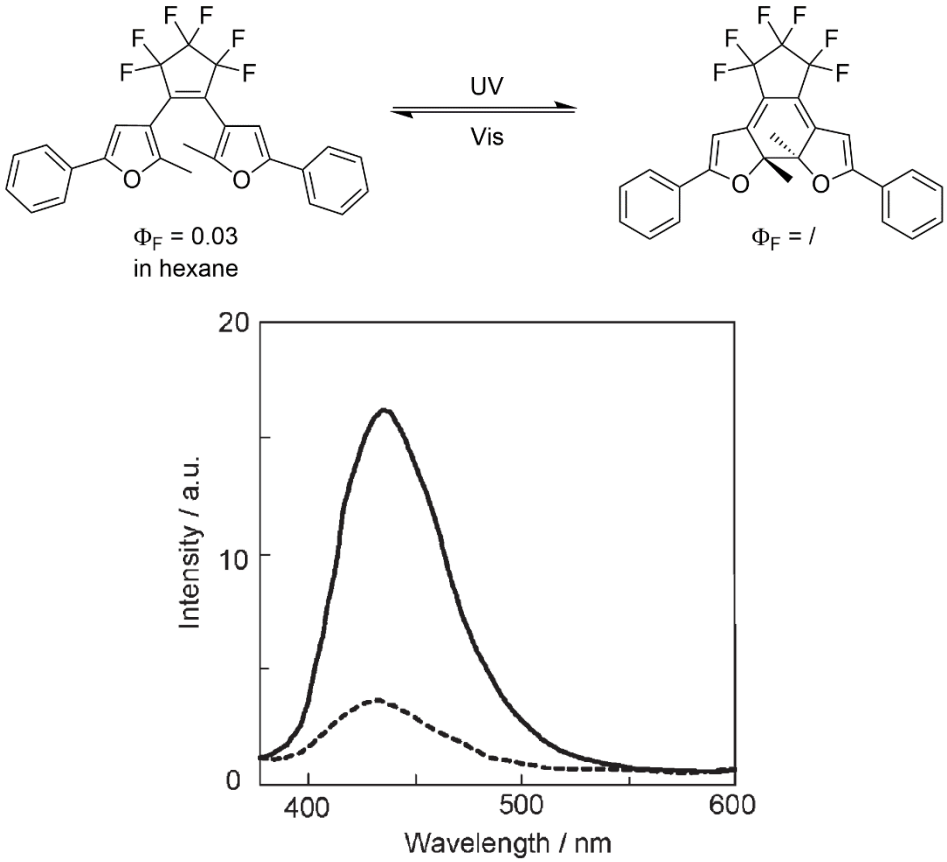

Figure 72: (top) isomerization reaction of the Type 1 DAE investigated in ref. [175]; (bottom) emission spectrum in hexane of the OF (solid line) and at the PSS (dashed line), as presented in ref. [175]

This kind of derivative is also defined as "turn off mode" fluorescent diarylethene. Similarly, our group has reported that the ESIPT fluorescence (Excited State Intramolecular Proton Transfer [176]) of a salen-type terarylene could be reduced to its 20% by reaching the photostationary state. [177]

Also so-called "turn on mode" systems where the closed form is the emissive isomer have been studied. [178,179] Well-established switches showing this kind of fluorescence modulation present benzothiophene-S,S-dioxide-based arms, as in the molecule shown in Figure 73. [180]

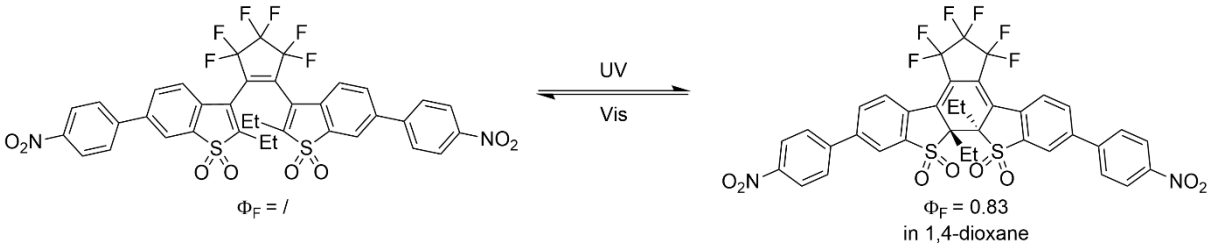

Figure 73: Type 1 "turn on mode" fluorescent DAE, investigated in ref. [180]

The impressively high fluorescence quantum yield of these photochromes (in addition to other properties such as the isomerization quantum yield and the fatigue resistance) made them suitable for super-resolution microscopy techniques such as RESOLFT or PALM. [181,182]

Fluorescence and the photochromic reactions are competing excited state processes since both generally occur in the S_1. Type 2 derivatives try to avoid this drawback by covalently linking the photochromes and fluorophores in dyads. The emission modulation is then expected to occur through electron transfer [183–187] or energy transfer. Generally, fluorescence can be observed when the diarylethene unit is in its open form while it is quenched in presence of the closed form, a species that absorbs at wavelengths where the fluorophore emits. A pioneering work about this type of fluorescence modulation was published by Irie and co-workers in 2002. [188] An adamantyl linker allowed to bind a dithienylethene derivative and a fluorescent anthracene unit, as depicted in Figure 74.

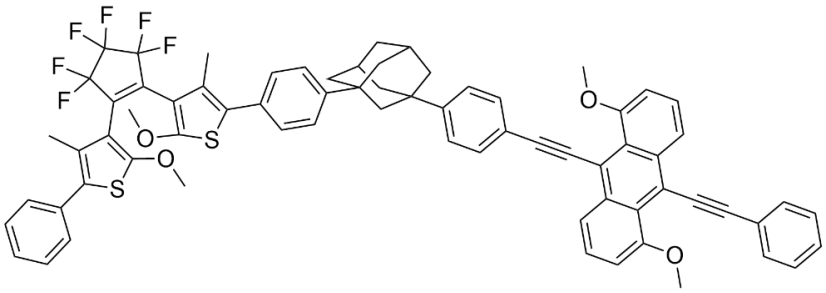

Figure 74: Photochromic-fluorescent dyad investigated in ref. [188]

The DAE unit underwent the photocyclization reaction under UV light irradiation and the cycloreversion when irradiated in the visible. Since the emission of the anthracene derivative occurred at 503 nm, the fluorescence could be modulated from 0.73 to 0 thanks to the OF↔CF isomerization. Moreover, the implementation of the dyad in a polymer film allowed to control single molecule fluorescence.

In this case and in many other examples in the literature (extensively summarized in several reviews [5,174,189,190]), a non-fluorescent photochrome is used. However, the combination of an inherently fluorescent photochrome to another fluorophore can offer interesting perspectives, as reported by Ouhenia-Ouadahi et *al.* [191] The authors studied the emissive "turn off mode" terarylene (Φ_F = 0.016 for the OF) linked by *click* chemistry to a dicyanomethylene (DCM) derivative, (Φ_F = 0.27) shown in Figure 75.

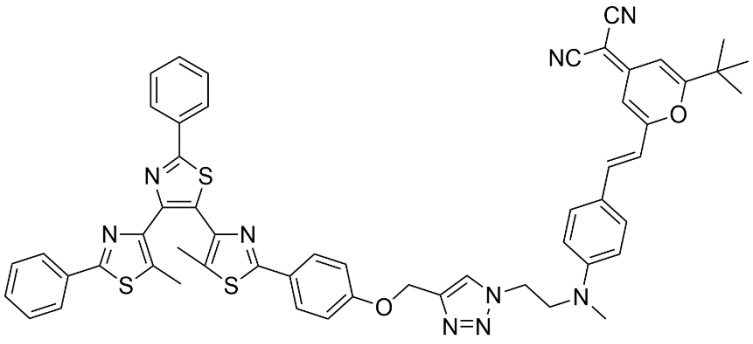

Figure 75: Terarylene-fluorophore dyad investigated in ref. [191]

The obtained dyad offered a two-way energy transfer since the emission band of the open form overlapped the absorption band of the DCM, while the band for the fluorescence of the dicyanomethylene species matched the absorption of the CF. The efficient modulation of the two fluorescent emissions occurred through Förster resonance energy transfer (FRET) and had significant impact on the properties of the DAE unit.

FRET is a non-radiative energy transfer through dipole-dipole interactions occurring between a donor molecule (D) and an acceptor one (A) when the emission band of D matches the absorption band of A and the vibronic transitions in the former are isoenergetic (or in resonance) to those in the latter (Figure 76). [192]

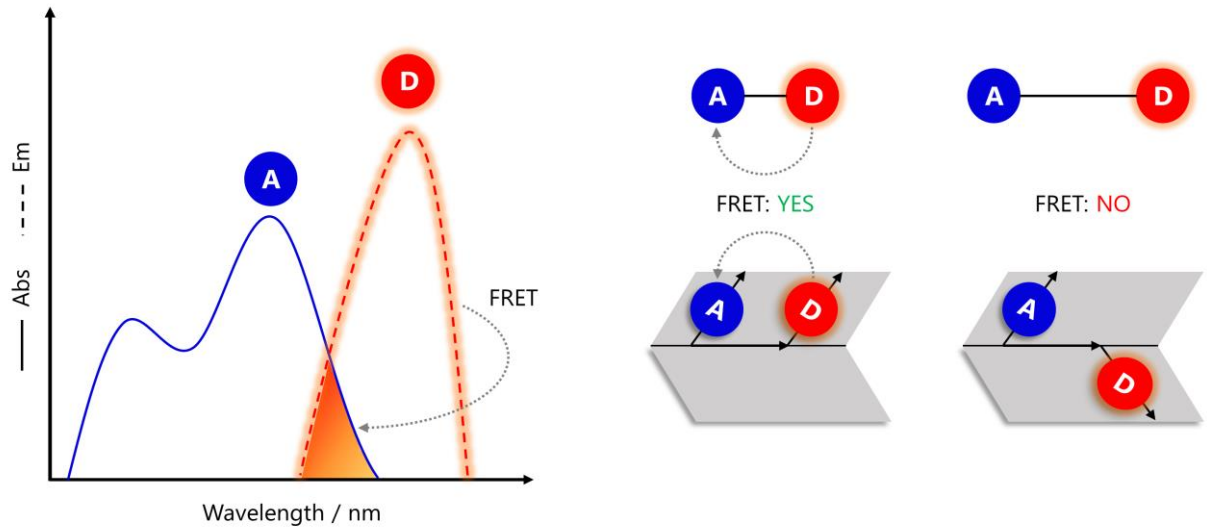

Figure 76: Schematic representation of FRET, the spectral overlay, the distance between donor (D) and acceptor (A) and their spatial disposition.

The rate constant for this transfer is defined as:

$$k_{FRET} = k_D \left[\frac{R_0}{r}\right]^6$$

Where k_D: emission rate constant of D in absence of A; R_0: Förster's radius; r: D-A distance.

The Förster's radius is the distance at which the resonance energy transfer has the same probability of occurring as the spontaneous deactivation of the donor (i.e. D* → D) and is generally around 15-60 Å. The R_0 value depends on several values like the fluorescence quantum yield of the donor unit, the refractive index of the medium, the molar absorption of the acceptor unit and the orientational factor, k^2. In particular, this parameter takes into account the spatial disposition of D and A. If the two units are perpendicular, $k^2 = 0$ and no FRET is expected to occur.

Overall, the efficiency of this process is determined as:

$$\Phi_{FRET} = \frac{1}{1 + (r/R_0)^6}$$

Which means that the efficiency is 0.5 if the D-A distance is equal to the Förster's radius, as it is summarized in Figure 77.

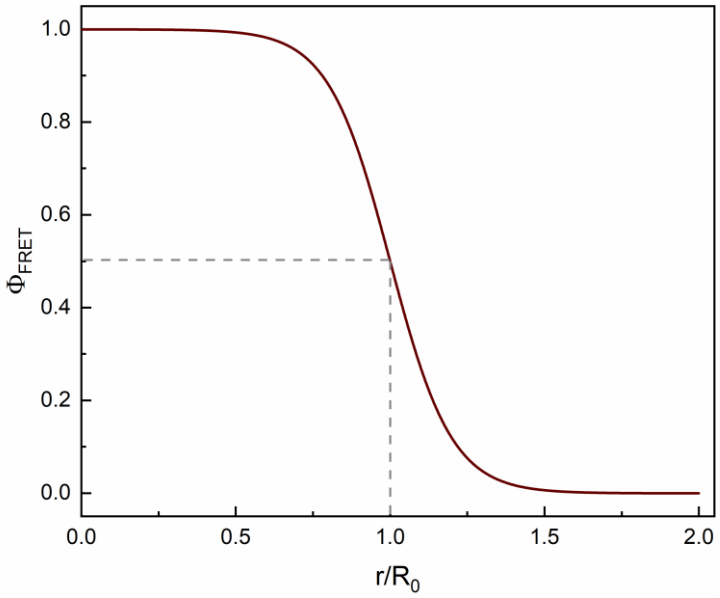

Figure 77: Φ_{FRET} dependence on the r/R_0 ratio.

The last category of systems capable to offer fluorescence modulation through the photochromic reaction is represented by hybrid materials, that is the Type 3. For example, DAEs and fluorophores can be combined in a polymer like PMMA [193] or in silica nanoparticles. [194,195] The dense packing in these systems can amplify the fluorescence signal and allow biological applications such as cell imaging.

It is also possible to develop fully organic nanoparticles [196–198] and polymers [199,200] capable to modulate fluorescence. A possible drawback of these systems is aggregation-caused quenching (ACQ), but it can be solved by properly selecting the fluorophore, so to have aggregation-induced effect (AIE) or aggregation-induced enhanced emission (AIEE) instead. [201–203] Recently, Fukaminato and co-workers have reported the case of a dyad (Figure 78) that wasn't particularly efficient in solution (i.e. fluorescence quenching ratio ~40% in THF) because of the poor overlap between the emission band of the D-A fluorophore and the absorption band of the DAE's CF isomer, but which showed "giant fluorescent quenching" if nanoparticles were prepared. [204]

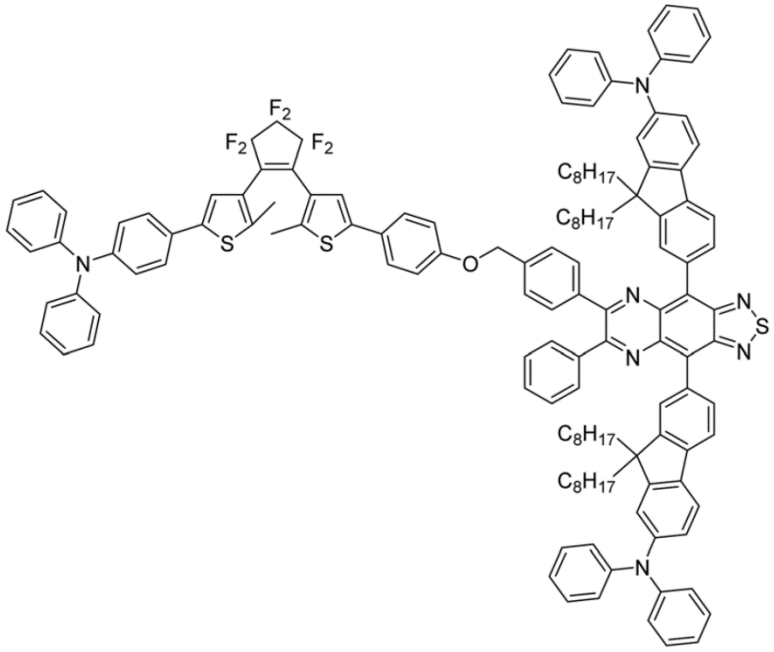

Figure 78: Photochromic-fluorescent dyad showing giant fluorescent quenching in nanoparticles. Adapted from ref. [204]

The better performances on fluorescence modulation are related to the fact that a single closed form can efficiently quench the emission of multiple fluorophores in the nanoparticles, since the units are more densely packed, improving the FRET efficiency that was low in solution. This was confirmed by the fact that an OF → CF conversion around 30% was enough to quench more than the 90% of the emission, thus making the relationship between the two parameters non-linear.

The same type of non-linear decrease of fluorescence with the conversion ratio of a diarylethene has been reported by Kobatake et *al*. in 2020 for hyperbranched polymers in which 20% of CF could quench the 70-80% of the emission. [205]

3.2 Aim of the study

In the perspective of developing smart materials, photoswitchable multichromophoric systems showing light-induced fluorescence hysteresis are unexplored in the literature, to the best of our knowledge. Consequently, the joint ANR SWIST project with Dr. Métivier, Pr. Xie, Dr. Maisonneuve and Yang Zhou, PhD student under their supervision (ENS Paris-Saclay – PPSM), has been started to design and develop molecular architectures containing a large number of fluorescent and photochromic units to be linked to a β-cyclodextrin platform by click chemistry [206–208], thus allowing an enhanced Förster energy transfer between the species. Moreover, Pr. Maurel (Université de Paris – ITODYS) has been involved for the theoretical modelling of such systems.

Preliminary studies had been previously conducted at ENS Paris-Saclay on dyads like the one shown in Figure 75 (previous Section, ref. [191]) and they have also been object of Dr. Maisonneuve's thesis. [209]

The fluorescence modulation is expected to occur through FRET from the dicyanomethylene derivative shown in Figure 79 (DCM, synthesized and characterized by Yang Zhou at ENS Paris-Saclay) to an appropriately functionalized terarylene, as Type 2 systems.

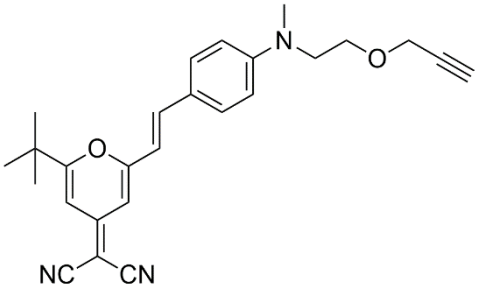

Figure 79: Dicyanomethylene derivative synthesized and characterized at ENS Paris-Saclay.

DCMs themselves allow photo-reversible fluorescence modulation because they undergo a light-induced *E/Z* isomerization between a strongly fluorescent *trans* isomer and a non-emissive *cis* one. [210,211] In particular, the efficiency of the *E/Z* isomerization for the derivative depicted above (i.e. $\Phi_{E\text{-}Z}$) is ~0.09-0.18 in THF and it is accompanied by a partial fluorescence quenching. [210] By combining it to a diarylethene or terarylene as in Figure 75 (previous Section, ref. [191]), bistable fluorescence photoswitching can be achieved, since the CF isomer of the DAE can quench the emission of *E*-DCM.

In particular, a hysteresis is expected to be observed if the fluorescence modulation doesn't occur with the same rate under UV and visible light irradiation, as schematized in Figure 80.

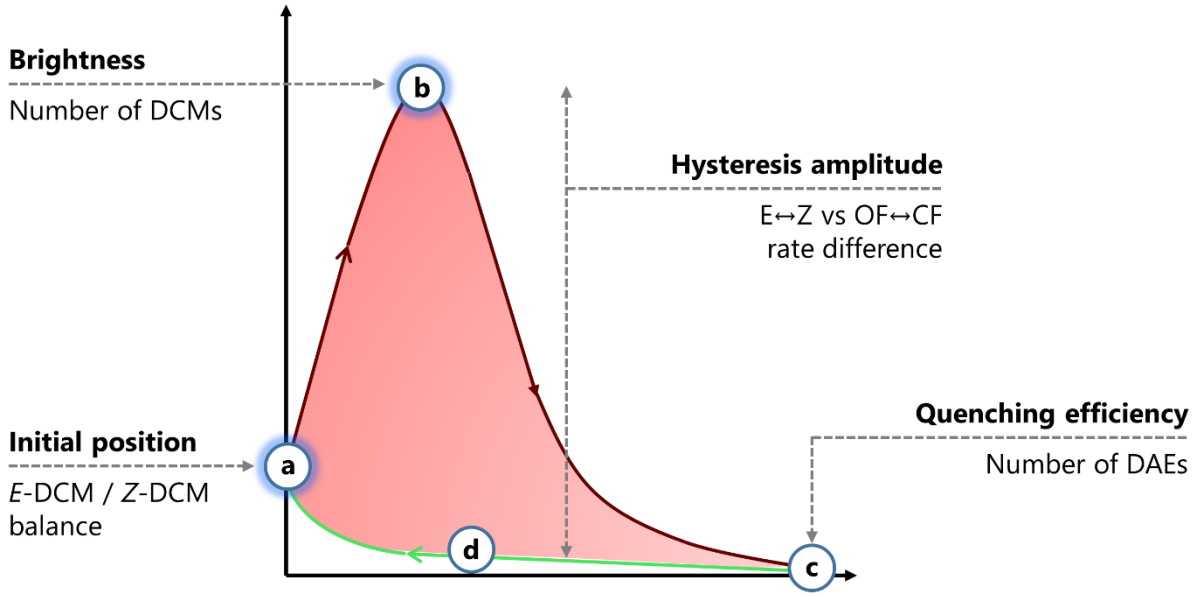

Figure 80: Schematic representation of the fluorescence hysteresis that can be obtained by combining DCM and DAE units in a Type 2 system and the parameters influencing it.

Generally, the DCM isomerization occurs rapidly thanks to its characteristic quantum yields and large extinction coefficients while the time-scale for the OF↔CF one is longer. Many parameters affect the shape of the hysteresis, such as the number of DCM and DAE units and the rate difference between the photochromic processes involving them. Since this last factor influences the amplitude of the hysteresis, a very slow isomerization of the diarylethene (or terarylene) thanks to small quantum yields is desired.

In fact, if the cycle is wide and showing multiple states at intermediate fluorescence, the molecular system can't be characterized by evaluating only the absorption or the fluorescence. An association of both becomes mandatory to properly define the state of the molecule, thus allowing the development of optical memories.

Initially, mono-N-alkylated-pyridinium terarylenes (examples in Figure 81) have been considered for this project. In fact, it has been explained in Chapter 1 that some studies in the literature have reported a decrease of the quantum yields as a consequence of this type of functionalization.

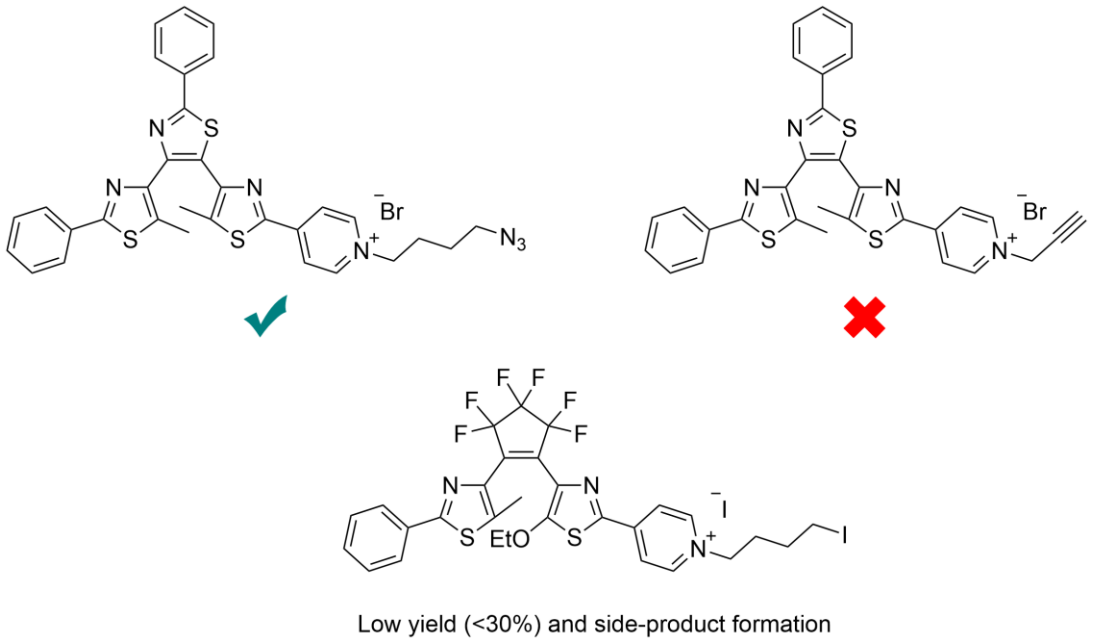

Figure 81: Structures of the cationic derivatives that have been initially considered for the project. The green tick indicates that the photochrome could be obtained; the red cross indicates that the product couldn't be prepared in the different experimental conditions that were attempted.

However, the synthesis of these cationic derivatives revealed to be occurring with high-to-moderate yields or not working at all in the attempted experimental conditions. Moreover, the introduction of multiple positive charges in a small "test" dendron made the purification by column chromatography difficult. Consequently, another route to achieve low photocyclization quantum yields has been selected.

As it has been explained in the previous Chapter, a control over the photocyclization quantum yield can be exerted by exploiting the charge transfer character obtained by introduction of electron-withdrawing and donating groups. Eventually, in accordance with the proposed correlation, terthiazole **SWIST1** has been synthesized and fully characterized, so to be used in this project (Figure 82).

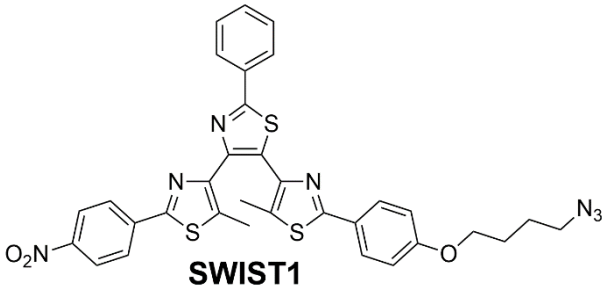

Figure 82: Investigated terarylene for the development of the molecular architectures showing light-induced fluorescence hysteresis.

3.3 Synthesis and characterizations

3.3.1 Synthesis route

Starting from terarylene **6**, whose synthesis has been described in Chapter 2, the first step to obtain **SWIST1** has been the demethylation with boron tribromide (BBr_3) to restore the hydroxyl group (Figure 83).

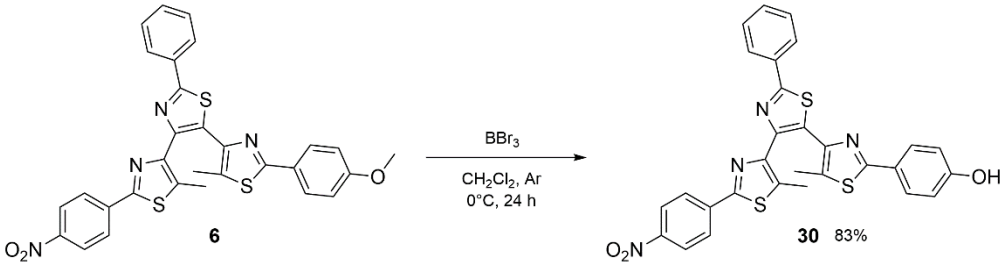

Figure 83: Synthesis of the photochromic intermediate **30**.

The alkyl chain has been introduced by using 1,4-dibromobutane in presence of a base such as potassium carbonate (K_2CO_3) in dimethylformamide (DMF), as depicted in Figure 84.

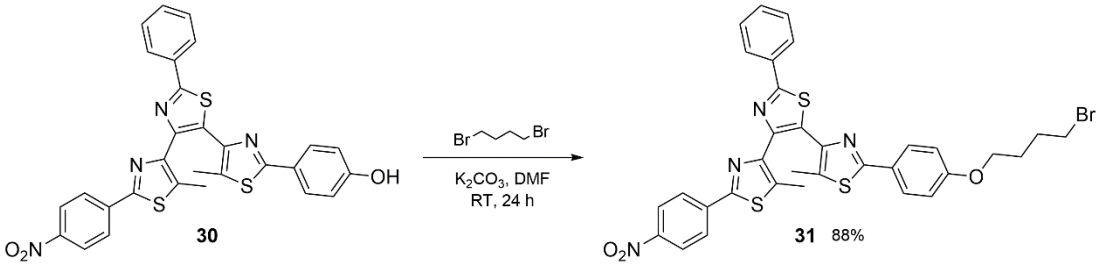

Figure 84: Synthesis of the photochromic intermediate **31**.

Finally, terthiazole **SWIST1** has been synthesized by exchanging the terminal bromide atom with an azide so to prepare a derivative suitable for click chemistry (Figure 85).

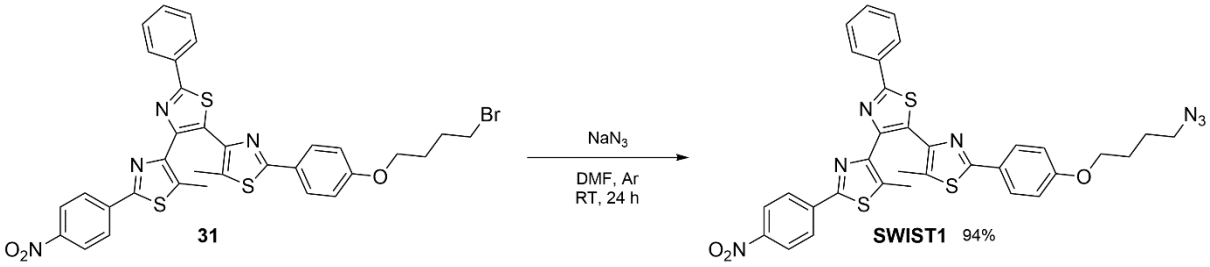

Figure 85: Synthesis of **SWIST1**.

The presence of such a functional group allows to afford molecular architectures as the one shown in Figure 86, whose synthesis has been carried out in ENS Paris-Saclay by Yang Zhou.

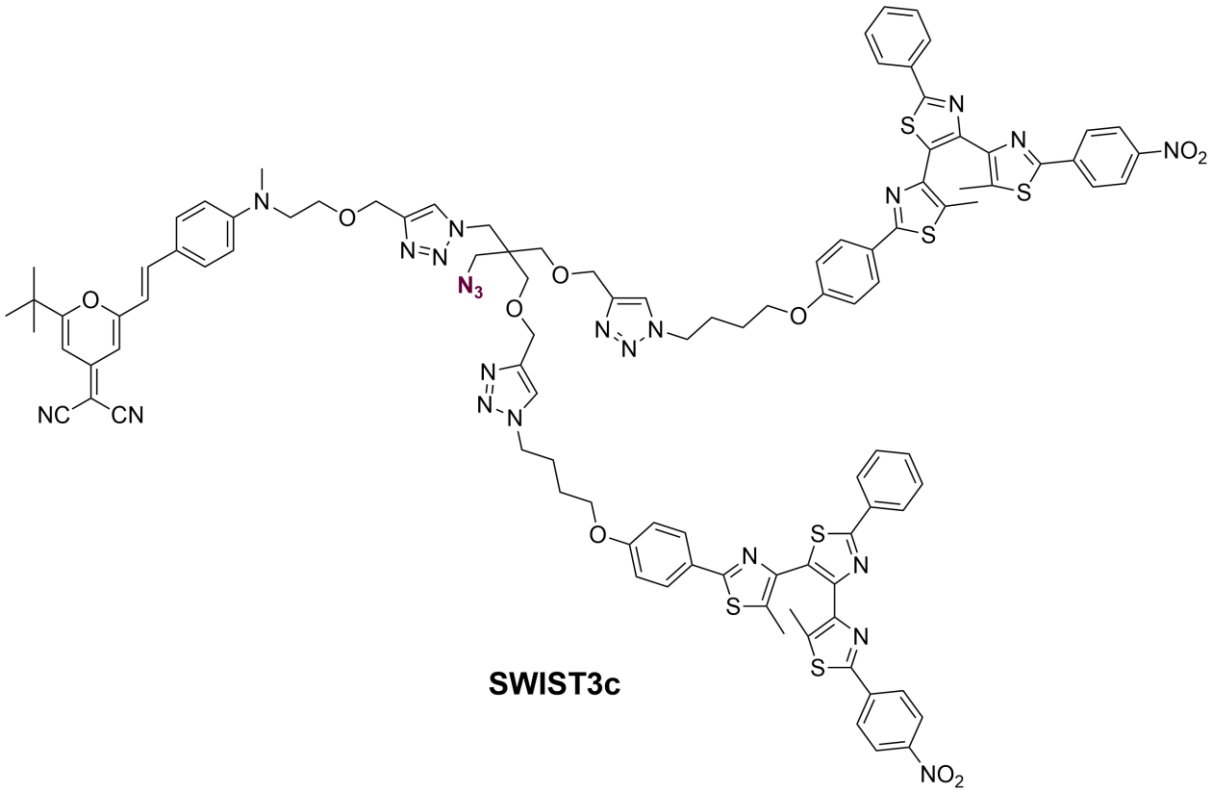

Figure 86: Example of achievable dendron by click chemistry with an aliphatic linker bearing the DCM unit.

An aliphatic linker bearing one DCM and two propargyl units has been reacted with 2 equivalents of **SWIST1** to prepare this first dendron (**SWIST3c**, where 3c stands for "three chromophores"). The presence of another azide group on the linker (indicated in prune in the Figure) allows the preparation of bigger architectures (i.e. 12, 42 or more chromophores) and the functionalization of O-propargyl- β-cyclodextrin.

3.3.2 Photochemical behavior

3.3.2.1 Stationary UV-vis spectroscopy, fluorescence and X-ray structure

Switch **SWIST1** has been investigated in acetonitrile at room temperature by irradiation at 320 nm and the corresponding spectra are provided in Figure 87.

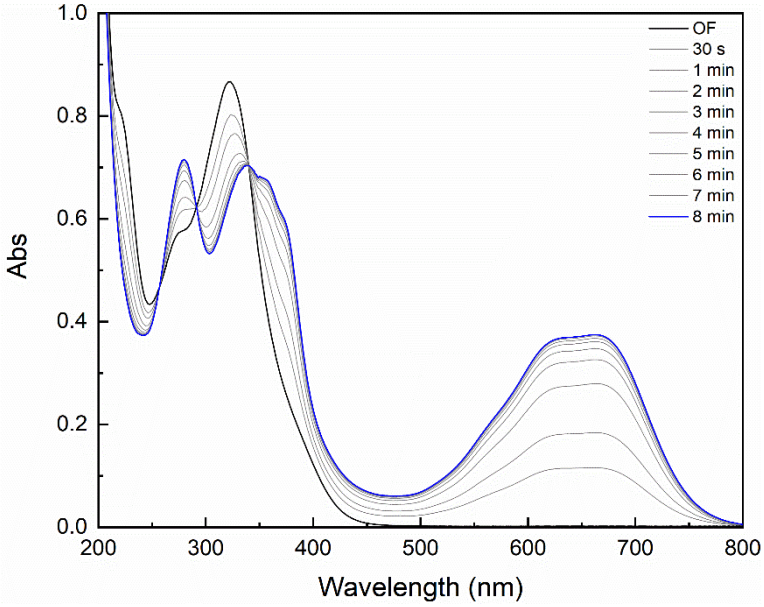

Figure 87: Absorption spectra of **SWIST1** (2.30 x 10^{-5} M) in acetonitrile, showing the evolution under UV light irradiation at 320 nm from the black line for the OF to the blue line indicating the reached photostationary state. Optical path of the cuvette: 1 cm.

The OF shows a very intense band at 322 nm while the band for the CF in the visible has a maximum absorption at 663 nm. These data are the same as those referring to photochrome **6** (see Chapter 2, Section 2.2.2.2, Table 1) and the spectra are actually superimposable. In fact, no significant difference was expected with the replacement of the methyl group on the oxygen atom with an azidobutyl chain and the quantum yields of **SWIST1** have been assumed to be similar to those determined for the photochromic reactions of the precursor **6**.

The possible fluorescence of the photochrome has been investigated, too. In fact, the emission of the terarylene, if present, would represent an additional process to take into account during the study of the fluorescence hysteresis in the multichromophoric system. An acetonitrile solution of **SWIST1** has been excited at 320 nm and the molecule didn't appear to be significantly fluorescent (the corresponding emission spectrum is provided in the Annexes, page 246).

Single crystals of **SWIST1** suitable for X-ray diffraction have been grown from acetone and distilled water (See the Annexes for the X-ray structure, page 246). No solid state reactivity has been detected for this terthiazole. The conformation is in fact parallel and the distance between

the two reactive carbons is 4.682 Å, above the limit to observe photochromism in the crystalline phase. [78]

*3.3.3 Theoretical modelling of **SWIST1***

To complete the characterization of this photochrome, DFT and TD-DFT calculations have been carried out in collaboration with Yang Zhou at ENS Paris-Saclay, so to apply functionals and basis sets in accordance with those used for the dicyanomethylene derivative and dendrons such as **SWIST3c**.

First, the geometries of the **SWIST1** in its open and closed forms have been optimized using PBE0/Def2SVP as functional. Since the solvent for the spectroscopic study of the DCM unit and **SWIST3c** is tetrahydrofuran (THF), it has been taken into account with IEFPCM.

Then, TD-DFT calculations have been performed by using CAM-B3LYP/Def2SVP always including the solvent in the computations. The accordance between the experimental spectra in THF and the theoretical ones is shown in Figure 88, where the most important calculated transitions are indicated with dashed lines.

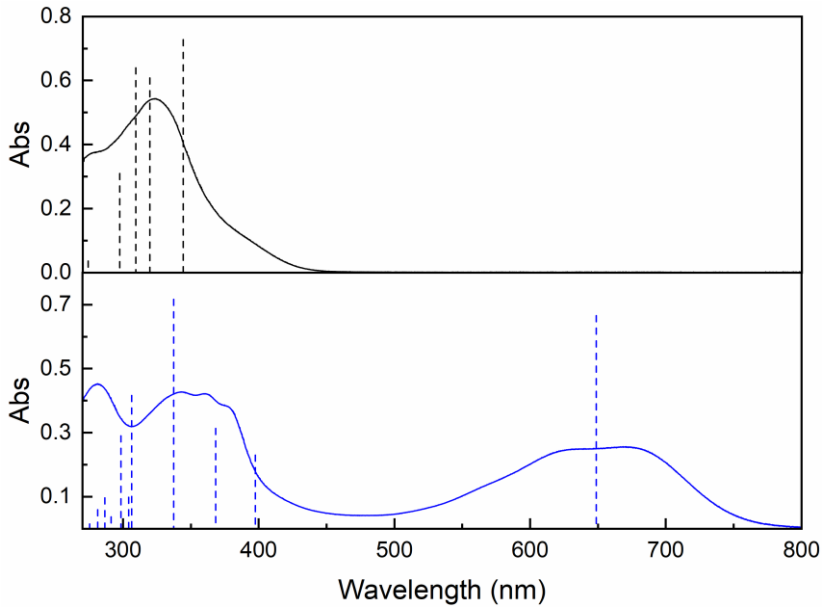

Figure 88: Experimental spectra of **SWIST1** (1.41 x 10^{-5} M) in THF (black solid line) in the OF and (blue solid line) at the PSS. The transitions determined by TD-DFT calculations are indicated in black solid lines for the OF and in blue solid lines for the CF. Optical path of the cuvette: 1 cm.

As it can be observed, the experimental spectra are well reproduced by the computations, thus validating the selected functional, that is suitable for molecules showing a CT character as **SWIST1**, as explained in the previous Chapter.

In fact, the lowest energy transition for the OF, which is HOMO → LUMO, a clear charge transfer is remarked (Figure 89).

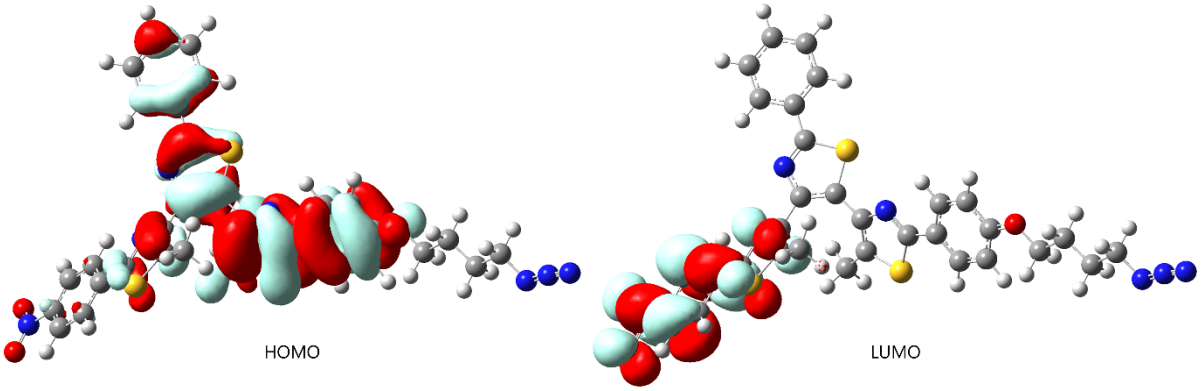

Figure 89: CAM-B3LYP/Def2SVP modelling of HOMO and LUMO of **SWIST1** in THF.

While the HOMO is mainly localized on the arm bearing the 4-azidobutoxy group and the central bridging unit, the LUMO is exclusively on the arm bearing the nitro group, as it has already been observed and described for the photochromic precursor **6** and the other donor-acceptor terarylenes in Chapter 2.

3.3.4 Preliminary studies on the fluorescence hysteresis

In this section, the results obtained by Yang Zhou at ENS Paris-Saclay on **SWIST3c** will be briefly described to provide a proof-of-concept about the achievement of the hysteresis. More details are available in his PhD thesis manuscript.

First, the photoinduced isomerization of the dendron has been investigated in THF at room temperature and the spectra evolution under irradiation at 335 nm has been monitored by UV-vis spectroscopy. Its fluorescence (λ_{exc} = 450 nm) has been recorded, too (Figure 90).

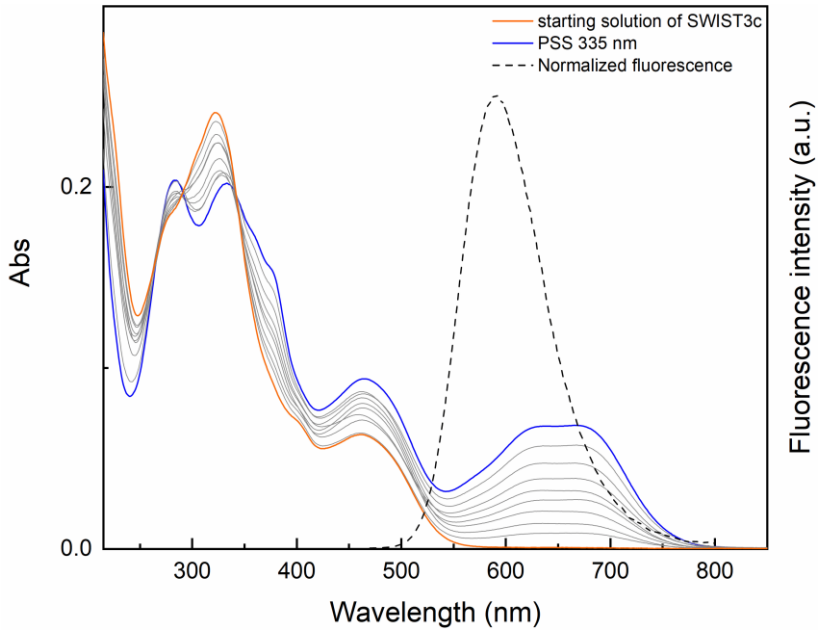

Figure 90: Absorption spectra of **SWIST3c** in THF, showing the evolution under UV light irradiation at 335 nm from the orange to the blue line indicating the reached photostationary state. The emission spectrum (λ_{exc} = 450 nm) is indicated with a black dashed line.

The band related to the DCM unit is observed at 485 nm and the characteristic emission of this fluorophore has been detected at 580 nm. Concerning the terarylene unit, the evolution of the bands in the UV region and between 600 nm and 700 nm resembles that of **SWIST1**.

The possibility of achieving the hysteresis has been verified by irradiating a THF solution of **SWIST3c** at 335 nm for 1 s followed by the recording of a UV-vis spectrum and then a fluorescence emission spectrum. Multiple points have been collected till the achievement of the PSS. Then, the back reactions have been induced by irradiation at 485 nm and several spectra have been recorded again. Finally, an irradiation at 635 nm has been carried out to guarantee the total cycloreversion of the terarylene units to the OF.

By plotting the data in terms of absorbance at 467 nm vs fluorescence intensity at 580 nm, the graph presented in Figure 91 has been obtained.

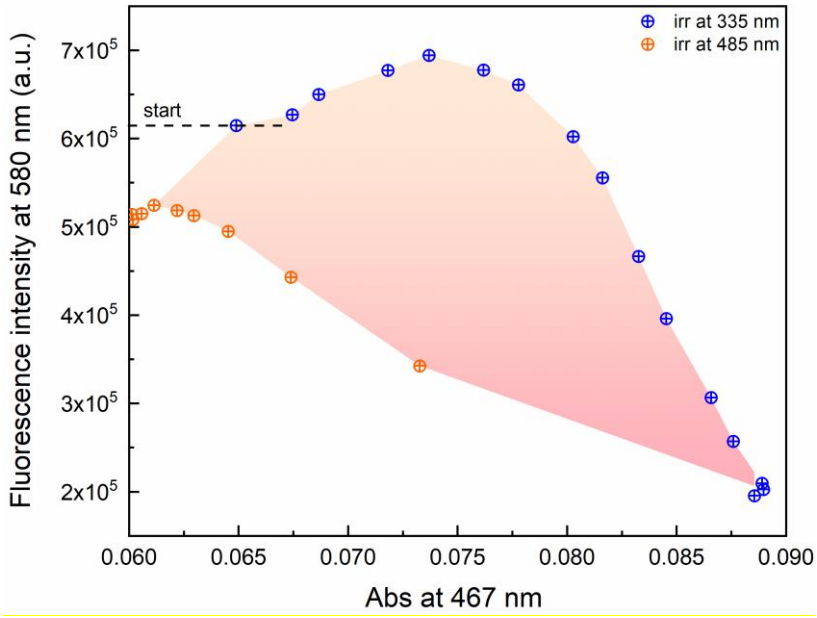

Figure 91: Plot of the fluorescence (at 580 nm) variation vs the absorbance at 467 nm of **SWIST3c** in THF, showing the evolution under UV light irradiation at 335 nm (blue circles) and under visible light irradiation at 485 nm (orange circles) and confirming the occurrence of the fluorescence hysteresis.

As it can be observed, the switchable light-induced fluorescence hysteresis could be achieved by combining the DCM unit with the low-$\Phi_{O\text{-}C}$-**SWIST1** terarylene. In fact, the fluorescence intensity initially increased thanks to the irradiation at 335 nm which promoted the *Z* → *E* isomerization. Then a progressive quenching of the fluorescence has been observed because of the generation of the closed forms of the two **SWIST1** units, which absorbed where the *E*-dicyanomethylene derivative was emitting. When the irradiation has been switched to 485 nm, the fluorescence was restored. However, a return to the initial state has not been achieved even after an irradiation at 635 nm to assure a cycloreversion of the terarylenes units to the open form. This might be ascribed to a photodegradation of the DCM unit, since the THF solution hadn't been degassed before the experiment.

These preliminary results confirmed that the designed terthiazole allowed to obtain a switchable fluorescence hysteresis when combined to a dicyanomethylene derivative and they are encouraging in the perspective of developing bigger molecular architectures with 12, 42 or more chromophores.

3.4 Conclusions

Applying the charge transfer approach developed in Chapter 2, a terphenylthiazole with appropriate electron-donating and accepting groups has been designed and fully characterized. This switches possesses not only an adequate, low photocyclization quantum yield, necessary for the target photoswitchable fluorescence hysteresis (ANR SWIST project), but it can also be readily functionalized with either an alkyl bromide or azido funtion without affecting significantly its main photochromic features.

The photoswitch has been successfully coupled with an appropriately functionalized DCM derivative at ENS Paris-Saclay (PhD thesis of Yang Zhou under the supervision of Dr. Métivier and Pr. Xie). Preliminary results of such a molecular system containing two terthiazoles and one dicyanomethylene chromophore showed the expected photoswitchable fluorescence hysteresis. More about the impact of the molecular architecture on the fluorescence hysteresis can be found in the PhD thesis of Yang Zhou.

Nicolò Baggi

Chapter 4: Design of redox-active terarylenes showing reductive or oxidative cyclization

Nicolò Baggi

4.1 Aim of the study

As presented in Chapter 1 (Section 1.4.1), among all the interesting features of diarylethenes, there is the possibility of driving the isomerization by an electrochemical stimulus in addition to light. Moreover, most studies have focused on the electron-rich dithienylethenes and their oxidation induced ring-closing or ring-opening reaction, while examples of reductive electrocyclization are rare. In particular, since reductive and oxidative cyclization had never been described for terarylenes, we decided to focus on this sub-class of compounds.

Concerning terarylenes, it is important to remember that in these systems the central unit is neither a cyclopentene ring nor a hexafluorocyclopentene one and that the replacement with an (hetero)aryl arm makes the closed forms of these derivatives less thermally stable than those of their diarylethene analogues.

In the first part of this Chapter, our investigation about the reductive cyclization of the appropriately N-methylpyridinium-substituted molecules depicted in Figure 92 will be described. In particular, the results obtained on **Red1**$^{2+}$ and **Red2**$^{2+}$ have been published in July 2021. [212]

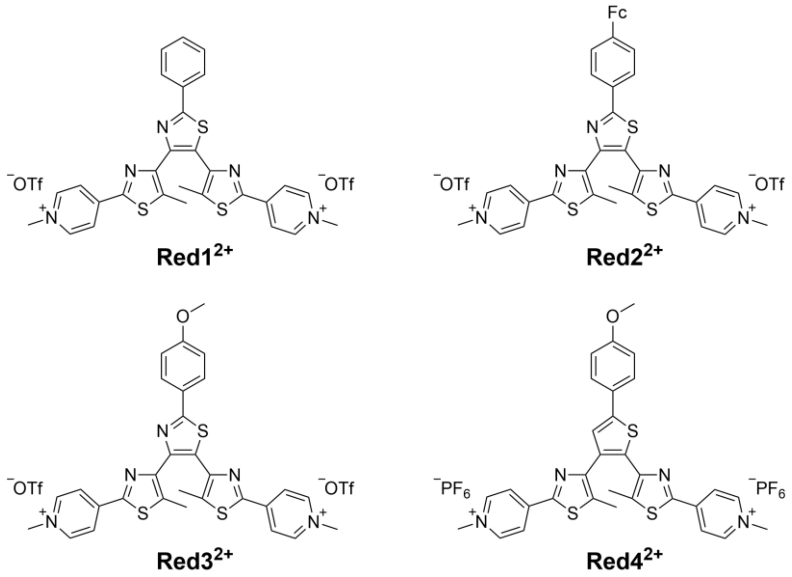

Figure 92: Investigated N-methylpyridinium-substituted terarylenes.

Red2^{2+}, **Red3**$^{2+}$ and **Red4**$^{2+}$ have been designed by exploiting the possibility of introducing a functionality even in the central (hetero)aryl arm of this DAE's sub-class. Ferrocene (Fc) has been chosen since it may provide a convenient way to tune the photo- and electrochromic properties of the switch as it can be reversibly switched between a diamagnetic electron donor (Fc) and a paramagnetic electron acceptor (Fc^+) via its redox chemistry. [213] Moreover, it can be used as covalently incorporated internal one-electron reference to determine the number of electrons that are involved in the redox processes.

Methoxy groups have been introduced in the other two switches to generate a CT character. Furthermore, **Red4**$^{2+}$ has been investigated to evaluate the possibility of observing the desired redox-active behavior also in the presence of a thiophene-based bridging unit.

The second part of this chapter will be dedicated instead to the photochromes that have been designed to verify the occurrence of oxidative cyclization.

Ox1 – **Ox6** contain thiophene rings, similarly to the DTEs that are known in the literature and that have been cited in Chapter 1 to explain this redox-active behavior (Figure 93). Various electron-donating groups have been introduced in *para* position to evaluate the impact on the electrochemical properties. **Ox2** has been functionalized differently (i.e. methoxy groups in *ortho* position), so to study how the position of the substituent influences the potential oxidative cyclization. Functionalization either in *ortho* or in *para* is provided with **Ox3**.

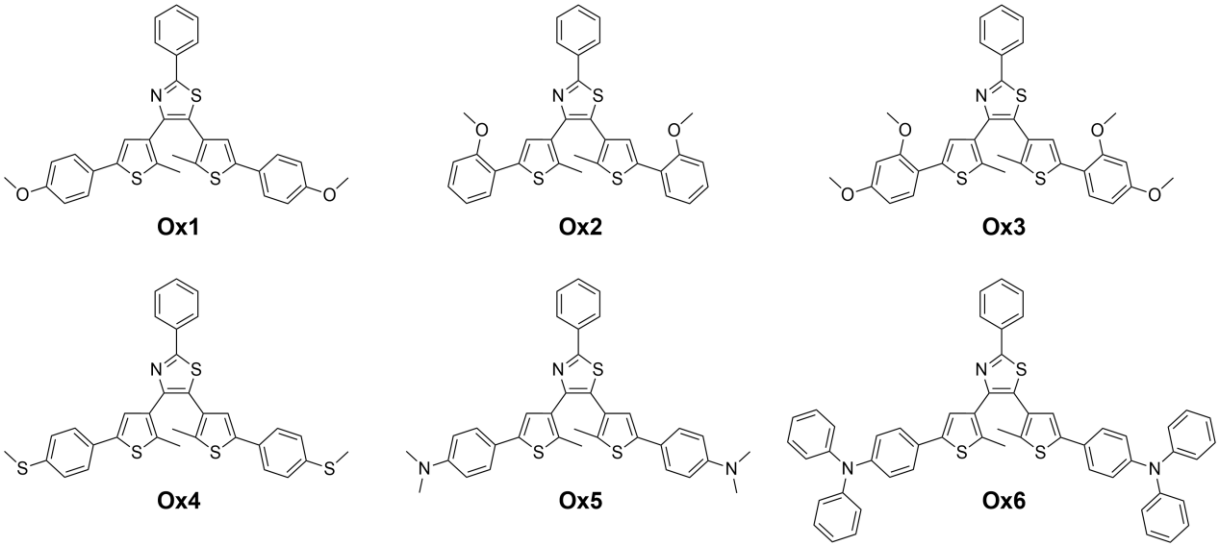

Figure 93: Investigated family of terarylenes bearing thiophene-based arms to study oxidative cyclization.

Ox7 – **Ox10** are terthiazoles, instead (Figure 94). Concerning the photochromic properties, thiazoles are interesting alternatives to thiophenes because they generally guarantee higher thermally-stable closed forms (since $ASE_{thiazole} < ASE_{thiophene}$ [214]) and better photoresistance (since thiazole is electron-poorer than thiophene).

However, as it has been explained previously, these electron-deficiency makes the oxidative cyclization difficult and only one example in the literature has demonstrated its feasibility in thiazole-containing systems, showing that the functionalization with strong electron-donors is mandatory. [118] Consequently, the effect of introducing functional groups in the shown terarylenes from the moderate electron-donating $–SCH_3$ up to $–N(CH_3)_2$ has been investigated in the attempt of achieving such a dual-responsive behavior.

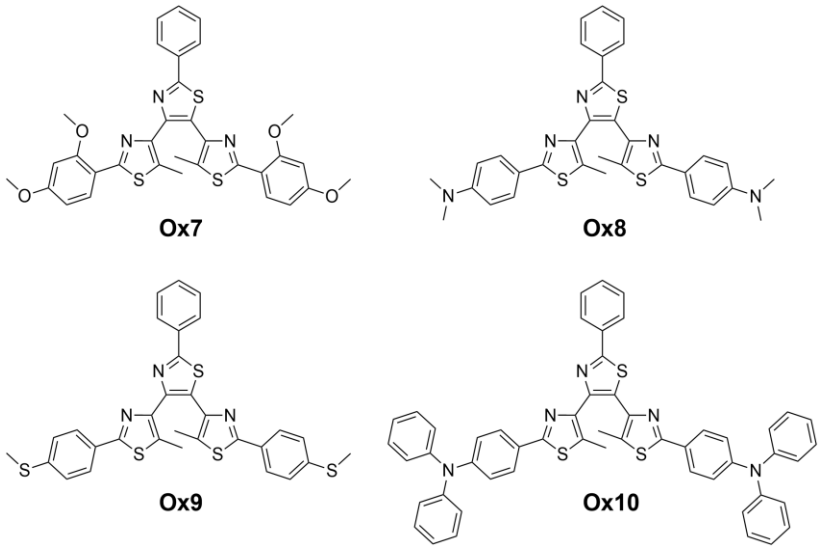

Figure 94: Investigated family of terarylenes bearing thiazole-based arms to study oxidative cyclization.

Finally, **Ox11** (Figure 95) represents the "bridging molecule" between the two studied families and it has been synthesized and characterized to evaluate what kind of electrochemical behavior is obtained in a mixed system.

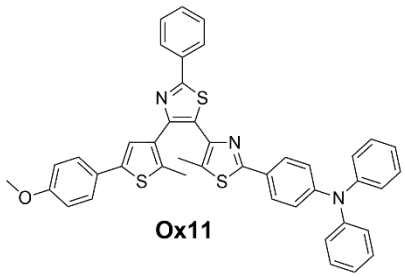

Figure 95: Investigated mixed terarylene bearing a thiazolyl-based and a thienyl-based arm.

4.2 Synthesis and characterizations of the photochromes designed for reductive cyclization

4.2.1 Synthesis route

In order to synthesize the terarylene **Red1**, the precursor 2-(4-pyridyl)-4-bromo-5-methyl-thiazole (**35**) has been initially obtained as shown in Figure 96.

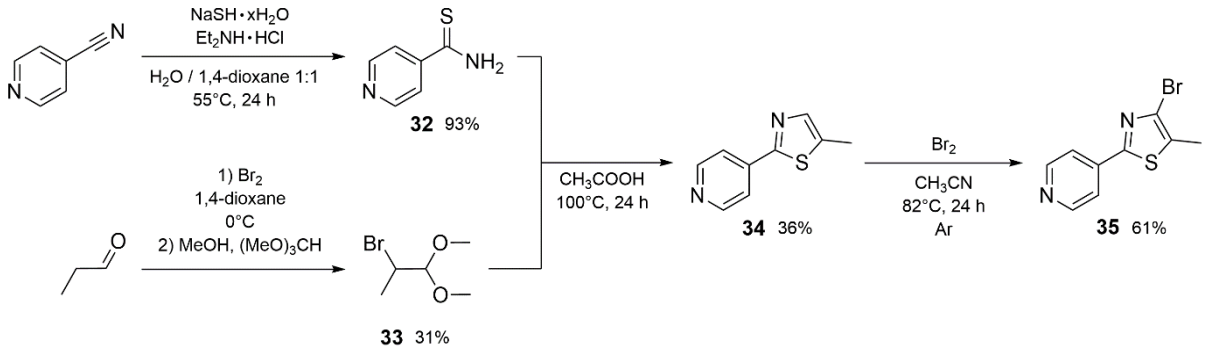

Figure 96: Synthesis route to intermediate **35**.

All the involved intermediates are known. The depicted steps have been consequently carried out by following (or slightly modifying) procedures described in the literature: for example, the thioamide (**32**) has been synthesized from the corresponding 4-cyanopyridine under Boys and Downs conditions [215] and **35** has been obtained as described by Irie and Takami, but by using only CH_3CN and not CH_3CN / $CHCl_3$ 1:1 as solvent mixture. [216]

Finally, **35** has been used to prepare the boronic acid pinacol ester **36** (Figure 97).

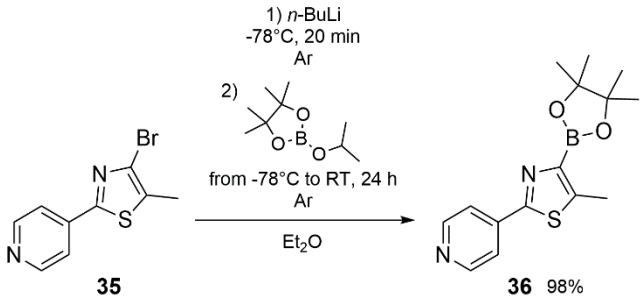

Figure 97: Synthesis of boronic acid pinacol ester **36**.

The needed bridging unit to complete the terthiazole skeleton has been synthesized through Halogen-Dance reaction (see Chapter 2, Section 2.2.1) by using 1,2-dibromo-tetrachloroethane as Br^+ source (Figure 98).

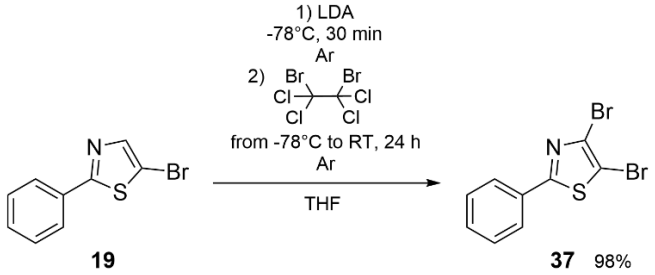

Figure 98: Synthesis of intermediate **37**.

Eventually, the neutral photochrome **38** has been obtained through double Suzuki-Miyaura coupling, as shown in Figure 99.

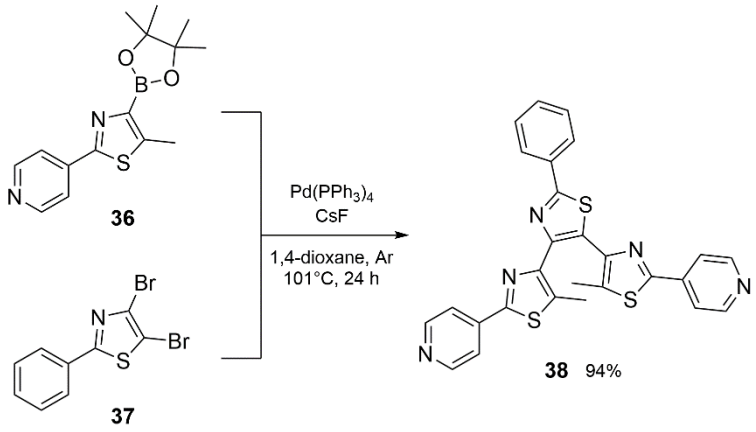

Figure 99: Synthesis of neutral photochrome **38**.

An excess of iodomethane (CH_3I) has been used to methylate the two pyridyl rings before exchanging the iodides with silver triflate (AgOTf) to afford **Red1**$^{2+}$, that bears two triflates as counter anions (Figure 100).

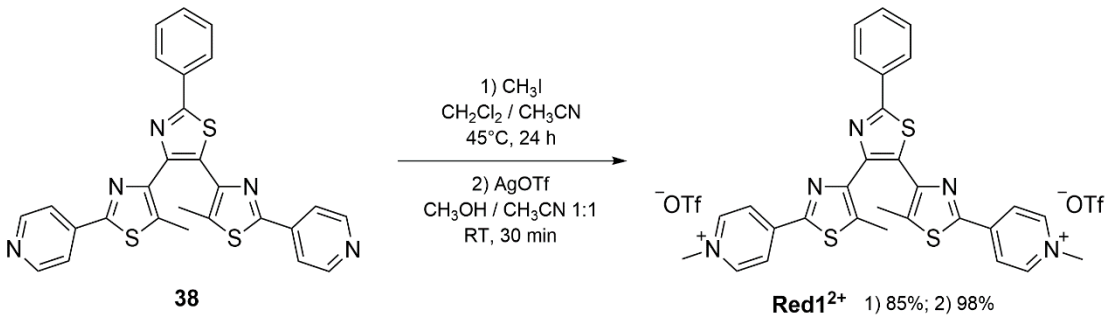

Figure 100: Synthesis of dicationic photochrome **Red1**$^{2+}$.

In the case of terthiazole **Red2**$^{2+}$, it has been necessary to prepare the Fc-containing bridging unit by adapting the procedure described by Lang and co-workers [217] on 2-(4-bromo)-phenyl-thiazole (whose preparation in described in the literature [218]), as depicted in Figure 101.

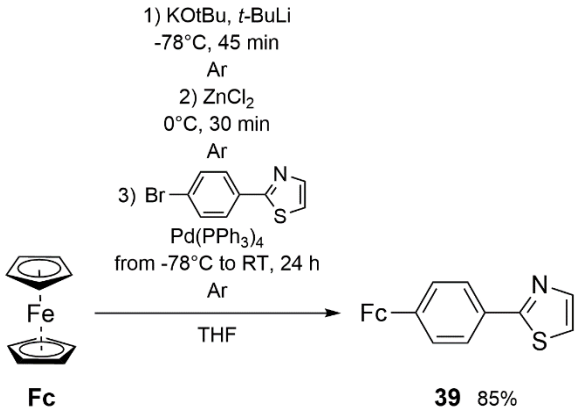

Figure 101: Synthesis of intermediate **39**.

Since it is not possible to introduce a bromine atom in C_5 of the thiazole ring neither by using Br_2 nor NBS as the electron-rich ferrocenyl part would be involved, a double Halogen Dance reaction with 1,2-dibromo-tetrachloroethane as brominating agent has been realized to prepare the dibrominated derivative **40** (Figure 102). Moreover, it has been possible to combine the two halogenation steps in a one-pot procedure.

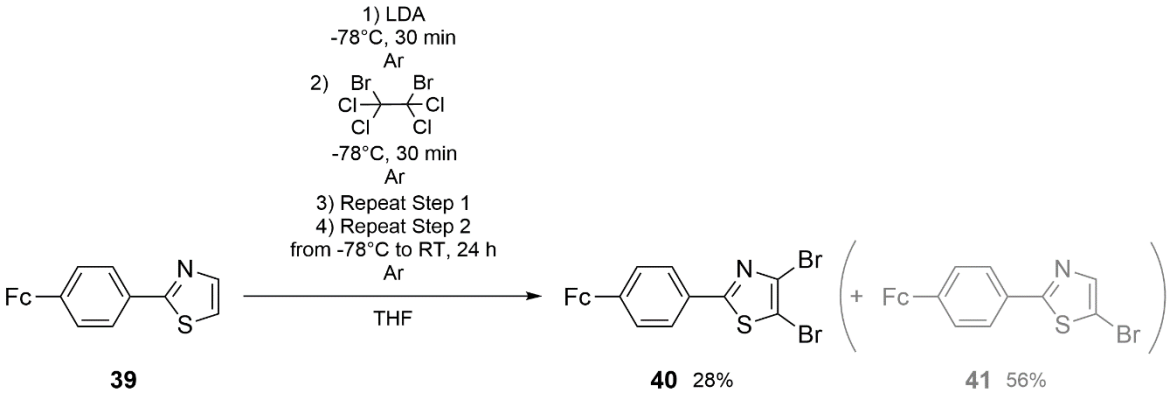

Figure 102: Synthesis of intermediate **40**.

The experimental conditions haven't been optimized and the main product is the monobrominated species (in grey in the Figure above). Nevertheless, this compound can be used as substrate in a classical HD reaction to obtain **40**.

Finally, terthiazole **Red2**$^{2+}$ has been synthesized by double Suzuki-Miyaura cross-coupling followed by bis-N-methylation and anion exchange (Figure 103).

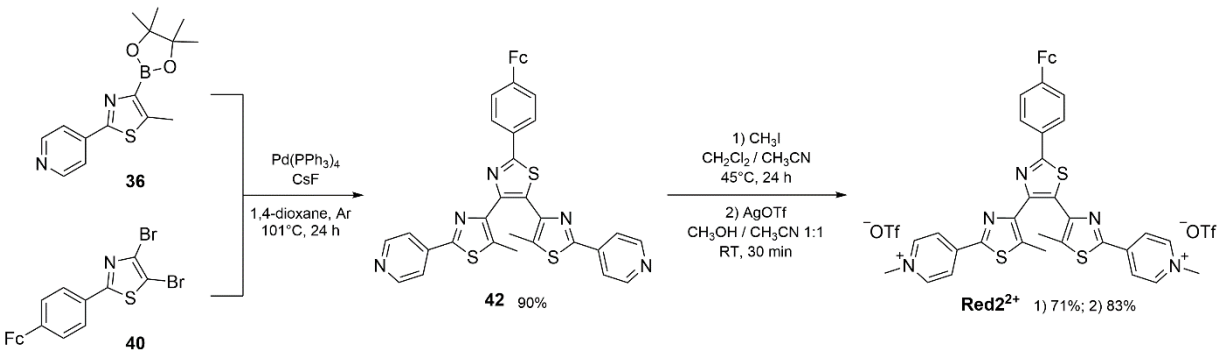

Figure 103: Synthesis route to dicationic photochrome **Red2**$^{2+}$.

Red3^{2+} has been obtained similarly, since the only difference is about the bridging unit, that has been synthesized as depicted in Figure 104.

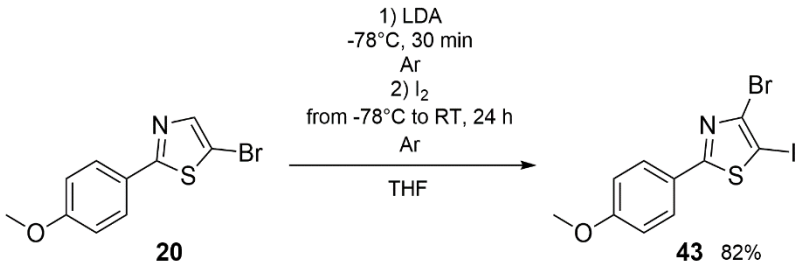

Figure 104: Synthesis of intermediate **43**.

The next steps are similar to those described for the other two dicationic derivatives (Figure 105).

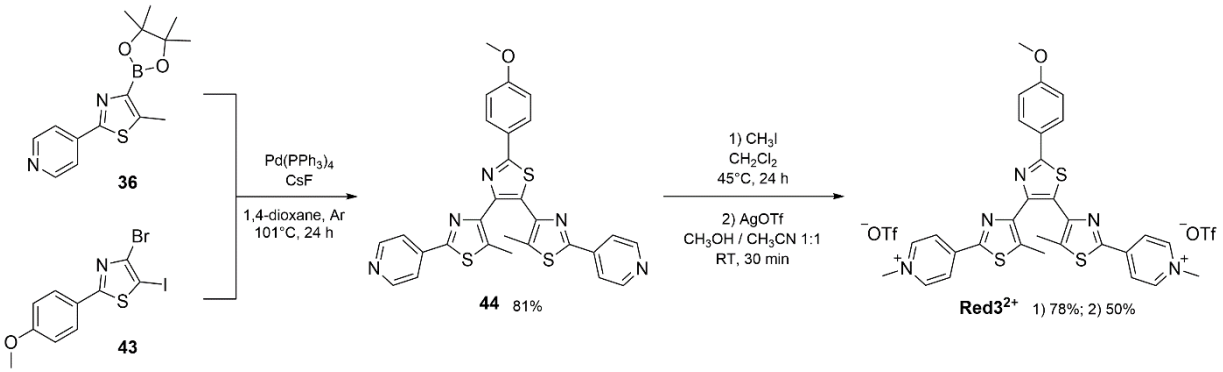

Figure 105: Synthesis route to dicationic photochrome **Red3**$^{2+}$.

Finally, in the case of **Red4**$^{2+}$, the bridging unit has been prepared by following the procedure described in the literature by Mori and co-workers (Figure 106). [219]

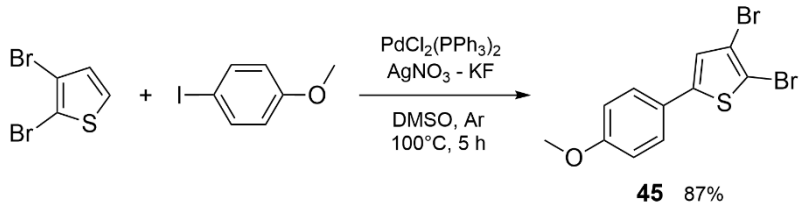

Figure 106: Synthesis of intermediate **45**.

Once again the desired photochrome has been obtained by double cross-coupling reaction followed by N-methylation of the pyridyl rings and iodide exchange (Figure 107). However, this last step has been carried out with KPF_6 in this case because the halide-containing dicationic intermediate couldn't be easily isolated, making the experimental conditions based on this salt preferable.

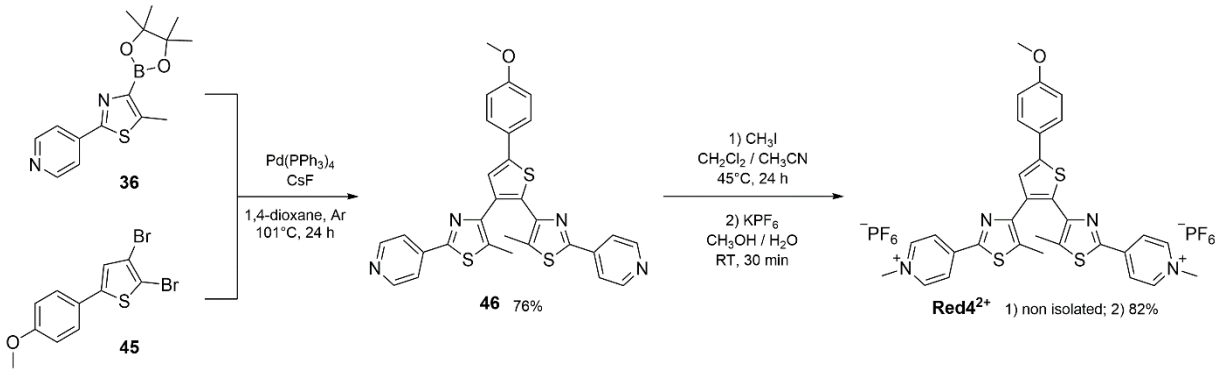

Figure 107: Synthesis route to dicationic photochrome **Red4^{2+}**.

*4.2.2 Photochemical and redox-active behavior of **Red1**$^{2+}$ and **Red2**$^{2+}$*

4.2.2.1 Stationary UV-vis spectroscopy, fluorescence and X-ray structure

The photochromic behavior of the dicationic terthiazoles **Red1**$^{2+}$ and **Red2**$^{2+}$ and their neutral precursors **38** and **42** have been investigated in acetonitrile at room temperature using steady-state absorption spectroscopy and their main photochromic data are listed in Table 5.

Table 5: Main photochromic data in acetonitrile of the investigated neutral and dicationic terarylenes.

	λ_{max} [nm] (ε [M^{-1} cm^{-1}])				
	OF	CF	Φ_{O-C}	α_{CF} (λ_{irr})	Φ_{C-O}
38	272 (26990) 319 (30360)	264 (28000), 308 (19465), 373 (18690), 632 (13540)	0.36	0.94 (320 nm)	0.015
Red1^{2+}	257 (20180) 322 (28900) 375 (17290)	277 (32780) 420 (10370) 744 (17430)	0.15	0.95 (365 nm)	0.002
42	294 (49310) 329 (60635) 455 (3540)	/	/		/
Red2^{2+}	340 (42775)	/	/		/

Only **38** and **Red1**$^{2+}$ show photochromism. On the contrary, Fc-containing derivatives **42** and **Red2**$^{2+}$ are non-photochromic and very poorly photochromic, respectively. The corresponding spectra are shown in Figure 108, where those of the OFs are indicated with black solid lines, the photostationary states reached under UV light irradiation (320 nm for **38** and **42**, 365 nm for **Red1**$^{2+}$ and 340 nm for **Red2**$^{2+}$) are in blue solid lines and the calculated spectra for the pure CFs are in blue dashed lines.

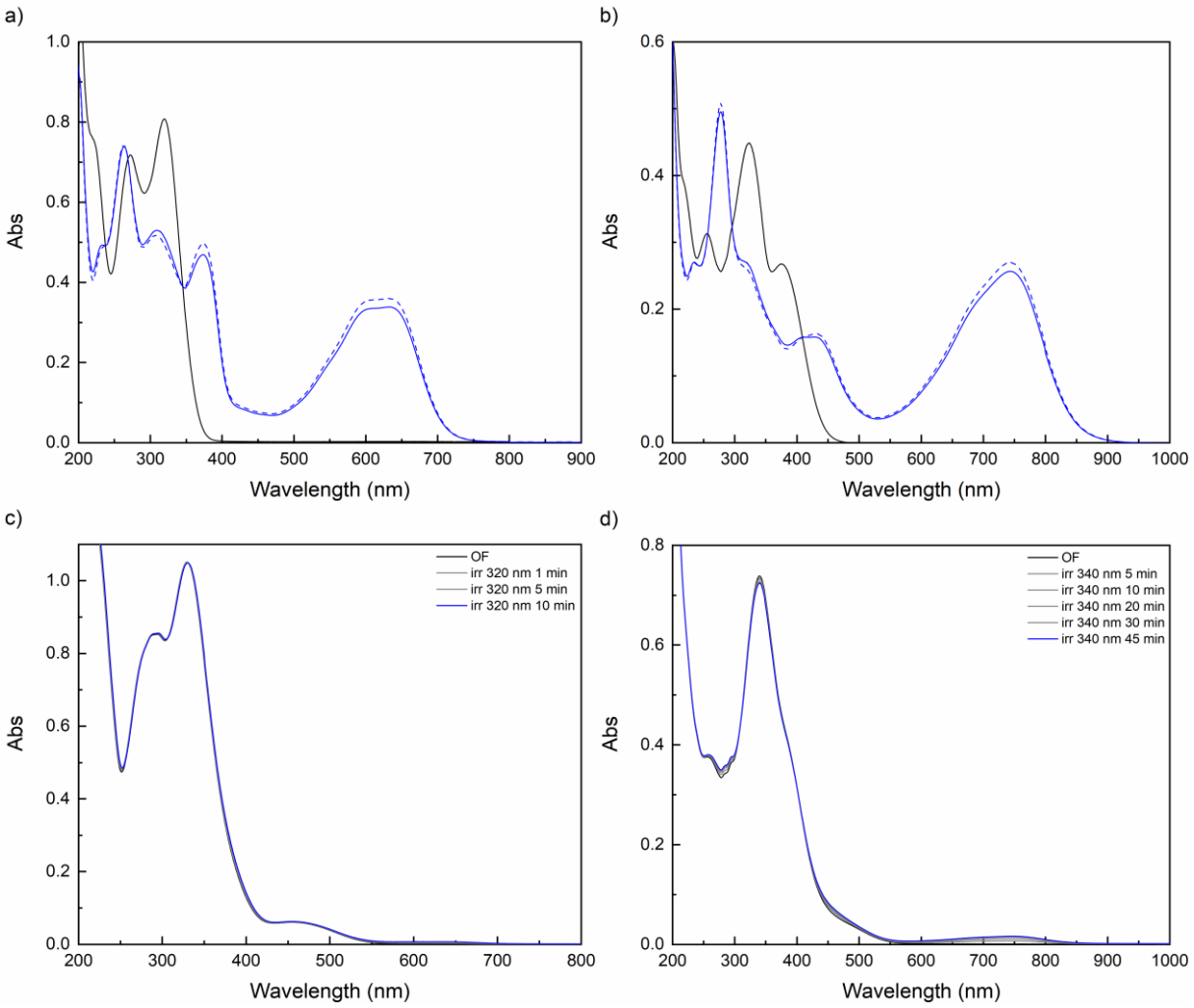

Figure 108: Absorption spectra in acetonitrile of (a) **38** (2.66 x 10^{-5} M), (b) **Red1^{2+}** (1.55 x 10^{-4} M), (c) **42** (1.73 x 10^{-5} M), (d) **Red2^{2+}** (1.73 x 10^{-5} M), showing the behavior under UV light irradiation (at 320 nm for **38** and **42**, at 365 nm for **Red1^{2+}** and at 340 nm for **Red2^{2+}**) from the black lines for the OFs to the blue lines to indicate the respective photostationary states. Optical path of the cuvette: 1 cm for **38**, **42** and **Red2^{2+}**; 1 mm for **Red1^{2+}**.

By comparing the optical properties of **38** and **Red1^{2+}**, it has been observed that the N-methylation had three marked effects on the photochromic properties:

1. Significant red-shift of the main absorption bands of the dicationic terthiazole in both its open and closed forms compared to those of the neutral precursor.
2. Decrease of the cyclization and cycloreversion quantum yields from 0.36 to 0.15 and from 0.015 to 0.002, respectively. A similar effect had been observed by our group previously (see ref. [121] in Chapter 1, Section 1.3.2.2).
3. Reduced thermal stability of the closed form isomer (**Red1c^{2+}**). While **38** is a P-type photochrome at room temperature, the bis-methylated species slowly reverted back to the open form in the dark. This is probably due to the weakening of the newly formed C-C single bond caused by the two strongly electron-withdrawing N-methylpyridinium groups.

In particular, by monitoring this thermal decay at different temperatures, an activation energy (E_a) of 94 kJ/mol for the thermal cycloreversion has been found. The half-lifetime ($\tau_{1/2}$) has been estimated to be of ~2 h at room temperature and ~6 h at 15°C.

Additionally, **Red1**$^{2+}$ is weakly fluorescent (emission spectrum in the Annexes, page 247). By exciting the molecule at 365 nm, an emission at 630 nm has been observed, with a quantum yield of ca. 1.2% that has been determined by using quinine sulfate in H_2SO_4 0.5 M as reference. Since the CF isomer is not fluorescent, the fluorescence turned off with the cyclization.

As said, the neutral ferrocene-substituted terthiazole **42** didn't show any isomerization under UV light irradiation, thus indicating that photochromism has been quenched by introducing the ferrocene group. This moiety has been oxidized to ferrocenium (Fc^+) by adding 1.5 eq of $Cu(OTf)_2$ to observe a slight light-induced spectral change. The same has been done to enhance the photochromism of **Red2**$^{2+}$ (spectra evolutions are provided in the Annexes, page 248).

For both the derivatives, the improvement is not comparable to that reported for redox-gated photochromism. [220] Nevertheless, it might be assumed that the quenching of the photochromic behavior is related to a charge transfer character that is developed with the introduction of electron-rich ferrocene into these rather electron-poor terthiazoles. Since CT is detrimental to the photocylization, an increase in reactivity can be expected when generating Fc^+.

Single crystals of **Red1**$^{2+}$ have grown by slow evaporation of a dichloromethane solution (the determined structure is shown in the Annexes, page 248). However, no photochromic activity has been observed. In fact, even if the conformation couldn't be unambiguously recognized, the distance separating the two reactive carbon atoms (C11 and C21) is 5.32 Å, largely above the limit for the observation of crystalline state photochromism (i.e. 4.2 Å). [78]

4.2.2.2 Electrochemical properties

The electrochemical properties of the four photochromes have been investigated by cyclic voltammetry (CV) at room temperature in acetonitrile / $TBAPF_6$ 0.1 M with a scan rate (ν) of 100 mV/s. The main data (i.e. half-wave potentials, $E_{1/2}$, and ΔE for reversible waves; peak potentials, E_p, for irreversible ones) referenced to a saturated calomel electrode (SCE) are reported in Table 6. In the case of neutral Fc-containing **42**, acetonitrile / dichloromethane 8:2 has been used as solvent mixture to guarantee a complete dissolution.

Table 6: Redox potentials vs SCE in CH_3CN / $TBAPF_6$ 0.1 M of the four investigated terarylenes.

	OF		CF	
	$E_{1/2}$ or E_p (V)	ΔE (mV)	$E_{1/2}$ or E_p (V)	ΔE (mV)
38	1.50 (irr)	/	0.90 (irr) 1.50 (irr) -0.88 -1.22 (qr)	/ / 70 100
Red1^{2+}	-0.91 (qr)	/	1.10 (irr) -0.21	/ 52
42[a]	1.60 (irr) 0.48	/ 60	/	/
Red2^{2+}	1.60 (irr) 0.46 -0.90	/ 90 110	1.22 (irr) 0.46 -0.21	/ 90 56

[a] solvents: 20% dichloromethane in acetonitrile.

Cyclic voltammograms for neutral terthiazole **38** are presented in Figure 109. This derivative is not redox-active over a large range of the potential window of the electrolytic solution in its OF, which shows only an irreversible oxidation wave at 1.50 V. The closed form isomer is instead characterized by one irreversible oxidation at ~0.90 V and two quasi-reversible reduction waves at -0.88 and -1.22 V.

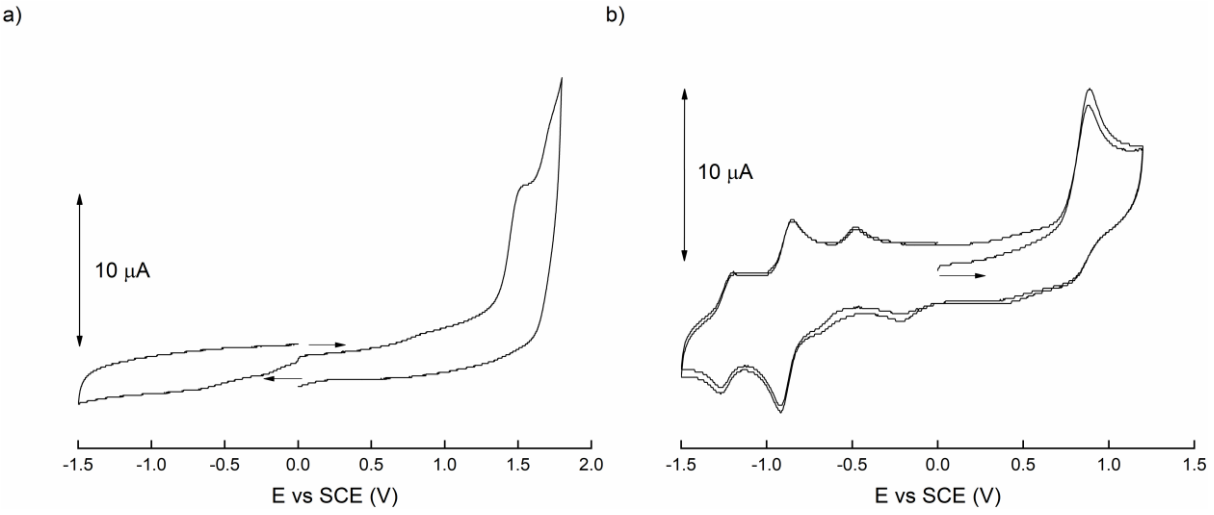

Figure 109: Cyclic voltammetry of **38** (1 mM) in CH_3CN / $TBAPF_6$ 0.1 M, (a) in the OF and (b) at the PSS, after irradiation at 365 nm. ν = 100 mV/s.

Differently from the cases about terarylenes that have been described in Chapter 1 - Section 1.4.1.1, no oxidative cycloreversion has been observed on the photogenerated CF.

In the case of **Red1**$^{2+}$, the open form isomer (**Red1o**$^{2+}$) doesn't show any oxidation waves. On the contrary, a quasi-reversible reduction wave is observed at $E_{1/2}$ = -0.91 V, as shown in Figure 110. On the back scan, one anodic peak appears at $E_{1/2}$ = -0.21 V, and its intensity grows at the expense of the initial one if multiple cycles are recorded. This new redox-active species corresponds to the dicationic closed form (**Red1c**$^{2+}$), as confirmed by the CV on the solution irradiated at 365 nm. In fact, it is characterized by the same two redox waves, with the relative intensity of the new one increasing with UV irradiation time at the expense of that related at $E_{1/2}$ = -0.91 V. This means that redox-active terthiazole **Red1**$^{2+}$ undergoes reductive cyclization.

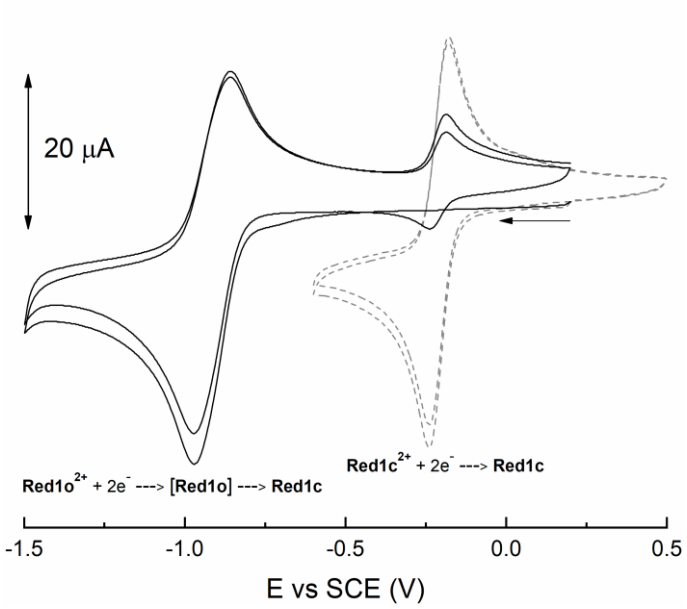

Figure 110: CVs of **Red1**$^{2+}$ (1 mM) in CH_3CN / $TBAPF_6$ 0.1 M in the OF (black solid lines) and at the PSS (grey dashed lines) indicating the reductive cyclization. ν = 100 mV/s.

Cyclic voltammetry at different scan rates has been carried out to estimate the kinetics of this redox-induced ring-closing reaction (Figure 111).

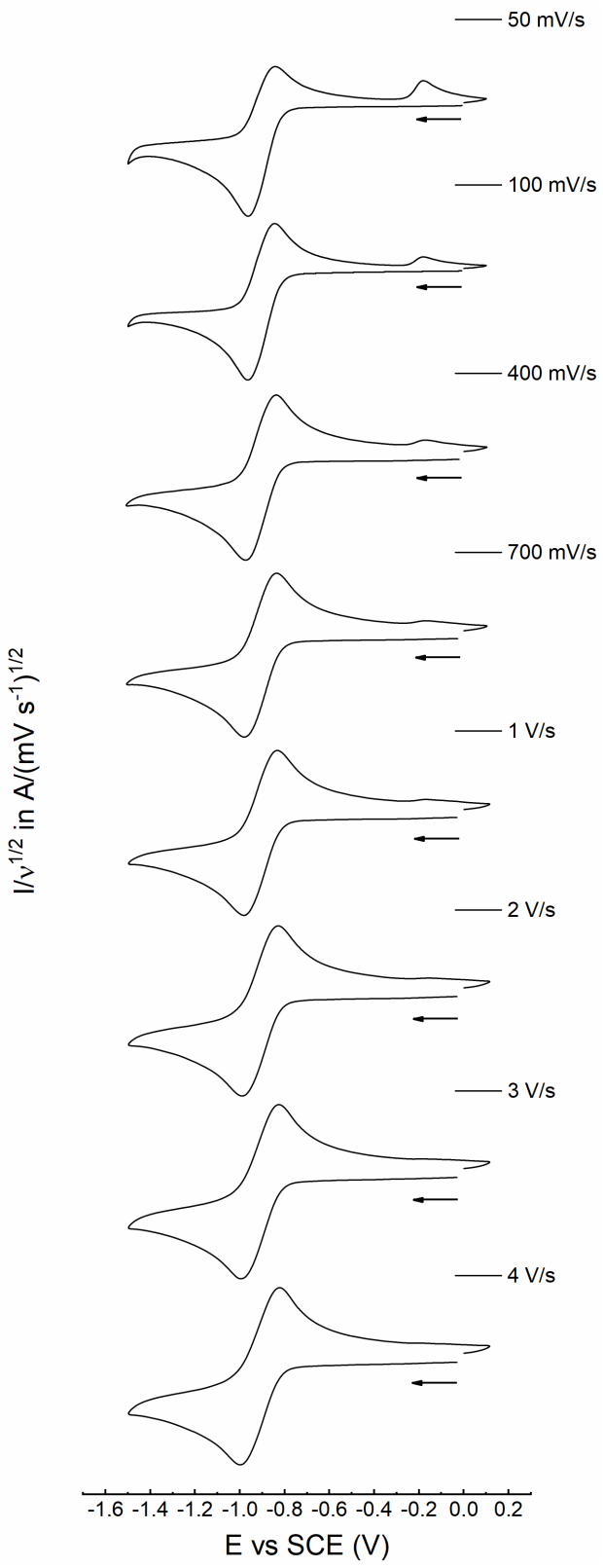

Figure 111: Reduction of **Red1o**$^{2+}$ (1 mM) in CH_3CN / $TBAPF_6$ 0.1 M at different scan rates.

The fact that the wave at -0.21 V gradually decreased by increasing the scan rate suggested that the process is quite slow. In particular, since the wave disappeared for ν = 3-4 V s^{-1}, the rate constant of the ring-closing reaction has been estimated to be in the range of ~10 s^{-1} by applying the following formula [221]:

$$k\ (s^{-1}) \leq 6\nu\ (V/s)$$

In addition to the reversible peak at –0.21 V, **Red1c**$^{2+}$ is also characterized by an irreversible wave at 1.10 V, as shown in Figure 112. The consequence of this oxidation to **Red1c**$^{3+}$ is a decrease of the intensity of the wave at -0.21 V and an increase of that at -0.91 V.

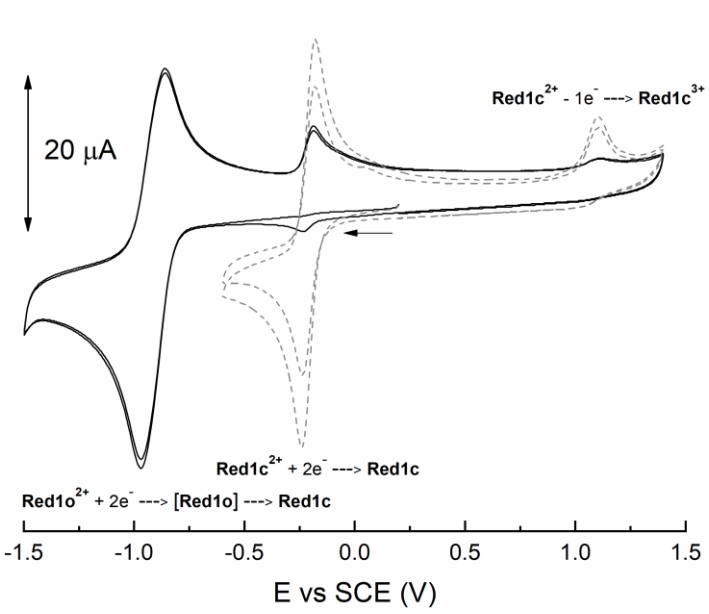

Figure 112: CVs of **Red1**$^{2+}$ (1 mM) in CH_3CN / $TBAPF_6$ 0.1 M in the OF (black solid lines) and at the PSS (grey dashed lines) indicating the reductive cyclization and the oxidative cycloreversion. ν = 100 mV/s.

This means that the oxidation at 1.10 V enhances the thermal ring-opening reaction of **Red1c**$^{2+}$, which is not otherwise detected on the time scale of cyclic voltammetry at room temperature. In fact, it has been shown that this species can be accumulated by performing multiple CV cycles. The irreversible oxidation peak at 1.10 V is consequently expected to cause a ring-opening: the generated **Red1c**$^{3+}$ reverts to **Red1o**$^{3+}$, a strong oxidant which is capable to immediately oxidize **Red1c**$^{2+}$ to **Red1c**$^{3+}$ while affording **Red1o**$^{2+}$, thus inducing a chain reaction.

Similarly to what has been done for the reductive ring-closing reaction, cyclic voltammetry at different scan rates has been performed to investigate this oxidative ring-opening process. By increasing the scan rate, it has been observed that the irreversible wave at 1.10 V became more reversible, meaning that also this reaction isn't very fast (Figure 113).

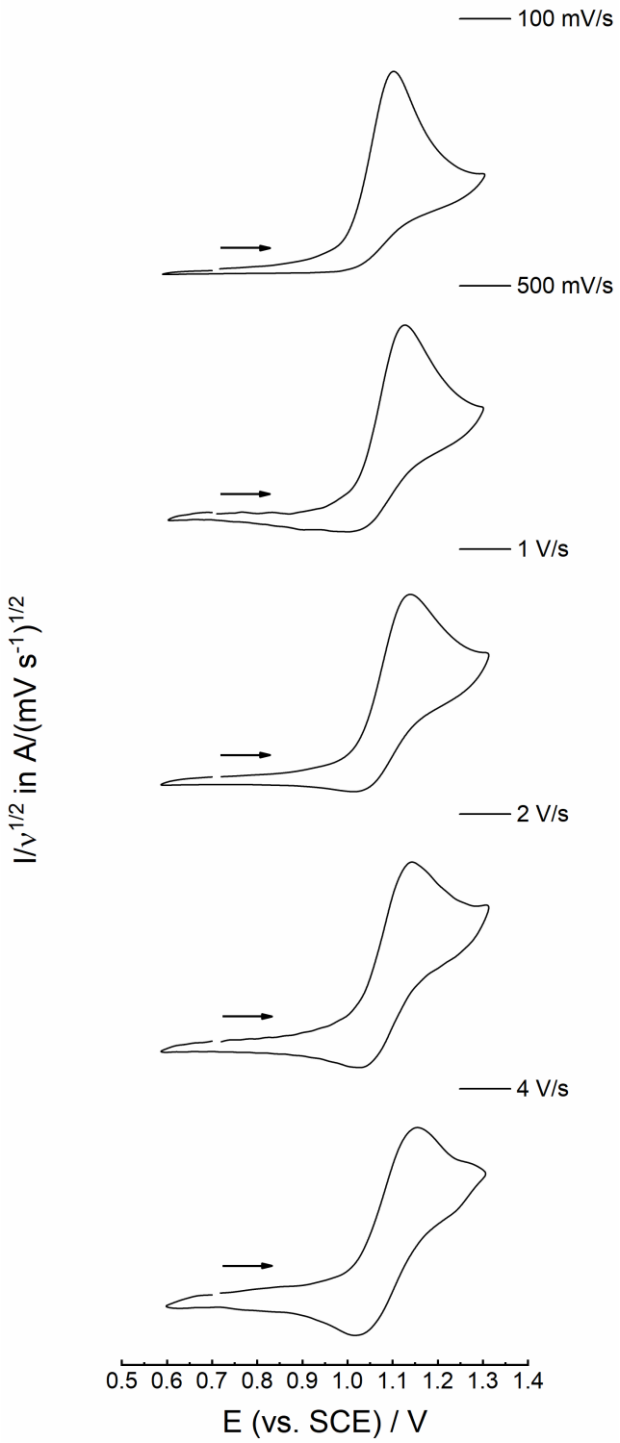

Figure 113: Oxidation of **Red1c^{2+}** (1 mM) in CH_3CN / $TBAPF_6$ 0.1 M at different scan rates.

In any case, the co-existence of reductive cyclization and oxidative cycloreversion makes **Red1^{2+}** the first-ever terarylene that fully operates photochemically as well as electrochemically.

Moving to the Fc-containing derivatives, neutral **42** is not electro-active toward reduction down to -1.5 V while it shows the reversible oxidation wave of ferrocene at 0.48 V. At higher potentials, an irreversible oxidation causing degradation has been observed (Figure 114).

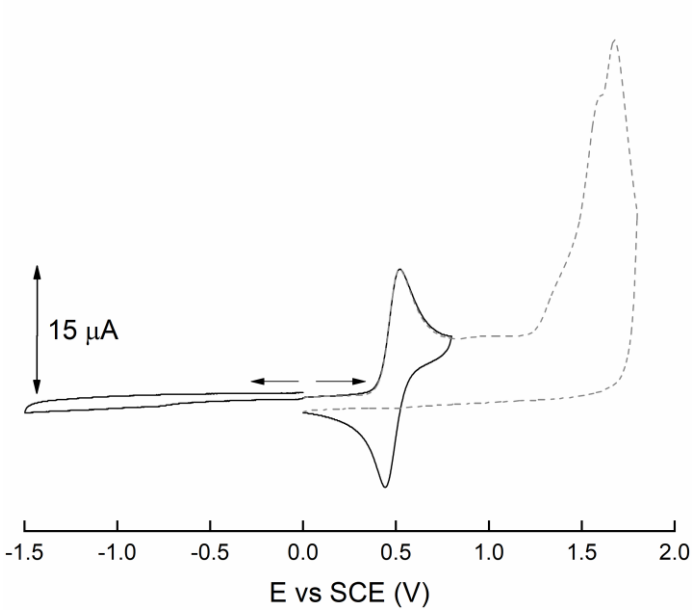

Figure 114: CVs of **42** (1 mM) in CH_3CN / CH_2Cl_2 8:2 / $TBAPF_6$ 0.1 M; (black solid lines) reduction up to -1.5 V and oxidation up to 0.8V; (grey dashed lines) oxidation up to 1.8 V leading to degradation. ν = 100 mV/s.

In the case of terthiazole **Red2**$^{2+}$, the obtained cyclic voltammogram when swiping to cathodic potentials is similar to that presented for **Red1**$^{2+}$. By oxidizing **Red2o**$^{2+}$, the reversible wave involving the ferrocenyl functional group has been observed instead (Figure 115).

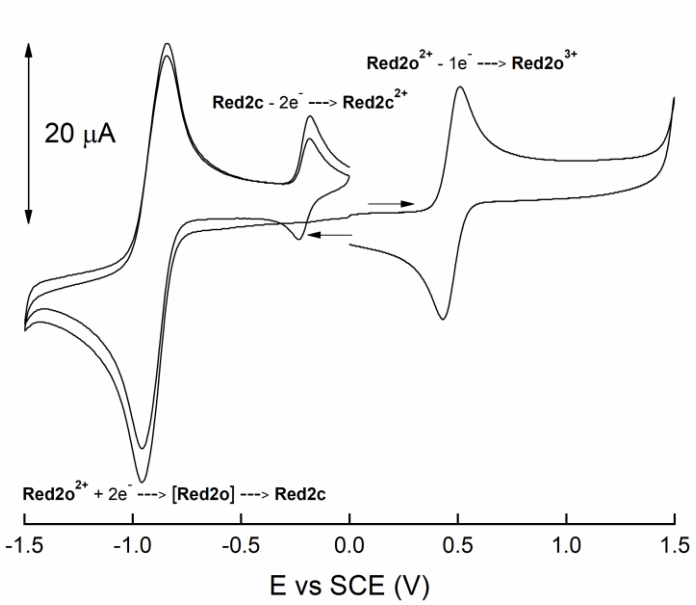

Figure 115: CVs of **Red2o**$^{2+}$ (1 mM) in CH_3CN / $TBAPF_6$ 0.1 M showing the reductive cyclization and the reversible oxidation of the covalently linked ferrocene unit. ν = 100 mV/s.

Reductive cyclization has been assumed to occur also in this case, as demonstrated by the appearance of a new reversible band that has been assigned to the **Red2c**$^{2+}$after the quasi-reversible reduction of the OF. It is important to remember that, differently from **Red1**$^{2+}$, this derivative is almost non-photochromic, so this dicationic species is not accessible photochemically.

Moreover, when the derivative has been reduced first and then oxidized up to 1.5 V, it has been possible to observe the Fc-centered oxidation wave followed by a second irreversible oxidation at ~1.22 V (Figure 116).

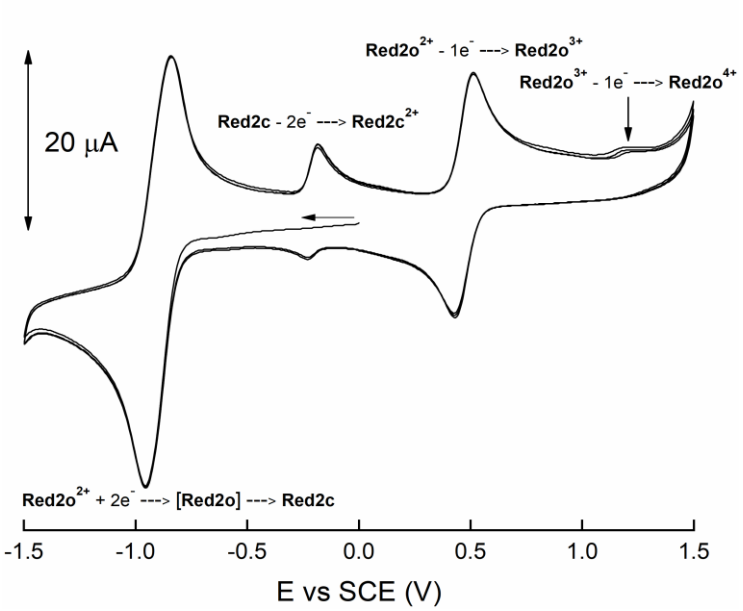

Figure 116: CV of **Red2o^{2+}** (1 mM) in CH_3CN / $TBAPF_6$ 0.1 M showing the reductive cyclization and the oxidative ring-opening. ν = 100 mV/s.

However, the cycloreversion appeared to occur even by stopping the oxidation after the generation of ferrocenium, thus meaning that the phenomenon could be induced at a much lower potential compared to **Red1^{2+}**, which needed an oxidation at 1.10 V (cyclic voltammogram in the Annexes, page 249). Nevertheless, no chain reaction is expected in this case because the redox potential for the reversible oxidation of ferrocene is the same for the two isomers. The thermal ring-opening is simply accelerated.

Finally, by taking advantage of Fc as one-electron reference, it has been concluded that **Red2o^{2+}**'s reduction wave (and consequently **Red1o^{2+}**'s one, too) is bielectronic, as well as the reversible wave at -0.21 V involving the CF isomer.

4.2.2.3 Spectroelectrochemical study of **Red1^{2+}**

Low-temperature spectroelectrochemistry has been carried out in collaboration with Dr. Anxolabéhère-Mallart (Université de Paris – LEM) to further investigate the redox-active behavior of terthiazole **Red1^{2+}** and to obtain additional evidences on the reductive cyclization and the oxidative cycloreversion that have been observed by cyclic voltammetry.

Furthermore, this experiment allows the identification of transient species to better understand the electrochemically induced ring-closing. In fact, the cyclization might occur on the one-electron reduced species as suggested by Branda and co-workers (see ref. [146] in

Chapter 1, Section 1.4.1.3) or after the bielectronic reduction, as described by our group (see ref. [121] in Chapter 1, Section 1.4.1.3).

A solution of **Red1**$^{2+}$ in acetonitrile / $TBAPF_6$ 0.2 M has been initially electrolyzed at -25 °C at -1.10 V. The induced spectral evolution has been followed by UV-vis spectroscopy (Figure 117).

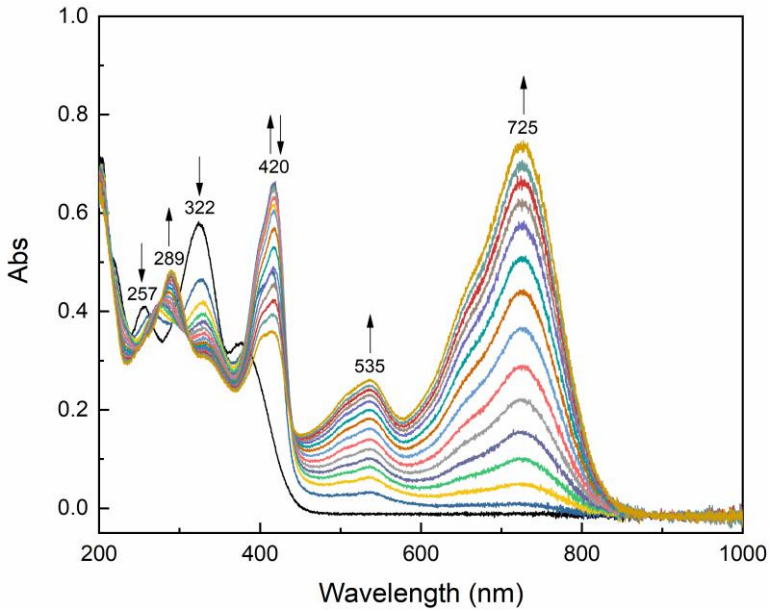

Figure 117: Absorption spectrum evolution of **Red1o**$^{2+}$ (1.75 x 10^{-4} M) in CH_3CN / $TBAPF_6$ 0.2 M under reduction at -1.10 V at -25°C. Optical path of the cuvette: 1 mm.

This reduction caused the decrease of the bands of **Red1o**$^{2+}$ at 257 nm, 322 nm and 375 nm with the concurrent appearance of two new bands at 535 nm and 725 nm, attributed to the neutral CF species (**Red1c**). Moreover, interesting information have been provided by the band at 420 nm, which initially grew and finally diminished in intensity with the progress of the electrolysis. In fact, as it will be shown in the section about the theoretical modelling, this band is related to the transient neutral open form (**Red1o**), thus indicating that the redox-induced cyclization occurs after the bielectronic reduction of **Red1o**$^{2+}$.

Next, an electrolysis has been carried out at 0.00 V to oxidize the generated **Red1c** so to afford the dicationic species and further confirm the occurrence of the reductive cyclization (Figure 118).

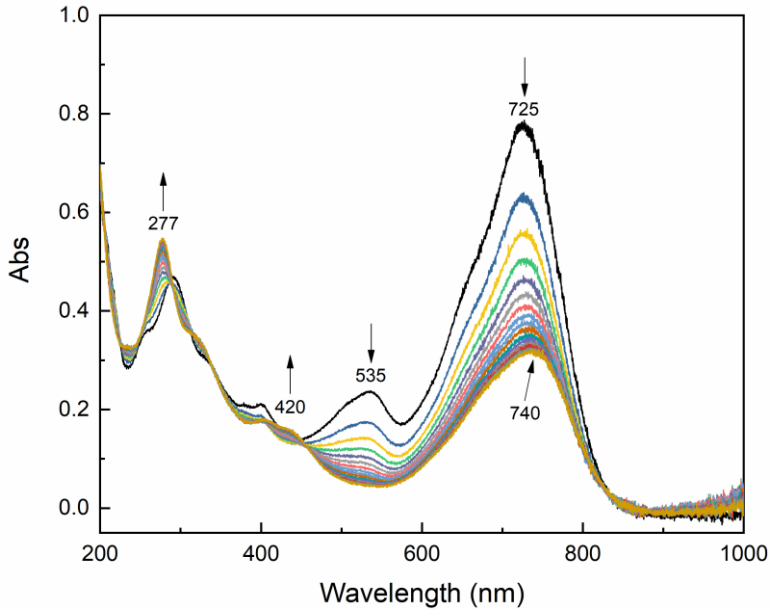

Figure 118: Absorption spectrum evolution of **Red1c** (1.75 x 10^{-4} M) in CH_3CN / $TBAPF_6$ 0.2 M under oxidation at 0.00 V at -25°C. Optical path of the cuvette: 1 mm.

The obtained absorption spectrum is in accordance with that of the photochemically generated **Red1c^{2+}**, thus certifying the expected redox-active behavior of the molecule. Moreover, the total redox-induced process (i.e. **Red1o^{2+}** → **Red1c^{2+}**) has shown a conversion higher than 90%.

However, as presented in the previous Section, this terthiazole appeared to undergo oxidative cycloreversion, too. To verify the happening of the redox-induced ring opening reaction, the spectroelectrochemical experiment has been repeated by electrolyzing the solution at 1.40 V after the initial reduction at -1.10 V. The obtained spectra are depicted in Figure 119.

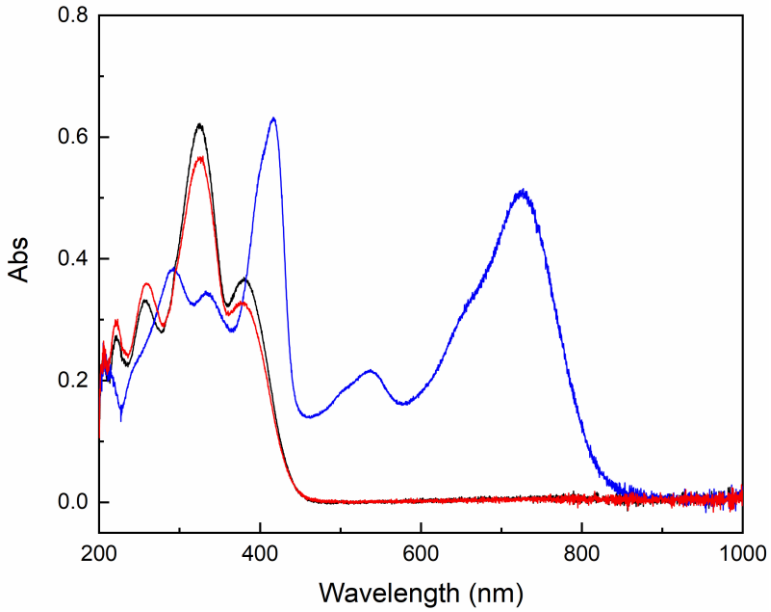

Figure 119: Absorption spectra of (black) **Red1o^{2+}** (1.75 x 10^{-4} M) in CH_3CN / $TBAPF_6$ 0.2 M at -25°C; (blue) after reduction at -1.10 V; (red) after oxidation at 1.40 V. Optical path of the cuvette: 1 mm.

As it can be observed, the oxidation at 1.40 V restored **Red1o^{2+}**. Furthermore, as for the reductive cyclization, also the oxidative cycloreversion allowed to restore more than the 90% of the dicationic open form.

Overall, the photochromic and redox-active behavior of **Red1^{2+}** can be summarized with the scheme presented in Figure 120.

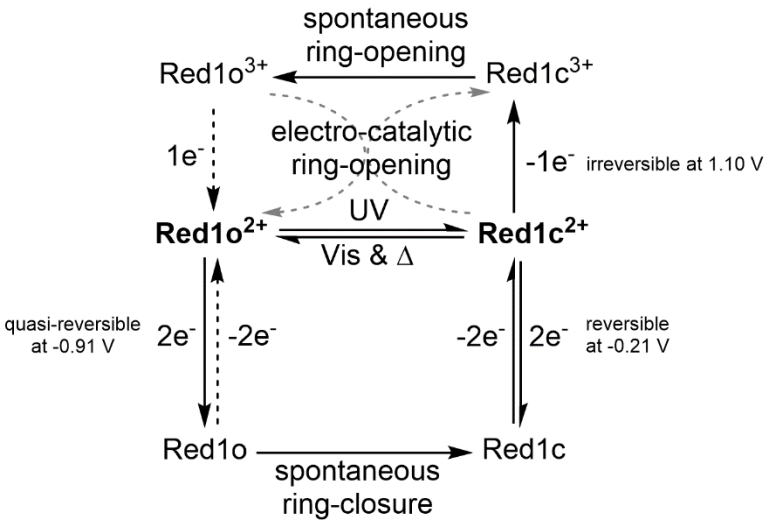

Figure 120: Summary of the photochemical and electrochemical transformations occurring on **Red1o^{2+}**.

4.2.3 Theoretical modelling of ***Red1^{2+}***

In order to better rationalize the bidirectional photo- and electro-chemical switching occurring on **Red1^{2+}**, DFT and TD-DFT calculations have been carried out in collaboration with Pr. Maurel (ITODYS – Université de Paris).

First, the geometry of **Red1o^{2+}** has been optimized using PBE0/6-311G(d,p) as functional by taking into account the solvent (i.e. acetonitrile) with the polarizable continuum model by using the integral equation formalism (IEFPCM). The computation has shown three possible conformations close in energy for the open form, one antiparallel and two parallel. Since only the former is photo-active, the calculations have been performed by taking this geometry at the ground state as starting point for the modelling of the OF and the CF in the different redox states.

It is important to remember that the electrochemical isomerization doesn't occur at the first excited state as the photochemical reaction. Consequently, the potential energy surface for the ring-closing reaction has been studied at the ground state for the redox states 0, +1, +2 and +3. The energies of the different closed forms and transition states (TS) have been determined by setting the energies of the respective open forms at 0 kJ/mol. The obtained values and the distances between the reactive carbons in those geometries are reported in Table 7.

Table 7: Relative energies of the closed forms and the transition states for the ring-closing reaction of **Red1^{2+}** at the ground state and distance between the two reactive carbon atoms in those geometries.

Redox state	Geometry	E (kJ/mol)	$d_{C\text{-}C}$ (Å)
+3	Red1o^{3+} TS Red1c^{3+}	0.0 95.2 13.6	3.487 1.982 1.542
+2	Red1o^{2+} TS Red1c^{2+}	0.0 190.1 74.9	3.583 1.728 1.532
+1	Red1o^{+} TS Red1c^{+}	0.0 89.1 -8.0	3.528 2.082 1.537
0	Red1o TS Red1c	0 16.3 -120.8	3.280 2.460 1.546

It is known that the energy difference between the OF and the CF at the ground state provides an indication about the thermal stability. By optimizing the geometry of the transition state, it is possible to estimate the barrier that has to be overcome to observe the ring-closing reaction.

By looking at the obtained data, a very high activation energy has been determined for **Red1o**$^{2+}$, thus indicating that this isomer is more stable than the CF at this redox state. By reducing this species, a lowering trend of the energy barrier has been observed. In particular, it appeared 10 times smaller for **Red1o**. Moreover, at this neutral redox state, **Red1c** is more stable than **Red1o** by 120.8 KJ/mol, in accordance with the proposition of a cyclization after a two-electron reduction.

Since this molecule has also shown oxidative cycloreversion, also the trend of the activation energy for the ring-opening reaction (i.e. $E_a = E_{TS} - E_{CF}$) in the four redox states has been considered. Furthermore, the theoretically determined value for the dicationic species has been compared to the experimental one (Table 8).

Table 8: Activation energy for the ring-opening reaction of **Red1c**$^{n+}$ at the ground state.

	Theoretical E_a (kJ/mol)	Experimental E_a (kJ/mol)
Red1c^{3+}	81.6	/
Red1c^{2+}	115.3	94.0
Red1c^{+}	97.1	/
Red1c	137.0	/

A good agreement between theoretical and experimental values has been observed for the redox state +2. Moreover, the calculations have shown that the oxidation to **Red1c**$^{3+}$ led to a decrease of the activation energy for the cycloreversion, consistently with the experimentally observed behavior.

Another computation that has been performed at the ground state is the modelling of the redox potentials in acetonitrile. The thermodynamic cycle that allows this computation is provided in the Annexes (Page 249).

The obtained values are reported in Table 9, where they are compared to the experimental ones, determined by cyclic voltammetry.

Table 9: Comparison between **Red1**'s calculated and experimental redox potentials.

Redox reaction	Theoretical E vs SCE (V)	Redox reaction	Experimental E vs SCE (V)
Red1o^{2+} → Red1o^{+} **Red1o^{+} → Red1o**	-1.00 -1.78	**Red1o^{2+} → Red1o**	-0.91
Red1c^{2+} → Red1c^{+} **Red1c^{+} → Red1c**	-0.26 -0.58	**Red1c^{2+} → Red1c**	-0.21
Red1c^{2+} → Red1c^{3+}	0.85	**Red1c^{2+} → Red1c^{3+}**	1.10

First, by looking at the computed values concerning the OF, the agreement between the redox potential for the one-electron reduction of **Red1o^{2+}** to **Red1o^{+}** and the experimental one suggested that the reduction of **Red1o^{2+}** to **Red1o** occurs through a concurrent one-electron process on both arms. Secondly, the observed redox couple at -0.21 V for the CF isomer is probably the made by two close one-electron redox couples that haven't been distinguished in the applied experimental conditions. Finally, the redox value for the oxidation **Red1c^{2+}** to **Red1c^{3+}**has been slightly underestimated.

Lastly, TD-DFT calculations have been performed by using CAM-B3LYP/6-311G(d,p) always including acetonitrile in the computations to determine the optical properties of **Red1** in the redox states 0 and +2. The modelled transitions (and the corresponding oscillator strengths, f) are presented in Table 10, where the wavelengths at which they occur are compared to the experimental ones.

Table 10: Comparison between **Red1**'s calculated and experimental optical properties.

	Theoretical λ (nm)	Experimental λ (nm)	f	Assigned transition
Red1o^{2+}	353 300 250	375 322 /	0.789 0.681 0.421	HOMO → LUMO HOMO → LUMO+2 HOMO-1 → LUMO+1
Red1c^{2+}	740 454 373	744 430 277 (320 sh[a])	0.538 0.305 0.362	HOMO → LUMO HOMO → LUMO+1 HOMO-1 → LUMO
Red1o	407	420	0.393	HOMO → LUMO+6
Red1c	635 494 420	725 535 289	1.431 0.311 0.361	HOMO → LUMO HOMO-1 → LUMO HOMO → LUMO+1

[a] sh: shoulder.

The corresponding theoretical spectra are presented in Figure 121.

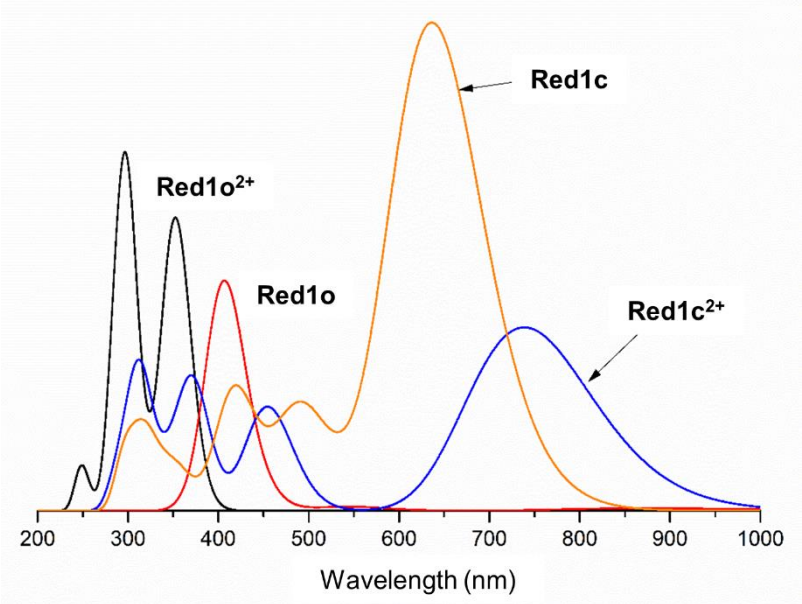

Figure 121: Theoretical spectra of **Red1o^{2+}**, **Red1o**, **Red1c^{2+}** and **Red1c**, adapted from ref. [212]

The two main transitions of the UV-vis spectrum of **Red1o^{2+}** at 322 nm and 375 nm have been well estimated by the calculations, with an error of ~20 nm (301 nm and 353 nm, respectively). Similarly, a very good result has been obtained for the lowest energy band of **Red1c^{2+}** (740 nm vs 744 nm) and an error of only 24 nm has been observed for the band at 430 nm. However, the UV band has been overestimated by 100 nm.

Concerning the neutral redox state, **Red1o**'s spectrum is well represented by the computations (420 nm vs 407 nm), contrarily to what observed for the closed form. In fact, large errors have been reported. Nevertheless, the calculations reproduced the blue-shift and the enhancement in intensity of the lower energy band caused by the reduction.

The isocontour plots of the molecular orbitals involved in these transitions are shown in the Annexes (Page 250).

Additional computations on **Red1** have been carried out to support the observed spectral evolution during the spectroelectrochemical experiment with theoretical modelling.

The first step that has been considered is the reduction at -1.10 V, that has been described through a sequential mechanism 1) **Red1o**$^{2+}$ → **Red1o** and 2) **Red1o** → **Red1c**, with the assumption of a quantitative reduction and a full conversion. The simulation has been performed by adding progressively different weight of the involved species in the UV-vis spectra (Figure 122).

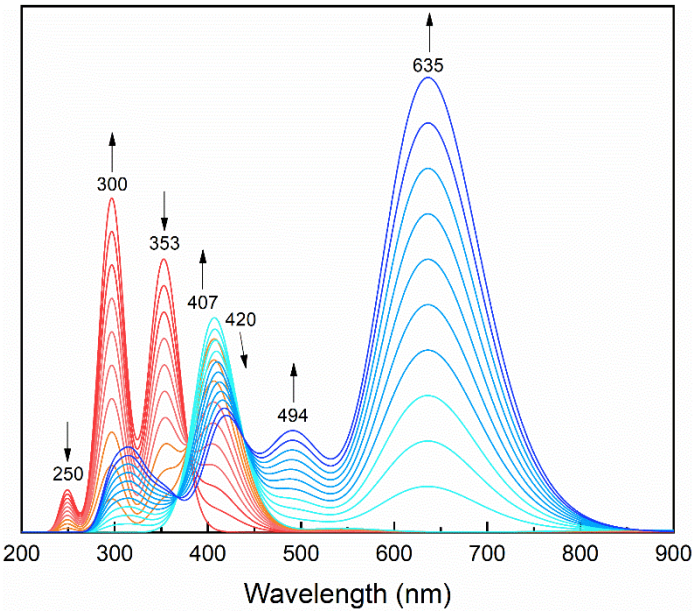

Figure 122: Theoretical UV-vis spectral evolution related to the reduction of **Red1o**$^{2+}$ to **Red1o** and the consequent conversion to **Red1c**, adapted from ref. [212]

Computations showed an evolution in agreement with the experimentally observed one. In particular, the initial appearance of the band at 407 nm that then faded well represented what has been observed for the band at 420 nm during the spectroelectrochemical experiment. Once again, the thesis that the cyclization occurs after the two-electron reduction of **Red1o**$^{2+}$ is reinforced.

Then, the second step of this simulation was the electrolysis at 0.0 V and **Red1c** → **Red1c**$^{2+}$ has been consequently modelled (Figure 123).

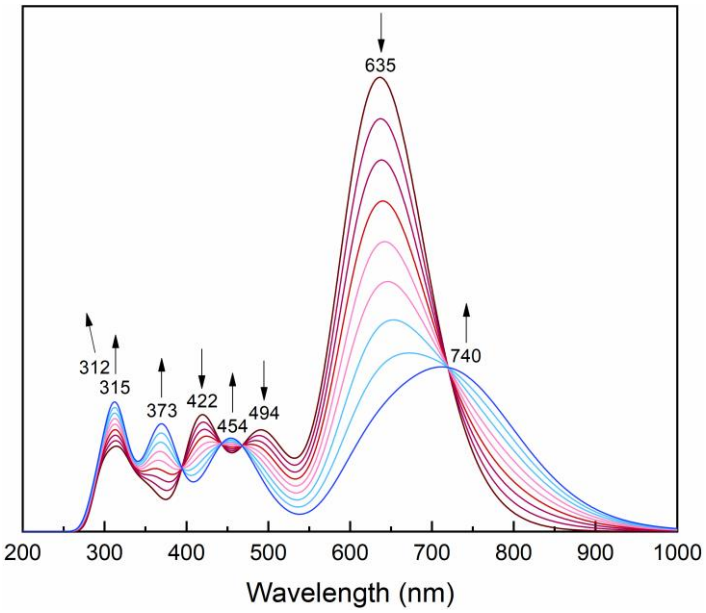

Figure 123: Theoretical UV-vis spectral evolution related to the oxidation of **Red1c** to **Red1c**$^{2+}$, adapted from ref. [212]

Again, even if the wavelength presented some non-negligible errors as mentioned earlier, the calculated spectral evolution resembled the experimental one. In fact, the band in the visible related to the neutral closed form decreased with a concurrent red-shift with the oxidation, as in the spectroelectrochemical experiment.

*4.2.4 Theoretical modelling of **Red2**$^{2+}$*

Fc-containing terthiazole **Red2**$^{2+}$ has been modelled in acetonitrile with the same functionals as **Red1**$^{2+}$.

Similarly, after the geometry optimization, the potential energies surfaces for the cyclization reaction at the ground state have been built at the redox states 0, +1, +2 and +3. The obtained values are indicated in Table 11.

Table 11: Relative energies of the closed forms and the transition states for the ring-closing reaction of **Red2^{2+}** at the ground state and distance between the two reactive carbon atoms in the TS geometry.

Redox state	Geometry	E (kJ/mol)	d_{C-C} (Å)
+3	Red2o^{3+} TS Red2c^{3+}	0.0 225.6 142.7	/ 1.997 /
+2	Red2o^{2+} TS Red2c^{2+}	0.0 188.7 72.8	/ 1.756 /
+1	Red2o^{+} TS Red2c^{+}	0.0 88.8 -8.6	/ 2.083 /
0	Red2o TS Red2c	0 15.8 -121.4	/ 2.462 /

Interesting, almost the same values previously reported for **Red1** have been observed with the exception of the redox state 3+, in which **Red2c^{3+}** appears remarkably more destabilized than **Red2o^{3+}** compared to what was observed for **Red1c^{3+}** / **Red1o^{3+}**. This is in accordance with the experimentally observed faster cycloreversion for this derivative.

Lastly, TD-DFT calculations have shown that the low energy and low intensity bands are exclusively based on Fc-centered transitions and that other bands present a charge transfer character that might be detrimental to the cyclization (Figure in the Annexes, page 251).

*4.2.5 Photochemical and redox-active behavior of **Red3^{2+}** and **Red4^{2+}***

4.2.5.1 Stationary UV-vis spectroscopy and fluorescence

The photochromic behaviors of the dicationic terthiazoles **Red3^{2+}** and **Red4^{2+}** have been investigated in acetonitrile at room temperature using steady-state absorption spectroscopy and the obtained spectra are shown in Figure 124.

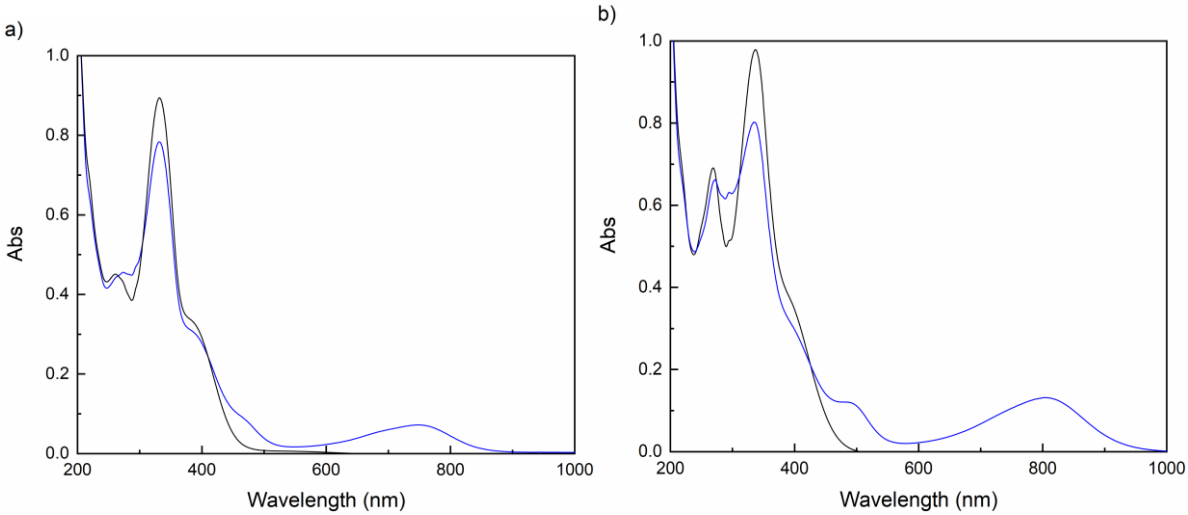

Figure 124: Absorption spectra in acetonitrile of (a) **Red3^{2+}** (6.09 x 10^{-5} M) and (b) **Red4^{2+}** (3.25 x 10^{-5} M), showing the behavior under UV light irradiation (at 340 nm for **Red3^{2+}** and with a diode at 405 nm for **Red4^{2+}**) from the black lines for the OFs to the blue lines to indicate the respective photostationary states. Optical path of the cuvette: 1 cm.

In the case of **Red4^{2+}**, degassing with Ar was required to observe the isomerization. Furthermore, a diode irradiating at 405 nm was needed since the lamp used for the other investigated photochromes wasn't powerful enough.

Red3^{2+} and **Red4^{2+}** in their open forms are characterized by intense absorption bands in the UV region, at 332 nm (ε = 14700 M^{-1} cm^{-1}) and 337 nm (ε = 30150 M^{-1} cm^{-1}), respectively. Both switches are poorly photochromic, a behavior that has been ascribed to the vertical charge transfer character developed by the presence of the electron-poor arms (because of the presence of N-methylated pyridyl rings) and the anisole in the bridging unit. The photogenerated CFs absorb at 750 nm and 800 nm, respectively.

Moreover, **Red4^{2+}** appeared to be even more thermally unstable than **Red1^{2+}**, being characterized by a half-lifetime ($\tau_{1/2}$) of ~30 min at room temperature, and this is consistent with the larger aromatic stabilization of thiophene compared to that of thiazole. [214]

Additionally, while **Red3^{2+}** isn't fluorescent, a degassed acetonitrile solution of **Red4^{2+}** showed an emission band centred at 525 nm and a quantum yield of ca. 7% that has been determined by using quinine sulfate in H_2SO_4 0.5 M as reference (emission spectrum is shown in the Annexes, page 252). The fluorescence diminished by irradiating the solution at 405 nm, thus indicating that the CF isomer is not fluorescent.

4.2.5.2 Electrochemical properties

The electrochemical properties of the two terarylenes have been investigated by cyclic voltammetry (CV) at room temperature in acetonitrile / $TBAPF_6$ 0.1 M with a scan rate (ν) of 100 mV/s. The main data (i.e. half-wave potentials, $E_{1/2}$, and ΔE for reversible waves; peak

potentials, E_p, for irreversible ones) referenced to a saturated calomel electrode (SCE) are reported in Table 12.

Table 12: Redox potentials vs SCE in CH_3CN / $TBAPF_6$ 0.1 M of **Red3^{2+}** and **Red4^{2+}**.

	OF		CF	
	$E_{1/2}$ or E_p (V)	ΔE (mV)	$E_{1/2}$ or E_p (V)	ΔE (mV)
Red3^{2+}	-0.91 (qr)	100	-0.22 (qr)	60
Red4^{2+}	-0.92 (qr)	110	0.90 (irr) -0.23	/ 50

Cyclic voltammograms for **Red3^{2+}** are presented in Figure 125.

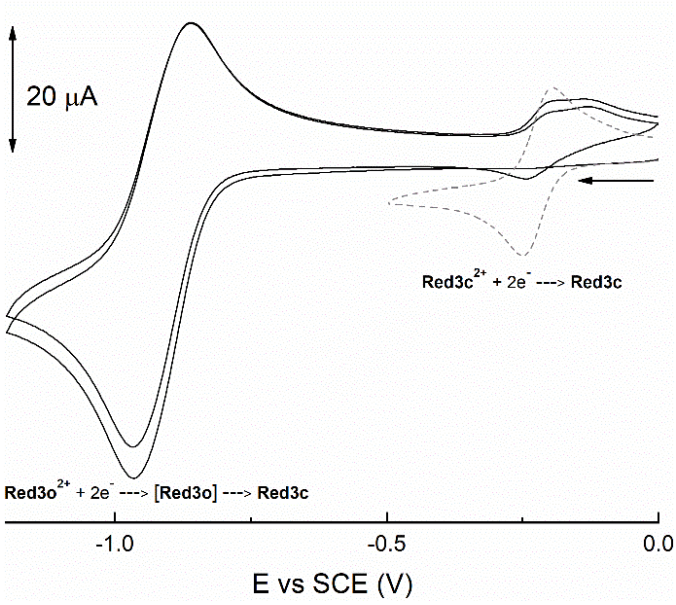

Figure 125: CVs of **Red3^{2+}** (1 mM) in CH_3CN / $TBAPF_6$ 0.1 M in the OF (black solid lines) and at the PSS (grey dashed lines) indicating the reductive cyclization. ν = 100 mV/s.

As for the previously presented terarylenes, a quasi-reversible reduction wave is observed at $E_{1/2}$ = -0.91 V also in the case of **Red3^{2+}**. On the back scan, two close anodic waves appear. The first one, at $E_{1/2}$ = -0.22 V, indicates the formation of the close form, as confirmed by the CV on the solution irradiated at 365 nm (grey dashed line). This means that redox-active terthiazole **Red3^{2+}** undergoes reductive cyclization, too, and a bielectronic mechanism is expected to remain valid. However, the reaction is not as clean as for **Red1^{2+}** and **Red2^{2+}**,

because of the presence of the irreversible wave at -0.13 V next to the wave related to CF. This additional wave is absent when recording the CV at the PSS and its attribution is still unclear.

In the case of **Red4^{2+}**, the open form isomer shows a quasi-reversible reduction wave at $E_{1/2}$ = -0.92 V, as shown in Figure 126. On the back scan, one anodic peak appears at $E_{1/2}$ = -0.23 V, due to a new species corresponding to the dicationic closed form (**Red4c^{2+}**), as confirmed by cyclic voltammetry on the same solution after irradiation at 405 nm. This means that reductive cyclization can be achieved also on this thiophene-containing terarylene. Once again, the two-electron ring-closure mechanism that has been described and confirmed by combination of spectroscopic and electrochemical data for **Red1^{2+}** is extended also to this molecule.

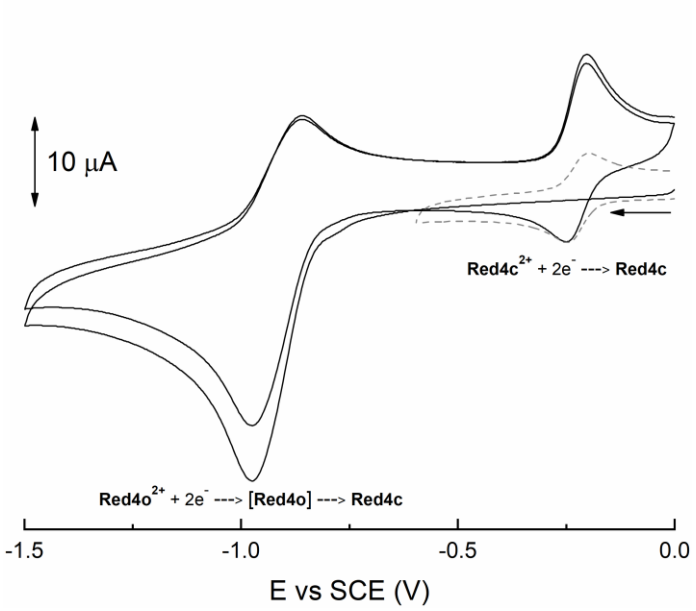

Figure 126: CVs of **Red4^{2+}** (1 mM) in CH_3CN / $TBAPF_6$ 0.1 M in the OF (black solid lines) and at the PSS (grey dashed lines) indicating the reductive cyclization. ν = 100 mV/s.

It is worth noting that the reduction wave of the OF is distinctly asymmetric and the current related to the CF in the back scan is significantly higher, thus suggesting a fast and efficient reductive cyclization that makes **Red4c^{2+}**more easily accessible by electrochemical means than by light (the irradiation at 405 nm of the 1 mM solution generated a very little amount of closed form, as indicated by the grey dashed line).

In addition to the reversible peak at –0.23 V, **Red4c^{2+}** is also characterized by an irreversible wave at 0.90 V, as shown in Figure 127. Moreover, a shoulder is present at ~0.05 V, but the corresponding redox process hasn't been understood yet.

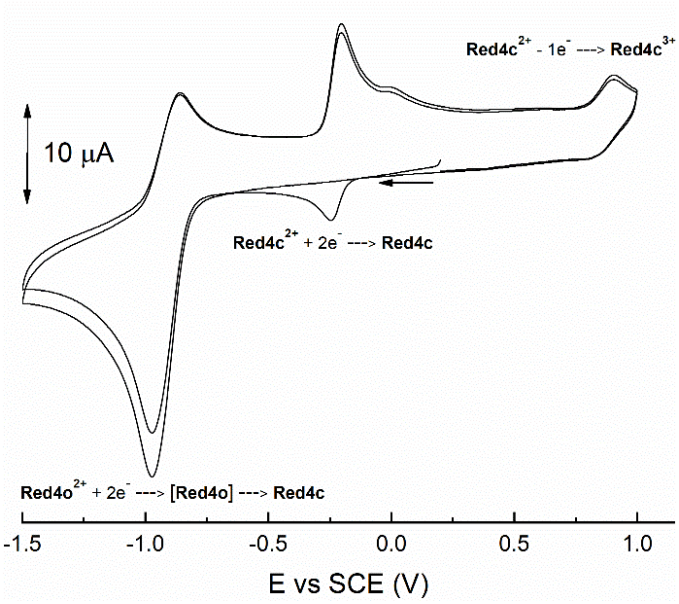

Figure 127: CVs of **Red4^{2+}** (1 mM) in CH_3CN / $TBAPF_6$ 0.1 M in the OF indicating the reductive cyclization and the oxidative cycloreversion. ν = 100 mV/s.

As for **Red1**, the oxidation at 0.90 V appears to speed up the thermal ring-opening reaction of the dicationic CF. This oxidative cycloreversion is expected to occur with the mechanism described in Section 4.2.2.4.

Overall, the main point to highlight concerning the investigation on these other two switches is the confirmation of the possibility of achieving the reductive cyclization also for these derivatives, even if the electrochemical route appears to be more complex than that observed for **Red1** and **Red2** because of the presence of unclear redox processes in addition to those showing the expected redox-active behavior.

4.3 Synthesis and characterizations of the photochromes designed for oxidative cyclization

*4.3.1 Synthesis route to **Ox1** – **6***

In order to synthesize the six terarylenes **Ox1** – **6**, the first step has been the preparation of the required 2-(4-substituted)-4-bromo-5-methyl-thiophene by reacting 3,5-dibromo-2-methyl-thiophene with the needed boronic acid in a Suzuki-Miyaura reaction (Figure 128).

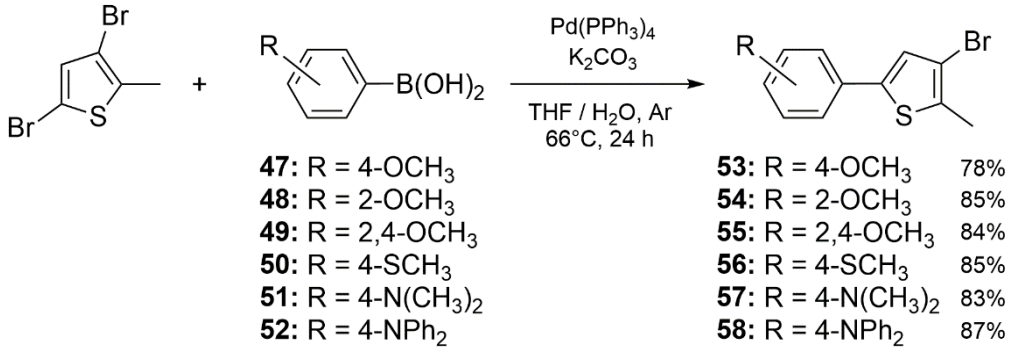

Figure 128: Synthesis of intermediates **53**-**58**.

Once obtained, these substrates could be used in two different synthetic routes to afford the desired photochromes. The first one was based on the synthesis of the respective boronic acid pinacol esters to be then reacted with **37** in a double cross-coupling reaction, as it has been done for the synthesis of **Red1**$^{2+}$ (Figure 129).

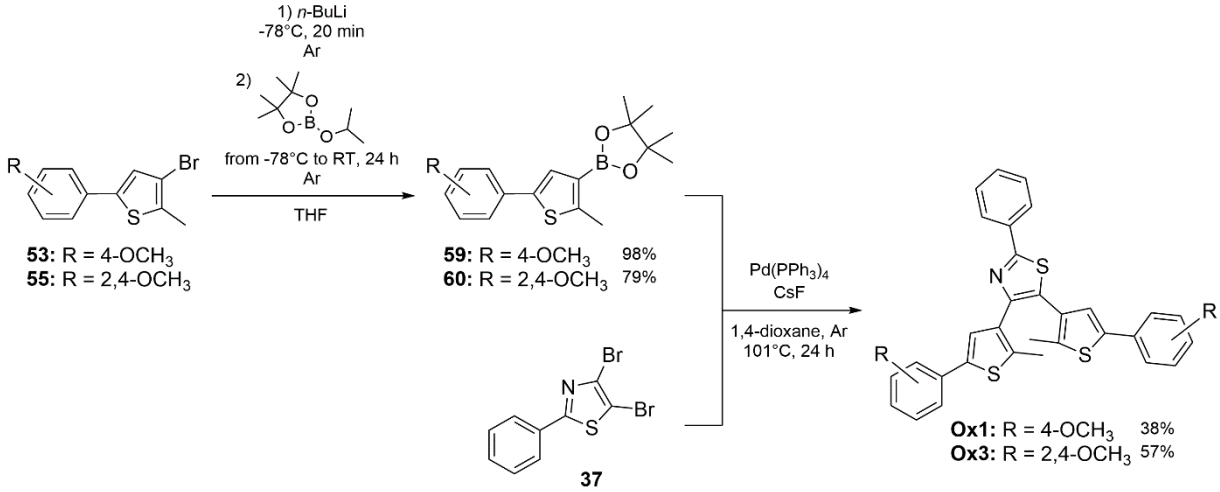

Figure 129: Synthesis route to **Ox1** and **Ox3**.

The second route involved instead the direct Suzuki-Miyaura reaction of the brominated intermediate with **28** (for its synthesis see Chapter 2, Section 2.2.1) followed by the direct arylation of the obtained derivative with the brominated intermediate again (Figure 130).

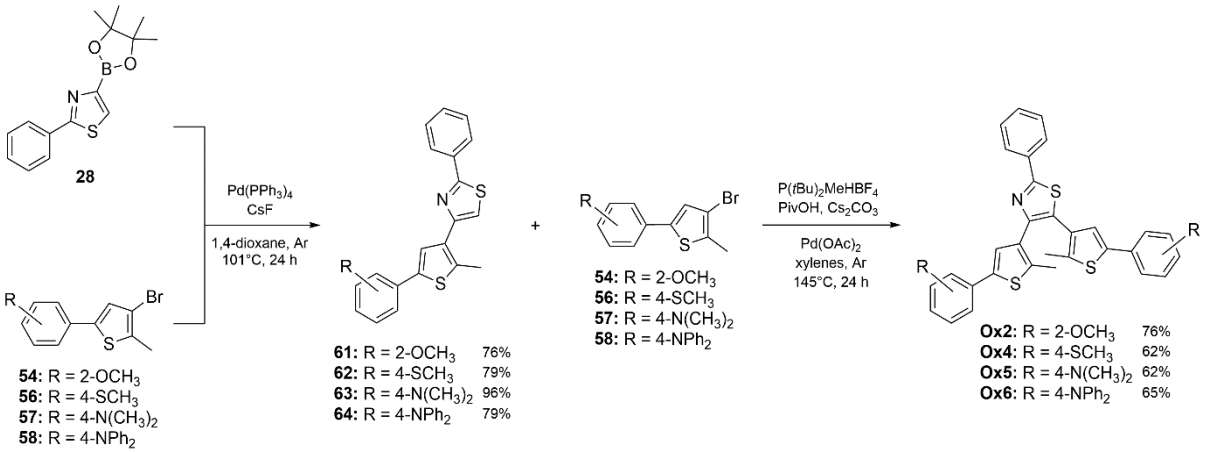

Figure 130: Synthesis route to **Ox2** and **Ox4** – **6**.

Both the routes are viable for the synthesis of these derivatives. Nevertheless, the second one allowed to obtain the photochromes in higher yields and consequently seems preferable. Moreover, it offers higher flexibility since the intermediates **61** – **64** potentially allow the synthesis of dissymmetric derivatives.

*4.3.2 Photochemical and redox-active behavior of **Ox1** – **6***

4.3.2.1 Stationary UV-vis spectroscopy

The photochromic behaviors of **Ox1** – **6** have been investigated in acetonitrile (or in presence of a minimum volume of dichloromethane to guarantee a complete dissolution) at room temperature using steady-state absorption spectroscopy. The solutions haven't been degassed unless stated otherwise. The obtained spectra are depicted in Figure 131, where the open forms are presented with black solid lines and the photostationary states with blue or green solid lines, depending on the color of the irradiated solution. If present, the effect of thermal cycloreversion in the dark at RT is shown with a red solid line.

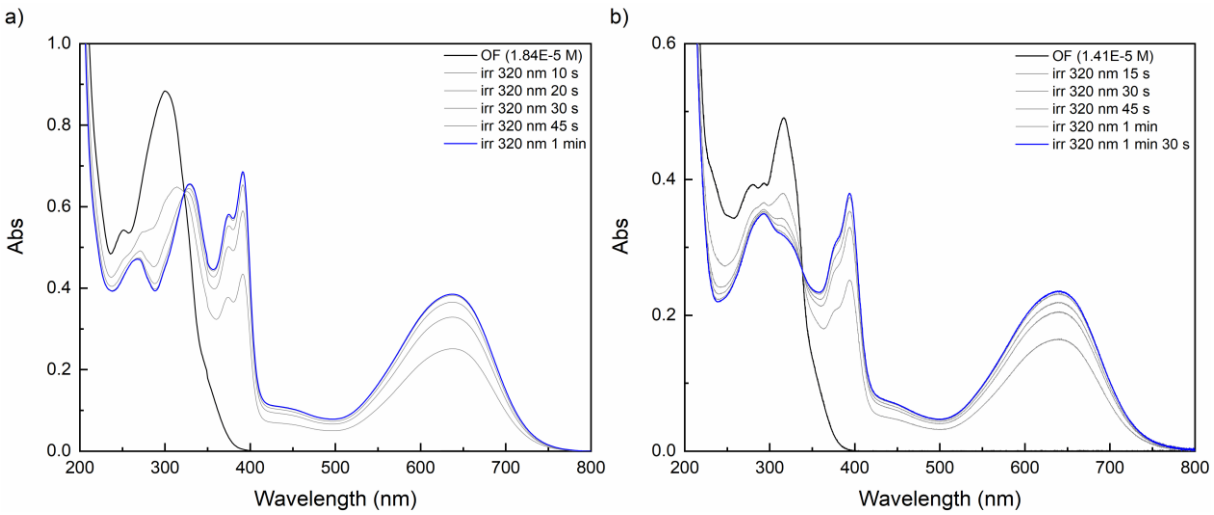

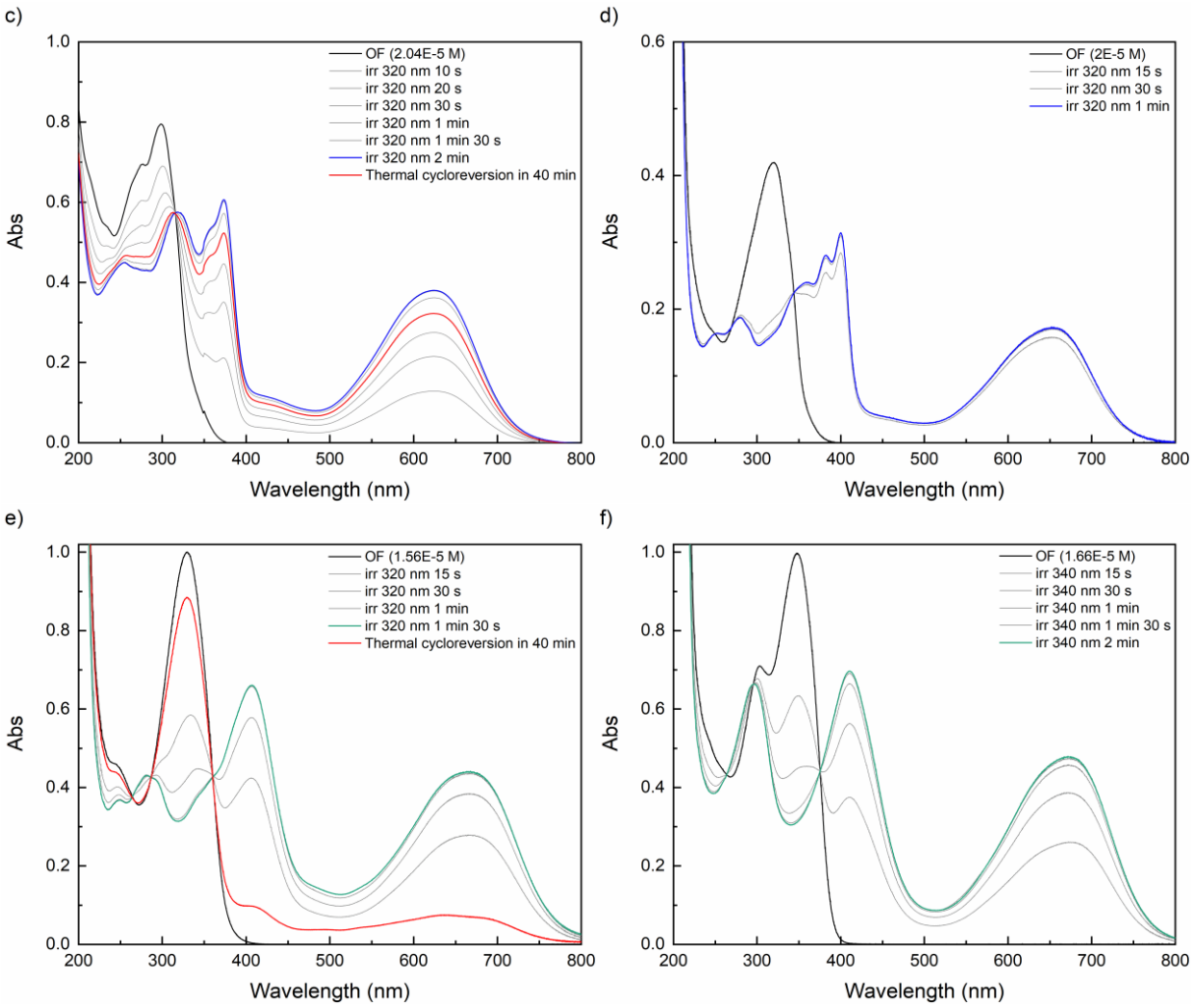

Figure 131: Absorption spectra in acetonitrile (+ minimum volume of dichloromethane) of (a) **Ox1**, (b) **Ox2**, (c) **Ox3**, (d) **Ox4**, (e) **Ox5**, (f) **Ox6**, showing the evolution under UV light irradiation (at 320 nm for **Ox1** – **5**, at 340 nm for **Ox6**) from the black lines for the OFs to the blue or green lines to indicate the respective photostationary states. Thermal cycloreversion of **Ox3** and **Ox5** is indicated in red solid lines. The concentrations are provided in the Figure. Optical path of the cuvette: 1 cm.

All the six derivatives show an intense absorption band in the UV region in their open forms, with λ_{max} between 300 and 350 nm. Good photochromic properties have been observed for these compounds, with a rapid conversion to the closed forms under light irradiation, as confirmed by the growth of broad absorption bands peaking between 600 and 700 nm.

Moreover, all the switches in their CF are also characterized by a band around 400 nm, that is sharp and accompanied by a shoulder as in the cases of **Ox1** – **4** or broad as remarked for **Ox5** and **Ox6**.

Unexpectedly, the closed forms of **Ox3** and **Ox5** didn't show thermal stability in the dark and non-negligible spontaneous cycloreversion has been observed after 40 minutes. This phenomenon was particularly pronounced for the $-N(CH_3)_2$-containing photochrome. Moreover, the formation of a side-product for this switch is suspected because of a residual

absorption between 400 nm and 700 nm when attempting to complete the cycloreversion to the open form by using visible light at 600 nm (Figure 132).

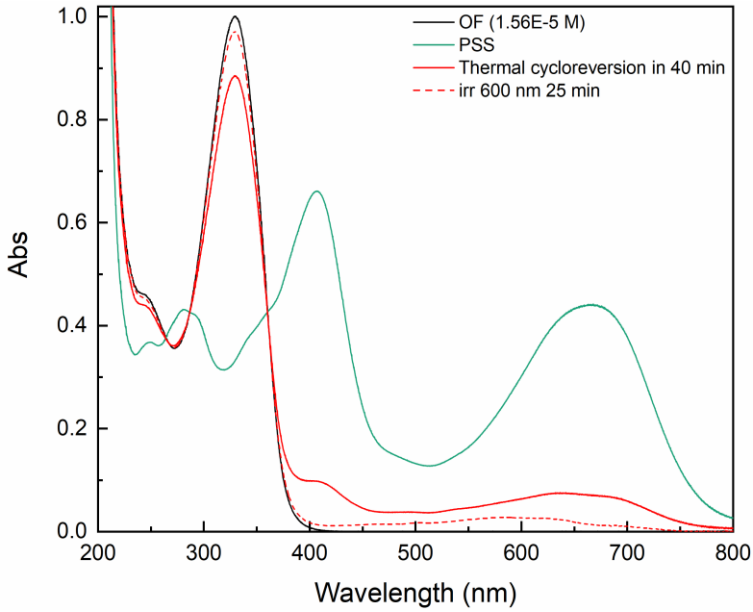

Figure 132: Absorption spectra in acetonitrile + minimum volume of dichloromethane of **Ox5**, showing in (black solid line) the OF, (green solid line) the PSS reached under light irradiation at 320 nm, (red solid line) the thermal cyloreversion in 40 minutes and (red dashed line) the obtained spectrum after irradiation at 600 nm. Concentration is provided in the Figure. Optical path of the cuvette: 1 cm.

The thermal instability and the side-product formation might be possibly ascribed to the presence of a percentage of dichloromethane, which, under UV irradiation, could generate tiny amounts of reactive radical species responsible either for a catalytic ring-opening reaction or the formation of the side-product.

4.3.2.2 Electrochemical properties

The electrochemical properties of the six photochromes have been investigated by cyclic voltammetry (CV) at room temperature in acetonitrile or dichloromethane / $TBAPF_6$ 0.1 M with a scan rate (ν) of 100 mV/s. In particular, dichloromethane has been used for **Ox2** and **Ox4** – **6**, photochromes whose total dissolution couldn't be achieved by using exclusively acetonitrile.

The main data (i.e. half-wave potentials, $E_{1/2}$, and ΔE for reversible waves; peak potentials, E_p, for irreversible ones) referenced to a saturated calomel electrode (SCE) are reported in Table 13.

Table 13: Redox potentials vs SCE in CH_3CN or CH_2Cl_2 / $TBAPF_6$ 0.1 M of the six investigated terarylenes.

	OF		CF	
	$E_{1/2}$ or E_p (V)	ΔE (mV)	$E_{1/2}$ or E_p (V)	ΔE (mV)
Ox1[a]	1.12 (irr)	/	0.28 0.42	60 60
Ox2[b]	1.17 (irr)	/	0.32 (irr) 0.39 (irr)	/ /
Ox3[a]	0.94 (irr)	/	0.17	50
Ox4[b]	1.18 (irr)	/	0.32 0.56	80 80
Ox5[b]	0.70 (irr)	/	0.03	120
Ox6[b]	0.90 (irr)	/	0.20	180

[a] solvent: acetonitrile; [b] solvent: dichloromethane.

For all the six compounds, either in the OF or the CF, no reduction wave has been observed when sweeping to negative potentials. Whatever the derivative, an irreversible two-electron oxidation wave has been detected for the open form. This oxidation became more and more easier with the introduction of stronger electron-donating groups.

Cyclic voltammograms for **Ox1** are presented in Figure 133. The open form isomer (**Ox1o**) is irreversibly oxidized at 1.12 V. On the back scan, two one-electron cathodic waves appear at $E_{1/2}$ = 0.28 V and 0.42 V, due to the reduction of the twice oxidized closed form (**Ox1c**$^{2+}$), so to afford **Ox1c**, as confirmed by the CV on the solution irradiated at 365 nm. In fact, the same two redox waves have been observed. This suggests that redox-active **Ox1** undergoes oxidative cyclization.

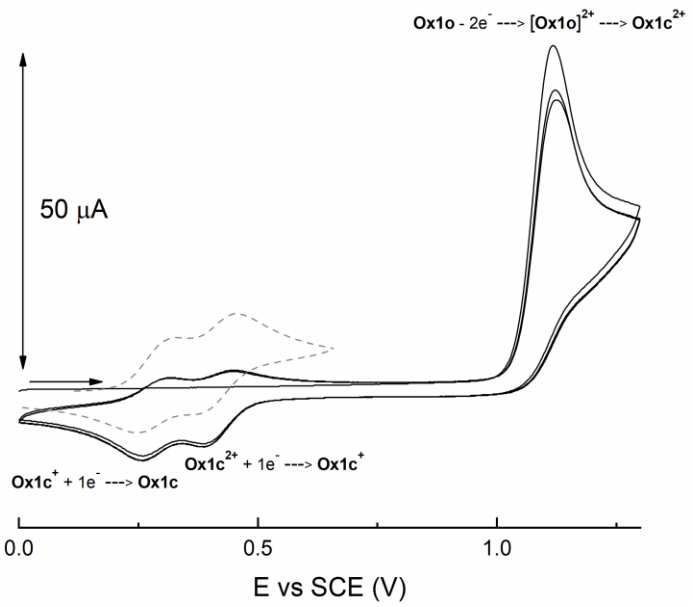

Figure 133: CVs of **Ox1** (1 mM) in CH_3CN / $TBAPF_6$ 0.1 M in the OF (black solid lines) and at the PSS (grey dashed lines) indicating the oxidative cyclization. ν = 100 mV/s.

The same general behavior has been detected for **Ox3** – **6** before and after irradiation at 365 nm (Figure 134). The main difference in the cyclic voltammograms concerns the redox waves of the closed form isomers. **Ox4c** shows two largely separated one-electron waves, also because of the use of dichloromethane as solvent, whose lower donating nature makes the oxidation of the radical species more difficult. [137] The other three derivatives are characterized by a single wave, possibly made of two one-electron redox processes occurring at close potentials.

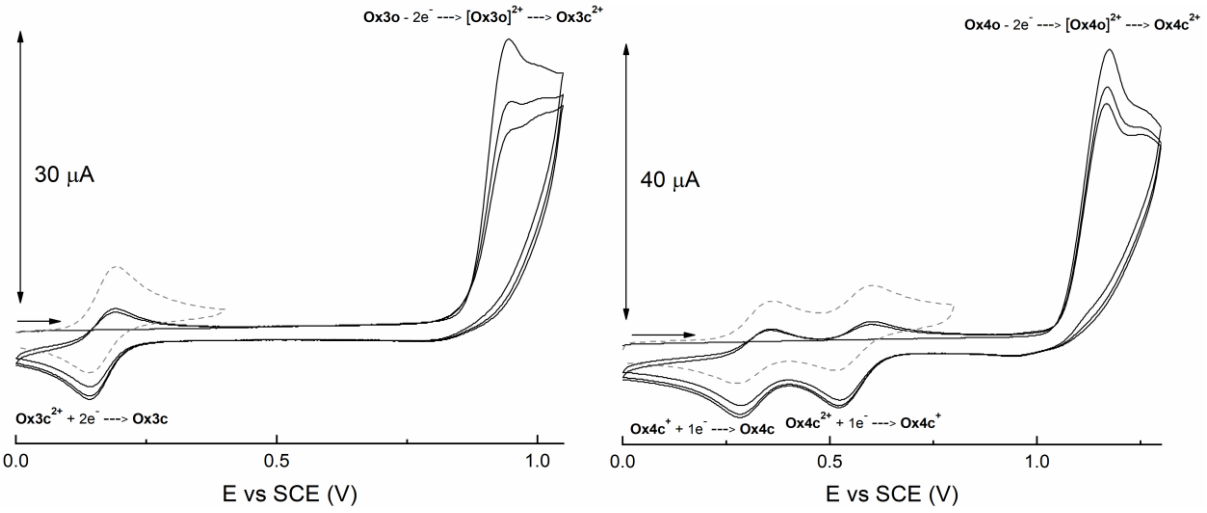

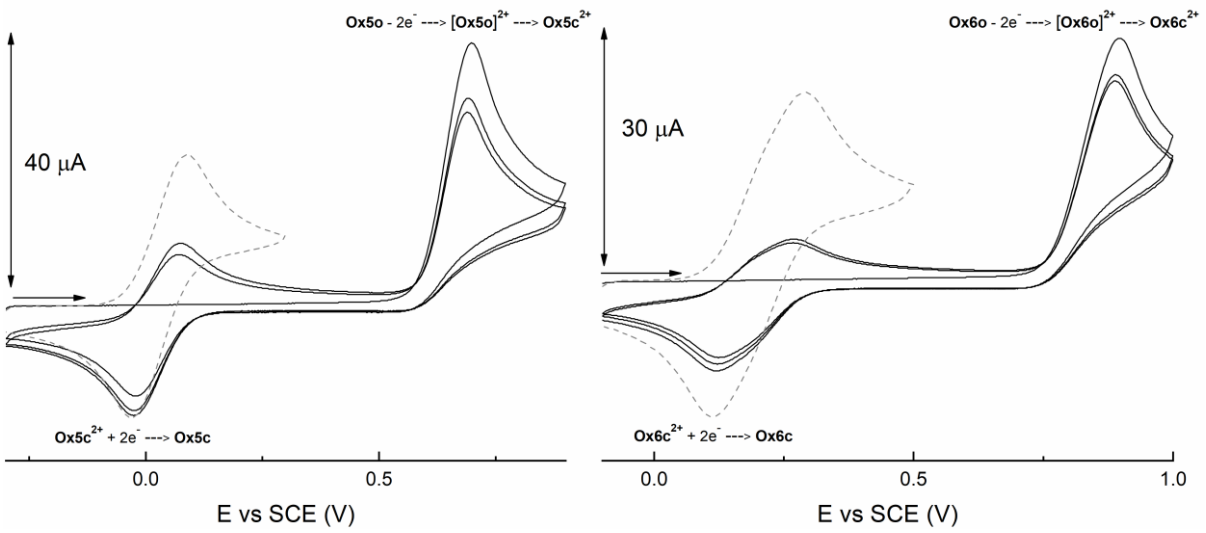

Figure 134: CVs of **Ox3** – **6** (1 mM) in CH_3CN (**Ox3**) or CH_2Cl_2 (**Ox4** – **6**) / $TBAPF_6$ 0.1 M in the OF (black solid lines) and at the PSS (grey dashed lines) indicating the oxidative cyclization. ν = 100 mV/s.

The only exception is represented by **Ox2**. The oxidation of its OF led to the appearance of a new large wave on the back scan (Figure 135), that is irreversible and consequently doesn't match to the wave detected when recording the CV on the PSS. Apparently, the oxidative cyclization doesn't occur on this molecule.

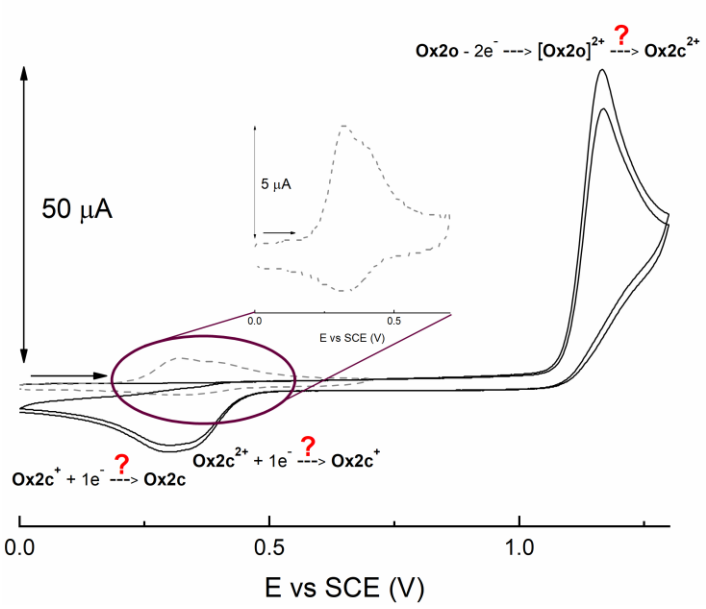

Figure 135: CVs of **Ox2** (1 mM) in CH_2Cl_2 / $TBAPF_6$ 0.1 M in the OF (black solid lines) and at the PSS (grey dashed lines and circled in prune to show an inset). ν = 100 mV/s.

This wave could be made slightly more reversible at higher scan rates, as shown by the cyclic voltammogram in Figure 136, that has been recorded at ν = 1 V/s. This suggests that the expected process might occur, but its kinetics are in the same order of magnitude of other detrimental side reactions.

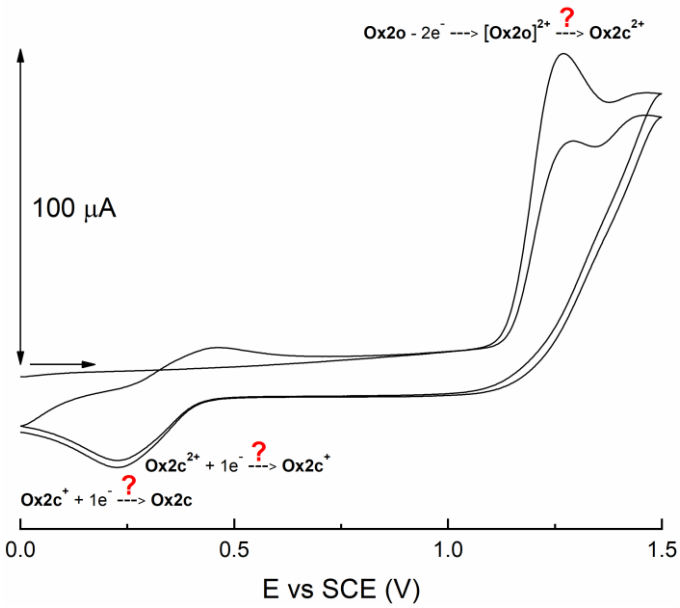

Figure 136: CV of **Ox2** (1 mM) in CH_2Cl_2 / $TBAPF_6$ 0.1 M at ν = 1 V/s.

About the kinetics of the oxidative cyclization, Feringa and co-workers proposed a rate constant larger than 10^4 s^{-1} for electron-donor-bearing dithienylethenes showing this redox-active behavior. [137] For our case, a similar constant can be expected, but the equipment available in our laboratory didn't allow an investigation at scan rates faster than 4 V/s, so it hasn't been possible to perform a proper estimation. However, a study up to at least 4 V/s has been carried out on **Ox1** and the two-electron oxidation of the open form remained unambiguously irreversible (Figure 137).

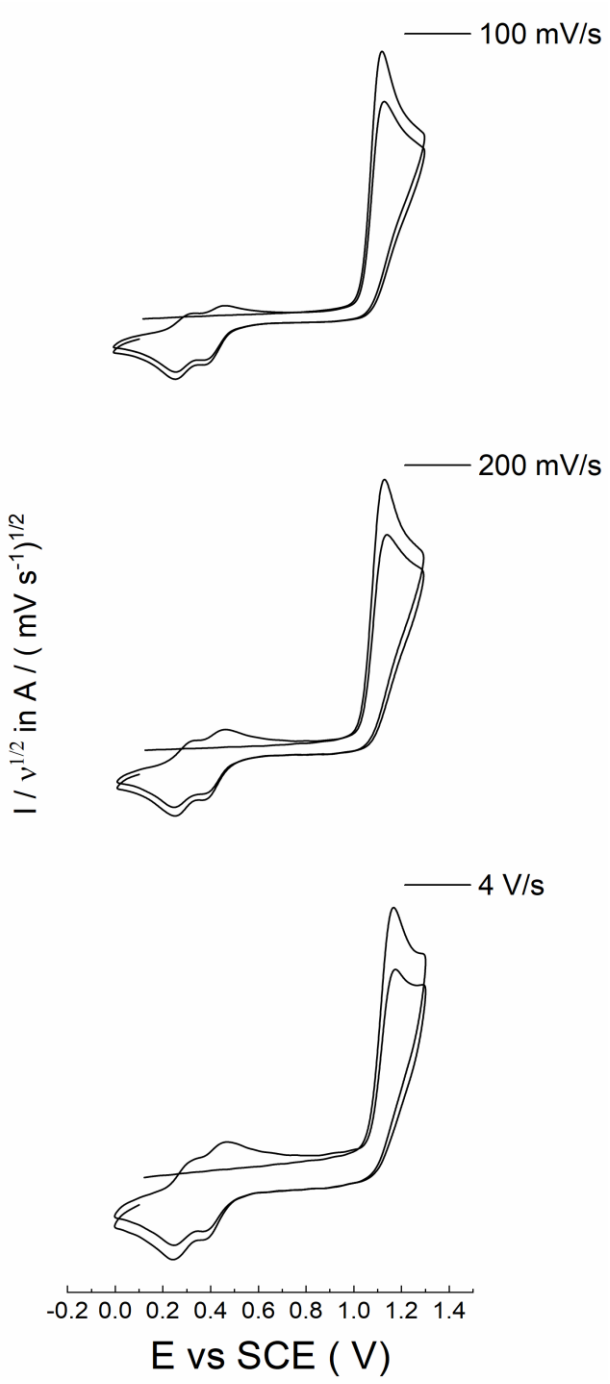

Figure 137: Oxidation of **Ox1o** (1 mM) in CH_3CN / $TBAPF_6$ 0.1 M at different scan rates.

As it can be observed, even if the oxidation of the open form wasn't affected by the increasing scan rate, an impact could be detected on the waves related to the closed form, that became more symmetric, thus suggesting an improved reversibility.

Overall, according to these preliminary results, the redox-active behavior of these thiophene-based terarylenes seemed comparable to that described by Feringa's group [137], even if no accumulation of the CF species in the diffusion layer has observed in our case during the recording of multiple cycles.

Nevertheless, an unexpected and striking difference has been detected during the recording of the CVs on the photostationary states: a loss of the closed form in the diffusion layer has been detected as if cycloreversion was occurring during the experiment (Figure 138).

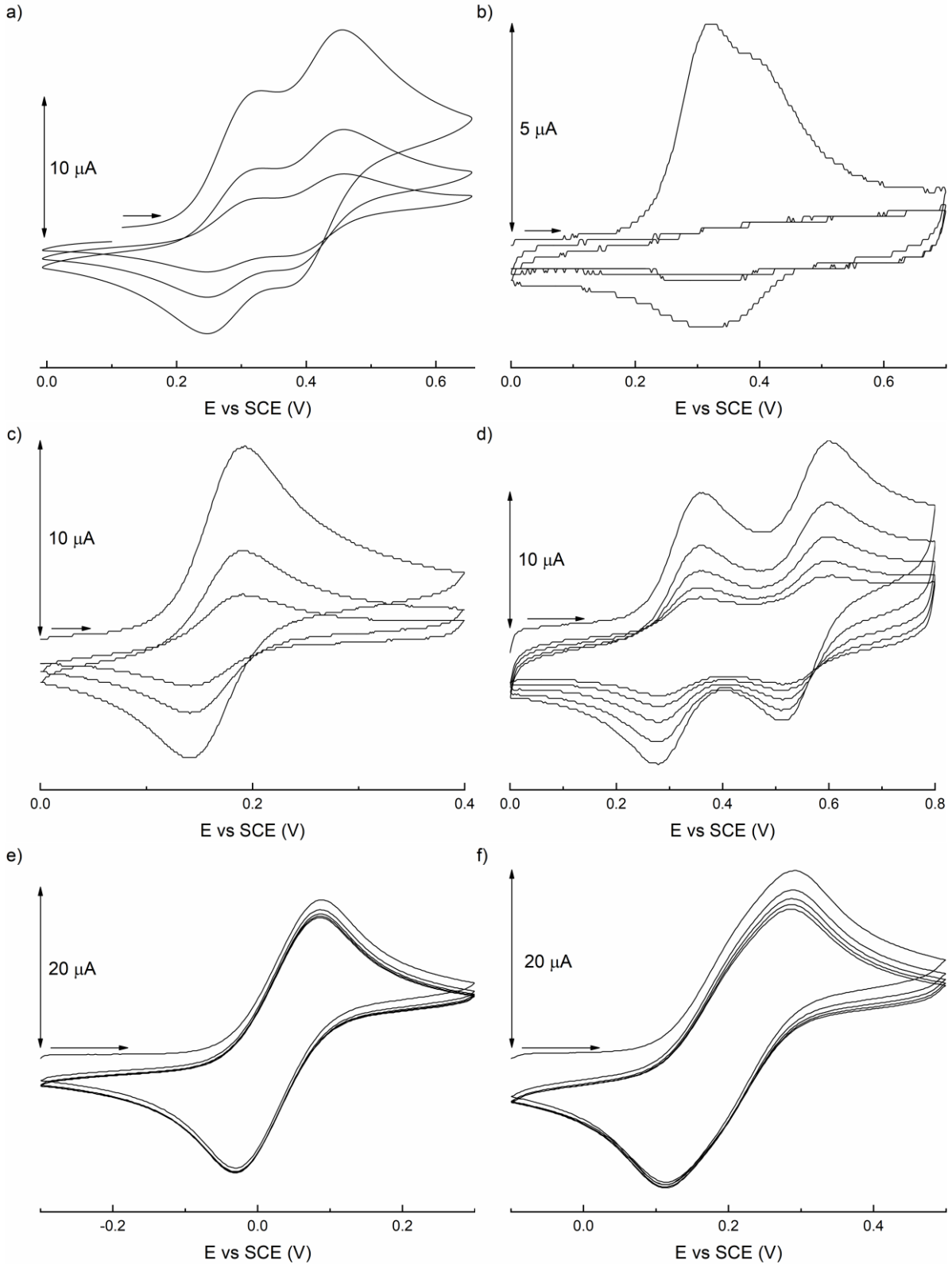

Figure 138: CVs of a) **Ox1c**, b) **Ox2c**, c) **Ox3c**, d) **Ox4c**, e) **Ox5c**, f) **Ox6c** (1 mM) in CH_3CN (**Ox1** and **Ox3**) or CH_2Cl_2 (**Ox2** and **Ox4** – **6**) / $TBAPF_6$ 0.1 M at the PSS (λ_{irr} = 365 nm). ν = 100 mV/s.

This disappearance of the closed form isomer is strongly dependent on the electron-donating strength of the substituents. While a rapid loss of the CF occurred for **Ox1c** – **4c**, the presence of stronger donors such as $–N(CH_3)_2$ and $–N(Ph)_2$ seemed to prevent or at least slow down the occurrence of this unexpected process. Moreover, the CVs related to **Ox2c** indicate that the functionalization in *ortho* stabilizes the redox-active species less than the one in *para* because of the different delocalization over the arms depending on the position of the substituent.

In conclusion, by looking at the results of the cyclic voltammetry experiments, these derivatives appeared to undergo oxidative cyclization. However, an unexpected rapid ring-opening reaction has been remarked when recording the CVs at the photostationary state. To further investigate this unanticipated redox-active behavior and to verify if the oxidative ring-closure could be really achieved, spectroelectrochemical experiments at room temperature have been carried out.

4.3.2.3 Spectroelectrochemical study of **Ox1**

A solution of **Ox1** in acetonitrile / $TBAPF_6$ 0.1 M has been initially electrolyzed at RT at 1.30 V. The induced spectral evolution has been followed by UV-vis spectroscopy (Figure 139).

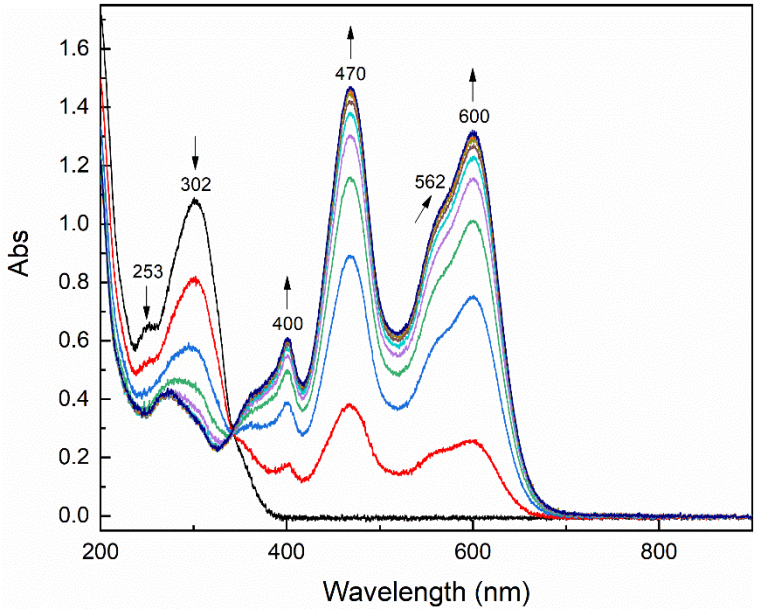

Figure 139: Absorption spectrum evolution of **Ox1o** (2.27×10^{-4} M) in CH_3CN / $TBAPF_6$ 0.1 M under oxidation at 1.30 V at RT. Optical path of the cuvette: 1 mm.

Because of the oxidation, the bands of **Ox1o** at 253 nm and 302 nm decreased while three new bands grew at 400 nm, 470 nm and 600 nm. They have been attributed to the dicationic CF species (**Ox1c**$^{2+}$). The formation of this species after the oxidation is so fast that no indication about monocationic radicals (either in the open or the closed form) has been obtained.

A second electrolysis has been carried out at 0.50 V (i.e. the potential at which the wave for the one-electron reduction of the dicationic species to the radical one starts), thus attempting to obtain the UV-vis spectrum of **Ox1c**$^{+\bullet}$. On the contrary, a return to the open form has been observed (Figure 140).

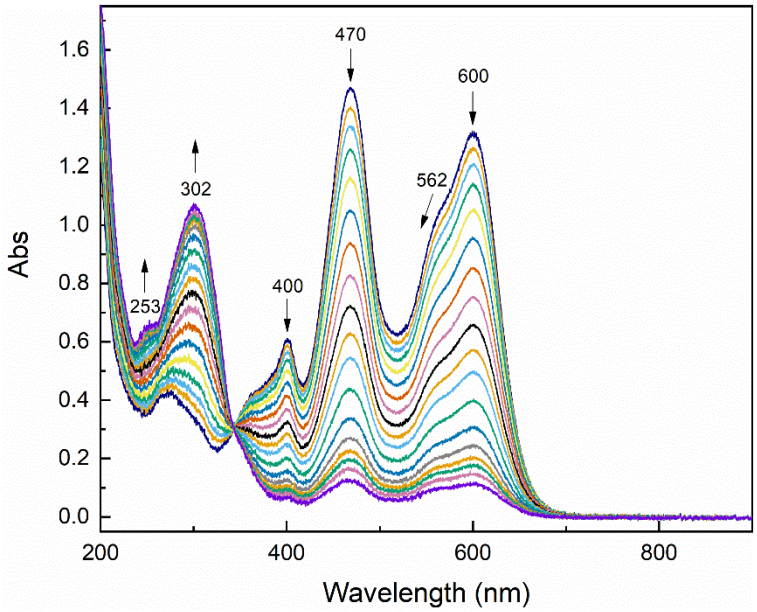

Figure 140: Absorption spectrum evolution of **Ox1c**$^{2+}$ (2.27 x 10^{-4} M) in CH_3CN / $TBAPF_6$ 0.1 M under reduction at 0.50 V at RT. Optical path of the cuvette: 1 mm.

No radical species has been detected during the electrolysis and an almost total conversion to the neutral open form has been achieved, thus providing additional evidence on the cycloreversion. The return to **Ox1o** has been completed by electrolyzing the solution at 0.00 V (Figure 141).

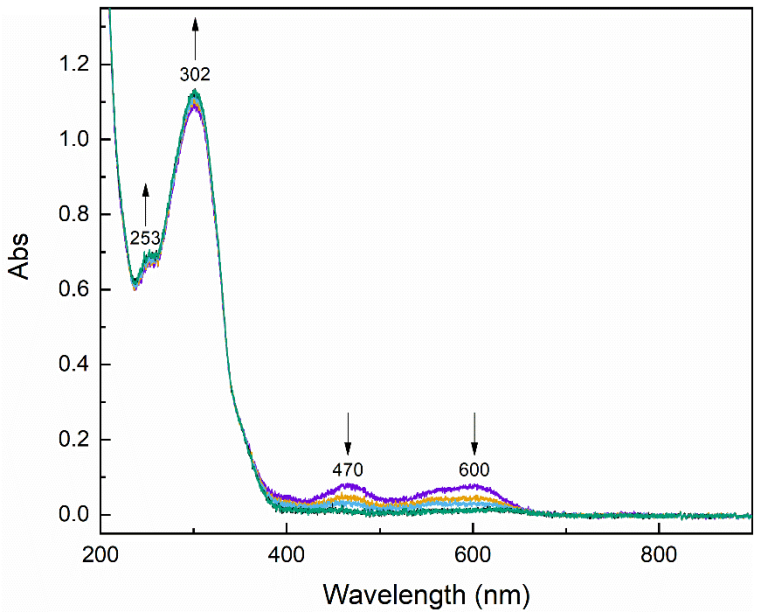

Figure 141: Absorption spectrum evolution of **Ox1c**$^{2+}$ (2.27 x 10^{-4} M) in CH_3CN / $TBAPF_6$ 0.1 M under reduction at 0.00 V at RT. Optical path of the cuvette: 1 mm.

4.3.2.4 Spectroelectrochemical study of **Ox2**, **Ox3** and **Ox4**

As it has been observed by cyclic voltammetry, the functionalization in *ortho* position led to a remarkably different redox-active behavior for **Ox2** compared to that shown by its regioisomer **Ox1**. The impact of this structural difference has been examined by spectroelectrochemistry, too.

The terarylene has been dissolved in dichloromethane / $TBAPF_6$ 0.1 M and electrolyzed at RT at 1.30 V. The induced spectral evolution has been followed by UV-vis spectroscopy (Figure 142).

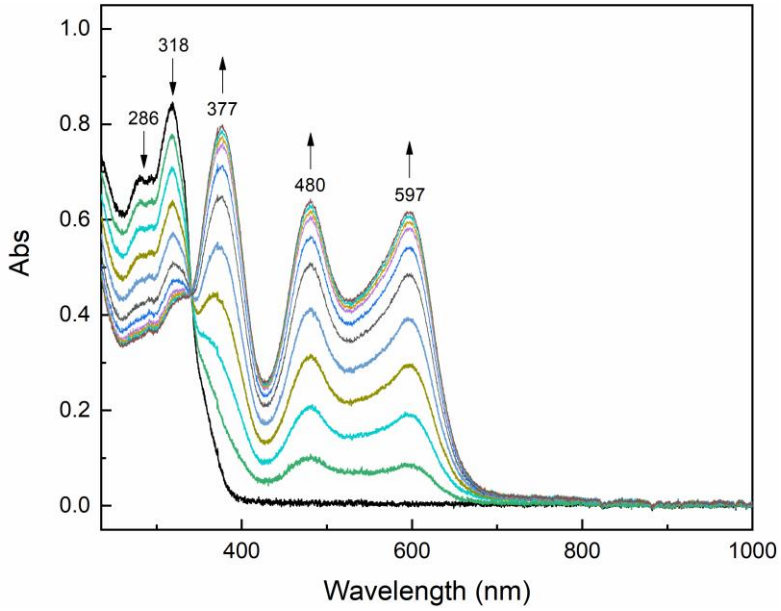

Figure 142: Absorption spectrum evolution of **Ox2o** (2.42×10^{-4} M) in CH_2Cl_2 / $TBAPF_6$ 0.1 M under oxidation at 1.30 V at RT. Optical path of the cuvette: 1 mm.

Similarly to what has been observed for **Ox1**, this oxidation caused a decrease of the bands of the neutral OF at 286 nm and 318 nm with a simultaneous appearance of new bands at 377 nm, 480 nm and 597 nm. The corresponding species might be the dicationic species **Ox2c**$^{2+}$.

This oxidation has been followed by a reduction at 0.40 V, that is a potential close to the E_p of the irreversible wave detected by cyclic voltammetry on the back scan at ν = 100 mV/s (Figure 143).

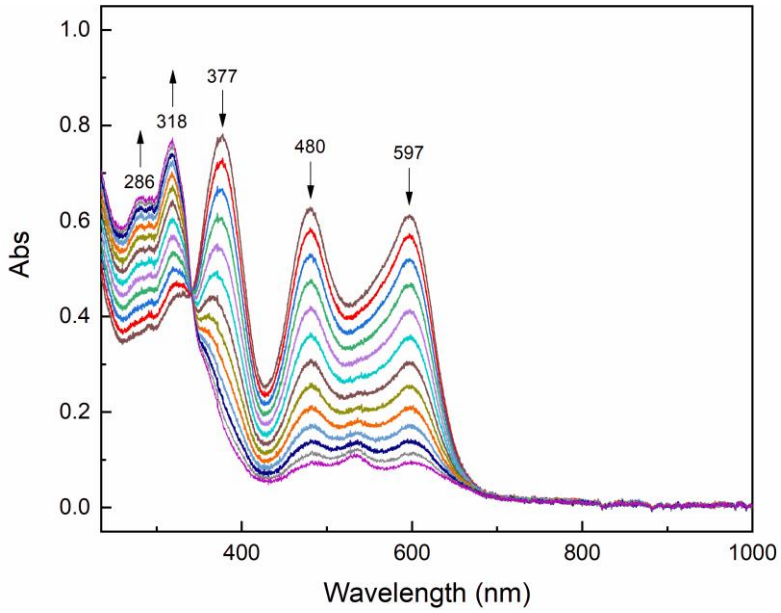

Figure 143: Absorption spectrum evolution of supposed **Ox2c**$^{2+}$ (2.42 x 10^{-4} M) in CH_2Cl_2 / $TBAPF_6$ 0.1 M under reduction at 0.40 V at RT. Optical path of the cuvette: 1 mm.

Again, no radical has been observed and this electrolysis seemed to cause the formation of a side-product in addition to the cycloreversion. This has been confirmed by the electrolysis at 0.00 V (Figure 144). In fact, differently from the case of the regiosiomer **Ox1**, **Ox2o** couldn't be completely recovered and a second species absorbing at 534 nm and 642 nm has been obtained.

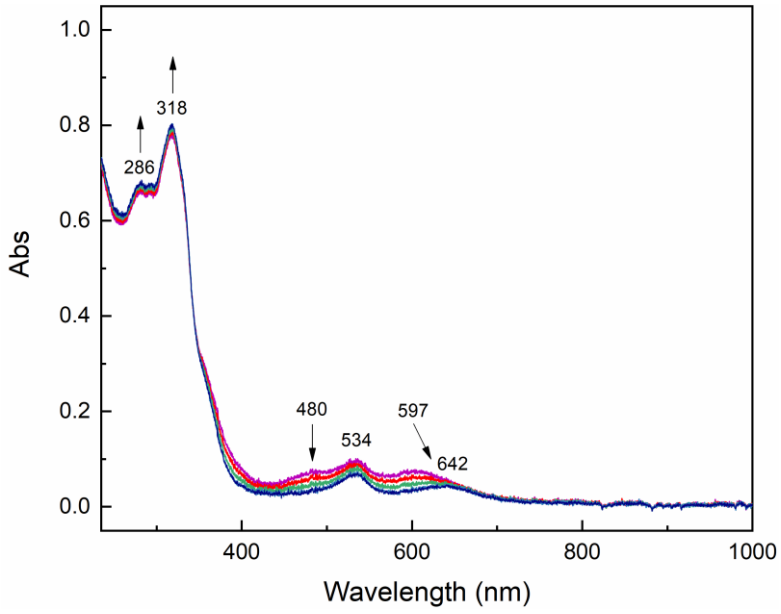

Figure 144: Absorption spectrum evolution of supposed **Ox2c**$^{2+}$ (2.42 x 10^{-4} M) in CH_2Cl_2 / $TBAPF_6$ 0.1 M under reduction at 0.00 V at RT. Optical path of the cuvette: 1 mm.

This spectral evolution confirms the non-negligible impact of the structural difference caused by the functionalization with the $–OCH_3$ groups in different positions. Once oxidized,

the *ortho*-methoxy-substituted terarylene seems more reactive than the *para*-substituted isomer and consequently more susceptible to side-reactions.

An intermediate behavior has been remarked for **Ox3**, since the formation of a side-product after oxidation and reduction was less pronounced. A solution of this molecule in acetonitrile / $TBAPF_6$ 0.1 M has been initially electrolyzed at RT at 1.00 V and the formation of **Ox3c^{2+}** has been monitored by UV-vis spectroscopy (Figure 145).

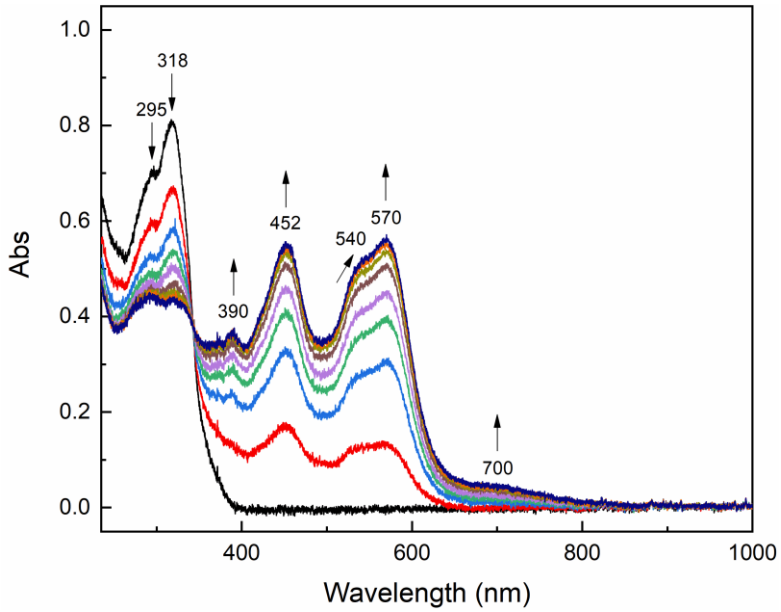

Figure 145: Absorption spectrum evolution of **Ox3o** (2.08×10^{-4} M) in CH_3CN / $TBAPF_6$ 0.1 M under oxidation at 1.00 V at RT. Optical path of the cuvette: 1 mm.

While the bands of the OF in the UV region (295 nm and 318 nm) decreased, new bands at 390 nm, 452 nm and 570 nm (with a shoulder at 540 nm) grew. Moreover, a broad low-intensity band appeared at 700 nm. Overall, the spectrum for the dicationic species is similar to that of **Ox1c^{2+}**, but the two main visible bands are shifted by 18 nm and 30 nm, respectively (i.e. 452 nm vs 470 nm and 570 nm vs 600 nm).

By carrying out a reduction initially at 0.20 V and then at 0.00 V, cycloreversion occurred and a side-product was formed also in this case, as suggested by the residual broad absorbance between 400 nm and 600 nm (Figure 146).

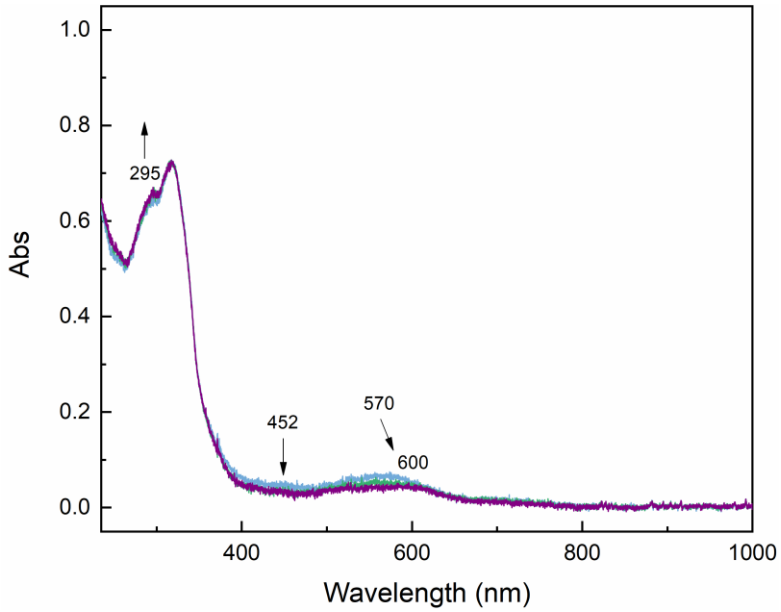

Figure 146: Absorption spectrum evolution of **Ox3c^{2+}** (2.08 x 10^{-4} M) in CH_3CN / $TBAPF_6$ 0.1 M under reduction at 0.00 V at RT. Optical path of the cuvette: 1 mm.

Last, methylthio-containing **Ox4** appeared as a promising candidate to observe a spectral signature of the closed form radical species since the two one-electron waves related to **Ox4c** ↔ **Ox4c$^{+\cdot}$** and **Ox4c$^{+\cdot}$** ↔ **Ox4c^{2+}** are separated by more than 200 mV, thus suggesting a certain stability of the monocationic intermediate. Nevertheless, after the generation of **Ox4c^{2+}** by oxidation of the solution in dichloromethane / $TBAPF_6$ 0.1 M at 1.30 V (Figure 147,a), the subsequent electrolysis at 0.55 V induced once again the cycloreversion without any detection of a radical (Figure 147,b).

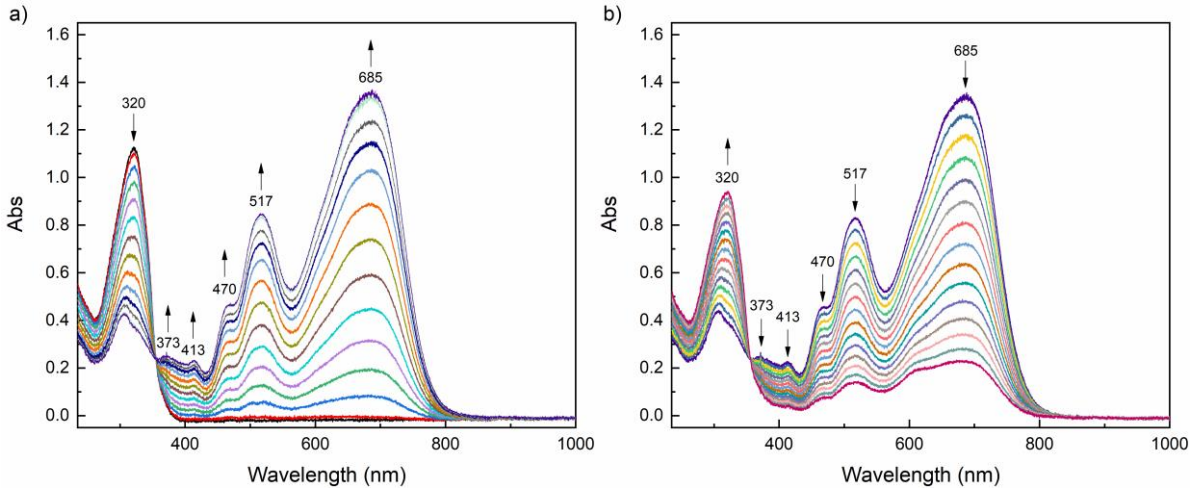

Figure 147: a) Absorption spectrum evolution of **Ox4o** (5.38 x 10^{-4} M) in CH_2Cl_2 / $TBAPF_6$ 0.1 M under oxidation at 1.30 V at RT; b) Absorption spectrum evolution of **Ox4c^{2+}** (5.38 x 10^{-4} M) in CH_2Cl_2 / $TBAPF_6$ 0.1 M under reduction at 0.55 V at RT. Optical path of the cuvette: 1 mm.

By lowering the potential to 0.00 V, the neutral open form has been recovered, but a side-product has been detected again, even if its formation seemed little compared to the cases of **Ox2** and **Ox3** (Figure 148).

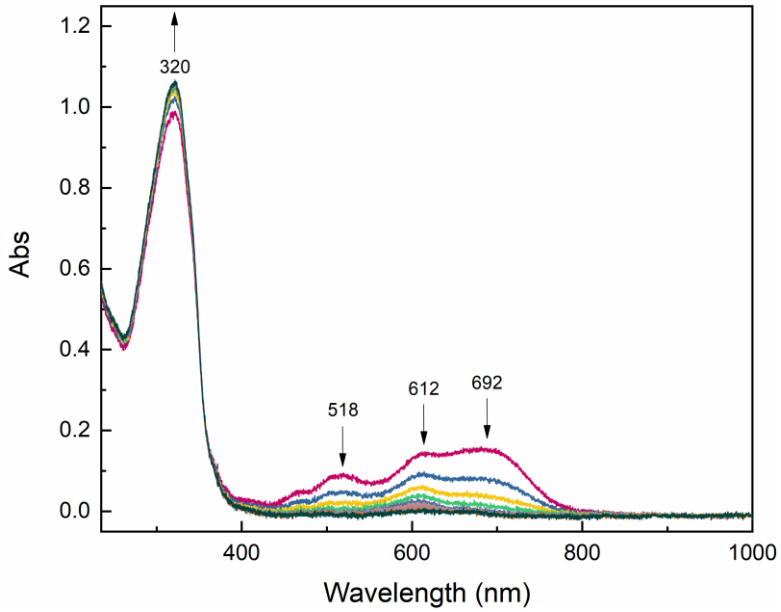

Figure 148: Absorption spectrum evolution of **Ox4c**$^{2+}$ (5.38 x 10^{-4} M) in CH_2Cl_2 / $TBAPF_6$ 0.1 M under reduction at 0.00 V at RT. Optical path of the cuvette: 1 mm.

4.3.2.5 Spectroelectrochemical study of **Ox5** and **Ox6**

Similar experiments have been conducted on **Ox5** and **Ox6** to verify if the neutral CF could be obtained for these derivatives or such a return to the neutral OF occurred even in the presence of the strongest electron-donating groups that have been selected for this investigation.

A solution of **Ox5** in dichloromethane / $TBAPF_6$ 0.1 M has been initially electrolyzed at RT at 0.80 V. The induced spectral evolution has been followed by UV-vis spectroscopy (Figure 149).

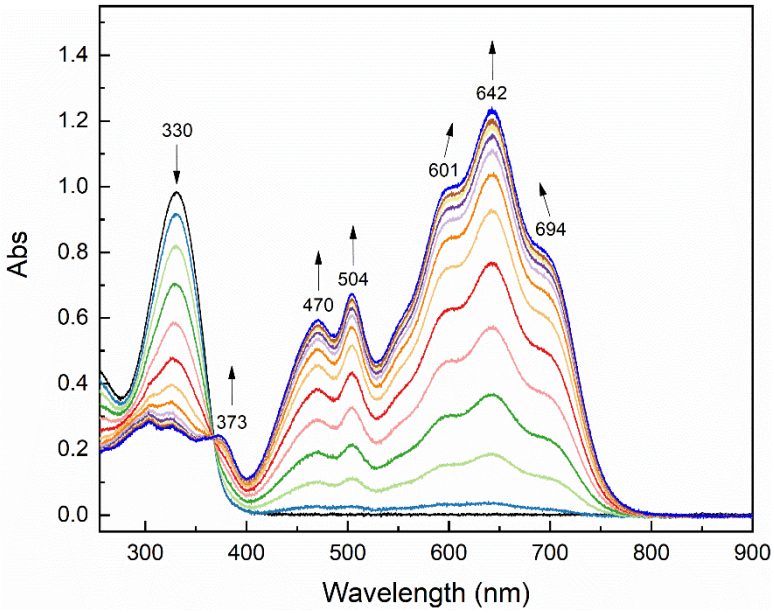

Figure 149: Absorption spectrum evolution of **Ox5o** (1.53 x 10^{-4} M) in CH_2Cl_2 / $TBAPF_6$ 0.1 M under oxidation at 0.80 V at RT. Optical path of the cuvette: 1 mm.

Similarly to what happened for the other four terarylenes, the oxidation led to a decrease of the characteristic band of the open form at 330 nm with the concurrent growth of a low-intensity band at 400 nm and several other bands in the visible (470 nm, 504 nm and 642 nm, with two shoulders at 601 nm and 694 nm). The corresponding species is **Ox5c^{2+}**.

A second electrolysis has been started at 0.05 V to reduce this dication. Even if a small band at 920 nm initially grew and then started to decrease, a slow conversion to the neutral OF seemed to happen (Figure 150).

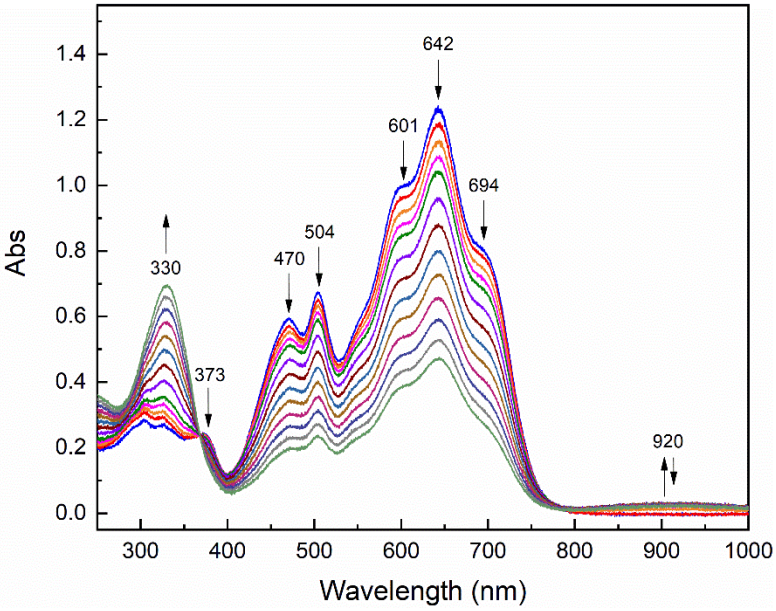

Figure 150: Absorption spectrum evolution of **Ox5c^{2+}** (1.53 x 10^{-4} M) in CH_2Cl_2 / $TBAPF_6$ 0.1 M under reduction at 0.05 V at RT. Optical path of the cuvette: 1 mm.

The possibility that the increase → decrease of the low-intensity infrared band (920 nm) was related to the generation of a detectable amount of the radical species **Ox5c**$^{+\cdot}$ that was then reduced again to **Ox5c** has been disproved when the potential for the electrolysis was moved to 0.00 V. In fact, a residual band in the visible peaking at 650 nm was afforded, but the spectrum didn't resemble that of the photo-generated neutral closed form isomer (Figure 151).

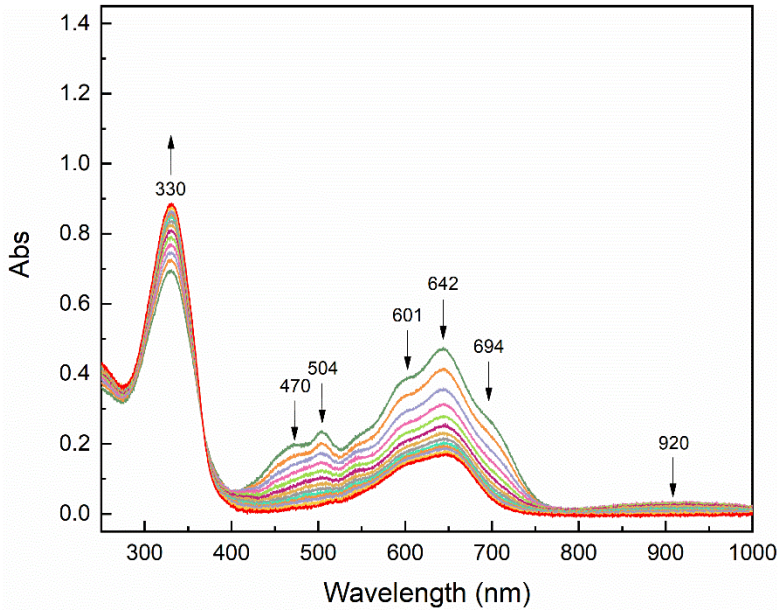

Figure 151: Absorption spectrum evolution of **Ox5c**$^{2+}$ (1.53 x 10^{-4} M) in CH_2Cl_2 / $TBAPF_6$ 0.1 M under reduction at 0.00 V at RT. Optical path of the cuvette: 1 mm.

To further confirm that this electrochemically generated species was a side-product, two other oxidation and reduction cycles have been performed to accumulate it so to compare the obtained UV-vis spectrum with that for the photostationary state at 320 nm (Figure 152).

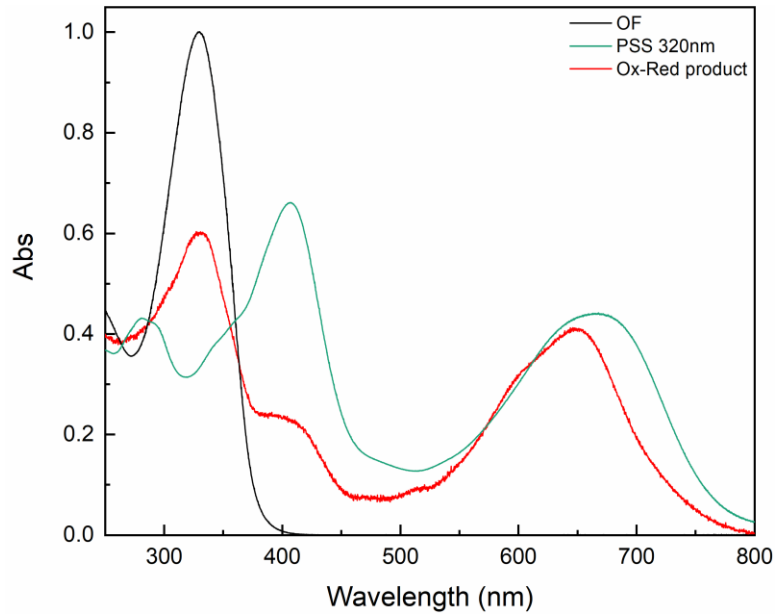

Figure 152: Comparison between the absorption spectrum (green solid line) at the PSS (320 nm) and (red solid line) after oxidation and reduction during the spectroelectrochemical experiment.

The residual bands between 300 nm and 450 nm for the species obtained by electrolysis are different compared to those of the photogenerated **Ox5c**. Moreover, the band in the visible of this electrochemically generated side-product has a different shape and it is blue-shifted by ~20 nm.

Concerning **Ox6**, a solution in dichloromethane / $TBAPF_6$ 0.1 M has been initially electrolyzed at RT at 1.00 V. The related spectral evolution is provided in Figure 153.

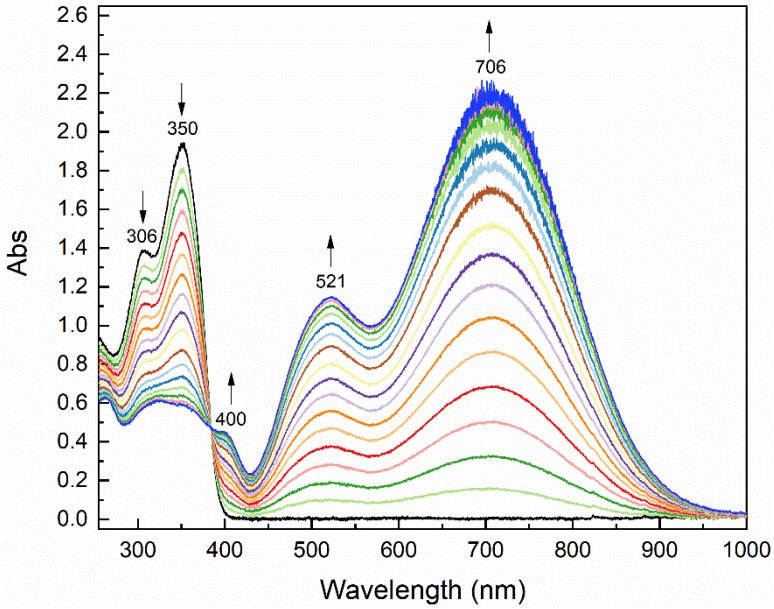

Figure 153: Absorption spectrum evolution of **Ox6o** (3.17×10^{-4} M) in CH_2Cl_2 / $TBAPF_6$ 0.1 M under oxidation at 1.00 V at RT. Optical path of the cuvette: 1 mm.

Ox6c^{2+} has been generated, as confirmed by the growth of the shoulder at 400 nm and the bands centered at 521 nm 706 nm, that are so broad to cover the whole visible region, while the bands of **Ox6o** (306 nm and 350 nm) diminished. As for the other two derivatives, no indication about monocationic radicals (either in the open or the closed form) have been obtained during the oxidation.

Step-by-step reduction has been tried to observe an optical signature of the radical species, expecting a possible stabilizing effect by the triphenylamino moieties. The electrolysis has been initially carried out at 0.25 V, the potential at with the reduction wave of **Ox6c**$^{2+}$ starts, according to the previously shown CV (Figure 154).

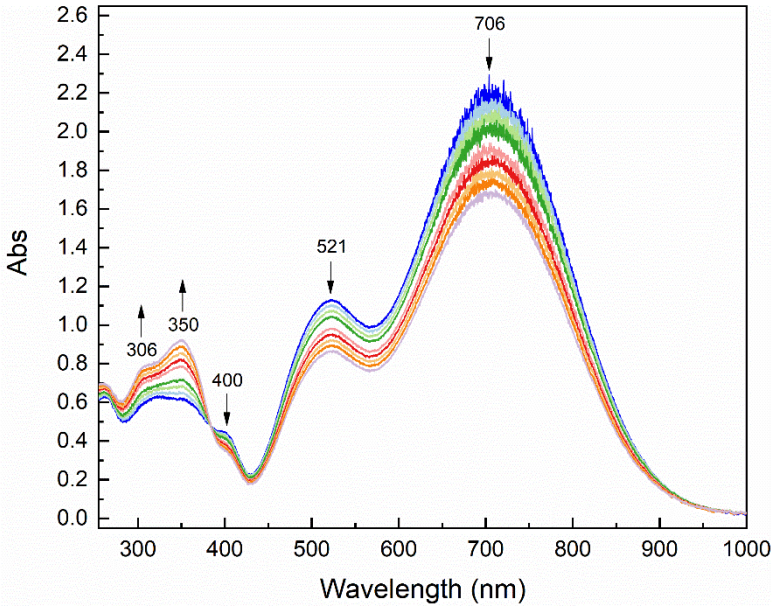

Figure 154: Absorption spectrum evolution of **Ox6c^{2+}** (3.17 x 10^{-4} M) in CH_2Cl_2 / $TBAPF_6$ 0.1 M under reduction at 0.25 V at RT. Optical path of the cuvette: 1 mm.

The spectral variation at such a potential was very slow and no radical has been observed. Then, the reduction has been performed at 0.00 V and a band in the visible (677 nm) has been eventually obtained (Figure 155).

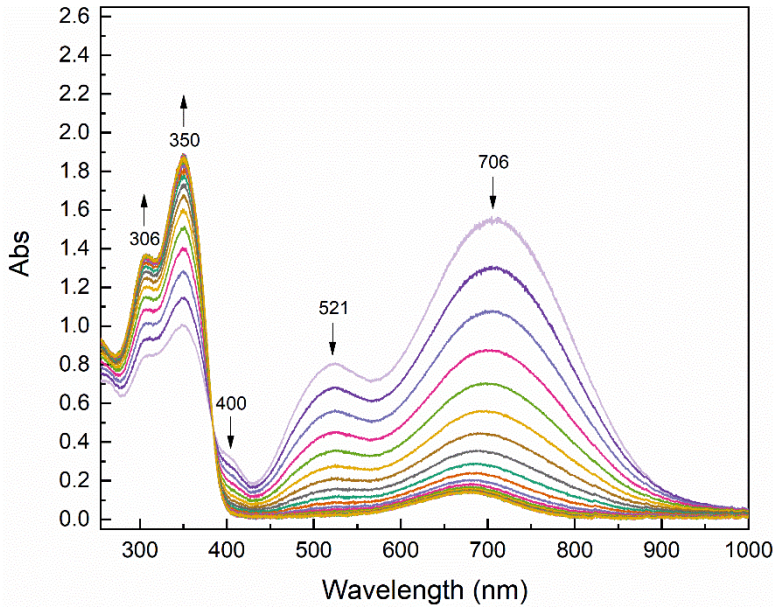

Figure 155: Absorption spectrum evolution of **Ox6c^{2+}** (3.17 x 10^{-4} M) in CH_2Cl_2 / $TBAPF_6$ 0.1 M under reduction at 0.00 V at RT. Optical path of the cuvette: 1 mm.

Once again, this band wasn't indicative of the obtainment of the neutral closed form species. Moreover, a last reduction at -0.20 V caused its disappearance and the conversion to **Ox6o** has been completed (Figure 156).

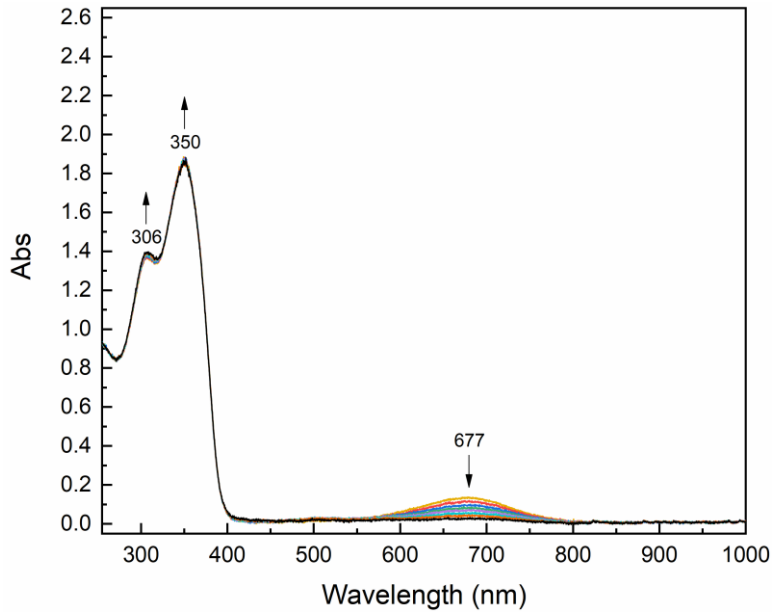

Figure 156: Absorption spectrum evolution of **Ox6c^{2+}** (3.17 x 10^{-4} M) in CH_2Cl_2 / $TBAPF_6$ 0.1 M under reduction at -0.20 V at RT. Optical path of the cuvette: 1 mm.

In conclusion, all the photochromes (excluding **Ox2**) appeared to undergo the expected oxidative cyclization in the timescale of a fast experiment such as cyclic voltammetry. However, the CVs at the photostationary states and the spectroelectrochemical experiments proved that no neutral closed form could be obtained, because of an unexpectedly fast redox-induced ring-opening. The supposed mechanism that might rationalize this process is presented in the following Section.

4.3.2.6 Mechanism ruling the redox-active behavior of **Ox1** – **6**

Ox1 has been chosen to investigate the mechanism that hinders the electrochemical generation of the neutral closed form of these terarylenes by electrolysis, contrarily to what has been reported for similarly functionalized diarylethenes by Feringa and co-workers [137]. Given their qualitatively similar redox behavior, the presented mechanism should hold for the other derivatives of this group, too.

Since photo-generated **Ox1c** is thermally stable, the ring-opening reaction might occur on **Ox1c^{2+}** or **Ox1c$^{+\cdot}$**. In the Supporting Information of ref. [141], work where a DAE derivative showing oxidative cyclization had been linked to an indium tin oxide (ITO) surface, Feringa and co-workers stated that an oxidative ring-opening reaction could also occur even if thermodynamically disfavored. It would happen because of the dismutation of $CF^{+\cdot}$ to afford neutral CF and CF^{2+} and this latter species is in equilibrium with OF^{2+}. Moreover, the authors suggested that this equilibrium shifts in favor of the dicationic open form at slower scan rates and a return to the open form could be achieved.

To verify the thermal stability of the dicationic species, a solution of **Ox1o** in acetonitrile has been oxidized with two equivalents of tris(4-bromophenyl)ammoniumyl

hexachloroantimonate (also known as "magic blue", $E^{0'}$ = 0.67 vs Fc in acetonitrile [222]) and the obtained spectrum is shown in Figure 157.

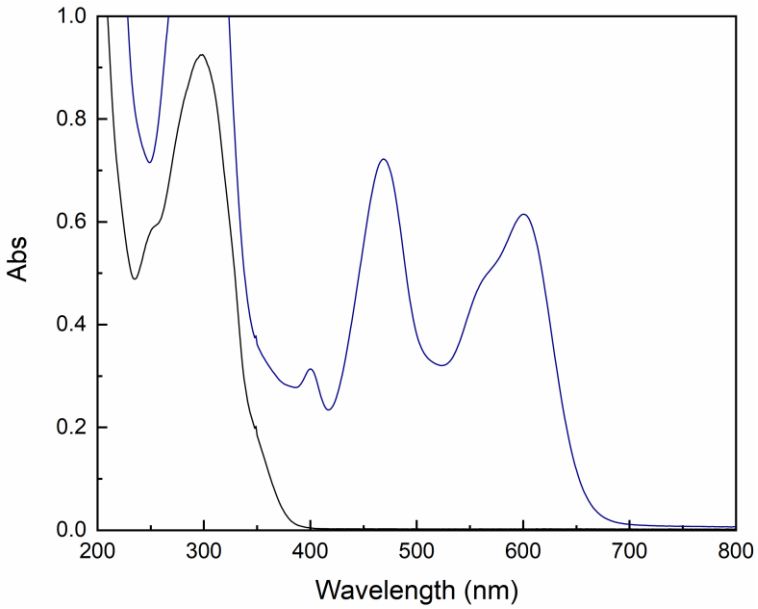

Figure 157: Absorption spectrum of **Ox1o** (1.92 x 10^{-5} M) in acetonitrile (black solid line) before and (navy solid line) after oxidation to **Ox1c^{2+}** with 2 eq of magic blue. Optical path of the cuvette: 1 cm.

While the visible region of the spectrum is equivalent to that obtained during the spectroelectrochemical experiment and confirmed that the oxidation of the OF leads to **Ox1c^{2+}**, the UV region is dominated by an intense band related to the chemical oxidant.

Then, the solution has been kept in the dark for 1 h and the observed spectral evolution at RT is shown in Figure 158.

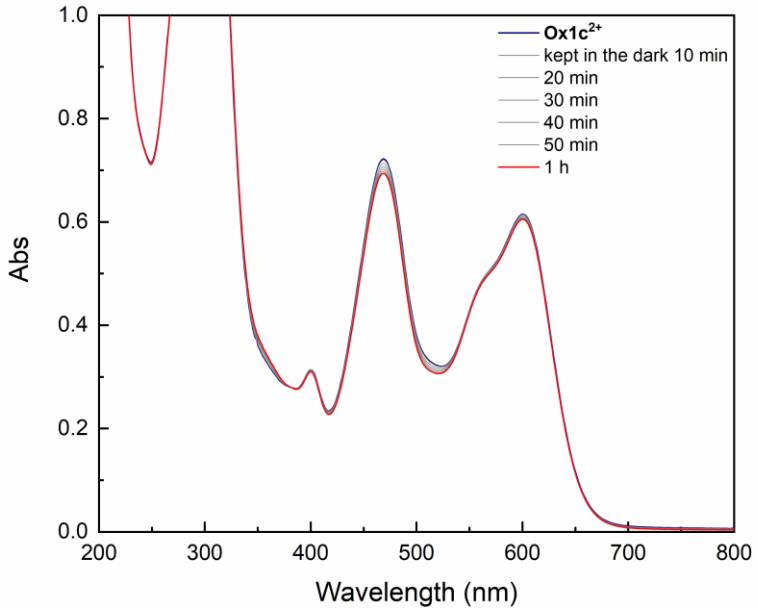

Figure 158: Thermal evolution of **Ox1c^{2+}** in acetonitrile in the dark.

Since only a slight decrease has been detected in 1 h, a certain degree of thermal stability can be supposed for this dication. Consequently, a different mechanism from that indicated by Feringa's group will be proposed to rationalize the occurrence of the cycloreversion, that has been ascribed to the generation of **Ox1c**$^{+\cdot}$ and its spontaneous ring-opening.

However, no radical has been observed at all during the spectroelectrochemical experiment. To prove the generation of the radical, a coupled electrolysis-EPR experiment has been attempted in collaboration with Dr. Herrero at Université Paris-Saclay. Since acetonitrile couldn't be used for an EPR experiment at room temperature, dichloromethane has been chosen as solvent.

With an in-house setup based on two Pt spirals as working and counter electrodes and an Ag wire as pseudo-reference electrode [223], it has been possible to perform the desired electrochemical experiment inside an EPR tube. First, a CV has been recorded to verify the potentials at which the redox processes occurred in such a system (Figure 159).

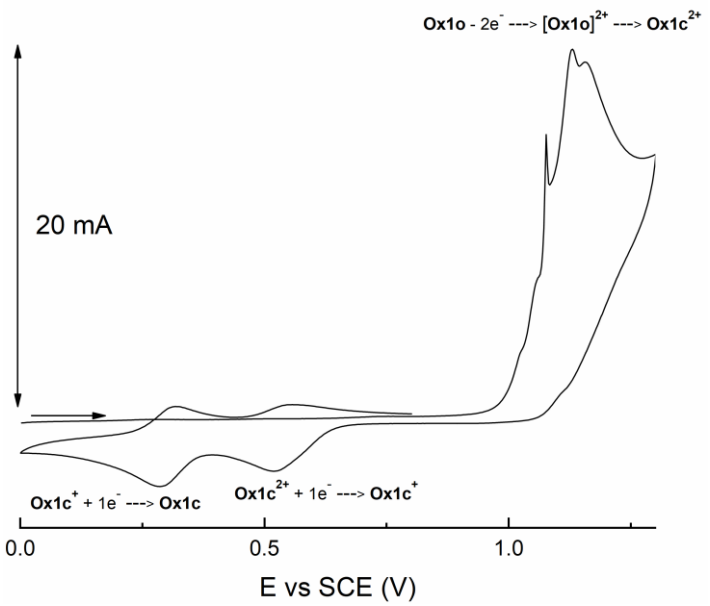

Figure 159: CV of **Ox1o** (2.5 mM) in CH_2Cl_2 / $TBAPF_6$ 0.24 M. ν = 100 mV/s.

Even if the cyclic voltammogram shows some noise for the oxidation wave of **Ox1o**, it provides qualitative useful information about the redox properties of the switch in CH_2Cl_2 / $TBAPF_6$ 0.24 M: the open form is irreversibly oxidized at ~1.15 V leading to the appearance of the waves related to the closed form at ~0.30 V and ~0.54 V. Compared to the data obtained in CH_3CN / $TBAPF_6$ 0.1 M, these two one-electron waves are significantly more separated (240 mV vs 140 mV) because of the use of a less donating solvent.

Accordingly, EPR spectra (microwave frequency = 9.63 GHz; microwave power = 1 mW; modulation amplitude = 8 Gauss; gain = 50 dB) have been recorded before the electrolysis, after the oxidation at 1.3 V and after the reduction at 0.5 V and they are provided in Figure 160.

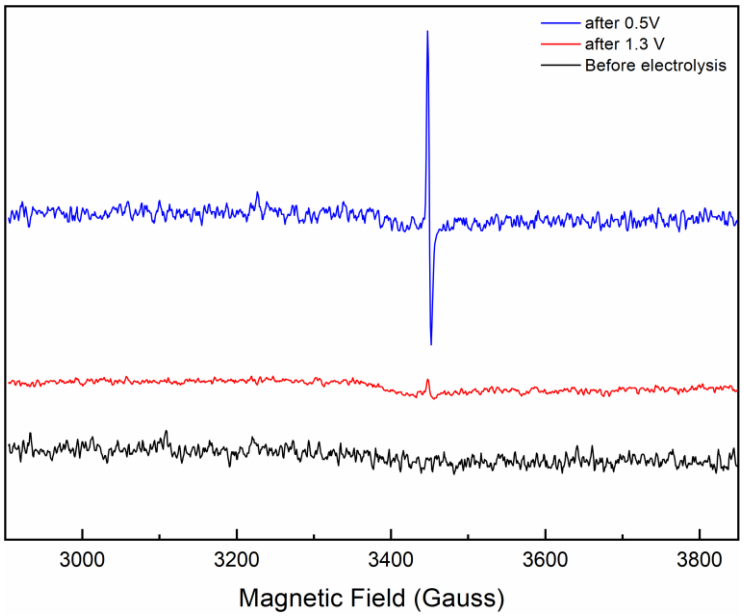

Figure 160: Absorption spectra of **Ox1** in CH_2Cl_2 / $TBAPF_6$ 0.24 M (black solid line) before the electrolysis, (red solid line) after the oxidation at 1.3 V and (blue solid line) after the reduction at 0.5 V.

As expected, the neutral open form didn't show any signal, being diamagnetic. Similarly, no signal has been observed for the twice oxidized **Ox1c**$^{2+}$ that has been generated by the electrolysis at 1.3 V. On the contrary, the formation of an organic radical species has been detected after the reduction at 0.5 V. This species wasn't persistent and it hasn't been possible to record multiple spectra to increase the intensity of the signal. Clearly, this experiment doesn't allow to state that the observed radical is **Ox1c**$^{+\cdot}$ instead of **Ox1o**$^{+\cdot}$, but it proves the formation of such an intermediate.

If the open form radical is generated, it is reasonable to think that the oxidative cycloreversion mechanism proposed by Kawai and co-workers and described in Chapter 1 is occurring also on **Ox1** (and the other members of the investigated family). In fact, **Ox1o**$^{+\cdot}$ is expected to be a stronger oxidant than **Ox1c**$^{+\cdot}$ and to afford the neutral open form by oxidizing a neighbor electrochemically generated **Ox1c** molecule to **Ox1c**$^{+\cdot}$, that would undergo the same process again and again until the total conversion to **Ox1o**.

The occurrence of such a mechanism could explain why, after the oxidation of the open form, the waves of the two redox processes involving the closed form in the CV are not symmetric. During the experiment:

1. At 1.12 V, **Ox1o** is oxidized to **Ox1o**$^{2+}$ that rapidly evolves to **Ox1c**$^{2+}$.
2. On the back scan, **Ox1c**$^{2+}$ is reduced to **Ox1c**$^{+\cdot}$ at $E_{1/2}$ = 0.42 V. However, if a spontaneous ring-opening is occurring, the obtained open form radical would be rapidly reduced to **Ox1o** at such a potential, thus lowering the quantity of closed form species in the diffusion layer and consequently affecting the symmetry of the waves.
3. The remaining **Ox1c**$^{+\cdot}$ is reduced to the neutral CF at $E_{1/2}$ = 0.28 V.

At this point, if a second cycle is started:

4. The electrochemically generated **Ox1c** is oxidized at $E_{1/2}$ = 0.28 V to **Ox1c**$^{+\cdot}$. Again, this species might isomerize to **Ox1o**$^{+\cdot}$. Nevertheless, this species can't be oxidized at this potential while sweeping anodically. In fact, a potential of at least 1.12 V should be required to generate **Ox1o**$^{2+}$. This means that, differently from what has been proposed in point 2, the species might remain in the diffusion layer and participate in the oxidative cycloreversion in addition to a possible reduction at the surface of the electrode.
5. The remaining **Ox1c**$^{+\cdot}$ is oxidized to the dicationic CF at $E_{1/2}$ = 0.42 V.

Moreover, the improved reversibility at higher scan rates suggests that this unexpected cycloreversion is limited in shorter timescales.

In support to the validity of this mechanism causing a return to the neutral open form, cyclic voltammetry on the irradiated solution of **Ox1** in CH_3CN / $TBAPF_6$ 0.1 M has shown that the wave related to the oxidation of **Ox1o** grew in intensity at expense of the waves related to the closed form if two cycles were recorded (Figure 161).

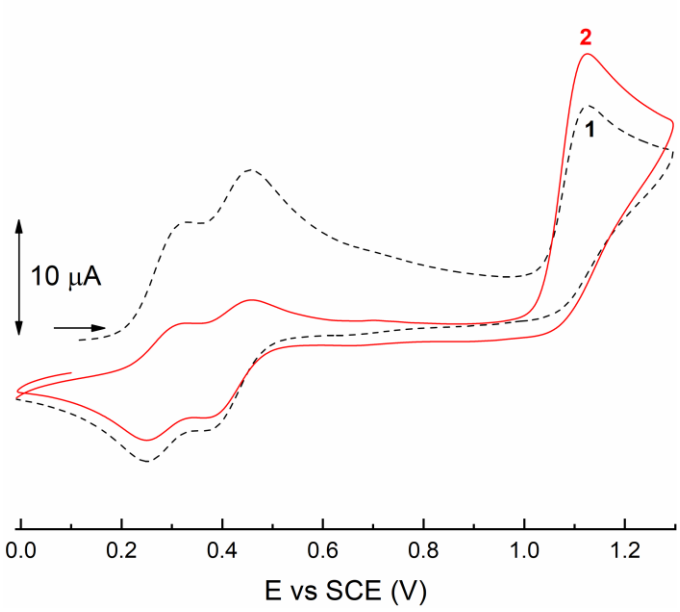

Figure 161: CVs of **Ox1** (1 mM) in CH_3CN / $TBAPF_6$ 0.1 M at the PSS, (black dashed line) 1st cycle and (red solid line) 2nd cycle, indicating the occurrence of a ring-opening reaction. ν = 100 mV/s.

The overall mechanism can be summarized as in Figure 162.

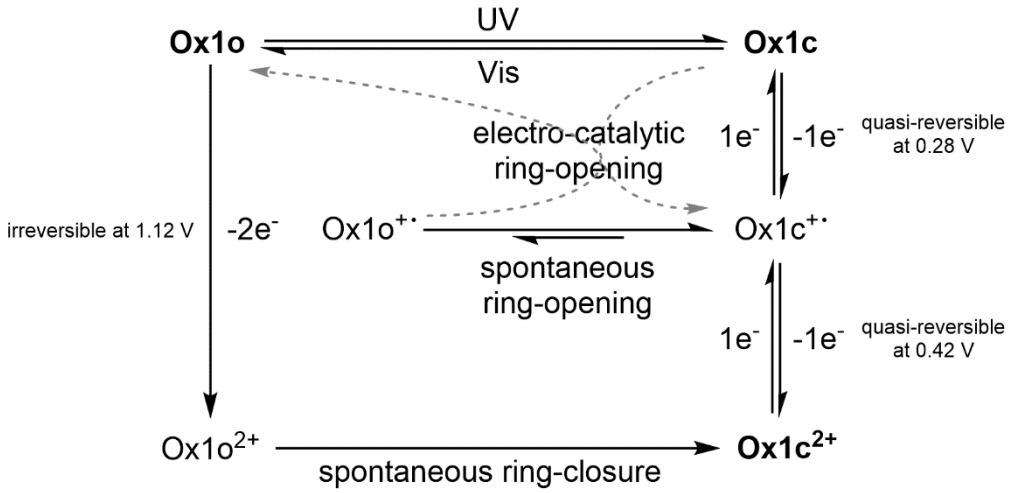

Figure 162: Summary of the photochemical and electrochemical transformations occurring on **Ox1o**.

4.3.2.7 Theoretical modelling of **Ox1** – **6**

In the attempt of reinforcing this mechanism, theoretical modelling has been carried out on the six investigated terarylenes, in collaboration with Pr. Maurel (ITODYS – Université de Paris).

The geometries of the six compounds have been optimized in acetonitrile (for the sake of comparison) in the three redox states 0, +1 and +2. The energy differences between CF and OF in these states have been calculated by using two different functionals, wb97XD/6-311g(d,p) in one case and CAM-B3LYP/6-311g(d,p)//wb97XD/6-311g(d,p) in the other one. The results are presented in Figure 163,a and Figure 163,b, respectively. In both graphs, the energies of the open forms have been arbitrarily set to 0 kJ/mol for every compound.

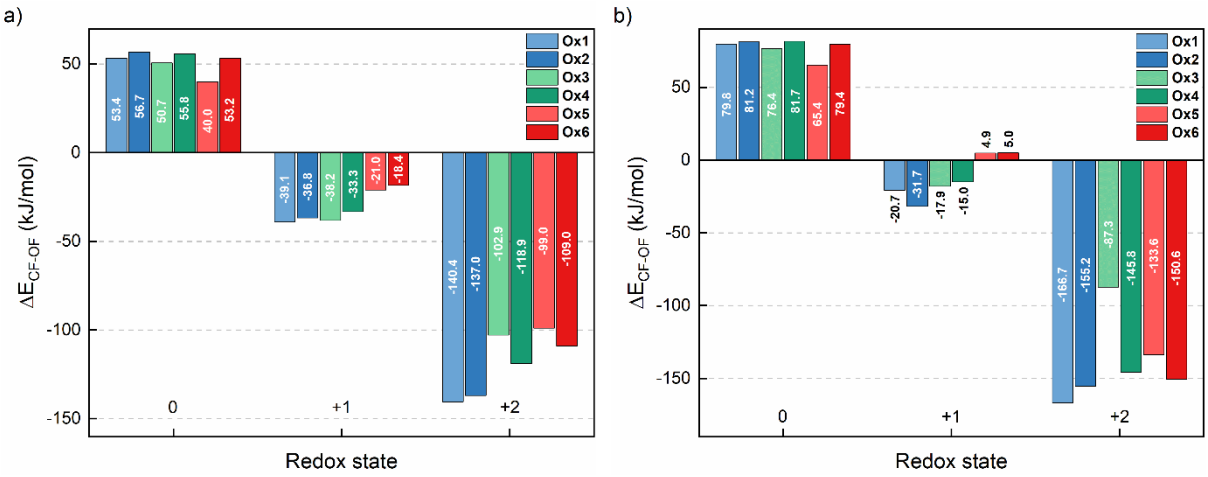

Figure 163: Relative energies of the closed forms and the open forms for **Ox1** – **6** at the ground state in the three different redox states in acetonitrile at a) wb97XD/6-311g(d,p) and b) CAM-B3LYP/6-311g(d,p)//wb97XD/6-311g(d,p) level of calculations.

Whatever the chosen functional, the neutral open forms are more stable than the respective closed forms, according to the calculations. The energy difference between the two isomers

appears to be only slightly dependent on the nature of the substituents in this redox state. In the dicationic state, the CF is strongly stabilized, coherent with the cyclization occurring after the two-electron oxidation of the OF. In this case, the impact of the different substituents seems to be more pronounced, as suggested by the variation of the stability of the closed form by ~21 kJ/mol and ~16 kJ/mol when $–OCH_3$ (i.e. **Ox1**) is replaced with $–SCH_3$ (i.e. **Ox4**) and $–NPh_2$ (i.e. **Ox6**), respectively.

Concerning the radical species, the energy difference between the isomers is smaller than in the other redox-states. Moreover, when CAM-B3LYP/6-311g(d,p)//wb97XD/6-311g(d,p) has been used, the radical open and closed forms appeared to be even closer in energy.

Clearly, the obtained results can't be used to definitively confirm the proposed mechanism and a correlation between the energy values of each molecule with its experimentally observed behavior is not straightforward. Nevertheless, the overall trend of these computations, showing that the stability of the closed forms is significantly higher in the dicationic state compared to the radical one, can be considered in accordance with the hypothesis of a ring-opening occurring when **Ox1c**$^{+\cdot}$ – **6c**$^{+\cdot}$ are generated.

Additionally, it is interesting to compare the results of the computations at the wb97XD/6-311g(d,p) level in acetonitrile concerning **Ox1** to those obtainable by modelling the DTE investigated by Feringa in ref. [137] in the same conditions (Figure 164, showing the reference DTE molecule on the top).

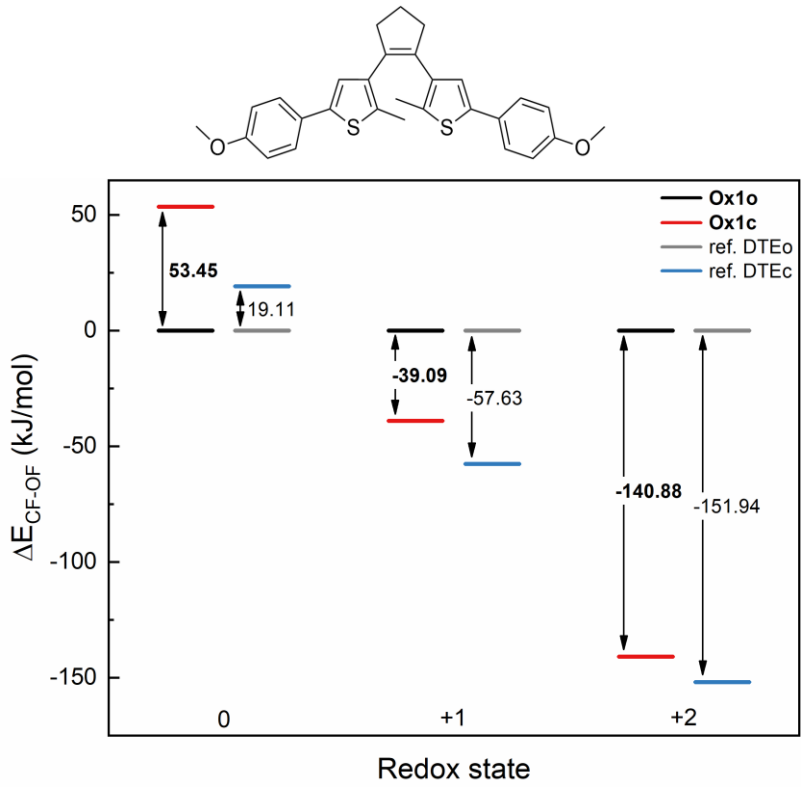

Figure 164: top) DTE undergoing oxidative cyclization, investigated in ref. [137]; bottom) relative energies of the closed forms and the open forms for the **Ox1** and ref. DTE at the ground state in the three different redox states at wb97XD/6-311g(d,p) level in acetonitrile.

As it can be observed, the neutral open forms (i.e. **Ox1o** and DTEo) are more stable than the respective closed forms. However, the energy difference is significantly larger in the case of **Ox1**, in good accordance with the lower stability of the ring-close species in terarylenes. In the case of the redox state +2, the ref. DTEc is strongly stabilized, coherently with the cyclization occurring after the two-electron oxidation of the OF.

At the monocationic state, it is worth noting that the energy difference between **Ox1o**$^{+\cdot}$ and **Ox1c**$^{+\cdot}$ is smaller than that determined for the reference DTE derivative, another result that seems compatible with the different redox-induced behavior of **Ox1** and the other members of the investigated family of switches here presented compared to that described in the work about ref. DTE.

*4.3.3 Synthesis route to **Ox7** – **10***

Regarding the four terthiazoles that have been shown at the beginning of this Chapter, **Ox7** – **9** have been prepared by using the respective thioamides (concerning the intermediate **66**, the procedure described by Aki and co-workers has been followed [224]) and **33** so to synthesize the required 2-(4-substituted)-5-methyl-thiazoles (Figure 165).

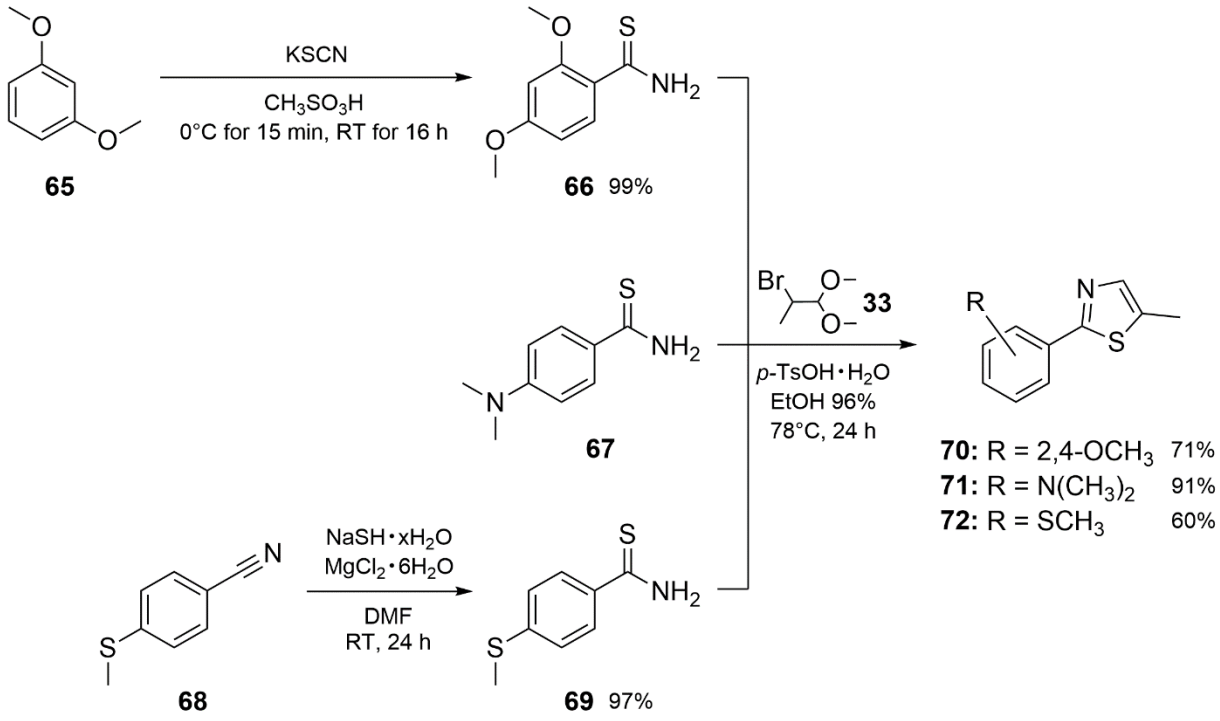

Figure 165: Synthesis routes to intermediates **70**-**72**.

Once obtained, these substrates have been converted to their boronic pinacol esters by directly functionalizing the C_4 as shown in Figure 166.

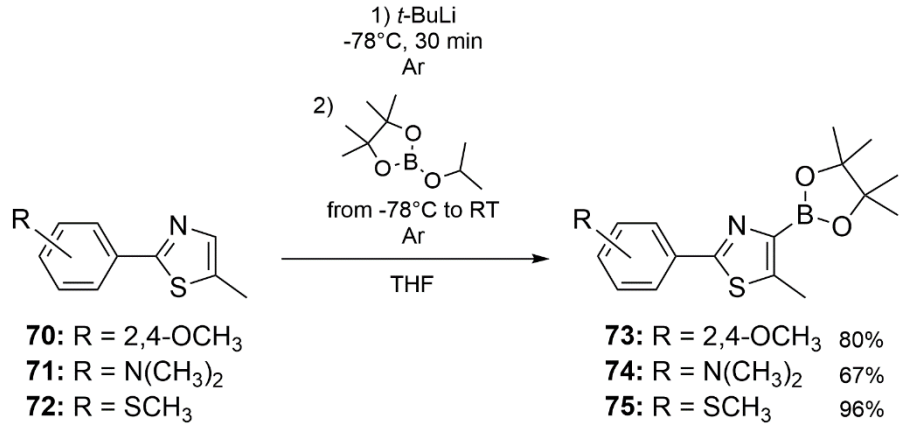

Figure 166: Synthesis of intermediates **73**-**75**.

Finally, these intermediates have been reacted with **37** in a double cross-coupling reaction (Figure 167).

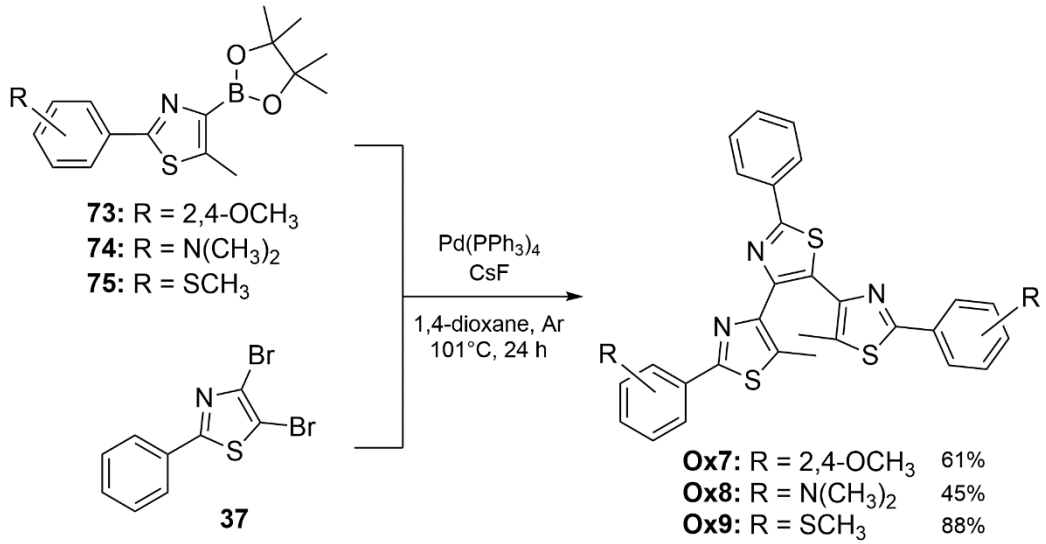

Figure 167: Synthesis of **Ox7** – **9**.

In the case of **Ox10**, 2,4-dibromo-5-methylthiazole and (4-(diphenylamino)phenyl)boronic acid (**52**) have been used for the synthesis of 2-(4-(diphenylamino)phenyl)-4-bromo-5-methyl-thiazole, **76** (Figure 168).

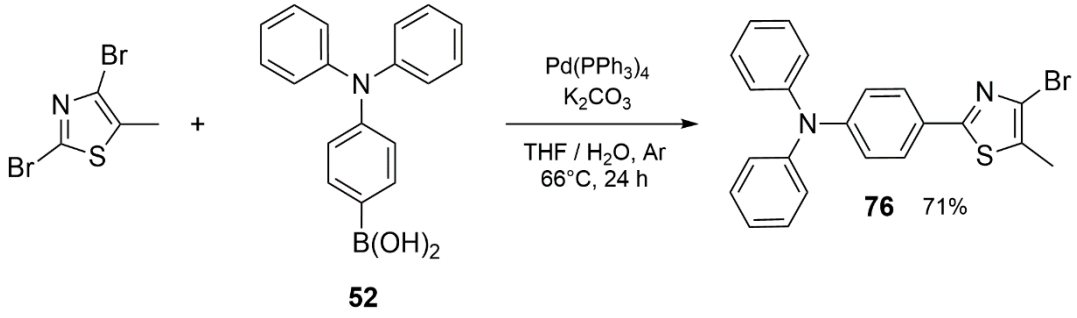

Figure 168: Synthesis of intermediate **76**.

A direct Suzuki-Miyaura reaction of this brominated intermediate with **28**, followed by the direct arylation of the obtained derivative with **76** again, afforded the desired terthiazole (Figure 169).

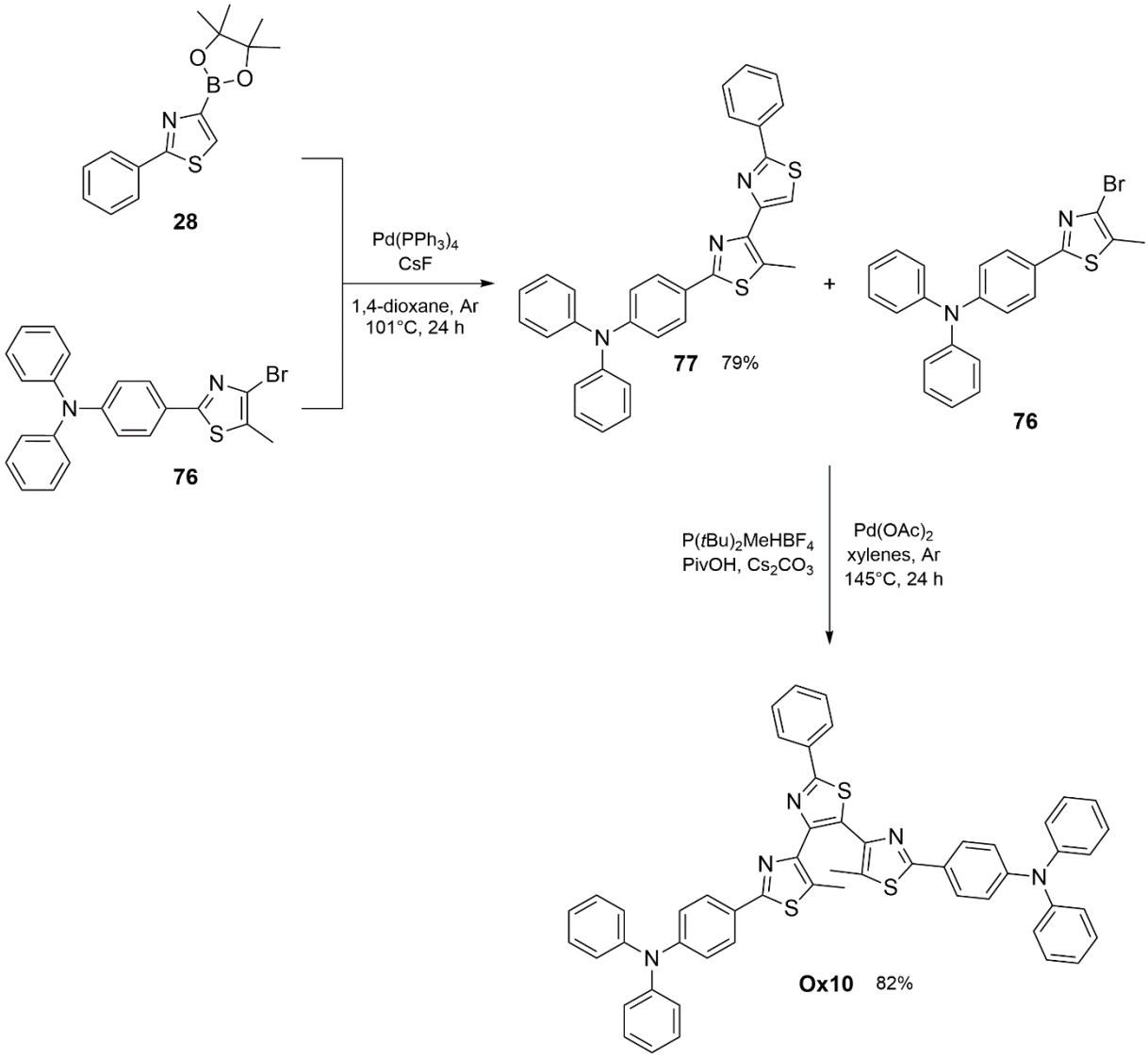

Figure 169: Synthesis route to **Ox10**.

*4.3.4 Photochemical and redox-active behavior of **Ox7** – **10***

4.3.4.1 Stationary UV-vis spectroscopy and fluorescence

The photochromic behaviors of **Ox8** has been investigated in acetonitrile at room temperature while **Ox7** and **Ox9** have been studied in acetonitrile + a minimum volume of dichloromethane to guarantee a complete dissolution using steady-state absorption spectroscopy. For solubility reasons, **Ox10** has been examined in dichloromethane. The solutions haven't been degassed unless stated otherwise. The obtained spectra are provided in Figure 170, where the open forms are presented with black solid lines and the

photostationary states with blue or green solid lines, depending on the color of the irradiated solution.

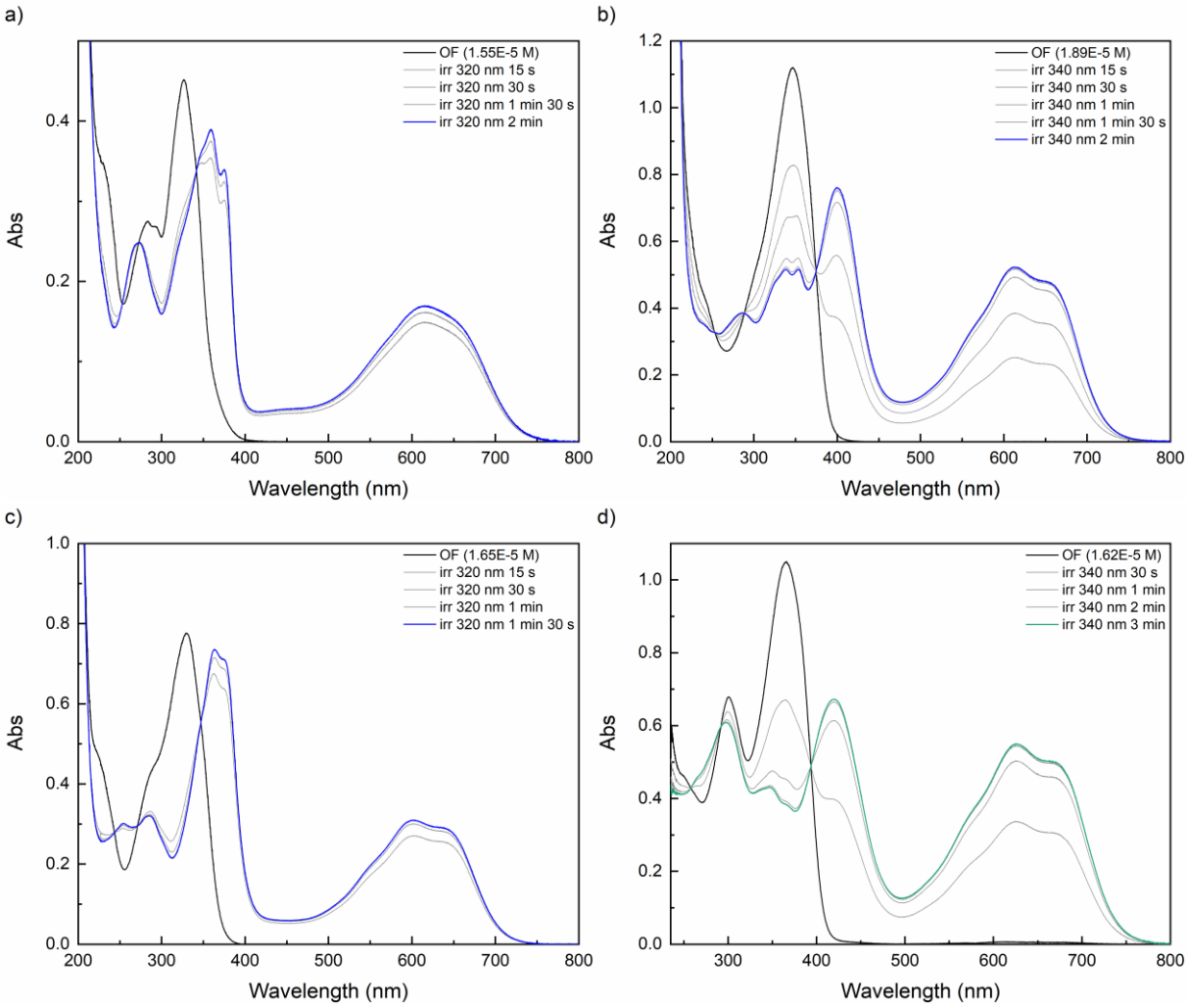

Figure 170: Absorption spectra in acetonitrile (a minimum volume of dichloromethane is needed for **Ox7** and **Ox9**) of (a) **Ox7**, (b) **Ox8**, (c) **Ox9** and in dichloromethane of (d) **Ox10**, showing the evolution under UV light irradiation (at 320 nm for **Ox7** and **Ox9**, at 340 nm for **Ox8** and **Ox10**) from the black lines for the OFs to the blue or green lines to indicate the respective photostationary states. Concentrations are indicated on the Figure. Optical path of the cuvette: 1 cm.

Ox7 – **10** show an intense absorption band in the UV region in their open forms, with λ_{max} between 300 and 350 nm. As for the thiophene-based derivatives, good photochromic properties have been observed also for these switches, with a rapid conversion to the thermally stable closed forms under light irradiation, as confirmed by the growth of broad absorption bands covering the 500 - 700 nm spectral region.

As for **Ox1** – **6**, all the switches in their CF are also characterized by a band around 400 nm, that is broad for **Ox8** and **Ox10**, while a shoulder can be detected in the cases of **Ox7** and **Ox9**.

Additionally, since **76** is strongly fluorescent (emission spectrum in the Annexes, page 252) with a quantum yield of 67% in dichloromethane determined by using 9,10-

diphenylanthracene in cyclohexane as reference, an emission band at 445 nm has been observed also for **Ox10o** (emission spectrum in the Annexes, page 253). By investigating the fluorescence of this switch in CH_2Cl_2, a quantum yields of 7% (always with respect to the same reference) has been determined.

The coexistence of fluorescence and the redox-active behavior for this derivatives and its precursor would make them potentially appealing for electrofluorochromism.

4.3.4.2 Electrochemical properties

The electrochemical properties of the four photochromes have been investigated by cyclic voltammetry (CV) at room temperature in acetonitrile or dichloromethane / $TBAPF_6$ 0.1 M with a scan rate (ν) of 100 mV/s. In particular, acetonitrile has been used for **Ox8**.

The main data (i.e. half-wave potentials, $E_{1/2}$, and ΔE for reversible waves; peak potentials, E_p, for irreversible ones) referenced to a saturated calomel electrode (SCE) are reported in Table 14.

Table 14: Redox potentials vs SCE in CH_3CN or CH_2Cl_2 / $TBAPF_6$ 0.1 M of the four investigated terarylenes.

	OF		CF	
	$E_{1/2}$ or E_p (V)	ΔE (mV)	$E_{1/2}$ or E_p (V)	ΔE (mV)
Ox7[b]	1.16 (irr) 1.36 (qr)	/ 160	0.37 0.52	80 90
Ox8[a]	0.83 (irr)	/	0.29	60
Ox9[b]	1.32 (irr)	/	0.65 0.86	80 80
Ox10[b]	1.03 (irr)	/	0.47	120

[a] solvent: acetonitrile; [b] solvent: dichloromethane.

The four molecules, either in the OF or the CF, didn't show any reduction wave when sweeping cathodically in the considered potential window. Whatever the derivative, an irreversible two-electron oxidation wave has been detected for the open form. The oxidation potential has been lowered from 1.32 V (in CH_2Cl_2 / $TBAPF_6$ 0.1 M) for **Ox9** to 0.83 V (in CH_3CN / $TBAPF_6$ 0.1 M) for **Ox8** with the replacement of the thiomethyl group with a much stronger electron-donating group such as the dimethylamino.

Cyclic voltammograms for **Ox7** – **10** are presented in Figure 171.

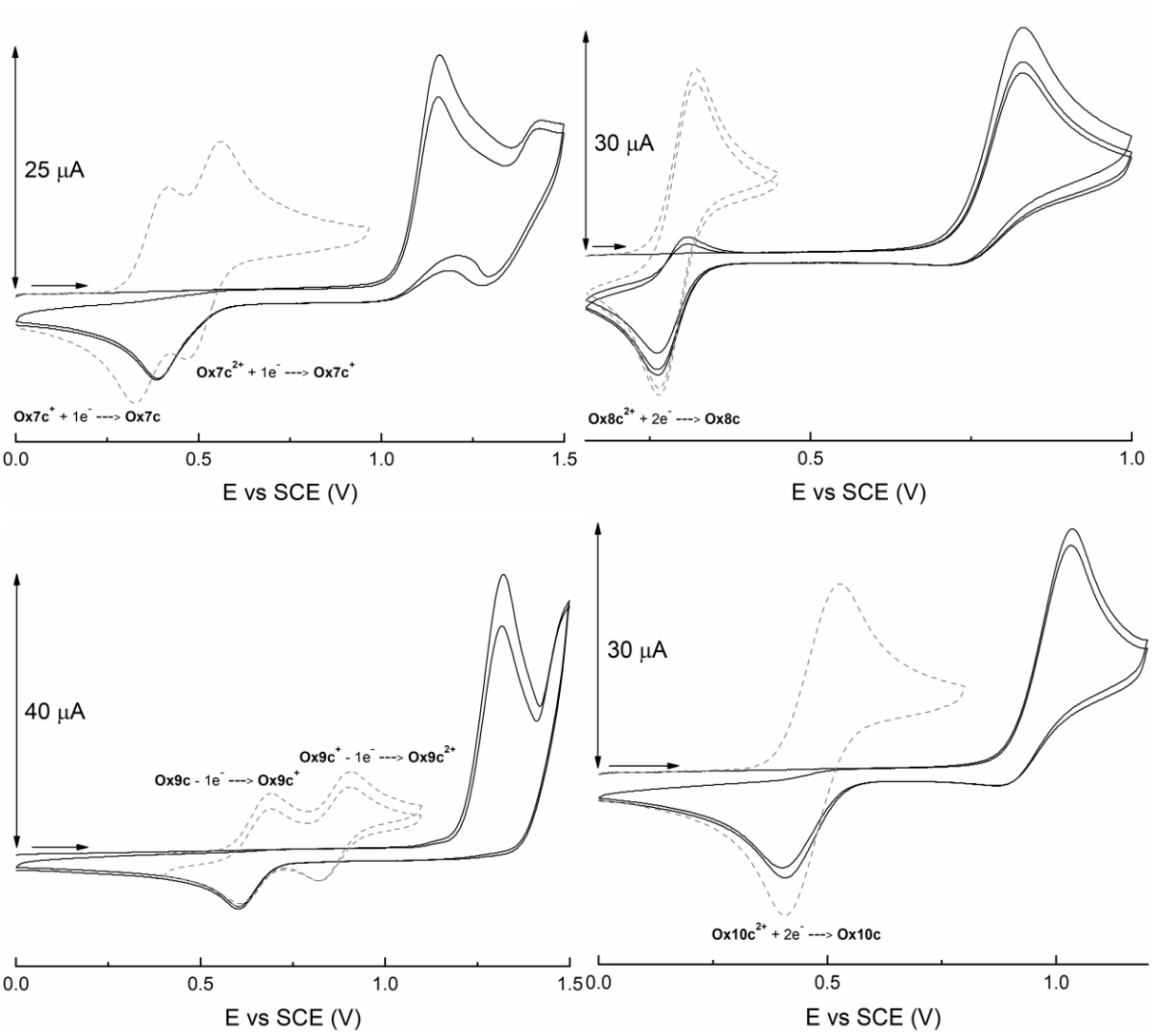

Figure 171: CVs of **Ox7** – **10** (1 mM) in CH_3CN (**Ox8**) or CH_2Cl_2 (**Ox7** and **Ox9** – **10**) / $TBAPF_6$ 0.1 M in the OF (black solid lines) and at the PSS (grey dashed lines). ν = 100 mV/s.

After the irreversible oxidation of the open form isomers, a wave has been observed at 0.39 V of **Ox7**, at 0.26 V for **Ox8**, at 0.60 V for **Ox9** and at 0.40 V for **Ox10**. These waves are irreversible for **Ox7** and **Ox9** – **10** and they don't match the waves detected in the CVs of the solutions irradiated at 365 nm. In fact, reversible redox waves have been remarked, either two one-electron waves (as for **Ox7** and **Ox9**) or a single one (**Ox10**), for the photochemically-generated closed forms. This suggests that these three compounds don't undergo oxidative cyclization, probably because the introduced functional groups aren't electron-donating enough, but the oxidation leads to another redox-active species. Surprisingly, the general shape of the CVs is similar for all the compounds, as if the nature of the generated species after the oxidation is the same, whatever the terthiazole.

Furthermore, by recording multiple CV cycles for **Ox7** (up to the first oxidation wave) and **Ox10**, it has been possible to verify that, whatever the species that is generated after the

oxidation of the open form, the irreversible reduction led to the OF again almost quantitatively, especially in the case of **Ox10** (Figure 172).

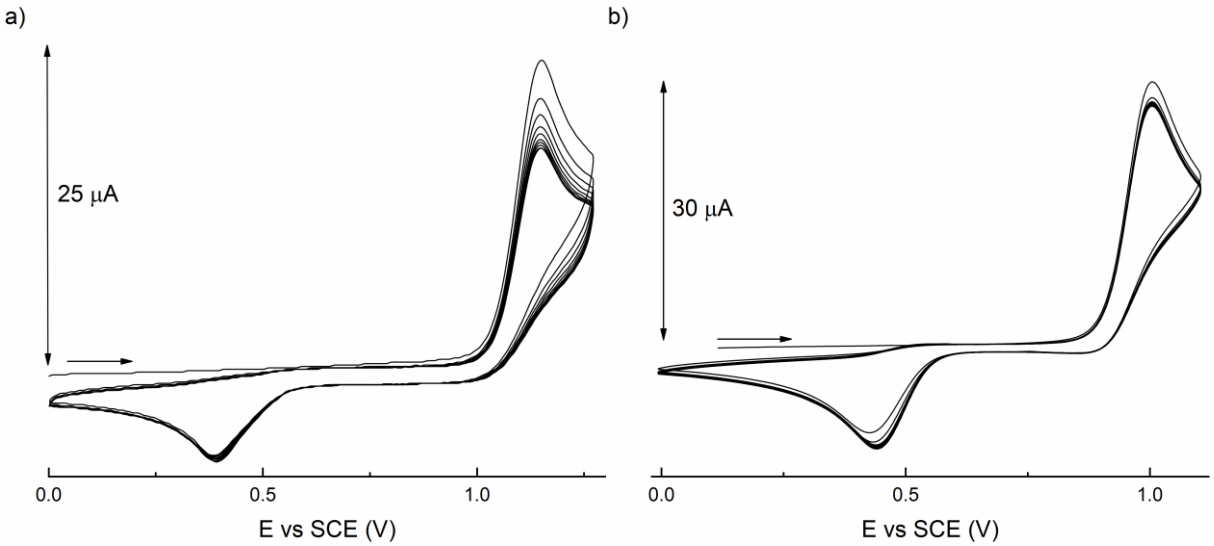

Figure 172: Multiple CV cycles of a) **Ox7** (1 mM) and b) **Ox10** (1 mM) in CH_2Cl_2 / $TBAPF_6$ 0.1 M in the OF. ν = 100 mV/s.

A minor difference has been noticed for **Ox8**, which bears the strongest donor groups among these four switches. The wave appearing after the oxidation of **Ox8o** is at the same potential of that related to the closed form and a small reversibility can be recognized, thus suggesting that the oxidative ring-closing reaction might occur on this switch. Nevertheless, the wave is pronouncedly asymmetric and this might be possibly due to the fact that the wave for the closed form isomer is merged with the irreversible one that has been detected for the other three terthiazoles.

Multiple CV cycles have been recorded on the photostationary states to verify if the loss of the closed form could be detected also for the four terthiazoles (Figure 173).

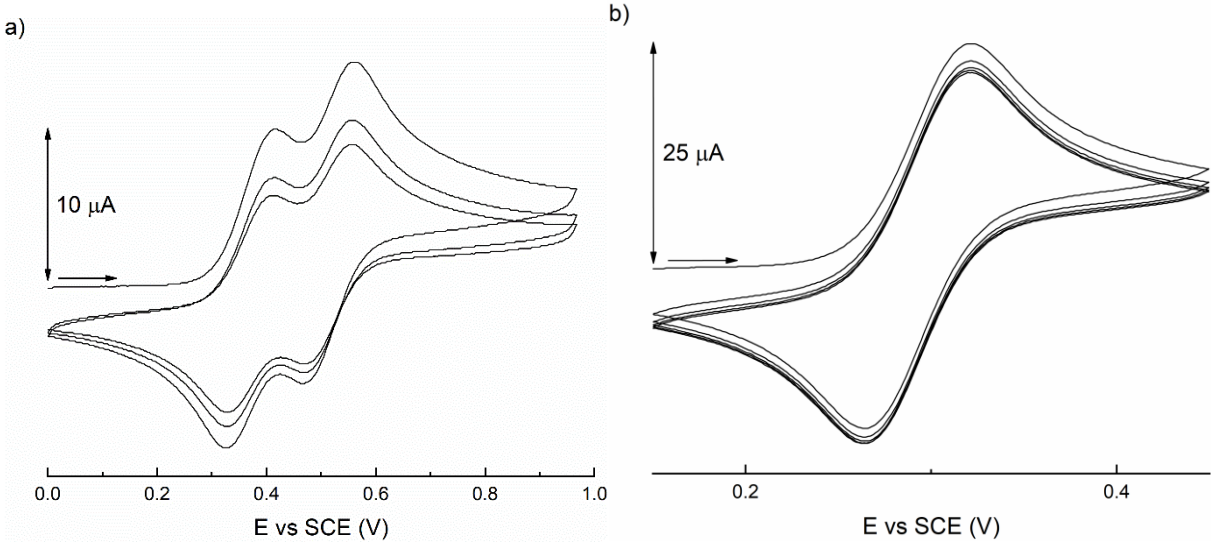

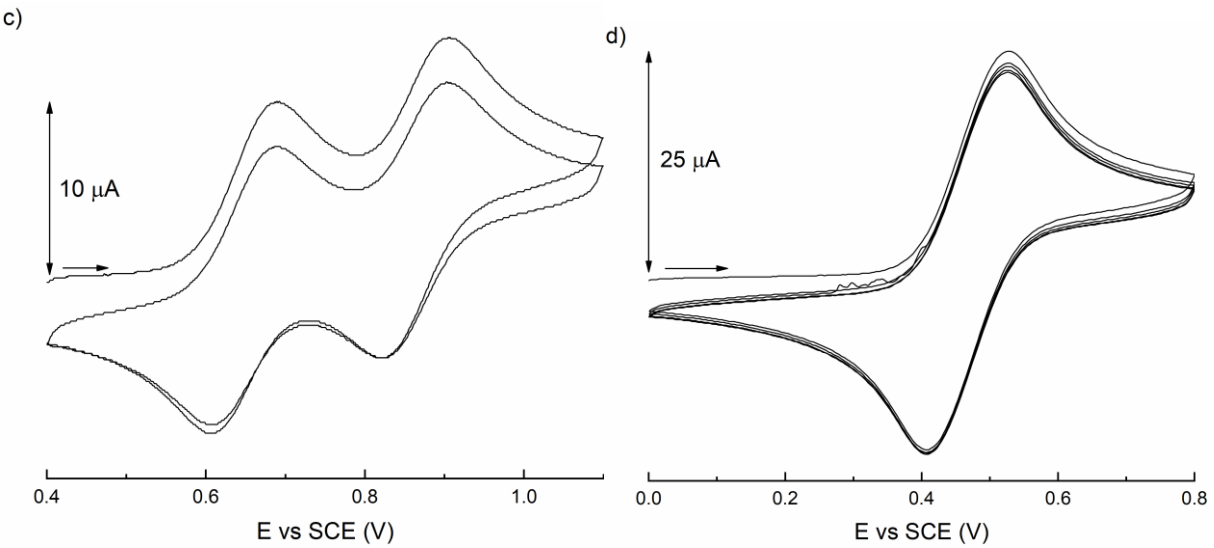

Figure 173: CVs of a) **Ox7c**, b) **Ox8c**, c) **Ox9c** and d) **Ox10c** (1 mM) in CH_3CN (**Ox8**) or CH_2Cl_2 (**Ox7**, **Ox9** and **Ox10**) / $TBAPF_6$ 0.1 M at the PSS (λ_{irr} = 365 nm). ν = 100 mV/s.

This disappearance of the closed form isomer seemed to be more limited than in the thiophene-based systems, even in presence of functional groups such as $–SCH_3$.

In conclusion, the results of the cyclic voltammetry experiments indicate that the investigated terthiazoles don't undergo oxidative cyclization with the selected functional groups to afford the closed form isomer. In fact, the oxidation led to a redox-species whose redox wave is different from that of the CF. An exception is partially observed for **Ox8**, which bears dimethylamino substituents.

4.3.4.3 Spectroelectrochemical study of **Ox10**

Ox10 has been selected to further investigate the consequences of the oxidation of the OF since the cyclic voltammetry has shown that several oxidations and reductions could be carried out without significant degradation or side-product formation. A solution of **Ox10** in dichloromethane / $TBAPF_6$ 0.1 M has been initially electrolyzed at RT at 1.10 V. The induced spectral evolution has been followed by UV-vis spectroscopy (Figure 174).

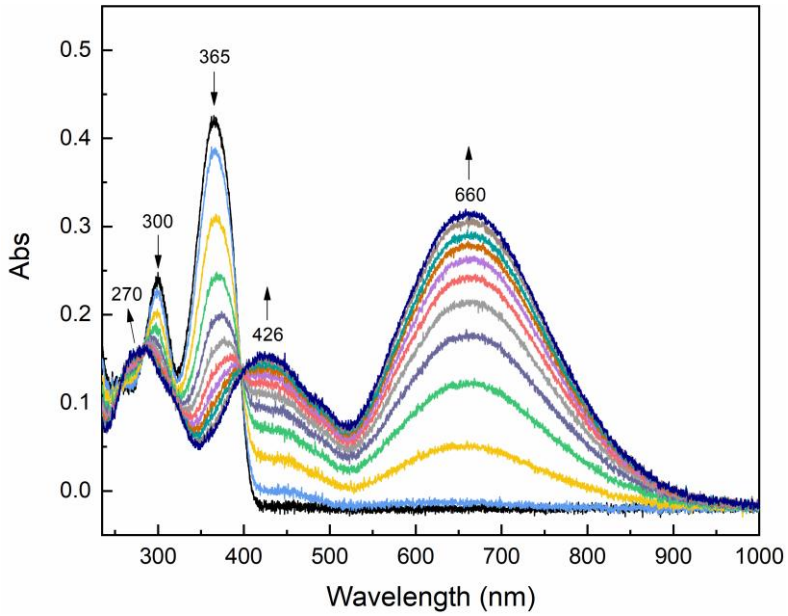

Figure 174: Absorption spectrum evolution of **Ox10o** ($6.44 \cdot 10^{-5}$ M) in CH_2Cl_2 / $TBAPF_6$ 0.1 M under oxidation at 1.10 V at RT. Optical path of the cuvette: 1 mm.

The oxidation caused the decrease of the bands of **Ox10o** at 300 nm and 365 nm and the growth of three new bands at 270 nm, 426 nm and 660 nm. The formation of this unidentified species after the oxidation is fast and no radicals have been observed during the electrolysis.

A second electrolysis has been carried out at 0.00 V and the OF has been restored almost completely (conversion: ~ 95%, Figure 175).

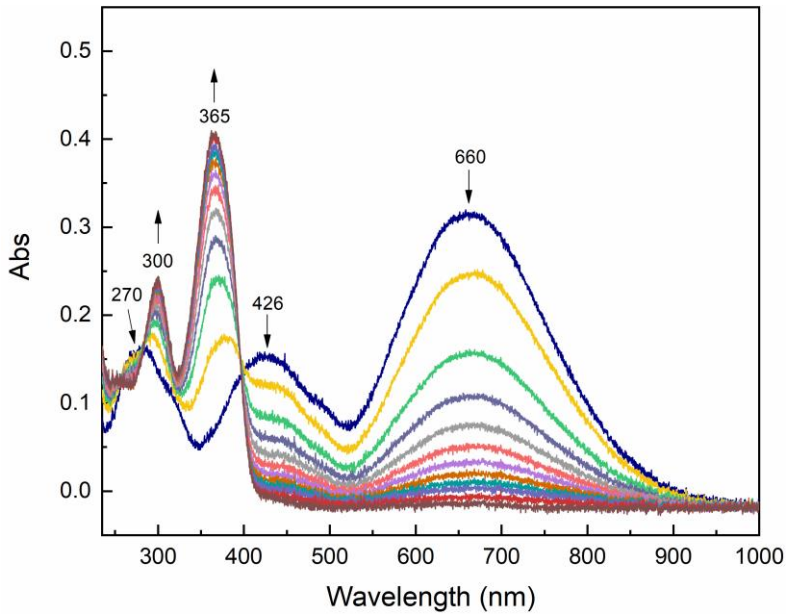

Figure 175: Absorption spectrum evolution of twice-oxidized **Ox10** ($6.44 \cdot 10^{-5}$ M) in CH_2Cl_2 / $TBAPF_6$ 0.1 M under reduction at 0.00 V at RT. Optical path of the cuvette: 1 mm.

The recovery of the neutral open form occurred rapidly at the beginning and then it became slower and slower with the conversion of the oxidized species.

To further confirm that the species achieved with the oxidation was not the dicationic closed form, the spectrum obtained during the spectroelectrochemical experiment has been compared to that recorded after the chemical oxidation of the photo-generated neutral closed form (by light irradiation at 340 nm) with two equivalents of $Cu(OTf)_2$. As it can be observed in Figure 176, the λ_{max} for the bands in the visible region differs by 30 nm (i.e. 630 nm vs 660 nm) and the bands in the UV region didn't match.

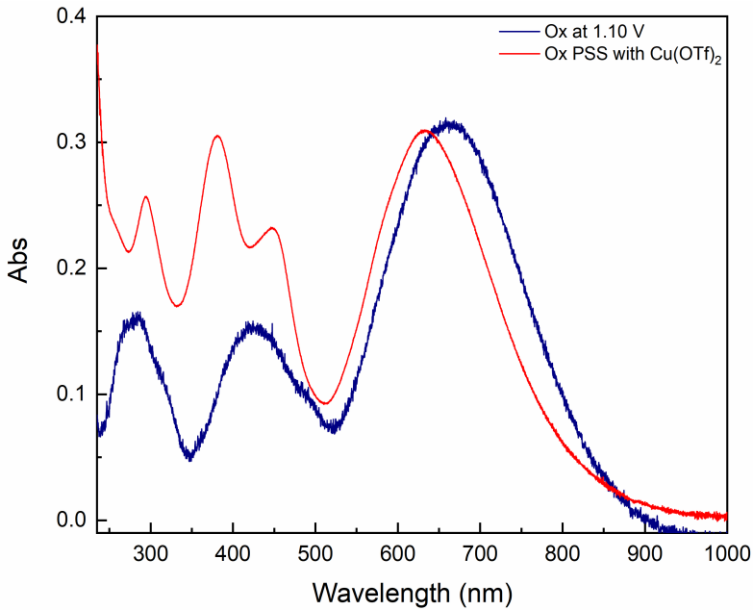

Figure 176: Comparison between the absorption spectra of **Ox10** (navy solid line) after oxidation at 1.10 V in CH_2Cl_2 / $TBAPF_6$ 0.1 M and (red solid line) after oxidation of the photogenerated neutral closed form with $Cu(OTf)_2$ in dichloromethane.

*4.3.5 Synthesis route to **Ox11***

"Bridging molecule" between the thiophene-based family and the thiazole-based one, **Ox11** has been eventually obtained with the synthesis of intermediate **78** using 2-(4-methoxyphenyl)-4-bromo-5-methyl-thiophene (**53**) and **28** followed by direct arylation of this substrate with **76** (Figure 177), thus exploiting the flexibility of this synthetic route.

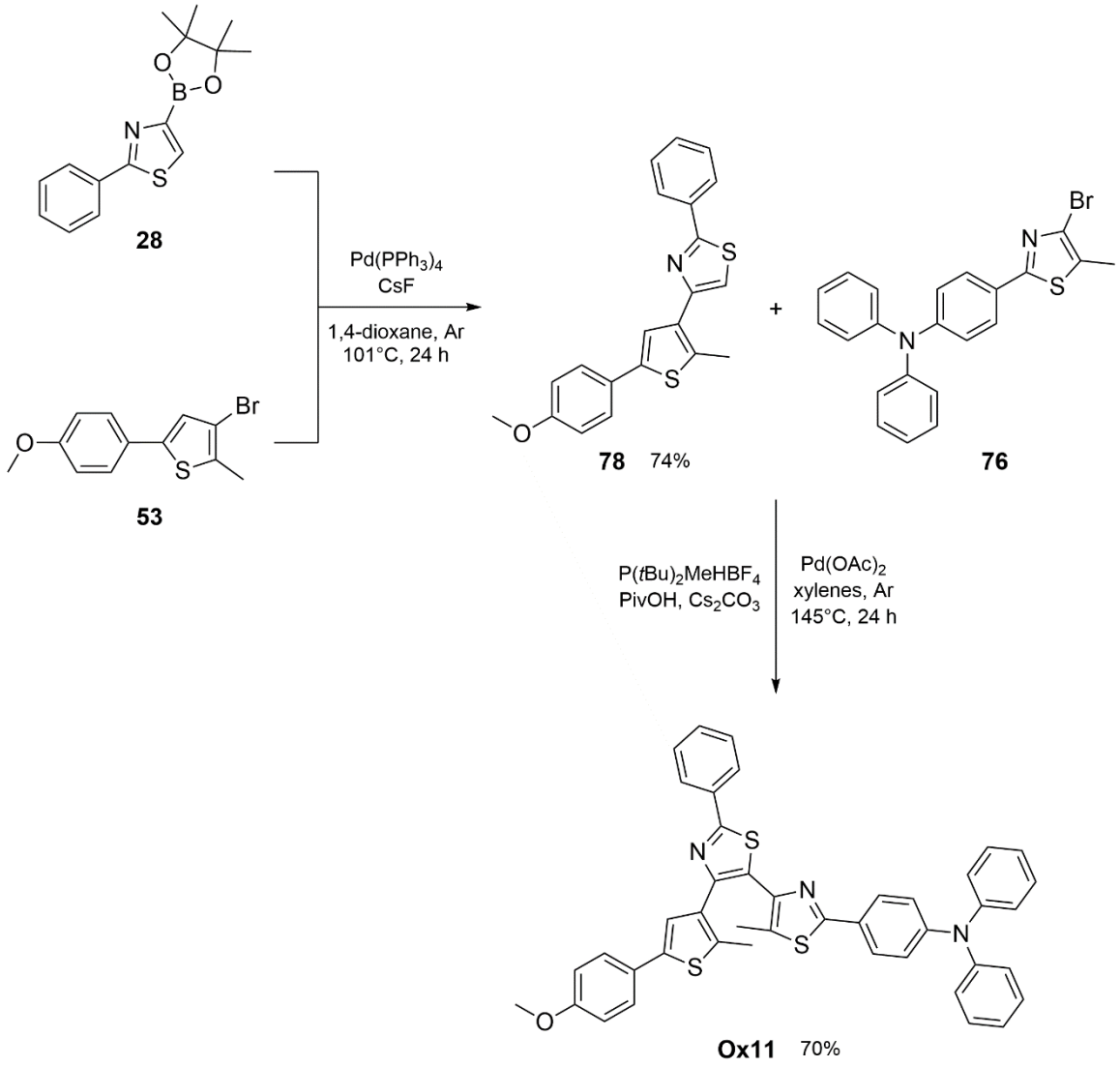

Figure 177: Synthesis route to **Ox11**.

*4.3.6 Photochemical and redox-active behavior of **Ox11***

4.3.6.1 Stationary UV-vis spectroscopy and fluorescence

The photochromic behavior of **Ox11** has been examined in dichloromethane. The obtained spectrum is shown in Figure 178, where the open form is indicated with a black solid line and the photostationary state (reached by irradiation at 340 nm) with a green solid one. **Ox11c** didn't show thermal stability in the dark at RT and the effect of the thermal ring-opening is shown with a red solid line.

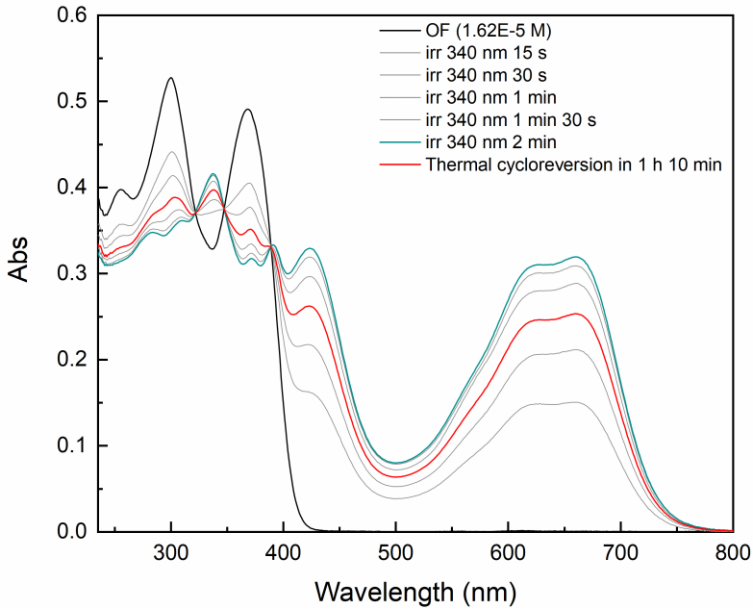

Figure 178: Absorption spectrum in dichloromethane of **Ox11** (1.62 x 10^{-5} M), showing the evolution under UV light irradiation at 340 nm from the black line for the OF to the green solid line at the PSS. Thermal cycloreversion is indicated with a red solid line. Optical path of the cuvette: 1 cm.

However, this thermal ring-opening appeared to be solvent-dependent, because it hasn't been observed when acetonitrile + minimum amount of dichloromethane has been used as solvent mixture (UV-vis spectra in the Annexes, page 253).

Again, also this molecule is fluorescent in its open form since it is obtained from **77** and an emission band at 445 nm has been observed in CH_2Cl_2 (emission spectrum in the Annexes, page 254). A quantum yields of 11% has been determined by using 9,10-diphenylanthracene in cyclohexane as reference. This molecule is consequently potentially appealing for electrofluorochromic studies, too.

4.3.6.2 Electrochemical properties

The electrochemical properties of **Ox11** has been investigated by cyclic voltammetry (CV) at room temperature in dichloromethane / $TBAPF_6$ 0.1 M with a scan rate (ν) of 100 mV/s.

The main data (i.e. half-wave potentials, $E_{1/2}$, and ΔE for reversible waves; peak potentials, E_p, for irreversible ones) referenced to a saturated calomel electrode (SCE) are reported in Table 15.

Table 15: Redox potentials vs SCE in CH_2Cl_2 / $TBAPF_6$ 0.1 M of **Ox11**.

	OF		CF	
	$E_{1/2}$ or E_p (V)	ΔE (mV)	$E_{1/2}$ or E_p (V)	ΔE (mV)
Ox11	1.02 (irr)	/	0.35 0.51	90 90

Compared to the four investigated terthiazoles, a distinctive behavior has been remarked for this mixed system (Figure 179).

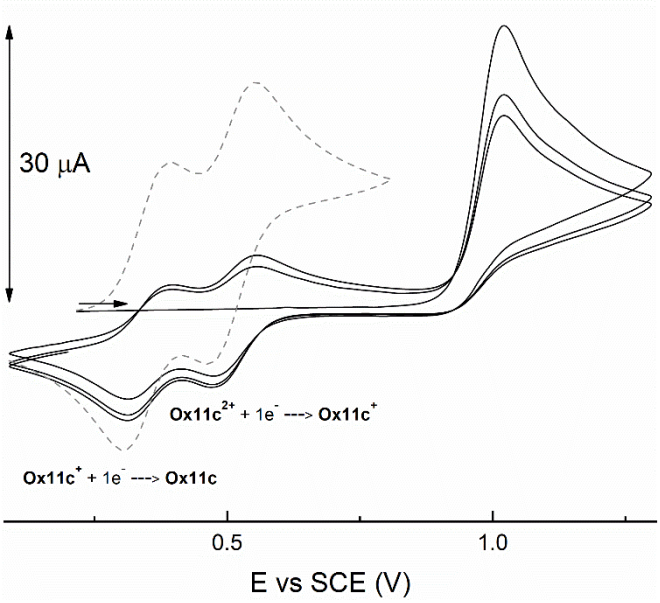

Figure 179: CVs of **Ox11** (1 mM) in CH_2Cl_2 / $TBAPF_6$ 0.1 M in the OF (black solid lines) and at the PSS (grey dashed lines) indicating the oxidative cyclization. ν = 100 mV/s.

The open form isomer is irreversibly oxidized at 1.02 V. On the back scan, two one-electron cathodic waves appear at $E_{1/2}$ = 0.35 V and 0.51 V, indicating the reduction of the dicationic closed form (**Ox11c^{2+}**) to **Ox11c**, as confirmed by the CV on the solution irradiated at 365 nm, where the same two redox waves have been observed. This indicates that the presence of at least one electron-richer and more reactive thiophene-based arm is needed for the oxidative cyclization to take place.

The redox-active behavior has also been investigated by recording the CVs at different scan rates on the open form and at the photostationary state. In particular, by working at a slow

scan rate such as 25 mV/s, in the case of the oxidation of the **Ox11o** solution, the waves related to the closed form isomer appeared strikingly lower in intensity compared to the oxidation wave of the open form, dissymmetric and irreversible (Figure 180, left). We speculate that the decrease in intensity could be possibly ascribed to some leaking of the involved species from the diffusion layer due to the large ΔE between the oxidation and the first reduction. To account for the dissymmetry and the irreversibility, we initially supposed that a ring-opening of **Ox11c**$^{+\cdot}$ to afford **Ox11o**$^{+\cdot}$ as in the cycloreversion mechanism proposed for **Ox1** – **6** was favored at such a slow scan rate. The open form radical would be rapidly reduced to **Ox11o** at the electrode surface during the back scan, thus causing the irreversible and dissymmetric waves. However, this hypothesis was invalidated by the CVs recorded at 25 mV/s at the photostationary state (Figure 180, right). In fact, the disappearance of the closed form isomer was undetectable over multiple cycles. This result suggests that the observed behavior can't be explained only by the ring-opening mechanism at the radical state proposed so far without invoking a possible, more favorable disproportionation of **Ox11c**$^{+\cdot}$ at slow scan rates (details in the Annexes, page 254). In fact, this reaction should amplify the intensity of the first reduction wave (related to **Ox11c**$^{2+}$) at the expenses of the second one. The fact that this is not observed on the CVs at the PSS might be due to the fact that the equilibrium is even more shifted towards the closed form radical if the bulk solution contains the photogenerated neutral **Ox11c**.

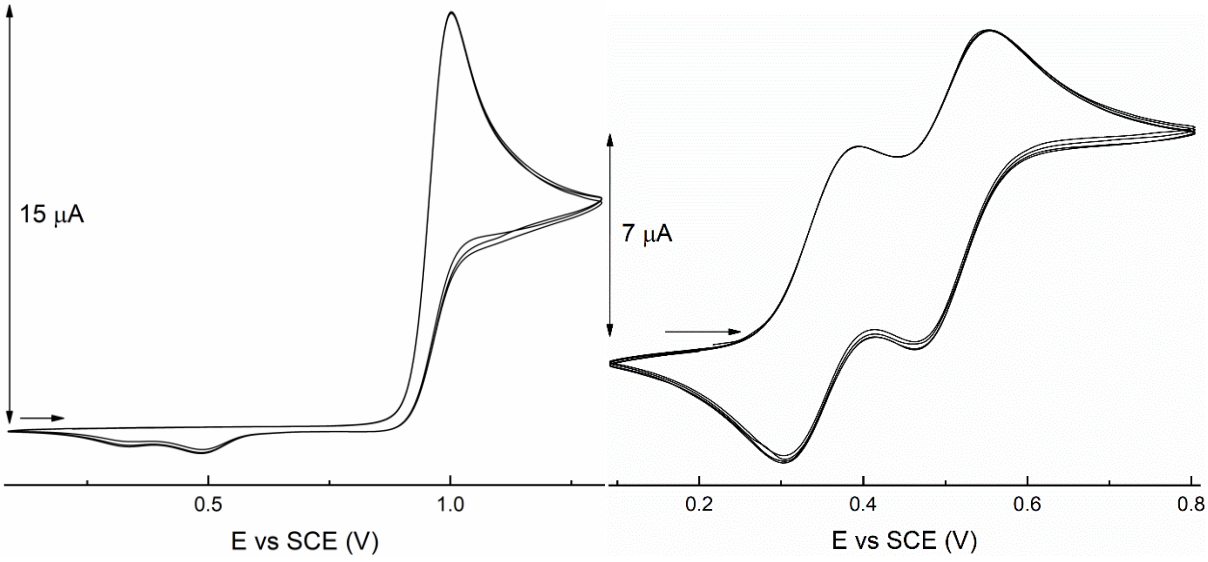

Figure 180: left) CV of **Ox11** (1 mM) in CH_2Cl_2 / $TBAPF_6$ 0.1 M. ν = 25 mV/s; right) CV of **Ox11c** (1 mM) in CH_2Cl_2 / $TBAPF_6$ 0.1 M. ν = 25 mV/s.

On the other hand, by increasing the scan rate (e.g. 1 V/s), it has been possible to partially split the oxidation wave of the open form in two at 1.06 V and 1.15 V, coherent with the presence of two different arms (Figure in the Annexes, page 255).

Overall, the CVs of the "bridging molecule" **Ox11** appeared to show the redox-active behavior of the thiophene-based switches (i.e. **Ox1** – **6**) when the open form was oxidized and the higher stability of the closed form in the diffusion layer during multiple cycles as in the cases of the four thiazyl-containing molecules (i.e. **Ox7** – **10**).

4.3.6.3 Spectroelectrochemical study of **Ox11**

A solution of **Ox11** in dichloromethane / $TBAPF_6$ 0.1 M has been initially electrolyzed at RT at 1.30 V. The induced spectral evolution has been followed by UV-vis spectroscopy (Figure 181).

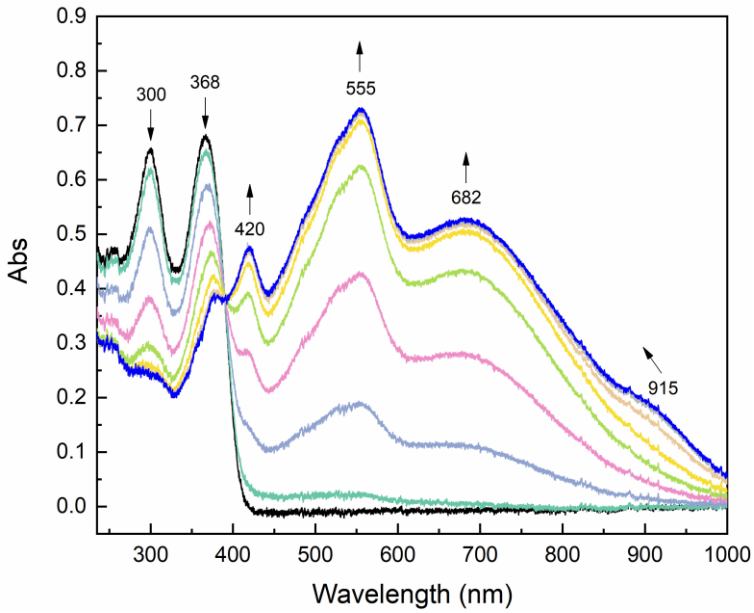

Figure 181: Absorption spectrum evolution of **Ox11o** ($2.25 \cdot 10^{-4}$ M) in CH_2Cl_2 / $TBAPF_6$ 0.1 M under oxidation at 1.30 V at RT. Optical path of the cuvette: 1 mm.

The oxidation led to a decrease of the characteristic band of the open form at 300 nm and 368 nm while bands at 420 nm, 555 nm and 682 nm grew. Moreover, a shoulder has been detected at 915 nm. According to the CV experiment, the generated species is **Ox11c**$^{2+}$.

Then the solution has been reduced at 0.45 V, aiming to obtain the spectrum of the closed form radical. However, a slow return to the neutral open form seemed to occur for this compound too, as for the **Ox1** – **6** series (Figure 182).

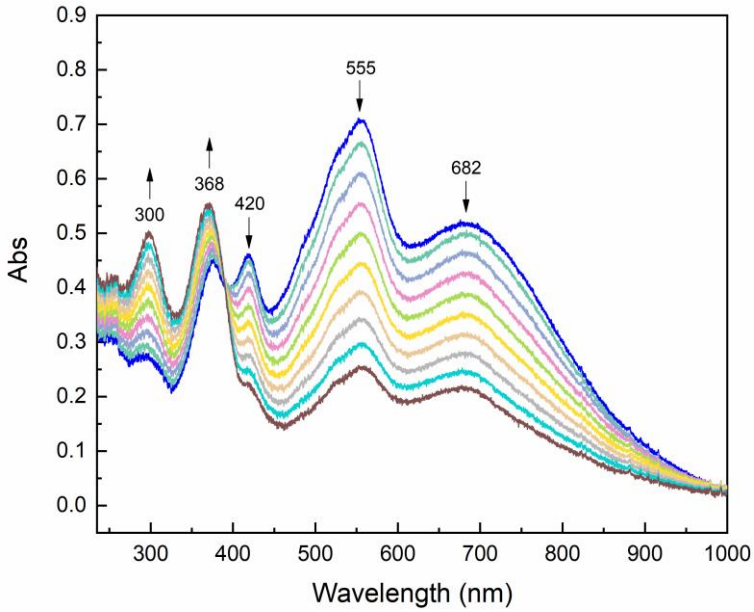

Figure 182: Absorption spectrum evolution of **Ox11c^{2+}** ($2.25 \cdot 10^{-4}$ M) in CH_2Cl_2 / $TBAPF_6$ 0.1 M under reduction at 0.45 V at RT. Optical path of the cuvette: 1 mm.

The reduction potential has been consequently changed to 0.00 V. The neutral open form hasn't been obtained cleanly because of the presence of a band in the visible (centered at 653 nm) likely ascribed to the formation of a side-product (Figure 183). As a possibility, it is known in the literature that the oxidation of triphenylamine and its derivatives can lead to the formation of dimers or other products. [225–227]

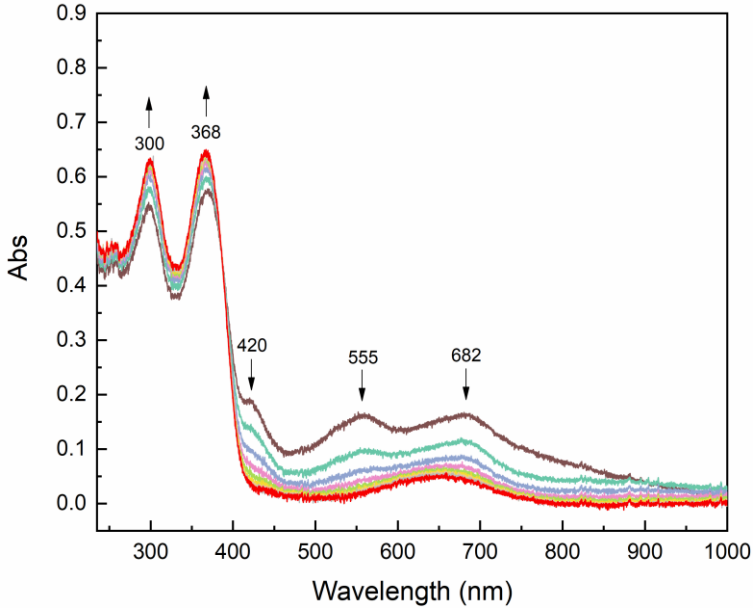

Figure 183: Absorption spectrum evolution of **Ox11c^{2+}** ($1.53 \cdot 10^{-4}$ M) in CH_2Cl_2 / $TBAPF_6$ 0.1 M under reduction at 0.00 V at RT. Optical path of the cuvette: 1 mm.

Since the cycloreversion seems to occur also in this mixed terarylene, the possibility that the mechanism proposed in Section 4.3.2.5 is occurring also in this case can't be excluded.

4.4 Conclusions

In the first part of this chapter, we have shown that terthiazoles, when functionalized with two strongly electron-withdrawing and redox-active N-methylpyridinium arms, can undergo not only similar reductive cyclization as reported diarylethenes with a classic ethene bridge but also display oxidative ring-opening reaction, thus leading to first terarylenes capable of bi-directional photo- and redox-switching. It is also worth noting that the redox switching may provide a more robust and valuable alternative when the photoisomerization is inhibited. A mechanism for different switching steps is proposed based on a joint experimental and theoretical investigation.

The second part of the chapter focused on the oxidative ring-closing of terarylenes. Depending on the nature of the two side aryl arms different redox behaviors have been observed:

1. With one central thiazole group and two electron-rich side thienyl-based arms, the cyclic voltammograms suggested a similar behavior as their diarylethene counterparts, i.e. an oxidative-ring closing reaction followed by subsequent reduction leading to the neutral closed form, while the bulk electrolysis clearly showed that an identical oxidation and reduction sequence gave instead the initial neutral open form. To account for the apparent contradiction between the two electrochemical techniques, a new mechanism has been proposed.
2. All the investigated thiazole-based terarylenes did not undergo oxidative ring-closing reaction even when functionalized with electron-rich substituents like dimethylamino or diphenylamino groups. However, the presence of one electron-rich thienyl arm proved effective to recover the oxidative ring-closing reaction observed for the series of terarylenes with two thienyl-based arms.

Nicolò Baggi

General Conclusion and Perspectives

Nicolò Baggi

The work of this PhD thesis is devoted to terarylenes-based switches with focus on two main topics: (i) modulation of the photocyclization quantum yield and (ii) search of photo- and redox- dual-responsive behavior.

The first topic has been covered in Chapters 2 and 3. A predictive model for the control of the photocyclization quantum yield ($\Phi_{O\text{-}C}$) through the tuning of the charge transfer (CT) character has been developed thanks to a joint experimental and theoretical study of a homogeneous series of terarylenes with increasing CT character. A correlation between the quantum yield of cyclization of the terarylene and its CT character has been clearly established. Moreover, the validity of the model seemed not limited to the investigated terarylenes as similar correlations have been found when applied to several homogeneous families of diarylethenes reported in the literature with a "horizontal" CT character. However, the model needs to be further checked and improved as it failed with known diarylethenes showing "vertical" CT. Nonetheless, to our knowledge, this is the first systematic study intended to correlate the photocyclization quantum yield, one of the most important photochromic feature for a given diarylethene, with one straightforward and readily tunable structural feature of the switch.

Applying the model, a suitably functionalized terphenylthiazole with low cyclization quantum yield has been designed and successfully combined through click chemistry with a dicyanomethylene (DCM)-based fluorophore to achieve switchable fluorescence hysteresis within a multichromophoric molecular assembly, target of a joint ANR project (SWIST, coordinator Dr. R. Métivier, ENS Paris-Saclay).

The second topic has been object of Chapter 4, where the results on a large family of photo- and redox-active switches have been presented. All these terarylenes are more or less photochromic while their redox behavior depends on the nature of the two side aryl arms.

1. When functionalized with two strongly electron-withdrawing and redox-active N-methylpyridinium groups, the resulting terarylenes underwent not only reductive cyclization as their diarylethenes counterparts with classic ethene bridges, but also oxidative cycloreversion, thus leading to first terarylenes capable of bi-directional photo- and redox-switching. Moreover, the redox-switching remained active even though the photo-isomerization was inhibited.
2. Terarylenes with two electron-rich thienyl groups as side arms displayed similar cyclovoltammograms as their corresponding diarylethenes reported in the literature while the bulk electrolysis clearly indicated that the same oxidation and reduction sequence didn't give the expected neutral closed forms, but led instead to the initial neutral open forms. To account for this unexpected redox-switching behavior, a different mechanism has been proposed. Clearly, the proposed mechanism needs to be confirmed by future works such as simulation of experimental CVs in order to get access to different kinetics of the various processes which are involved. It would also be interesting to depose such molecules directly on an electrode surface *via* diazonium

electroreduction [228,229] and investigate their photo- and redox-switching behaviors as potential candidates for dual-responsive molecular junctions.

3. No oxidative ring-closing reaction could be observed with electron-poorer thiazolyl side arms even when they have been functionalized with electron-donating groups like dimethylamino or diphenylamino. However, introduction of one electron-rich thienyl arm allowed to recover the oxidative ring-closing reaction discussed above. It is also worth noting that, in at least one case, upon oxidation of the open form a new electroactive species has been generated and could be reversibly switched at least 20 times without significant degradation within the cyclovoltammetry timescale. What is the nature of the new electroactive species remains an open question. Cyclic voltammetry experiments at different concentrations could be helpful to rule out the occurrence of competitive intermolecular processes. [230]

Finally, the study of above photo- and redox-active terarylene-based switches paves the way for the design of more complex switching systems by combining those dual-responsive terarylene units.

Materials and Methods

Nicolò Baggi

5.1 General methods

Reagents have been purchased at Alfa-Aesar, Fischer Scientific (Acros), Merck (Sigma-Aldrich), TCI, BLDPharm or Fluorochem and used without further purification, unless otherwise stated.

Solvents have been purchased at Carlo Erba and VWR and distilled, if necessary, according to standard drying procedures (i.e. THF: Na / benzophenone; Et_2O: Na / benzophenone; CH_2Cl_2: CaH_2; CH_3OH: Mg; CH_3CN: CaH_2).

Thin layer chromatography (TLC) has been performed on silica gel 60 F_{254} while column chromatography has been carried out on silica gel 60 (0.063-0.2 mm).

5.2 Analytical methods

5.2.1 NMR spectroscopy

NMR spectra have been recorded on a Bruker Avance I (400 MHz), Bruker Avance I (360 MHz), Bruker Avance I (300 MHz) or Bruker DPX 250 (250 MHz).

Euriso-Top deuterated solvents ($CDCl_3$, CD_3CN, Methanol-d_4, Acetone-d_6, DMSO-d_6) have been used to prepare the samples and residual proton signals have been used as standards (7.26 ppm, 1.94 ppm, 3.31 ppm, 2.05 ppm and 2.50 ppm, respectively).

Chemical shifts are provided in δ (ppm) and the coupling constants J in Hz. The splitting patterns are indicated as: s (singlet); d (doublet); t (triplet); q (quartet) and m (multiplet).

5.2.2 Mass spectrometry

Samples have been analyzed by Tanya Inceoglu and Hélène Maisonneuve at ICMMO (Université Paris-Saclay) on a Bruker MicroTOF-Q in ESI (Electrospray Ionization).

5.2.3 X-ray diffraction

X-ray diffraction data have been collected by Régis Guillot at ICMMO (Univeristé Paris-Sacly) by using a Kappa X8 APPEX II Bruker diffractometer with graphite-monochromated Mo_K radiation (λ = 0.71073 Å).

Crystals have been mounted on a CryoLoop (Hampton Research) with Paratone-N (Hampton Research) as cryoprotectant and then flashfrozen in a nitrogen-gas stream at 100 K.

The temperature of the crystal was maintained at the selected value by means of a 700 series Cryostream cooling device to within an accuracy of ±1K.

5.2.4 EPR spectroscopy

EPR spectra have been recorded by Christian Herrero at ICMMO (Université Paris-Saclay) on a Bruker Elexsys ESP 300E.

Cyclic voltammetry and electrolysis in a EPR tube have been carried out with a PGSTAT204 potentiostat (AUTOLAB) and an in-house three-electrode setup. Electrochemical data have been collected with NOVA 2.1.

5.2.5 UV-vis and fluorescence spectroscopy

UV-vis spectra have been recorded on a Varian Cary 5000 spectrometer and on a Varian Cary 60 during the spectroelectrochemical experiment.

Cyclization and cycloreversion of the investigated photochromes have been induced by light irradiation with a lamp (Oriel Hg(Xe) 200 W) equipped with narrow-band interference filters of appropriate wavelengths (Semrock: 320 ± 20 nm, 340 ± 13 nm; Andover Corporation 600 ± 40 nm).

The fluorescence spectra have been recorded on a Fluoromax 4 instrument from Jobin-Yvon/Horiba Co. The fluorescence quantum yields have been determined by using quinine sulfate in H_2SO_4 0.5 M or 9,10-diphenylanthracene in cyclohexane as standard reference (Φ = 0.54 and Φ = 0.90, respectively).

5.2.6 Setup for the photochromism quantum yields determination

The photochromic reactions have been induced by continuous irradiation through a Hg/Xe lamp (Hamamatsu, LC6 Lightingcure, 200 W) equipped with narrow-band interference filters of appropriate wavelengths (Semrock) and attenuation filters (Melles Griot, DO 1 or 2).

The irradiation power has been measured by a photodiode (Ophir, PD300-UV). The photochromic quantum yields have been determined by probing the sample with a Xenon lamp during the photochromic reaction.

Absorption changes have been monitored by a CCD camera mounted with a spectrometer (Princeton Instruments) and the kinetic profiles have been finally analyzed by an Igor-implemented in-house procedure developed by Dr. Métivier.

5.2.7 Electrochemical measurements

Cyclic voltammetry measurements have been carried out with an EGG PAR (model 273A) electrochemical workstation or a PGSTAT302 potentiostat (AUTOLAB).

Measurements have been performed at 20°C with a glassy carbon electrode (3 mm diameter) as working electrode, a saturated KCl calomel electrode as reference and a platinum counter electrode.

Dry acetonitrile and/or dichloromethane have been used to prepare the solutions of the investigated photochromes (10 mL, 1 mM). Tetrabutylammonium hexafluorophosphate ($TBAPF_6$, 0.1M) has been used as electrolyte.

The solutions have been introduced in an argon-purged heart-shaped cell and protected with aluminum foil.

5.2.8 Spectroelectrochemical experiments

The low-temperature analysis of **Red1**$^{2+}$ has been performed by using a three-electrode setup in a thin cell (optical path length = 1 mm) placed in a UV-vis Varian Cary 60 spectrophotometer, equipped with a transparent dewar.

The optical part was surmounted by a glass compartment. The working electrode was a 3 cm x 0.7 cm x 0.3 mm Pt grid with a Teflon-covered wire to avoid electrolysis elsewhere than in the quartz cell. A $Ag/AgNO_3$ electrode ($E_{Ag/AgNO_3}$ = 0.284 V vs SCE) was used as the reference and a platinum grid as counter. They were separated from the solution with fritted bridges.

The cell was filled under argon with a dry acetonitrile solution of the photochrome and $TBAPF_6$ (0.2 M). The cell was cooled to -25°C by a Julabo circulation cryostat.

Room temperature experiments have been carried out with a similar setup, but with a saturated KCl calomel electrode as reference.

5.2.9 Computational details

Calculations have been performed with Gaussian 09 [Gaussian] using Density Functional Theory (DFT) and the 6-311G(d,p) or Def2SVP basis sets and with CAM-B3LYP or PBE0 as functionals.

The first low-lying electronic singlet excited states have been calculated using the time-dependent density functional theory (TD-DFT) method using the CAM-B3LYP functional to obtain theoretical absorption spectra. All the calculations (geometry optimizations, TD-DFT calculations) have been performed in acetonitrile as in the experiments and solvent has been included in the calculations by means of the polarizable continuum model by the integral equation formalism (IEFPCM). All the geometry optimizations were performed without symmetry constraints and followed by a vibrational frequency computation to ensure that they correspond to true energetic minima.

Nicolò Baggi

5.3 Experimental procedures

The syntheses of the investigated photochromes and their precursors will be provided in different sections for each chapter. References are provided for known compounds whose characterizations are available in the literature.

5.3.1 Intermediates, Chapter 2

2-phenylthiazole, **10**[231]

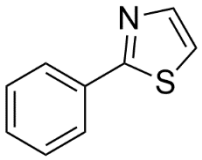

10

Thiobenzamide, **9** (4.12 g, 30 mmol) has been partially dissolved in ethanol 96% (20 mL) and then bromoacetaldehyde diethyl acetal (6.50 g, 5 mL, 33 mmol) and *p*-toluenesulfonic acid monohydrated (0.29 g, 1.5 mmol) have been added to it. The mixture has been stirred at reflux for 24 h. The solvent has been finally removed under vacuum to afford 2-phenylthiazole, **10** (4.60 g, 28.5 mmol, 95%), as a brown liquid that has been used without further purification.

^{1}H-NMR ($CDCl_3$, 360 MHz): δ (ppm) 8.20 (m, 2H), 8.16 (d, *J* = 3.8 Hz, 1H), 7.86 (d, *J* = 3.8 Hz, 1H), 7.56 (m, 3H).

5-methyl-2,2'-diphenyl-4,4'-bithiazole, **11**[232]

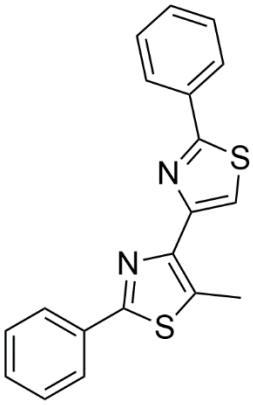

11

Thiobenzamide, **9** (5.50 g, 40 mmol) has been partially dissolved in CH_3OH (60 mL) and crude 1,4-dibromopentane-2,3-dione (5.20 g, 20 mmol) has been added. The mixture has been stirred at room temperature for 20 min and then refluxed 24 h. After cooling down to room temperature, 5-methyl-4,4′-bi-(2-phenyl)-thiazole, **11** (3.41 g, 10.2 mmol, 51%) precipitated as a sand-colored crystalline solid that has been used without further purification.

^{1}H-NMR ($CDCl_3$, 360 MHz): δ (ppm) 8.02 (d, *J* = 7.9 Hz, 2H), 7.96 (d, *J* = 7.9 Hz, 2H), 7.90 (s, 1H), 7.44 (m, 6H), 2.97 (s, 3H).

4-methoxybenzothioamide, **14**[233], and 4-(dimethylamino)benzothioamide, **15**[234]

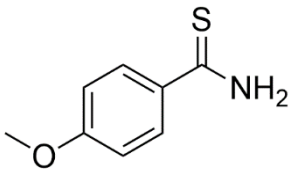

14

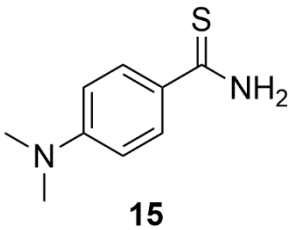

15

4-methoxybenzonitrile, **12** (4 g, 30 mmol) has been added to a slurry of 67% sodium hydrosulfide hydrate (6.48 g, 78 mmol) and magnesium chloride hexahydrate (6.71 g, 22 mmol) in DMF (40 mL) and the mixture has been stirred at room temperature for 24 h. The resulting green slurry has been poured into 100 mL of water, stirred for 20 min in 1M HCl, then filtered and washed with water to give pure 4-methoxybenzothioamide, **14** (4.51 g, 27 mmol, 90%) as a pale yellow solid.

^{1}H-NMR ($CDCl_3$, 300 MHz): δ (ppm) 7.91 (dt, *J* = 9.3, 2.7 Hz, 2H), 7.54 (bs, 1H), 7.12 (bs, 1H), 6.91 (dt, *J* = 9.3, 2.7 Hz, 2H), 3.87 (s, 3H).

The same procedure has been followed on 4-(dimethylamino)benzonitrile, **13** (730 mg, 5 mmol) to afford pure 4-(dimethylamino)benzothioamide, **15** (721 mg, 4 mmol, 80%) as a yellow solid.

^{1}H-NMR (300 MHz, Acetone-d_6): δ (ppm) 8.48 (bs, 2H), 8.02 (d, *J* = 9.0 Hz, 2H), 7.49 (d, *J* = 9.0 Hz, 2H), 3.03 (s, 6H).

2-(4-methoxyphenyl)thiazole, **16**[235], and N,N-dimethyl-4-(thiazol-2-yl)aniline, **17**[236]

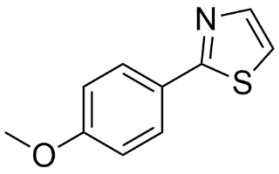

16

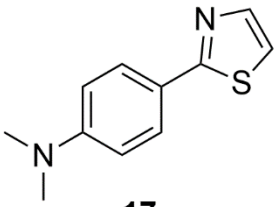

17

The procedure described for the synthesis of **10** has been followed on 4-methoxybenzothioamide, **14** (4.00 g, 24 mmol) to obtain 2-(4-methoxyphenyl)thiazole, **16** (4.36 g, 22.8 mmol, 95%) as a light brown oil that was used without further purification.

^{1}H-NMR ($CDCl_3$, 360 MHz): δ (ppm) 8.19 (d, *J* = 8.9 Hz, 2H), 8.00 (d, *J* = 3.8 Hz, 1H), 7.61 (d, *J* = 3.8 Hz, 1H), 7.02 (d, *J* = 8.9 Hz, 2H), 3.87 (s, 3H).

In the case of 4-(dimethylamino)benzothioamide, **15** (721 mg, 4 mmol), the crude product obtained by following this procedure has been purified by silica gel column chromatography (eluent: dichloromethane / petroleum ether 1:1) and N,N-dimethyl-4-(thiazol-2-yl)aniline, **17** (441 mg, 2.16 mmol, 54%) has been isolated as light yellow solid.

^{1}H-NMR ($CDCl_3$, 360 MHz): δ (ppm) 7.84 (d, *J* = 9.0 Hz, 2H), 7.76 (d, *J* = 3.3 Hz, 1H), 7.17 (d, *J* = 3.3 Hz, 1H), 6.73 (d, *J* = 9.0 Hz, 2H), 3.03 (s, 6H).

2,2'-bis(4-methoxyphenyl)-5-methyl-4,4'-bithiazole, **18**

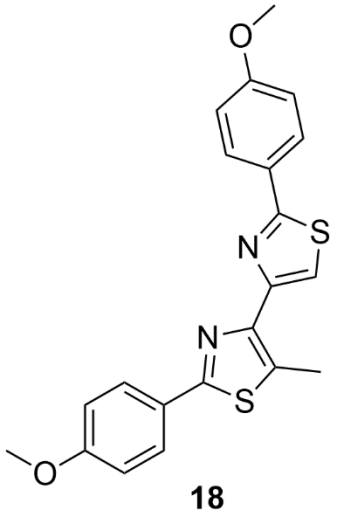

18

The procedure described for the synthesis of **11** has been followed on 4-methoxybenzothioamide, **14** (2.90 g, 17 mmol) to obtain 2,2'-bis(4-methoxyphenyl)-5-methyl-4,4'-bithiazole, **18** (1.73 g, 4.4 mmol, 52%) as beige crystalline solid.

^{1}H-NMR ($CDCl_3$, 300 MHz): δ (ppm) 7.96 (m, 5H), 6.97 (m, 4H), 3.88 (s, 3H), 3.87 (s, 3H), 2.95 (s, 3H).
^{13}C-NMR ($CDCl_3$,101 MHz): δ (ppm) 167.41, 163.89, 161.20, 161.07, 152.42, 145.49, 130.17, 128.09, 127.95, 127.01, 126.78, 115.70, 114.37, 114.31, 55.55, 13.20.
HRMS (ESI): calcd. for $C_{21}H_{19}N_2O_2S_2^+$ $[M+H]^+$ 395.0882, found $[M+H]^+$ 395.0877; calcd. for $C_{21}H_{18}N_2NaO_2S_2^+$ $[M+Na]^+$ 417.0702, found $[M+Na]^+$ 417.0692.

5-bromo-2-phenylthiazole, **19**[237], 5-bromo-2-(4-methoxyphenyl)thiazole, **20**[237], and 4-(5-bromothiazol-2-yl)-N,N-dimethylaniline, **21**

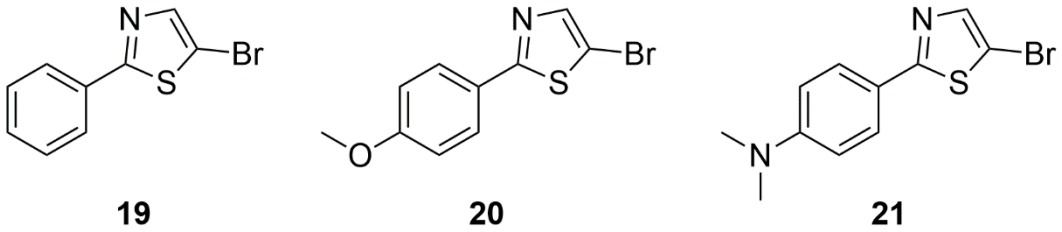

19 **20** **21**

N-bromosuccinimide (5.60 g, 31.4 mmol) has been added to a solution of 2-phenylthiazole, **10** (4.60 g, 28.5 mmol) in DMF (35 mL) and the obtained solution has been stirred at room temperature for 24 hours. Sodium thiosulfate pentahydrate (0.25 g, 1 mmol) in distilled water (25 mL) has been added to the solution to induce a solid precipitation that has been filtered and washed with water. The crude product has been dissolved in diethyl ether to remove insoluble impurities by filtration. 5-bromo-2-phenylthiazole, **19** (6.02 g, 25.1 mmol, 88%) has recovered by evaporation of the solvent under vacuum as an off-white solid.

^{1}H-NMR ($CDCl_3$, 360 MHz): δ (ppm) 7.87 (m, 2H), 7.74 (s, 1H), 7.44 (m, 3H).

The same procedure has been followed on 4-methoxybenzothioamide, **14** (4.60 g, 24 mmol) to obtain 5-bromo-2-(4-methoxyphenyl)thiazole, **20** (5.05 g, 18.7 mmol, 78%) as a white solid.

^{1}H-NMR ($CDCl_3$, 300 MHz): δ (ppm) 7.80 (d, *J* = 8.9 Hz, 2H), 7.67 (s, 1H), 6.95 (d, *J* = 8.9 Hz, 2H), 3.86 (s, 3H).

In the case of N,N-dimethyl-4-(thiazol-2-yl)aniline, **17** (430 mg, 2.10 mmol), the crude product obtained by following this procedure has been purified by silica gel column chromatography (eluent: dichloromethane / petroleum ether 1:1) and 4-(5-bromothiazol-2-yl)-N,N-dimethylaniline, **21** (208 mg, 0.74 mmol, 35%) has been isolated as light yellow crystalline solid.

^{1}H-NMR ($CDCl_3$, 300 MHz): δ (ppm) 7.72 (d, *J* = 8.8 Hz, 2H), 7.61 (s, 1H), 6.70 (d, *J* = 8.9 Hz, 2H), 3.03 (s, 6H).
^{13}C-NMR ($CDCl_3$, 63 MHz): δ (ppm) 170.58, 151.77, 144.28, 127.48, 121.31, 111.82, 105.69, 40.18.
HRMS (ESI): calcd. for $C_{11}H_{12}BrN_2S^+$ $[M+H]^+$ 282.9899, found $[M+H]^+$ 282.9896.

2-phenyl-4-bromo-5-methylthiazole, **22**[238], 2-(4-methoxyphenyl)-4-bromo-5-methylthiazole, **23**[232], and 4-(4-bromo-5-methylthiazol-2-yl)-N,N-dimethylaniline, **24**

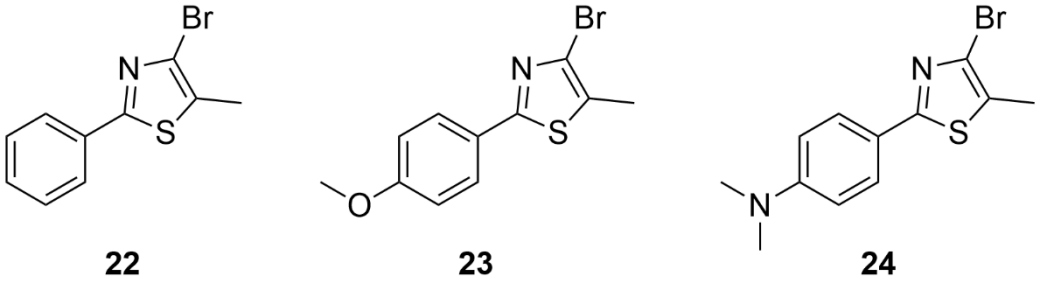

22 **23** **24**

5-bromo-2-phenylthiazole, **19** (1.92 g, 8 mmol) has been dissolved in distilled dry THF (20 mL) under argon and the obtained solution has been cooled at -78°C with a dry ice/acetone bath. Lithium diisopropylamine (2M solution, 6 mL, 12 mmol) has been added dropwise and the system has been stirred at -78°C for 30 min. Iodomethane (1.70 g, 0.75 mL, 12 mmol) has been finally added and the resulting solution has been stirred for 24 h letting the temperature rise up to room temperature under argon. The system has been quenched with NH_4Cl 1M solution (20 mL) and the organic layer has been extracted with diethyl ether. The combined extracts have been washed with water, dried over anhydrous Na_2SO_4 and filtered. The filtrate has been concentrated under vacuum giving the crude product as a light brown crystalline solid. Silica gel column chromatography (eluent: dichloromethane) of the residue afforded pure 2-phenyl-4-bromo-5-methylthiazole, **22** (1.83 g, 7.2 mmol, 90%) as a white crystalline solid.

^{1}H-NMR ($CDCl_3$, 360 MHz): δ (ppm) 7.87 (m, 2H), 7.42 (m, 3H), 2.44 (s, 3H).

The same procedure has been followed on 5-bromo-2-(4-methoxyphenyl)thiazole, **20** (1.35 g, 5 mmol) to obtain 2-(4-methoxyphenyl)-4-bromo-5-methylthiazole, **23** (1.28 g, 4.45 mmol, 74%) as a white crystalline solid after purification by silica gel column chromatography (eluent: dichloromethane).

^{1}H-NMR ($CDCl_3$, 360 MHz): δ (ppm) 7.81 (d, *J* = 8.9 Hz, 2H), 6.93 (d, *J* = 8.9 Hz, 2H), 3.85 (s, 3H), 2.41 (s, 3H).

Similarly, the procedure has been followed on 4-(5-bromothiazol-2-yl)-N,N-dimethylaniline, **21** (205 mg, 0.72 mmol) to obtain 4-(4-bromo-5-methylthiazol-2-yl)-N,N-dimethylaniline, **24** (159 mg, 0.53 mmol, 74%) as a pale yellow crystalline solid after purification by silica gel column chromatography (eluent: dichloromethane / petroleum ether 1:1).

^{1}H-NMR ($CDCl_3$, 360 MHz): δ (ppm) 7.74 (d, *J* = 9.0 Hz, 2H), 6.70 (d, *J* = 8.6 Hz, 2H), 3.02 (s, 6H), 2.39 (s, 3H).
^{13}C-NMR (CDCl3, 63 MHz): δ (ppm) 166.79, 151.75, 127.23, 125.98, 124.15, 120.90, 111.76, 40.14, 12.88.
HRMS (ESI): calcd. for $C_{12}H_{14}BrN_2S^+$ $[M+H]^+$ 297.0055, found $[M+H]^+$ 297.0054.

2-(4-formylphenyl)-4-bromo-5-methylthiazole, **25**[239]

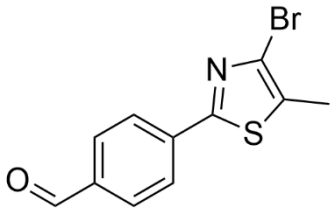

25

4-formylphenylboronic acid (165 mg, 1.10 mmol), 2,4-dibromo-5-methylthiazole (257 mg, 1 mmol), xantphos (18 mg, 0.03 mmol), $Pd(OAc)_2$ (7 mg, 0.03 mmol) and K_3PO_4 (637 mg, 3 mmol) have been partially dissolved in distilled dry THF (10 mL). The obtained mixture has been stirred at reflux under argon for 24 h. Once cooled down to room temperature, it has been filtered on Celite. Multiple washings with dichloromethane have been carried out and the obtained filtrate has been concentrated under vacuum. The obtained crude product has been purified by silica gel column chromatography (eluent: initially dichloromethane / petroleum ether 1:1, then dichloromethane / petroleum ether 7:3) to afford 2-(4-formylphenyl)-4-bromo-5-methylthiazole, **25** (228 mg, 0.81 mmol, 81%) as a yellow crystalline solid.

^{1}H-NMR ($CDCl_3$, 300 MHz): δ (ppm) 10.04 (s, 1H), 8.04 (d, *J* = 8.4 Hz, 2H), 7.93 (d, *J* = 8.4 Hz, 2H), 2.47 (s, 3H).

2-(4-nitrophenyl)-4-bromo-5-methylthiazole, **26**[240]

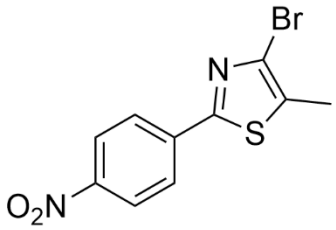

26

2-phenyl-4-bromo-5-methylthiazole, **22** (762 mg, 3 mmol) has been dissolved in H_2SO_4 (3 mL). The system has been stirred at room temperature for 10 min to achieve a complete dissolution. The solution has been cooled down to 0°C before the addition of KNO_3 (312 mg, 3.09 mmol). Water has been added to make the product precipitate after 1 h of stirring at 0°C and 1 h at room temperature. The solid has been recovered by filtration and then re-dissolved in acetone. Slow evaporation of the solvent and the addition of water (10 mL) allowed to obtain 2-(4-nitrophenyl)-4-bromo-5-methylthiazole, **26** (834 mg, 2.79 mmol, 93%) as a yellow crystalline solid to be recovered by filtration.

^{1}H-NMR ($CDCl_3$, 250 MHz): δ (ppm) 8.29 (d, *J* = 8.9 Hz, 2H), 8.04 (d, *J* = 8.9 Hz, 2H), 2.49 (s, 3H).

4-bromo-2-phenylthiazole, **27**[237]

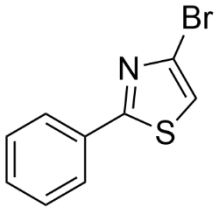

27

5-bromo-2-phenylthiazole, **19** (1.20 g, 5 mmol) has been dissolved in distilled dry THF (15 mL) under argon and the obtained solution has been cooled at -78°C with a dry ice/acetone bath. Lithium diisopropylamine (2M solution, 3.75 mL, 7.5 mmol) has been added dropwise and the system has been stirred at -78°C for 30 minutes. Methanol (2 mL) has been added and the resulting solution has been stirred for 20 min letting the temperature rise up to room temperature under argon. The system has been quenched with NH_4Cl 1M solution (20 mL) and the organic layer has been extracted with diethyl ether. The combined extracts have been washed with water, dried over anhydrous Na_2SO_4 and filtered. The filtrate has been concentrated under vacuum giving the crude product. Silica gel column chromatography (eluent: dichloromethane) of the residue afforded pure 4-bromo-2-phenylthiazole, **27** (1.12 g, 4.65 mmol, 93%) as a white crystalline solid.

^{1}H-NMR ($CDCl_3$, 300 MHz): δ (ppm) 7.94 (m, 2H), 7.46 (m, 3H), 7.22 (s, 1H).

2-phenyl-4-(4,4,5,5-tetramethyl-1,3,2-dioxaborolan-2-yl)thiazole, **28**[241]

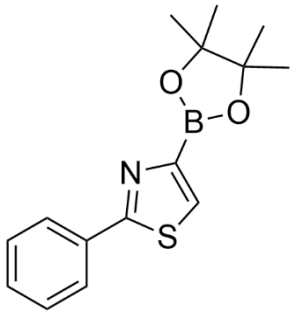

28

4-bromo-2-phenylthiazole, **27** (960 mg, 4 mmol) has been dissolved in distilled dry Et_2O (30 mL) under argon and the obtained solution has been cooled at -78°C with a dry ice/acetone bath. *n*-BuLi (2.5 M, 2 mL, 5 mmol) has been added dropwise and the system has been stirred at -78°C for 20 min. 2-isopropoxy-4,4,5,5-tetramethyl-1,3,2-dioxaborolane (930 mg, 1 mL, 5 mmol) has been slowly added to the solution and the resulting system has been stirred for 24 h letting the temperature rise up to room temperature under argon. The obtained mixture has been quenched with NH_4Cl 1M solution (30 mL) and the organic layer has been extracted with Et_2O. The combined extracts have been washed with water, dried over anhydrous Na_2SO_4 and filtered. The filtrate has been concentrated under vacuum giving 2-phenyl-4-(4,4,5,5-tetramethyl-1,3,2-dioxaborolan-2-yl)thiazole, **28** (1.06 g, 3.68 mmol, 92%) as an oil that later crystallized as a whitish solid that was used without further purification.

^{1}H-NMR ($CDCl_3$, 300 MHz): δ (ppm) 8.04 (m, 2H), 7.97 (s, 1H), 7.42 (m, 3H), 1.39 (s, 12H).

5-methyl-2-(4-nitrophenyl)-2'-phenyl-4,4'-bithiazole, **29**

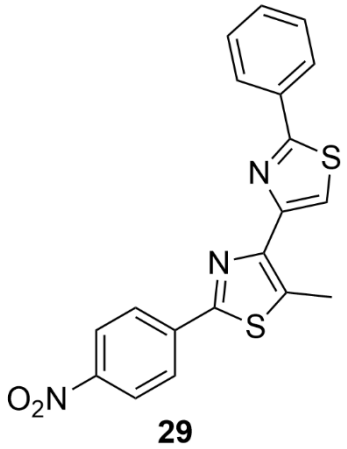

29

2-(4-nitrophenyl)-4-bromo-5-methylthiazole, **26** (299 mg, 1 mmol), 2-phenyl-4-(4,4,5,5-tetramethyl-1,3,2-dioxaborolan-2-yl)thiazole, **28** (373 mg, 1.3 mmol), CsF (380 mg, 2.50 mmol) and $Pd(PPh_3)_4$ (46 mg, 0.04 mmol) have been partially solubilized in dry 1,4-dioxane (20 mL) and the obtained yellow mixture has been stirred at reflux under argon for 24 h. The reaction has been quenched with water (20 mL) and extracted with chloroform. The combined extracts have been washed with water, dried over anhydrous Na_2SO_4 and filtered. The filtrate has been concentrated under vacuum giving the crude product as a dark yellow solid. It has been dissolved in dichloromethane and recrystallized from methanol to afford pure 5-methyl-2-(4-nitrophenyl)-2'-phenyl-4,4'-bithiazole, **29** (327 mg, 0.87 mmol, 87%) as a dark yellow crystalline solid.

^{1}H-NMR ($CDCl_3$, 300 MHz): δ (ppm) 8.31 (d, *J* = 8.9 Hz, 2H), 8.14 (d, *J* = 8.9 Hz, 2H), 8.04 (m, 2H), 7.95 (s, 1H), 7.48 (m, 3H), 3.03 (s, 3H).
^{13}C-NMR ($CDCl_3$, 91 MHz): δ (ppm) 167.90, 160.76, 152.15, 148.29, 146.98, 139.29, 133.79, 133.75, 130.28, 129.12, 126.93, 126.61, 124.43, 117.14, 13.49.
HRMS (ESI): calcd. for $C_{19}H_{14}N_3O_2S_2^+$ $[M+H]^+$ 380.0522, found $[M+H]^+$ 380.0510; calcd. for $C_{19}H_{13}N_3NaO_2S_2^+$ $[M+Na]^+$ 402.0341, found $[M+Na]^+$ 402.0327.

5.3.2 Photochromes, Chapter 2

Terthiazoles **1**[77], **2**[232], **3**, **4** and **5**

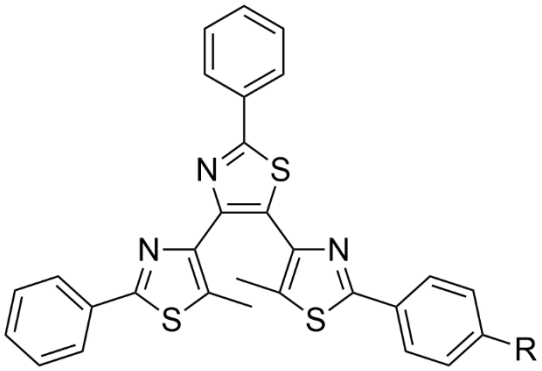

1: R = H
2: R = OCH_3
3: R = $N(CH_3)_2$
4: R = CHO
5: R= NO_2

5-methyl-2,2'-diphenyl-4,4'-bithiazole, **11** (334 mg, 1 mmol), 2-phenyl-4-bromo-5-methylthiazole, **22** (240 mg, 1 mmol), $P(tBu)_2MeHBF_4$ (32.3 mg, 0.13 mmol), Cs_2CO_3 (424 mg, 1.30 mmol), pivalic acid (31 mg, 0.30 mmol) and $Pd(OAc)_2$ (23 mg, 0.10 mmol) have been partially solubilized in dry xylenes (5 mL) and the obtained mixture has been stirred at reflux for 24 h. The reaction has been diluted with chloroform and filtered through a Celite pad. The obtained solution has been washed with water, dried over anhydrous Na_2SO_4 and filtered. The filtrate has been concentrated under vacuum and silica gel column chromatography (eluent: dichloromethane) of the residue afforded pure terthiazole **1** (344 mg, 0.68 mmol, 68%) as a whitish-light blue crystalline solid.

^{1}H-NMR ($CDCl_3$, 300 MHz): δ (ppm) 8.07 (m, 2H), 7.94 (m, 2H), 7.80 (m, 2H), 7.45 (m, 6H), 7.35 (m, 3H), 2.53 (s, 3H), 2.12 (s, 3H).
HRMS (ESI): calcd. for $C_{29}H_{22}N_3S_3^+$ $[M+H]^+$ 508.0970, found $[M+H]^+$ 508.0974.

The same procedure has been followed by replacing **22** with 2-(4-methoxyphenyl)-4-bromo-5-methylthiazole, **23** (142 mg, 0.50 mmol) to afford pure terthiazole **2** (108 mg, 0.20 mmol, 40%) as an off-white solid after purification by silica gel column chromatography (eluent: initially dichloromethane, then dichloromethane / ethyl acetate 95:5).

^{1}H-NMR ($CDCl_3$, 300 MHz): δ (ppm) 8.04 (m, 2H), 7.88 (d, *J* = 8.9 Hz, 2H), 7.81 (m, 2H), 7.46 (m, 3H), 7.35 (m, 3H), 6.95 (d, *J* = 8.9 Hz, 2H), 3.86 (s, 3H), 2.51 (s, 3H), 2.08 (s, 3H).
^{13}C-NMR ($CDCl_3$, 100 MHz): δ (ppm) 167.19, 164.27, 164.02, 161.19, 147.72, 146.59, 143.44, 133.86, 133.77, 133.09, 131.45, 130.28, 129.79, 129.72, 129.04, 128.86, 128.00, 126.77, 126.64, 126.47, 114.36, 55.58, 12.81, 12.41.
HRMS (ESI): calcd. for $C_{30}H_{24}N_3OS_3^+$ $[M+H]^+$ 538.1076, found $[M+H]^+$ 538.1087.

The same procedure has been followed by replacing **22** with 4-(4-bromo-5-methylthiazol-2-yl)-N,N-dimethylaniline, **24** (149 mg, 0.50 mmol) to afford pure terthiazole **3** (205 mg, 0.37 mmol, 74%) as a green amorphous solid after purification by silica gel column chromatography (eluent: dichloromethane / acetonitrile 99:1).

^{1}H-NMR ($CDCl_3$, 300 MHz): δ (ppm) 8.07 (m, 2H), 7.84 (m, 2H), 7.81 (d, *J* = 9.0 Hz, 2H), 7.46 (m, 3H), 7.36 (m, 3H), 6.71 (d, *J* = 9.0 Hz, 2H), 3.03 (s, 6H), 2.45 (s, 3H), 2.04 (s, 3H).
^{13}C-NMR ($CDCl_3$, 75 MHz): δ (ppm) 167.06, 165.28, 164.01, 151.62, 147.50, 146.72, 142.95, 133.90, 133.83, 132.97, 130.28, 130.16, 130.09, 129.65, 128.98, 128.82, 127.69, 126.75, 126.49, 121.94, 111.95, 40.37, 12.70, 12.31.
HRMS (ESI): calcd. for $C_{31}H_{27}N_4S_3^+$ $[M+H]^+$ 551.1392, found $[M+H]^+$ 551.1373; calcd. for $C_{31}H_{26}N_4NaS_3^+$ $[M+Na]^+$ 573.1212, found $[M+Na]^+$ 573.1185.

The same procedure has been followed by replacing **22** with 2-(4-formylphenyl)-4-bromo-5-methylthiazole, **25** (141 mg, 0.50 mmol) to afford pure terthiazole **4** (203 mg, 0.38 mmol, 76%) as a light green crystalline solid after purification by silica gel column chromatography (eluent: dichloromethane / acetonitrile 99:1).

^{1}H-NMR ($CDCl_3$, 300 MHz): δ (ppm) 10.05 (s, 1H), 8.11 (d, *J* = 8.3 Hz, 2H), 8.07 (m, 2H), 7.94 (d, *J* = 8.4 Hz, 2H), 7.75 (m, 2H), 7.48 (m, 3H), 7.33 (m, 3H), 2.60 (s, 3H), 2.17 (s, 3H).
^{13}C-NMR ($CDCl_3$,75 MHz): δ (ppm) 191.55, 167.23, 163.75, 162.19, 148.17, 146.21, 144.92, 138.67, 136.93, 134.38, 133.70, 133.59, 133.30, 130.37, 129.71, 129.05, 128.81, 128.61, 126.80, 126.67, 126.27, 12.93, 12.56.
HRMS (ESI): calcd. for $C_{30}H_{22}N_3OS_3^+$ $[M+H]^+$ 536.0919, found $[M+H]^+$ 536.0892.

Lastly, the same procedure has been followed by replacing **22** with 2-(4-nitrophenyl)-4-bromo-5-methylthiazole, **26** (299 mg, 1 mmol) to afford pure terthiazole **5** (200 mg, 0.40 mmol, 40%) as a yellow-brownish solid after purification by silica gel column chromatography (eluent: initially dichloromethane, then dichloromethane / acetonitrile 99:1).

^{1}H-NMR ($CDCl_3$, 300 MHz): δ (ppm) 8.29 (d, *J* = 8.9 Hz, 2H), 8.09 (d, *J* = 8.9 Hz, 2H), 8.06 (m, 2H), 7.73 (m, 2H), 7.49 (dd, *J* = 5.1, 1.9 Hz, 3H), 7.33 (dd, *J* = 5.3, 2.0 Hz, 3H), 2.65 (s, 3H), 2.20 (s, 3H).
^{13}C-NMR ($CDCl_3$, 75 MHz): δ (ppm) 167.19, 163.65, 160.83, 148.18, 146.01, 145.23, 138.96, 135.11, 133.53, 133.44, 133.36, 130.39, 129.73, 129.02, 128.78, 128.19, 126.81, 126.59, 126.16, 124.29, 12.95, 12.56.
HRMS (ESI): calcd. for $C_{29}H_{21}N_4O_2S_3^+$ $[M+H]^+$ 553.0821, found $[M+H]^+$ 553.0798.

Terthiazole **6**

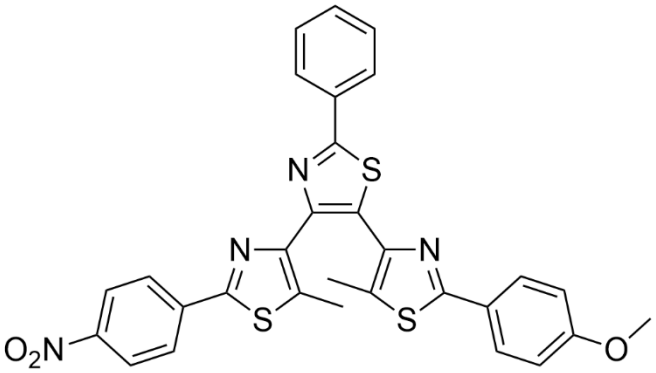

6

5-methyl-2-(4-nitrophenyl)-2'-phenyl-4,4'-bithiazole, **29** (304 mg, 0.80 mmol), 2-(4-methoxyphenyl)-4-bromo-5-methylthiazole, **23** (227 mg, 0.80 mmol), $P(tBu)_2MeHBF_4$ (25 mg, 0.10 mmol), Cs_2CO_3 (326 mg, 1 mmol), pivalic acid (25 mg, 0.24 mmol) and $Pd(OAc)_2$ (18 mg, 0.08 mmol) have been partially solubilized in dry xylenes (5 mL) and the obtained mixture has been stirred at reflux for 24 h. The reaction has been diluted with chloroform and filtered through a Celite pad. The obtained solution has been washed with water, dried over anhydrous Na_2SO_4 and filtered. The filtrate has been concentrated under vacuum and silica gel column chromatography (eluent: initially dichloromethane / acetonitrile 99:1, then 97:3) of the residue afforded pure terthiazole **6** (216 mg, 0.37 mmol, 46%) as a light orange crystalline solid.

^{1}H-NMR ($CDCl_3$, 300 MHz): δ (ppm) 8.18 (d, *J* = 9.0 Hz, 2H), 8.06 (m, 2H) 7.91 (d, *J* = 9.0 Hz, 2H), 7.86 (d, *J* = 8.8 Hz, 2H) 7.48 (m, 3H), 6.95 (d, *J* = 8.9 Hz, 2H), 3.86 (s, 3H), 2.63 (s, 3H), 2.12 (s, 3H).
^{13}C-NMR ($CDCl_3$, 101 MHz): δ (ppm) 167.31, 164.40, 161.39, 160.49, 148.17, 147.62, 147.51, 143.19, 139.29, 135.80, 133.60, 131.49, 130.43, 129.11, 128.01, 126.81, 126.70, 126.28, 124.28, 114.45, 55.56, 13.17, 12.41.
HRMS (ESI): calcd. for $C_{30}H_{23}N_4O_3S_3^+$ $[M+H]^+$ 583.0926, found $[M+H]^+$ 583.0902; calcd. for $C_{30}H_{22}N_4NaO_3S_3^+$ $[M+Na]^+$ 605.0746, found $[M+Na]^+$ 605.0721.

Nicolò Baggi

Terthiazole **7**

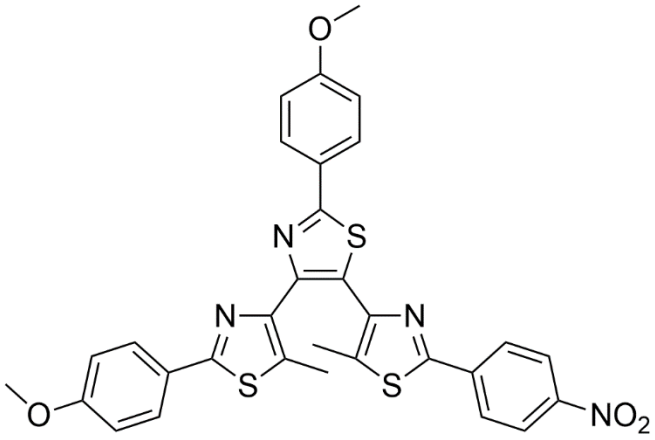

7

2,2'-bis(4-methoxyphenyl)-5-methyl-4,4'-bithiazole, **18** (395 mg, 1 mmol), 2-(4-nitrophenyl)-4-bromo-5-methylthiazole, **26** (299 mg, 1 mmol), $P(tBu)_2MeHBF_4$ (31 mg, 0.12 mmol), Cs_2CO_3 (652 mg, 2 mmol), pivalic acid (40 mg, 0.40 mmol) and $Pd(OAc)_2$ (23 mg, 0.10 mmol) have been partially solubilized in dry xylenes (5 mL) and the obtained mixture has been stirred at reflux for 24 hours. The reaction has been diluted with chloroform (40 mL) and water (30 mL). The organic layer has been extracted with chloroform. The obtained solution has been washed with water, dried over anhydrous Na_2SO_4 and filtered. The filtrate has been concentrated under vacuum and silica gel column chromatography (eluent dichloromethane) of the residue followed by recrystallization from methanol afforded pure terthiazole **7** (460 mg, 0.75 mmol, 75%) as a yellow crystalline solid.

^{1}H-NMR ($CDCl_3$, 360 MHz): δ (ppm) 8.27 (d, *J* = 8.9 Hz, 2H), 8.06 (d, *J* = 8.9 Hz, 2H), 8.01 (d, *J* = 8.9 Hz, 2H), 7.74 (d, *J* = 8.9 Hz, 2H), 6.99 (d, *J* = 8.9 Hz, 2H), 6.86 (d, *J* = 8.9 Hz, 2H), 3.89 (s, 3H), 3.82 (s, 3H), 2.55 (s, 3H), 2.22 (s, 3H).
^{13}C-NMR ($CDCl_3$, 91 MHz): δ (ppm) 167.18, 163.73, 161.44, 160.92, 160.77, 148.17, 147.92, 145.82, 145.40, 139.00, 134.86, 132.20, 128.15, 127.69, 127.28, 126.82, 126.54, 126.39, 124.31, 114.34, 114.12, 55.47, 55.40, 12.80, 12.56.
HRMS (ESI): calcd. for $C_{31}H_{25}N_4O_4S_3^+$ $[M+H]^+$ 613.1032, found $[M+H]^+$ 613.1007; calcd. for $C_{31}H_{24}N_4NaO_4S_3^+$ $[M+Na]^+$ 635.0852, found $[M+Na]^+$ 635.0822.

Terthiazole **8**

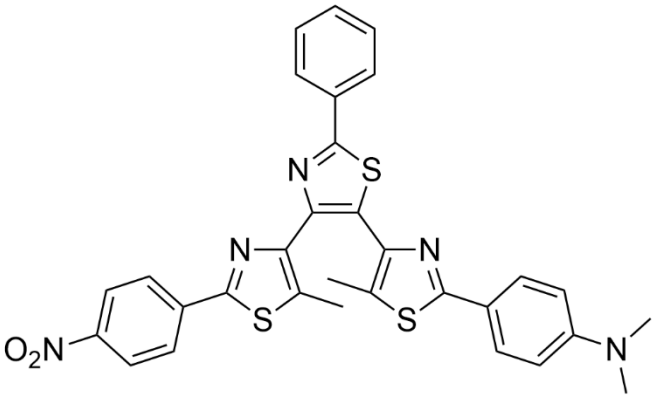

8

5-methyl-2-(4-nitrophenyl)-2'-phenyl-4,4'-bithiazole, **29** (190 mg, 0.50 mmol), 4-(4-bromo-5-methylthiazol-2-yl)-N,N-dimethylaniline, **24** (149 mg, 0.50 mmol), $P(tBu)_2MeHBF_4$ (16 mg, 0.07 mmol), Cs_2CO_3 (212 mg, 0.65 mmol), pivalic acid (15 mg, 0.15 mmol) and $Pd(OAc)_2$ (11 mg, 0.05 mmol) have been partially solubilized in dry xylenes (5 mL) and the obtained mixture has been stirred at reflux for 24 h. The reaction has been diluted with chloroform and filtered through a Celite pad. The obtained solution has been washed with water, dried over anhydrous Na_2SO_4 and filtered. The filtrate has been concentrated under vacuum and silica gel column chromatography (eluent: initially dichloromethane / acetonitrile 99:1, then 98:2 and finally 96:4) of the residue afforded pure terthiazole **8** (100 mg, 0.17 mmol, 34%) as a light orange crystalline solid.

^{1}H-NMR ($CDCl_3$, 300 MHz): δ (ppm) 8.17 (d, *J* = 8.9 Hz, 2H), 8.06 (m, 2H), 7.92 (d, *J* = 8.9 Hz, 2H), 7.80 (d, *J* = 8.9 Hz, 2H), 7.47 (m, 3H), 6.72 (d, *J* = 8.9 Hz, 2H), 3.03 (s, 6H), 2.63 (s, 3H), 2.10 (s, 3H).
^{13}C-NMR ($CDCl_3$, 75 MHz): δ (ppm) 167.08, 165.26, 160.45, 151.55, 148.03, 147.68, 147.20, 142.78, 139.25, 135.60, 133.59, 130.30, 130.09, 129.03, 127.61, 126.79, 126.63, 124.21, 121.71, 111.95, 40.34, 13.05, 12.32.
HRMS (ESI): calcd. for $C_{31}H_{26}N_5O_2S_3^+$ $[M+H]^+$ 596.1243, found $[M+H]^+$ 596.1227.

5.3.3 Intermediates, Chapter 3

Terthiazole **30**

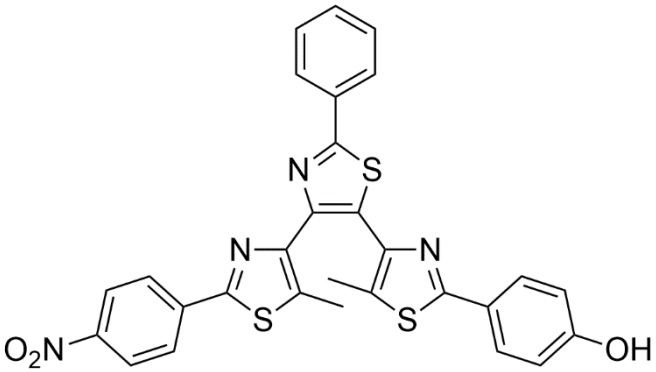

30

Terthiazole **6** (200 mg, 0.34 mmol) has been dissolved in distilled dry CH_2Cl_2 (15 mL) under argon and the obtained solution has been cooled at 0°C. BBr_3 (426 mg, 0.164 mL, 1.70 mmol) has been slowly added and the resulting system has been stirred for 24 h letting the temperature rise up to room temperature under argon. The obtained mixture has been quenched with water (20 mL) and the organic layer has been extracted with dichloromethane. The combined extracts have been washed with a saturated solution of $NaHCO_3$ (50 mL), dried over anhydrous Na_2SO_4 and filtered. The filtrate has been concentrated under vacuum before adding Et_2O to induce the precipitation of terthiazole **30** (161 mg, 0.28 mmol, 83%), that has been recovered by filtration as an orange solid.

^{1}H-NMR ($CDCl_3$, 300 MHz): δ (ppm) 8.18 (d, *J* = 8.9 Hz, 2H), 8.05 (m, 2H), 7.90 (d, *J* = 8.9 Hz, 2H), 7.80 (d, *J* = 8.9 Hz, 2H), 7.48 (m, 3H), 6.87 (d, *J* = 8.9 Hz, 2H), 2.64 (s, 3H), 2.13 (s, 3H).
^{13}C-NMR ($CDCl_3$, 91 MHz): δ (ppm) 167.55, 165.18, 160.75, 158.88, 148.05, 147.40, 147.28, 142.74, 139.11, 135.81, 133.32, 131.32, 130.49, 129.46, 129.09, 128.00, 126.78, 126.65, 125.15, 124.26, 115.96, 12.96, 12.29.
HRMS (ESI): calcd. for $C_{29}H_{19}N_4O_3S_3^-$ $[M-H]^-$ 567.0625, found $[M-H]^-$ 567.0610.

Terthiazole **31**

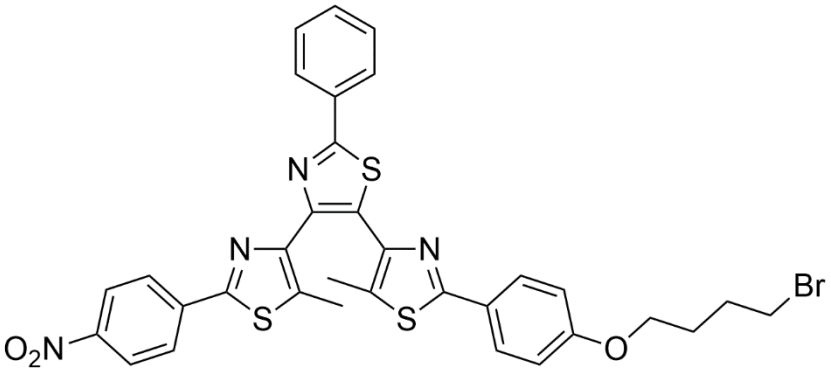

31

Terthiazole **30** (160 mg, 0.28 mmol) has been dissolved in DMF (5 mL) and then K2CO3 (58 mg, 0.42 mmol) has been added to the it. The system has been stirred for 10 min before the addition of 1,4-dibromobutane (182 mg, 0.105 mL, 0.84 mmol). The mixture has been stirred at room temperature for 24 h and then quenched with water (15 mL) and extracted with dichloromethane. The combined extracts have been washed with water, dried over anhydrous Na_2SO_4 and filtered. The filtrate has been concentrated under vacuum and silica gel column chromatography (eluent: dichloromethane / acetonitrile 99:1) of the residue afforded pure terthiazole **31** (176 mg, 0.25 mmol, 88%) as a yellow solid.

^{1}H-NMR ($CDCl_3$, 300 MHz): δ (ppm) 8.16 (d, *J* = 8.9 Hz, 2H), 8.06 (m, 2H), 7.88 (m, 4H), 7.48 (m, 3H), 6.93 (d, *J* = 8.9 Hz, 2H), 4.06 (t, *J* = 5.9 Hz, 2H), 3.50 (t, *J* = 6.5 Hz, 2H), 2.68 (s, 3H), 2.15 (s, 3H), 2.12 – 1.92 (m, 4H).
^{13}C-NMR ($CDCl_3$, 91 MHz): δ (ppm) 167.16, 164.19, 160.46, 160.41, 148.00, 147.50, 147.28, 143.21, 139.15, 135.65, 133.46, 131.39, 130.34, 129.62, 129.01, 127.83, 126.70, 126.57, 126.35, 124.18, 114.78, 67.05, 33.45, 29.41, 27.83, 13.06, 12.32.
HRMS (ESI): calcd. for $C_{33}H_{28}BrN_4O_3S_3^+$ $[M+H]^+$ 703.0501, found $[M+H]^+$ 703.0482.

5.3.4 Photochrome, Chapter 3

Terthiazole **SWIST1**

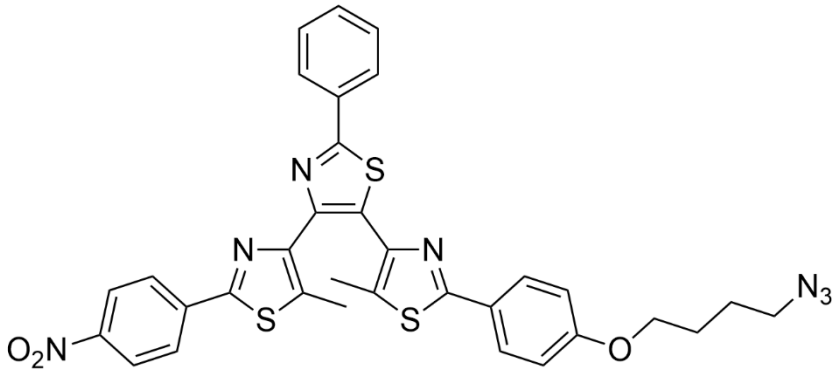

SWIST1

Terthiazole **31** (170 mg, 0.24 mmol) has been dissolved in DMF (5 mL) and then NaN_3 (130 mg, 2 mmol) has been added to it. The solution has been stirred for 24 h at room temperature under Ar. Water has been added to induce the precipitation of terthiazole **SWIST1** (150 mg, 0.23 mmol, 94%), that has been recovered by filtration as a yellow solid.

^{1}H-NMR ($CDCl_3$, 360 MHz): δ (ppm) 8.17 (d, *J* = 8.9 Hz, 2H), 8.06 (m, 2H), 7.90 (d, *J* = 8.9 Hz, 2H), 7.85 (d, *J* = 8.8 Hz, 2H), 7.48 (m, 3H), 6.93 (d, *J* = 8.8 Hz, 2H), 4.05 (t, *J* = 5.9 Hz, 2H), 3.39 (t, *J* = 6.6 Hz, 2H), 2.65 (s, 3H), 2.13 (s, 3H), 2.00 – 1.73 (m, 4H).
^{13}C-NMR ($CDCl_3$, 91 MHz): δ (ppm) 167.23, 164.25, 160.53, 160.48, 148.08, 147.58, 147.36, 143.28, 139.23, 135.72, 133.53, 131.45, 130.41, 129.69, 129.08, 127.91, 126.77, 126.65, 126.42, 124.25, 114.84, 67.43, 51.25, 26.52, 25.80, 13.13, 12.40.
HRMS (ESI): calcd. for $C_{33}H_{28}N_7O_3S_3^+$ $[M+H]^+$ 666.1410, found $[M+H]^+$ 666.1380.

5.3.5 Intermediates, Chapter 4

pyridine-4-carbothioamide, **32**[242]

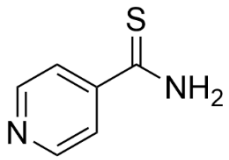

32

4-pyridinecarbonitrile (5.21 g, 50 mmol), 67% sodium hydrosulfide hydrate (12.45 g, 150 mmol) and diethylamine hydrochloride (16.44 g, 150 mmol) have been dissolved in water / 1,4-dioxane 1:1 (80 mL) and the system has been stirred at room temperature for 24 h. Water has been added to make pure pyridine-4-carbothioamide, **32** (6.41 g, 46.43 mmol, 93%) precipitate as a yellow solid to be recovered by filtration.

^{1}H-NMR (DMSO-d_6, 300 MHz): δ (ppm) 10.20 (bs, 1H), 9.79 (bs, 1H), 8.65 (d, *J* = 6.2 Hz, 2H), 7.70 (d, *J* = 6.2 Hz, 2H).

2-bromo-1,1-dimethoxypropane, **33**[243]

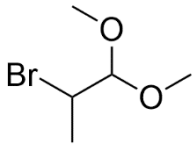

33

Propionaldehyde (11.62 g, 14.60 mL, 200 mmol) and 1,4-dioxane (880 mg, 1.00 mL, 10 mmol) have been cooled at 0°C under stirring. Br_2 (32 g, 10.30 mL, 200 mL) has been added dropwise while maintaining the solution at ~0°C. It has been stirred for 15 min before the addition of CH_3OH (19.20 g, 24.30 mL, 600 mmol). The obtained biphasic system was stirred until the obtainment of a brown homogeneous solution. It has been cooled at 0°C again and $(CH_3O)_3CH$ (25.50 g, 26.30 mL, 240 mmol) has been added dropwise. The solution has been stirred for 16 h while letting the temperature rise to RT. A saturated solution of $NaHCO_3$ (50 mL) has been added and the organic layer has been extracted with diethyl ether. Combined extracts have been washed with water, dried over anhydrous Na_2SO_4 and filtered. Volatile solvents have been removed under reduced pressure before obtaining pure 2-bromo-1,1-dimethoxypropane, **33** (11.18 g, 61 mmol, 31%) as a colorless liquid by distillation.

^{1}H-NMR ($CDCl_3$, 300 MHz): δ (ppm) 4.32 (d, *J* = 5.7 Hz, 1H), 4.06 (m, 1H), 3.42 (s, 6H), 1.65 (d, *J* = 6.8 Hz, 3H).

5-methyl-2-(pyridin-4-yl)thiazole, **34**[216]

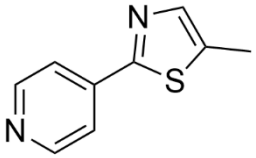

34

pyridine-4-carbothioamide, **32** (6.34 g, 46 mmol) has been dissolved in acetic acid (57.5 mL) before the addition of 2-bromo-1,1-dimethoxypropane, **33** (10.50 g, 57.50 mmol). The resulting mixture has been stirred at 100°C for 24 h. The solvent has been removed under reduced pressure. Water has been added to the residue followed by the addition of a saturated solution of $NaHCO_3$ until pH 8. Dichloromethane has been added to extract the product. Combined extracts have dried over anhydrous Na_2SO_4 and filtered. The solvent has been removed under vacuum. The crude product has been dissolved in diethyl ether to remove insoluble impurities by filtration. The filtrate has been concentrated under vacuum and silica gel column chromatography (eluent: dichloromethane / ethyl acetate 1:1) of the residue afforded pure 5-methyl-2-(pyridin-4-yl)thiazole, **34** (2.90 g, 16.50 mmol, 36%) as an off-white solid.

^{1}H-NMR ($CDCl_3$, 250 MHz): δ (ppm) 8.67 (d, *J* = 6.2 Hz, 2H), 7.75 (d, *J* = 6.2 Hz, 2H), 7.60 (s, 1H), 2.55 (s, 3H).

2-(pyridin-4-yl)-4-bromo-5-methylthiazole, **35**[216]

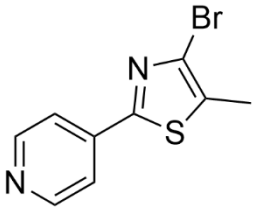

35

5-methyl-2-(pyridin-4-yl)thiazole, **34** (1.46 g, 8.28 mmol) has been dissolved in acetonitrile (40 mL) and Br_2 (8.41 g, 2.70 mL, 52.60 mmol) has been slowly added. The obtained mixture has been stirred at reflux under argon for 24 h. It has been quenched with $Na_2S_2O_3 \cdot 5H_2O$ (250 mg) in water (20 mL). A saturated solution of $NaHCO_3$ has been added until pH 8 and then the organic layer has been extracted with chloroform. The combined extracts have been dried over anhydrous Na_2SO_4 and filtered. The filtrate has been concentrated under vacuum and silica gel column chromatography (eluent: dichloromethane / ethyl acetate 7:3) of the residue afforded pure 2-(pyridin-4-yl)-4-bromo-5-methylthiazole, **35** (1.29 g, 5.05 mmol, 61%) as an off-white solid.

^{1}H-NMR ($CDCl_3$, 360 MHz): δ (ppm) 8.69 (d, *J* = 6.2 Hz, 1H), 7.73 (d, *J* = 6.2 Hz, 1H), 2.48 (s, 2H).

2-(pyridin-4-yl)-4-(4,4,5,5-tetramethyl-1,3,2-dioxaborolan-2-yl)-5-methylthiazole, **36**[212]

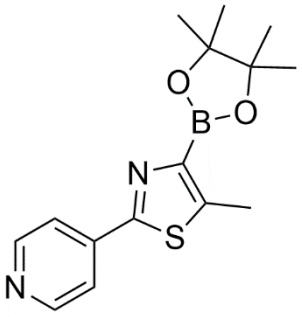

36

2-(pyridin-4-yl)-4-bromo-5-methylthiazole, **35** (510 mg, 2 mmol) has been dissolved in distilled dry Et_2O (30 mL). The resulting solution has been cooled to -78°C and *n*-BuLi (2.5 M, 1 mL, 2.5 mmol) has been added dropwise and the system has been stirred at -78°C for 2 h. 2-isopropoxy-4,4,5,5-tetramethyl-1,3,2-dioxaborolane (560 mg, 0.610 mL, 3 mmol) has been slowly added to the solution and the resulting system has been stirred for 24 h letting the temperature rise up to room temperature under argon. The obtained mixture has been quenched with NH_4Cl 1M solution (20 mL) and the organic layer has been extracted with Et_2O. The combined extracts have been washed with brine, dried over anhydrous Na_2SO_4 and filtered. The filtrate has been concentrated under vacuum giving 2-(pyridin-4-yl)-4-(4,4,5,5-tetramethyl-1,3,2-dioxaborolan-2-yl)-5-methylthiazole, **36** (590 mg, 1.96 mmol, 98%) as an oil that later crystallized as a light-brown solid that was used without further purification.

^{1}H-NMR ($CDCl_3$, 360 MHz): δ (ppm) 8.65 (d, *J* = 6.4 Hz, 2H), 7.84 (d, *J* = 6.4 Hz, 2H), 2.77 (s, 3H), 1.38 (s, 12H).

2-phenyl-4,5-dibromothiazole, **37**[212,244]

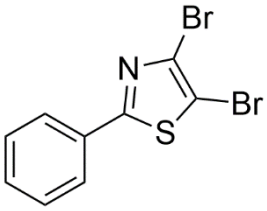

37

5-bromo-2-phenylthiazole, **19** (1.20 g, 5 mmol) has been dissolved in distilled dry THF (30 mL) under argon and the obtained solution has been cooled at -78°C with a dry ice/acetone bath. Lithium diisopropylamine (2M solution, 3.80 mL, 7.60 mmol) has been added dropwise and the system has been stirred at -78°C for 30 min. 1,2-dibromo-tetrachloroethane (1.63 g, 5 mmol) has been finally added in one portion in solid form and the resulting solution has been stirred for 24 h letting the temperature rise up to room temperature under argon. The system has been quenched with NH_4Cl 1M solution (30 mL) and the organic layer has been extracted with diethyl ether. The combined extracts have been washed with brine, dried over anhydrous Na_2SO_4 and filtered. The filtrate has been concentrated under vacuum giving the crude product that has been purified by silica gel column chromatography (eluent: dichloromethane / petroleum ether 7:3) to afford 2-phenyl-4,5-dibromothiazole, **37** (1.57 g, 4.90 mmol, 98%) as a colorless crystalline solid.

^{1}H-NMR ($CDCl_3$, 360 MHz): δ (ppm) 7.86 (m, 2H), 7.45 (m, 3H).

2-(4-ferrocenylphenyl)thiazole, **39**[212]

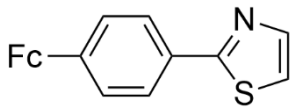

39

Ferrocene (372 mg, 2 mmol) and KOtBu (32 mg, 0.28 mmol) have been dissolved in distilled dry THF (25 mL) under argon and the obtained solution has been cooled at -78°C. *t*-BuLi (1.9 M, 2.30 mL, 4.4 mmol) has been added dropwise and the system has been stirred at -78°C for 45 min and then at 0°C before adding $ZnCl_2$ (1M, 2.3 ml, 2.3 mmol). The solution has been stirred at 0°C for 30 min before the addition of 2-(4-bromophenyl)thiazole (480 mg, 2 mmol) and $Pd(PPh_3)_4$ (23 mg, 0.02 mmol). The mixture has been stirred at 55°C for 24 h. It has been quenched with NH_4Cl 1M solution (30 mL) and the organic layer has been extracted with ethyl acetate. The combined organic phase has been washed with brine, dried over anhydrous Na_2SO_4 and filtered. The filtrate has been concentrated under vacuum and the residue has been purified by silica gel column chromatography (eluent: dichloromethane) to give 2-(4-ferrocenyl-phenyl)thiazole, **39** (588 mg, 1.70 mol, 85%) as an orange-red microcrystalline solid.

^{1}H-NMR ($CDCl_3$, 360 MHz): δ (ppm) 7.87 (m, 3H), 7.49 (d, *J* = 8.2 Hz, 2H), 7.31 (d, *J* = 3.2 Hz, 1H), 4.78 (s, 2H), 4.44 (s, 2H), 4.11 (s, 5H).
^{13}C-NMR ($CDCl_3$, 91 MHz): δ (ppm) 168.5, 143.7, 141.8, 131.1, 126.6, 126.4, 118.4, 84.1, 69.9, 69.6, 66.7.
HRMS (ESI): calcd. for $C_{19}H_{15}FeNS$ $[M]^+$ 345.0269, found $[M]^+$ 345.0259.

2-(4-ferrocenylphenyl)-4,5-dibromothiazole, **40** and 2-(4-ferrocenylphenyl)-5-bromothiazole, **41**[212]

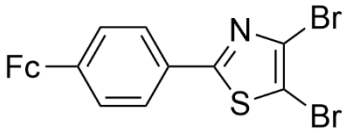

40

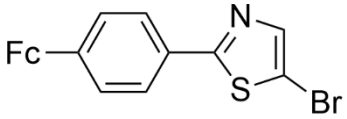

41

2-(4-ferrocenylphenyl)thiazole, **39** (580 mg, 1.68 mmol) has been dissolved in distilled dry THF (30 mL) under argon and the obtained solution has been cooled at -78°C. Lithium diisopropylamine (2 M, 1 ml, 2 mmol) has been added dropwise and the system has been stirred at -78°C for 30 min. 1,2-dibromo-tetrachloroethane (550 mg, 1.69 mmol) has been added in one portion in solid form and the resulting solution has been stirred for 30 min at that temperature. Always at -78°C, lithium diisopropylamine (2 M, 1 ml, 2 mmol) has been added dropwise again. The solution has been stirred at -78°C for 30 min before the addition of another portion of 1,2-dibromo-tetrachloroethane (550 mg, 1.69 mmol). The resulting mixture has been allowed to slowly warm up to room temperature while stirring for 24 h. The system has been quenched with NH_4Cl 1M solution (30 mL) and the organic layer has been extracted with ethyl acetate. The combined extracts have been washed with brine, dried over anhydrous Na_2SO_4 and filtered. The filtrate has been concentrated under reduced pressure and the residue has been purified by silica gel column chromatography (eluent: dichloromethane / petroleum ether 6:4). The first fraction gave 2-(4-ferrocenylphenyl)-4,5-dibromothiazole, **40** (235 mg, 0.47 mmol, 28%) as a red microcrystalline solid while the second fraction afforded 2-(4-ferrocenylphenyl)-5-bromothiazole, **41** (400 mg, 0.94 mmol, 56%) as a red microcrystalline solid, too.

About intermediate **40**:

^{1}H-NMR ($CDCl_3$, 250 MHz): δ (ppm) 7.75 (d, *J* = 8.3 Hz, 2H), 7.47 (d, *J* = 8.3 Hz, 2H), 4.71 (s, 2H), 4.40 (s, 2H), 4.06 (s, 5H).
^{13}C-NMR ($CDCl_3$, 91 MHz): δ (ppm) 168.9, 143.3, 129.7, 129.4, 126.4, 126.1, 106.0, 83.5, 69.9, 69.8, 66.8.
HRMS (ESI): calcd. for $C_{19}H_{13}Br_2FeNS$ $[M]^+$ 500.8482, found $[M]^+$ 500.8471.

About intermediate **41**:

^{1}H-NMR ($CDCl_3$, 360 MHz): δ (ppm) 7.76 (d, *J* = 8.2 Hz, 2H), 7.72 (s, 1H), 7.50 (d, *J* = 8.2 Hz, 2H), 4.77 (s, 2H), 4.44 (s, 2H), 4.10 (s, 5H).
^{13}C-NMR ($CDCl_3$, 91 MHz): δ (ppm) 169.7, 144.9, 142.5, 130.6, 126.4, 126.3, 107.9, 100.2, 83.9, 69.9, 69.7, 66.8.
HRMS (ESI): calcd. for $C_{19}H_{14}BrFeNS$ $[M]^+$: 422.9376, found $[M]^+$ 422.9379.

2-(4-methoxyphenyl)-4-bromo-5-iodothiazole, **43**

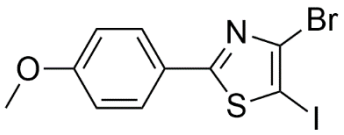

43

5-bromo-2-(4-methoxyphenyl)thiazole, **20** (1.05 g, 3.90 mmol) has been dissolved in distilled dry THF (20 mL) under argon and the obtained solution has been cooled at -78°C with a dry ice/acetone bath. Lithium diisopropylamine (2M solution, 3 mL, 6 mmol) has been added dropwise and the system has been stirred at -78°C for 1 h. I_2 (1.48 g, 5.85 mmol) has been finally added and the resulting solution has been stirred for 24 h letting the temperature rise up to room temperature under argon. The system has been quenched with NH_4Cl 1M solution (30 mL) before the addition of an aliquot of $Na_2S_2O_5$ to reduce the excess of iodine. The organic layer has been extracted with diethyl ether. The combined extracts have been washed with water, dried over anhydrous Na_2SO_4 and filtered. The filtrate has been concentrated under vacuum giving the crude product as an off-white solid. Silica gel column chromatography (eluent: chloroform) of the residue afforded pure 2-(4-methoxyphenyl)-4-bromo-5-iodothiazole, **43** (1.43 g, 3.61 mmol, 92%) as a white crystalline solid.

^{1}H-NMR ($CDCl_3$, 250 MHz): δ (ppm) 7.80 (d, *J* = 8.8 Hz, 2H), 6.94 (d, *J* = 8.9 Hz, 2H), 3.86 (s, 3H). HRMS (ESI): calcd. for $C_{10}H_8INOS$ $[M+H]^+$ 395.8549, found $[M+H]^+$ 395.8545.

2,3-dibromo-5-(4-methoxyphenyl)thiophene, **45**[219]

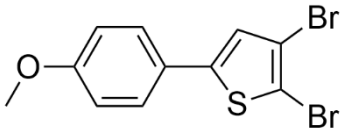

45

DMSO (5 mL) has been added to 4-iodoanisole (234 mg, 1 mmol), KF (145 mg, 2.50 mmol), $PdCl_2(PPh_3)_2$ (35 mg, 0.05 mmol), 2,3-dibromothiophene (290 mg, 1.20 mmol) and $AgNO_3$ (85 mg, 0.50 mmol). The mixture has been stirred at 100°C and $AgNO_3$ (436 mg) has been added in three portion over 3 h (3 x 112 mg). The obtained system has been stirred at 100°C for 3 h. The reaction has been diluted with chloroform (20 mL) and filtered through a Celite pad. The obtained solution has been washed with water, dried over anhydrous Na_2SO_4 and filtered. The filtrate has been concentrated under vacuum and silica gel column chromatography (eluent: petroleum ether / dichloromethane 9:1) of the residue afforded pure 2,3-dibromo-5-(4-methoxyphenyl)thiophene, **45** (303 mg, 0.87 mmol, 87%) as a pale yellow crystalline solid.

^{1}H-NMR ($CDCl_3$, 300 MHz): δ (ppm) 7.40 (d, *J* = 8.7 Hz, 2H), 6.98 (s, 1H), 6.91 (d, *J* = 8.7 Hz, 2H), 3.83 (s, 3H).

3-bromo-5-(4-methoxyphenyl)-2-methylthiophene, **53**[245], 3-bromo-5-(2-methoxyphenyl)-2-methylthiophene, **54**[245], 3-bromo-5-(2,4-dimethoxyphenyl)-2-methylthiophene, **55**, 3-bromo-2-methyl-5-(4-(methylthio)phenyl)thiophene, **56**[246], 4-(4-bromo-5-methylthiophen-2-yl)-N,N-dimethylaniline, **57**[247], and 4-(4-bromo-5-methylthiophen-2-yl)-N,N-diphenylaniline, **58**

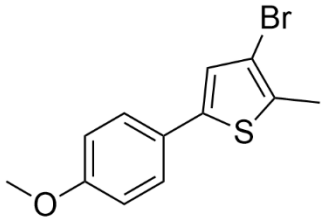

53

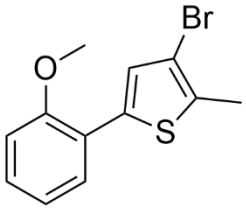

54

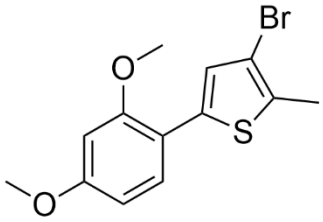

55

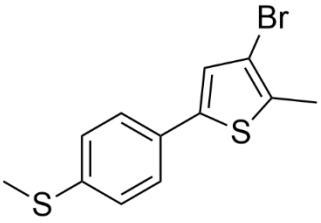

56

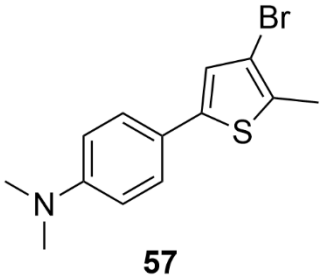

57

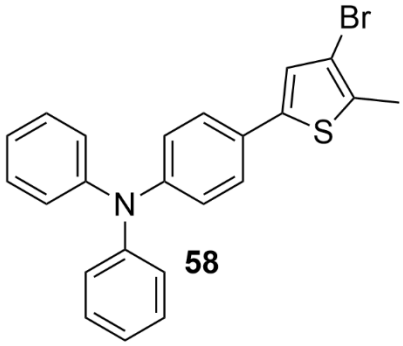

58

3,5-dibromo-2-methylthiophene (1.41 g, 0.705 mL, 5.5 mmol), 4-methoxyphenylboronic acid, **47** (920 mg, 6.05 mmol), $Pd(PPh_3)_4$ (254 mg, 0.22 mmol) and K_2CO_3 (835 mg, 6.05 mmol) have been dissolved in a water / THF 1:1 mixture (40 mL). The obtained biphasic system has been stirred at 66°C under argon for 24 h. It has been quenched with ethyl acetate (30 mL). The organic layer has been extracted with ethyl acetate. The combined extracts have been washed with brine, dried over anhydrous Na_2SO_4 and filtered. The filtrate has been concentrated under vacuum giving the crude product as yellow-brownish solid. Silica gel column chromatography (eluent: petroleum ether / dichloromethane 8:2) of the residue afforded pure 3-bromo-5-(4-methoxyphenyl)-2-methylthiophene, **53** (1.22 g, 4.31 mmol, 78%) as a white crystalline solid.

^{1}H-NMR ($CDCl_3$, 360 MHz): δ (ppm) 7.43 (d, *J* = 8.9 Hz, 1H), 6.98 (s, 1H), 6.90 (d, *J* = 8.9 Hz, 1H), 3.83 (s, 3H), 2.40 (s, 3H).

The same procedure has been followed by replacing **47** with 2-methoxyphenylboronic acid, **48** (312 mg, 2.05 mmol) to afford pure 3-bromo-5-(2-methoxyphenyl)-2-methylthiophene, **54** (480 mg, 1.70 mmol, 85%) as a white solid after purification by silica gel column chromatography (eluent: petroleum ether / dichloromethane 1:1).

^{1}H-NMR ($CDCl_3$, 360 MHz): δ (ppm) 7.54 (d, *J* = 8.0 Hz, 1H) 7.30 (s, 1H), 7.27 (s, 1H), 6.97 (m, 2H), 3.91 (s, 3H), 2.41 (s, 3H).

The same procedure has been followed by replacing **47** with 2,4-dimethoxyphenylboronic acid, **49** (382 mg, 2.10 mmol) to afford pure 3-bromo-5-(2,4-dimethoxyphenyl)-2-methylthiophene, **55** (525 mg, 1.68 mmol, 84%) as white crystalline solid after purification by silica gel column chromatography (eluent: petroleum ether / dichloromethane 7:3).

^{1}H-NMR ($CDCl_3$, 360 MHz): δ (ppm) 7.43 (d, *J* = 9.1 Hz, 1H), 7.17 (s, 1H), 6.52 (bs, 2H), 3.89 (s, 3H), 3.83 (s, 3H), 2.40 (s, 3H).

The same procedure has been followed by replacing **47** with 4-(methylthio)phenylboronic acid, **50** (505 mg, 3 mmol) to afford pure 3-bromo-2-methyl-5-(4-(methylthio)phenyl)thiophene, **56** (765 mg, 2.55 mmol, 85%) as a white solid after purification by silica gel column chromatography (eluent: petroleum ether / dichloromethane 8:2).

^{1}H-NMR ($CDCl_3$, 300 MHz): δ (ppm) 7.42 (d, *J* = 8.5 Hz, 2H), 7.24 (d, *J* = 8.5 Hz, 2H), 7.07 (s, 1H), 2.50 (s, 3H), 2.41 (s, 3H).

The same procedure has been followed by replacing **47** with 4-(N,N-dimethylamino)phenylboronic acid, **51** (662 mg, 4.01 mmol) to afford pure 4-(4-bromo-5-methylthiophen-2-yl)-N,N-dimethylaniline, **57** (935 mg, 3.14 mmol, 83%) as a pale yellow crystalline solid after having washed the residue first with NaOH (1 M, 60 mL) and then with ethanol 96% to recover it by filtration.

^{1}H-NMR ($CDCl_3$, 360 MHz): δ (ppm) 7.38 (d, *J* = 8.9 Hz, 2H), 6.93 (s, 1H), 6.70 (d, *J* = 8.9 Hz, 2H), 2.98 (s, 6H), 2.39 (s, 3H).

Last, the same procedure has been followed by replacing **47** with 4-(N,N-diphenylamino)phenylboronic acid, **52** (867 mg, 3 mmol) to afford pure 4-(4-bromo-5-methylthiophen-2-yl)-N,N-diphenylaniline, **58** (1.10 g, 2.61 mmol, 87%) as a light yellow solid after purification by re-precipitation from CH_3OH.

^{1}H-NMR ($CDCl_3$, 300 MHz): δ (ppm) 7.36 (d, *J* = 8.7 Hz, 2H), 7.30 – 7.24 (m, 4H), 7.11 (m, 4H), 7.04 (m, 4H), 7.00 (s, 1H), 2.40 (s, 3H).
HRMS (ESI): calcd. for $C_{23}H_{19}BrNS$ $[M+H]^+$ 420.0416, found $[M+H]^+$ 420.0401.

2-(5-(4-methoxyphenyl)-2-methylthiophen-3-yl)-4,4,5,5-tetramethyl-1,3,2-dioxaborolane, **59**, and 2-(5-(2,4-dimethoxyphenyl)-2-methylthiophen-3-yl)-4,4,5,5-tetramethyl-1,3,2-dioxaborolane, **60**

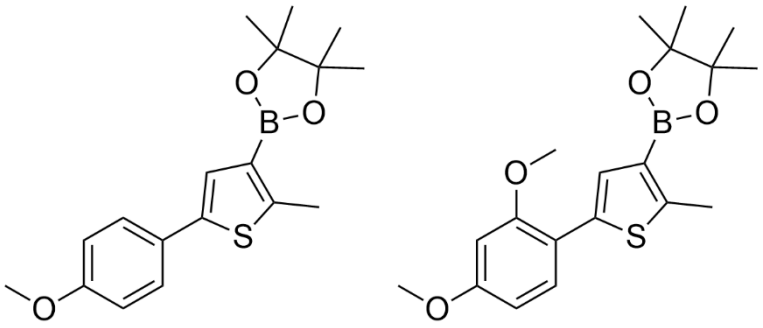

59 **60**

3-bromo-5-(4-methoxyphenyl)-2-methylthiophene, **53** (1.21 g, 4.28 mmol) has been dissolved in distilled dry THF (20 mL). The resulting solution has been cooled to -78°C and *n*-BuLi (2.5 M, 2.20 mL, 5.35 mmol) has been added dropwise and the system has been stirred at -78°C for 40 min. 2-isopropoxy-4,4,5,5-tetramethyl-1,3,2-dioxaborolane (995 mg, 1.10 mL, 5.35 mmol) has been slowly added to the solution and the resulting system has been stirred for 24 h letting the temperature rise up to room temperature under argon. The obtained mixture has been quenched with NH_4Cl 1M solution (30 mL) and the organic layer has been extracted with ethyl acetate. The combined extracts have been washed with brine, dried over anhydrous Na_2SO_4 and filtered. The filtrate has been concentrated under vacuum giving 2-(5-(4-methoxyphenyl)-2-methylthiophen-3-yl)-4,4,5,5-tetramethyl-1,3,2-dioxaborolane, **59** (1.39 g, 4.20 mmol, 98%) as an oil that later crystallized as a white solid that was used without further purification.

^{1}H-NMR ($CDCl_3$, 300 MHz): δ (ppm) 7.49 (d, *J* = 8.9 Hz, 2H), 7.30 (s, 1H), 6.87 (d, *J* = 8.9 Hz, 2H), 3.82 (s, 3H), 2.68 (s, 3H), 1.33 (s, 12H).

The same procedure has been followed by replacing **53** with 3-bromo-5-(2,4-dimethoxyphenyl)-2-methylthiophene, **55** (510 mg, 1.63 mmol) to afford 2-(5-(2,4-dimethoxyphenyl)-2-methylthiophen-3-yl)-4,4,5,5-tetramethyl-1,3,2-dioxaborolane, **60** (465 mg, 1.29 mmol, 79%) as a white solid.

^{1}H-NMR ($CDCl_3$, 300 MHz): δ (ppm) 7.52 (d, J = 9.2 Hz, 1H), 7.42 (s, 1H), 6.62 – 6.40 (m, 2H), 3.88 (s, 3H), 3.83 (s, 3H), 2.68 (s, 3H), 1.32 (s, 12H).

4-(5-(2-methoxyphenyl)-2-methylthiophen-3-yl)-2-phenylthiazole, **61**, 4-(2-methyl-5-(4-(methylthio)phenyl)thiophen-3-yl)-2-phenylthiazole, **62**, N,N-dimethyl-4-(5-methyl-4-(2-phenylthiazol-4-yl)thiophen-2-yl)aniline, **63**, and 4-(5-methyl-4-(2-phenylthiazol-4-yl)thiophen-2-yl)-N,N-diphenylaniline, **64**

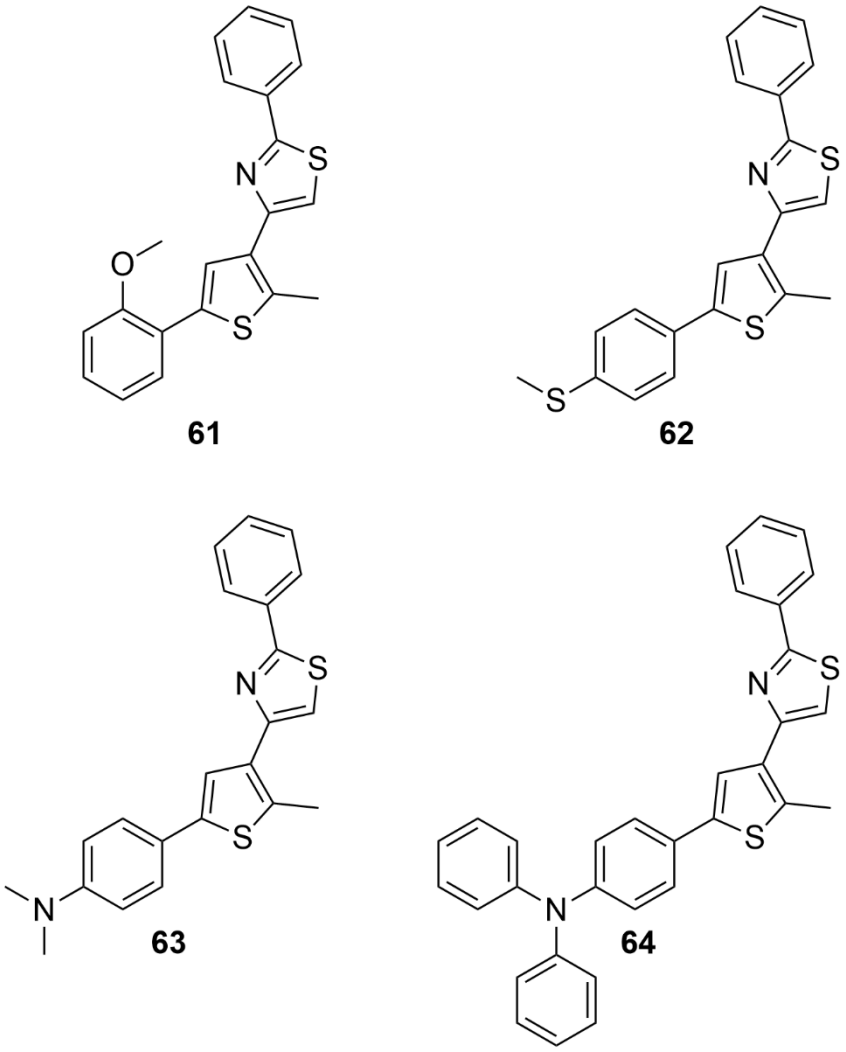

3-bromo-5-(2-methoxyphenyl)-2-methylthiophene, **54** (144 mg, 0.51 mmol), 2-phenyl-4-(4,4,5,5-tetramethyl-1,3,2-dioxaborolan-2-yl)thiazole, **28** (160 mg, 0.56 mmol), CsF (199 mg, 1.31 mmol) and $Pd(PPh_3)_4$ (23 mg, 0.02 mmol) have been partially solubilized in dry 1,4-dioxane (10 mL) and the obtained mixture has been stirred at reflux under argon for 24 h. The reaction has been quenched with water (15 mL) and extracted with chloroform. The combined extracts have been washed with brine, dried over anhydrous Na_2SO_4 and filtered. The filtrate has been concentrated under vacuum giving the crude product as an oil. It has been purified by silica gel column chromatography (eluent: petroleum ether / dichloromethane 6:4) to afford pure 4-(5-(2-methoxyphenyl)-2-methylthiophen-3-yl)-2-phenylthiazole, **61** (140 mg, 0.39 mmol, 76%) as a colorless solid.

^{1}H-NMR ($CDCl_3$, 360 MHz): δ (ppm) 8.05 (m, 2H), 7.79 (s, 1H), 7.69 (dd, *J* = 7.7, 1.7 Hz, 1H), 7.53 – 7.41 (m, 3H), 7.30 – 7.22 (m, 2H), 7.05 – 6.95 (m, 2H), 3.95 (s, 3H), 2.77 (s, 3H).
HRMS (ESI): calcd. for $C_{21}H_{18}NOS_2$ $[M+H]^+$ 364.0824, found $[M+H]^+$ 364.0815.

The same procedure has been followed by replacing **54** with 3-bromo-2-methyl-5-(4-(methylthio)phenyl)thiophene, **56** (150 mg, 0.50 mmol) to afford 4-(2-methyl-5-(4-(methylthio)phenyl)thiophen-3-yl)-2-phenylthiazole, **62** (150 mg, 0.40 mmol, 79%) as a white solid after purification by silica gel column chromatography (eluent: initially petroleum ether / dichloromethane 7:3, then petroleum ether / dichloromethane 6:4).

^{1}H-NMR ($CDCl_3$, 300 MHz): δ (ppm) 8.04 (m, 2H), 7.61 (s, 1H), 7.54 (d, *J* = 8.4 Hz, 2H), 7.47 (m, 4H), 7.28-7.25 (m, 2H), 2.76 (s, 3H), 2.51 (s, 3H).
HRMS (ESI): calcd. for $C_{21}H_{18}NS_3$ $[M+H]^+$ 380.0596, found $[M+H]^+$ 380.0589.

The same procedure has been followed by replacing **54** with 4-(4-bromo-5-methylthiophen-2-yl)-N,N-dimethylaniline, **57** (252 mg, 0.85 mmol) to afford N,N-dimethyl-4-(5-methyl-4-(2-phenylthiazol-4-yl)thiophen-2-yl)aniline, **63** (306 mg, 0.82 mmol, 96%) as a beige crystalline solid after purification by re-precipitation from ethanol 96%.

^{1}H-NMR ($CDCl_3$, 300 MHz): δ (ppm) 8.04 (d, *J* = 8.6 Hz, 2H), 7.72 – 7.38 (m, 6H), 6.74 (d, *J* = 8.6 Hz, 2H), 2.99 (s, 6H), 2.75 (s, 3H).
HRMS (ESI): calcd. for $C_{22}H_{21}N_2S_2^+$ $[M+H]^+$ 377.1141, found $[M+H]^+$ 377.1123.

Last, the same procedure has been followed by replacing **54** with 4-(4-bromo-5-methylthiophen-2-yl)-N,N-diphenylaniline, **58** (210 mg, 0.50 mmol) to afford 4-(5-methyl-4-(2-phenylthiazol-4-yl)thiophen-2-yl)-N,N-diphenylaniline, **64** (197 mg, 0.40 mmol, 79%) as a cream white solid after purification by re-precipitation from CH_3OH.

^{1}H-NMR ($CDCl_3$, 360 MHz): δ (ppm) 8.04 (dd, *J* = 7.6, 2.0 Hz, 2H), 7.54 (s, 1H), 7.50 – 7.43 (m, 5H), 7.33 – 7.21 (m, 4H), 7.17 – 6.99 (m, 9H), 2.75 (s, 3H)
HRMS (ESI): calcd. for $C_{32}H_{25}N_2S_2^+$ $[M+H]^+$ 501.1454, found $[M+H]^+$ 501.1435; calcd. for $C_{32}H_{24}N_2NaS_2^+$ $[M+Na]^+$ 523.1273, found $[M+Na]^+$ 523.1254.

2,4-dimethoxybenzothioamide, **66**

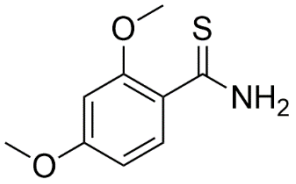

66

1,3-dimethoxybenzene, **65** (2.76 g, 20 mmol) has been dissolved in CH_3SO_3H (20 mL) and the obtained solution has been cooled at 0°C before the addition of KSCN (2.33 g, 24 mmol). It has been stirred at 0°C for 15 min and then at room temperature for 16 h. The reaction mixture has been poured in ice (~200 mL) and 2,4-dimethoxybenzothioamide, **66** (3.91 g, 19.80 mmol, 99%) precipitated as a cream yellow solid to be recovered by filtration that was used without further purification.

^{1}H-NMR ($CDCl_3$, 360 MHz): δ (ppm) 9.09 (s, 1H), 8.71 (d, *J* = 9.0 Hz, 1H), 7.95 (s, 1H), 6.60 (dd, *J* = 9.0, 2.4 Hz, 1H), 6.46 (d, *J* = 2.4 Hz, 1H), 3.95 (s, 3H), 3.87 (s, 3H).

4-(methylthio)benzothioamide, **69**[248]

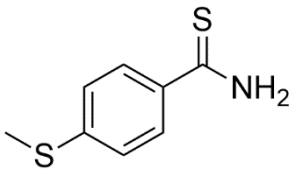

69

4-(methylthio)benzonitrile, **68** (2.98 g, 20 mmol) has been added to a slurry of 67% sodium hydrosulfide hydrate (5.00 g, 60 mmol) and magnesium chloride hexahydrate (4.06 g, 20 mmol) in DMF (20 mL) and the mixture has been stirred at room temperature for 24 h. The resulting slurry has been poured into 100 mL of water, stirred for 20 min in 1M HCl, then filtered and washed with water to give pure 4-(methylthio)benzothioamide, **69** (3.57 g, 19.40 mmol, 97%) as a yellow solid.

^{1}H-NMR ($CDCl_3$, 360 MHz): δ (ppm) 7.83 (d, *J* = 8.6 Hz, 2H), 7.23 (d, *J* = 8.6 Hz, 2H), 2.51 (s, 3H).

2-(2,4-dimethoxyphenyl)-5-methylthiazole, **70**, N,N-dimethyl-4-(5-methylthiazol-2-yl)aniline, **71**, and 2-(4-(methylthio)phenyl)-5-methylthiazole, **72**

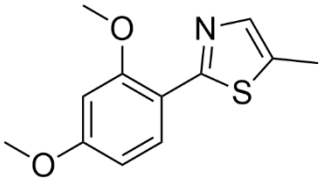

70

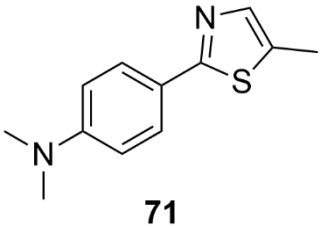

71

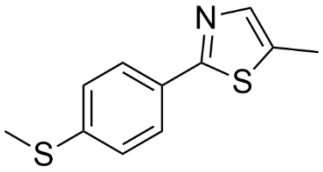

72

2,4-dimethoxybenzothioamide, **66** (945 mg, 4.80 mmol) has been dissolved in ethanol (35 mL) before the addition of 2-bromo-1,1-dimethoxypropane, **33** (1.05 g, 5.75 mmol) and *p*-toluenesulfonic acid monohydrate (50 mg, 0.26 mmol) in water (0.50 mL). The resulting mixture has been stirred at reflux for 24 h. A beige crystalline solid precipitated and it was recovered by filtration. It has been re-dissolved in dichloromethane and washed with a saturated solution of $NaHCO_3$. The organic phase has been dried over anhydrous Na_2SO_4 and filtered. The solvent has been removed under vacuum to afford pure 2-(2,4-dimethoxyphenyl)-5-methylthiazole, **70** (802 mg, 3.41 mmol, 71%) as light beige solid.

^{1}H-NMR ($CDCl_3$, 300 MHz): δ (ppm) 8.35 (d, *J* = 8.8 Hz, 1H), 7.54 (d, *J* = 1.2 Hz, 1H), 6.65 (dd, *J* = 8.8, 2.4 Hz, 1H), 6.55 (d, *J* = 2.4 Hz, 1H), 4.00 (s, 3H), 3.87 (s, 3H), 2.50 (d, *J* = 1.2 Hz, 3H).

The same procedure has been followed by replacing **66** with 4-(dimethylamino)benzothioamide, **67** (720 mg, 4 mmol) to afford N,N-dimethyl-4-(5-methylthiazol-2-yl)aniline, **71** (795 mg, 3.64 mmol, 91%) as a cream white crystalline solid.

^{1}H-NMR ($CDCl_3$, 360 MHz): δ (ppm) 8.09 (d, *J* = 9.2 Hz, 2H), 7.60 (d, *J* = 1.3 Hz, 1H), 6.78 (d, *J* = 9.2 Hz, 2H), 3.11 (s, 6H), 2.50 (d, *J* = 1.3 Hz, 3H).
HRMS (ESI): calcd. for $C_{12}H_{15}N_2S^+$ $[M+H]^+$ 219.0950, found $[M+H]^+$ 219.0949.

Last, the same procedure has been followed by replacing **66** with 4-(methylthio)benzothioamide, **69** (2.57 g, 14 mmol) to afford 2-(4-(methylthio)phenyl)-5-methylthiazole, **72** (1.87 g, 8.40 mmol, 60%) as an off-white crystalline solid after purification by re-precipitation from ethanol 96% and activated carbon filtration.

^{1}H-NMR ($CDCl_3$, 360 MHz): δ (ppm) 8.17 (d, *J* = 8.7 Hz, 2H), 7.81 (d, *J* = 1.2 Hz, 1H), 7.37 (d, *J* = 8.7 Hz, 2H), 2.60 (d, *J* = 1.2 Hz, 3H), 2.54 (s, 3H).
HRMS (ESI): calcd. for $C_{11}H_{12}NS_2^+$ $[M+H]^+$ 222.0406, found $[M+H]^+$ 222.0404.

2-(2,4-dimethoxyphenyl)-5-methyl-4-(4,4,5,5-tetramethyl-1,3,2-dioxaborolan-2-yl)thiazole, **73**, N,N-dimethyl-4-(5-methyl-4-(4,4,5,5-tetramethyl-1,3,2-dioxaborolan-2-yl)thiazol-2-yl)aniline, **74**, 5-methyl-2-(4-(methylthio)phenyl)-4-(4,4,5,5-tetramethyl-1,3,2-dioxaborolan-2-yl)thiazole, **75**

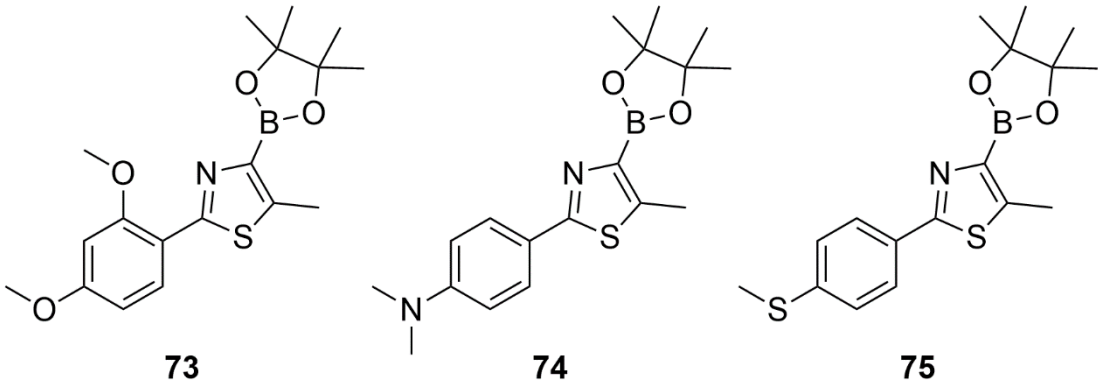

73 **74** **75**

2-(2,4-dimethoxyphenyl)-5-methylthiazole, **70** (470 mg, 2 mmol) has been dissolved in distilled dry THF (20 mL). The resulting solution has been cooled to -78°C and *t*-BuLi (1.9 M, 1.60 mL, 3 mmol) has been added dropwise and the system has been stirred at -78°C for 45 min. 2-isopropoxy-4,4,5,5-tetramethyl-1,3,2-dioxaborolane (558 mg, 0.60 mL, 3 mmol) has been slowly added to the solution and the resulting system has been stirred for 24 h letting the temperature rise up to room temperature under argon. The obtained mixture has been quenched with NH_4Cl 1M solution (25mL) and the organic layer has been extracted with ethyl acetate. The combined extracts have been washed with brine, dried over anhydrous Na_2SO_4 and filtered. The filtrate has been concentrated under vacuum giving 2-(2,4-dimethoxyphenyl)-5-methyl-4-(4,4,5,5-tetramethyl-1,3,2-dioxaborolan-2-yl)thiazole, **73** (580 mg, 1.60 mmol, 80%) as an orange oil that was used without further purification.

^{1}H-NMR ($CDCl_3$, 360 MHz): δ (ppm) 8.38 (d, *J* = 9.0 Hz, 1H), 6.57 (d, *J* = 9.0 Hz, 1H), 6.51 (s, 1H), 3.95 (s, 3H), 3.84 (s, 3H), 2.70 (s, 3H), 1.37 (s, 12H).

The same procedure has been followed by replacing **70** with N,N-dimethyl-4-(5-methylthiazol-2-yl)aniline, **71** (440 mg, 2 mmol) to afford N,N-dimethyl-4-(5-methyl-4-(4,4,5,5-tetramethyl-1,3,2-dioxaborolan-2-yl)thiazol-2-yl)aniline, **74** (461 mg, 1.34 mmol, 67%) as an orange solid that was used without further purification.

^{1}H-NMR ($CDCl_3$, 360 MHz): δ (ppm) 7.82 (d, *J* = 9.0 Hz, 2H), 6.68 (d, *J* = 9.0 Hz, 2H), 3.00 (s, 6H), 2.69 (s, 3H), 1.37 (s, 12H).

Last, the same procedure has been followed by replacing **70** with 2-(4-(methylthio)phenyl)-5-methylthiazole, **72** (442 mg, 2 mmol) to afford 5-methyl-2-(4-(methylthio)phenyl)-4-(4,4,5,5-tetramethyl-1,3,2-dioxaborolan-2-yl)thiazole, **75** (667 mg, 1.92 mmol, 96%) as a yellowish solid that was used without further purification.

^{1}H-NMR ($CDCl_3$, 360 MHz): δ (ppm) 7.86 (d, *J* = 8.5 Hz, 2H), 7.23 (d, *J* = 8.5 Hz, 2H), 2.72 (s, 3H), 2.51 (s, 3H), 1.37 (s, 12H).

4-(4-bromo-5-methylthiazol-2-yl)-N,N-diphenylaniline, **76**

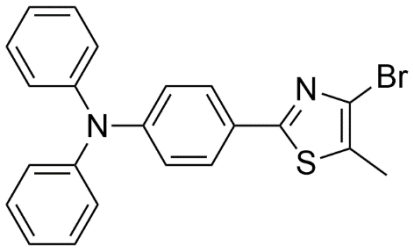

76

4-(N,N-diphenylamino)phenylboronic acid, **52** (292 mg, 1.01 mmol), 2,4-dibromo-5-methylthiazole (259 mg, 1.01 mmol), xantphos (15 mg, 0.03 mmol), $Pd(OAc)_2$ (7 mg, 0.03 mmol) and K_3PO_4 (658 mg, 3.1 mmol) have been partially dissolved in distilled dry THF (10 mL). The obtained mixture has been stirred at reflux under argon for 24 h. Once cooled down to room temperature, it has been diluted with chloroform (10 mL) and filtered on a Celite pad. Multiple washings with chloroform have been carried out and the obtained filtrate has been concentrated under vacuum. The obtained crude product has been purified by silica gel column chromatography (eluent: petroleum ether / dichloromethane 6:4) to afford 4-(4-bromo-5-methylthiazol-2-yl)-N,N-diphenylaniline, **76** (300 mg, 0.72 mmol, 71%) as a pale yellow crystalline solid.

^{1}H-NMR ($CDCl_3$, 300 MHz): δ (ppm) 7.70 (d, *J* = 8.8 Hz, 2H), 7.32 – 7.25 (m, 4H), 7.16 – 7.06 (m, 6H), 7.04 (d, *J* = 8.8 Hz, 2H), 2.41 (s, 3H).
HRMS (ESI): calcd. for $C_{22}H_{18}BrN_2S^+$ $[M+H]^+$ 421.0368, found $[M+H]^+$ 421.0360; calcd. for $C_{22}H_{17}BrN_2NaS^+$ $[M+Na]^+$ 443.0188, found $[M+Na]^+$ 443.0178.

4-(5-methyl-2'-phenyl-[4,4'-bithiazol]-2-yl)-N,N-diphenylaniline, **77**, and 4-(5-(4-methoxyphenyl)-2-methylthiophen-3-yl)-2-phenylthiazole, **78**

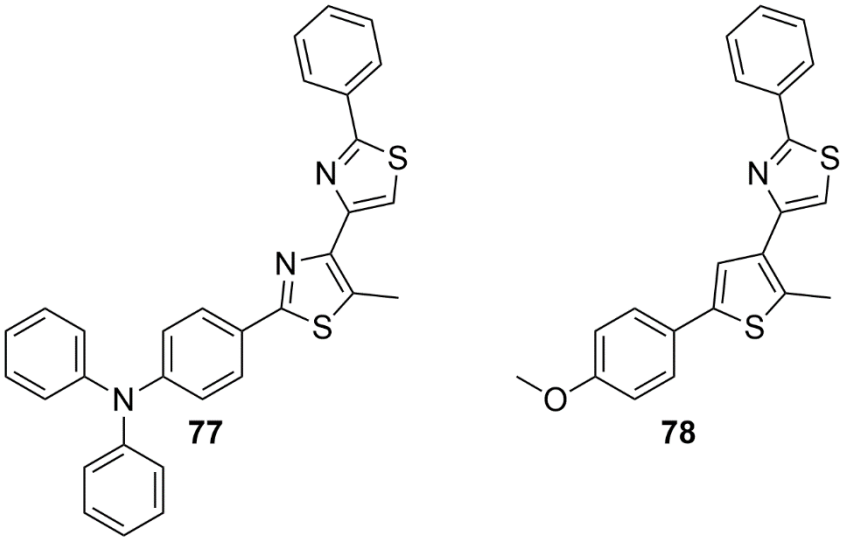

4-(4-bromo-5-methylthiazol-2-yl)-N,N-diphenylaniline, **76** (176 mg, 0.42 mmol), 2-phenyl-4-(4,4,5,5-tetramethyl-1,3,2-dioxaborolan-2-yl)thiazole, **28** (138 mg, 0.48 mmol), CsF (170 mg, 1.12 mmol) and $Pd(PPh_3)_4$ (27 mg, 0.02 mmol) have been partially solubilized in dry 1,4-dioxane (10 mL) and the obtained light yellow mixture has been stirred at reflux under argon for 24 h. The reaction has been quenched with water (20 mL) and extracted with chloroform. The combined extracts have been washed with brine, dried over anhydrous Na_2SO_4 and filtered. The filtrate has been concentrated under vacuum giving the crude product as a greenish solid. It has been purified by silica gel column chromatography (eluent: dichloromethane / petroleum ether 1:1) to afford pure 4-(5-methyl-2'-phenyl-[4,4'-bithiazol]-2-yl)-N,N-diphenylaniline, **77** (166 mg, 0.33 mmol, 79%) as a pale green solid.

^{1}H-NMR ($CDCl_3$, 250 MHz): δ (ppm) 8.04 (m, 2H), 7.88 (s, 1H), 7.81 (d, *J* = 8.7 Hz, 2H), 7.46 (m, 3H), 7.32 – 7.25 (m, 4H), 7.19 – 7.05 (m, 8H), 2.97 (s, 3H).
HRMS (ESI): calcd. for $C_{31}H_{24}N_3S_2^+$ $[M+H]^+$ 502.1406, found $[M+H]^+$ 502.1400; calcd. for $C_{31}H_{23}N_3NaS_2^+$ $[M+Na]^+$ 524.1226, found $[M+Na]^+$ 524.1219.

The same procedure has been followed by replacing **76** with 3-bromo-5-(4-methoxyphenyl)-2-methylthiophene, **53** (566 mg, 2 mmol) to afford 4-(5-(4-methoxyphenyl)-2-methylthiophen-3-yl)-2-phenylthiazole, **78** (538 mg, 1.48 mmol, 74%) as white crystalline solid after purification by silica gel column chromatography (eluent: initially petroleum ether / dichloromethane 7:3, then petroleum ether / dichloromethane 6:4).

^{1}H-NMR ($CDCl_3$, 300 MHz): δ (ppm) 8.03 (m, 2H), 7.54 (d, *J* = 8.8 Hz, 2H), 7.51 (s, 1H), 7.47 – 7.42 (m, 3H), 7.25 (s, 1H), 6.91 (d, *J* = 8.8 Hz, 2H), 3.83 (s, 3H), 2.75 (s, 3H).
HRMS (ESI): calcd. for $C_{21}H_{18}NOS_2^+$ $[M+H]^+$ 364.0824, found $[M+H]^+$ 364.0820.

5.3.6 Photochromes, Chapter 4

Terthiazole **38**[212]

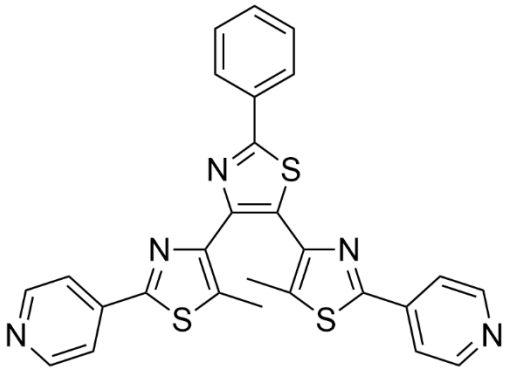

38

2-(pyridin-4-yl)-4-(4,4,5,5-tetramethyl-1,3,2-dioxaborolan-2-yl)-5-methylthiazole, **36** (377 mg, 1.25 mmol), 2-phenyl-4,5-dibromothiazole, **37** (160 mg, 0.50 mmol), CsF (395 mg, 2.60 mmol) and $Pd(PPh_3)_4$ (57 mg, 0.05 mmol) have been partially solubilized in dry 1,4-dioxane (15 mL) and the obtained mixture has been stirred at reflux under argon for 24 h. The reaction has been quenched with water (20 mL) and extracted with chloroform (30 mL). The combined organic phase has been washed with brine, dried over anhydrous Na_2SO_4 and filtered. The solvents have been removed under vacuum and the obtained residue has been purified by silica gel column chromatography (eluent: dichloromethane / ethanol 95:5) to give a brown solid that has been discolored by activated carbon filtration to afford terthiazole **38** (240 mg, 0.47 mmol, 94%) as a microcrystalline off-white powder.

^{1}H-NMR ($CDCl_3$, 400 MHz): δ (ppm) 8.69 (d, *J* = 5.0 Hz, 2H), 8.57 (d, *J* = 5.0 Hz, 2H), 8.05 (d, *J* = 5.0 Hz, 2H), 7.58 (d, *J* = 5.0 Hz, 2H), 7.55 (d, *J* = 5.0 Hz, 2H), 7.51 (m, 3H), 2.71 (s, 3H), 2.21 (s, 3H).
^{13}C-NMR ($CDCl_3$, 91 MHz): δ (ppm) 167.6, 160.9, 160.3, 150.2, 150.0, 147.6, 147.0, 144.8, 140.6, 140.4, 135.8, 134.9, 133.2, 130.5, 129.1, 128.4, 126.6, 120.2, 120.1, 13.1, 12.5.
HRMS (ESI): calcd. for $C_{27}H_{20}N_5S_3^+$ $[M+H]^+$ 510.0875, found $[M+H]^+$ 510.0865.

Terthiazole **Red1^{2+}**[212]

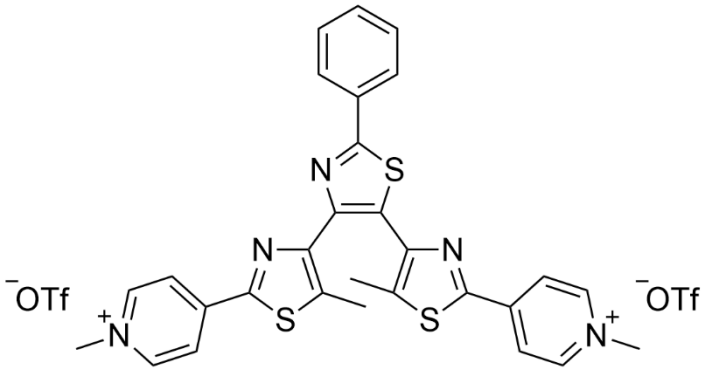

Red1^{2+}

Step 1: an excess of iodomethane (570 mg, 0.250 mL, 4 mmol) has been added to a solution of **38** (102 mg, 0.20 mmol) in a mixture of dichloromethane (10 mL) and acetonitrile (5 mL). It has been stirred at ~45°C overnight. Once cooled to room temperature, the orange solid has been recovered by suction, washed with dichloromethane and dried under vacuum to afford **Red1^{2+}2I^{-}** (125 mg, 0.17 mmol, 85%). *Step 2:* **Red1^{2+}2I^{-}** (88 mg, 0.11 mmol) has been dissolved in a mixture of methanol (25 mL) and acetonitrile (10 mL). AgOTf (57 mg, 0.22 mmol in 5 mL of methanol) has been added to the resulting solution and stirring has been continued for ~30 min at room temperature. The solid precipitate has been filtered off and washed with methanol. The yellow filtrate has been evaporated to dryness and the solid residue has been re-dissolved in dichloromethane (10-15 mL) and filtrated again to get rid of some suspension. The yellow filtrate has been concentrated to a volume of 3-5 mL before adding slowly some diethyl ether (~20 mL). After one night, the bright yellow crystalline powder has been collected by suction, washed with diethyl ether and dried under vacuum to afford **Red1^{2+}** (90 mg, 0.11 mmol, 98%).

^{1}H-NMR ($CDCl_3$, 360 MHz): δ (ppm) 8.68 (m, 4H), 8.36 (d, *J* = 6.8 Hz, 2H), 8.06 (m, 2H), 7.79 (d, *J* = 6.4 Hz, 2H), 4.38 (s, 3H), 4.31 (s, 3H), 3.05 (s, 3H), 2.52 (s, 3H).
^{13}C-NMR (CD_3CN, 101 MHz): δ (ppm) 167.8, 156.7, 156.1, 148.6, 147.4, 146.9, 146.5, 146.0, 145.8, 142.0, 141.1, 132.9, 131.0, 129.4, 128.2, 126.5, 123.3, 123.0, 47.9, 47.8, 12.9, 12.1.
HRMS (ESI): calcd. for $C_{29}H_{25}N_5S_3^{2+}$ $[M/2]^{2+}$ 269.5631, found $[M/2]^{2+}$ 269.5639.

Terthiazole **42**[212]

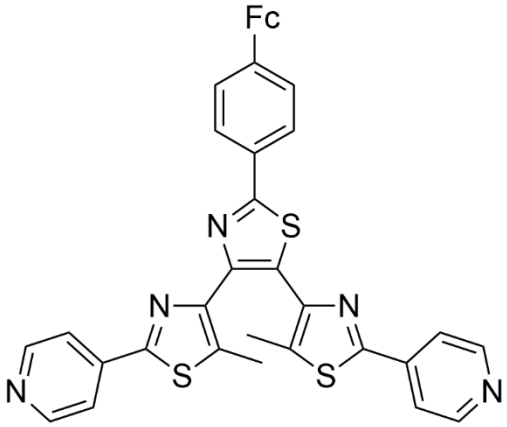

42

The same procedure used for the synthesis of terthiazole **38** has been followed by replacing **37** with 2-(4-ferrocenylphenyl)-4,5-dibromothiazole, **40** (202 mg, 0.40 mmol) to obtain terthiazole **42** (250 mg, 0.36 mmol, 90%) as a red-brown microcrystalline solid.

^{1}H-NMR ($CDCl_3$, 300 MHz): δ (ppm) 8.70 (d, *J* = 5.7 Hz, 2H), 8.58 (d, *J* = 5.3 Hz, 2H), 7.97 (d, *J* = 8.2 Hz, 2H), 7.79 (d, *J* = 5.3 Hz, 2H), 7.57 (m, 4H), 4.73 (s, 2H), 4.40 (s, 2H), 4.07 (s, 5H), 2.71 (s, 3H), 2.20 (s, 3H).
^{13}C-NMR ($CDCl_3$, 91 MHz): δ (ppm) 167.5, 161.1, 160.5, 150.6, 150.4, 147.7, 147.1, 144.9, 142.5, 140.2, 140.1, 135.5, 134.6, 130.7, 128.0, 126.6, 126.3, 120.1, 119.9, 83.9, 69.8, 69.6, 66.7, 13.2, 12.6.
HRMS (ESI): calcd. for $C_{37}H_{27}FeN_5S_3$ $[M]^+$ 693.0773, found $[M]^+$ 693.0767.

Terthiazole **Red2^{2+}**[212]

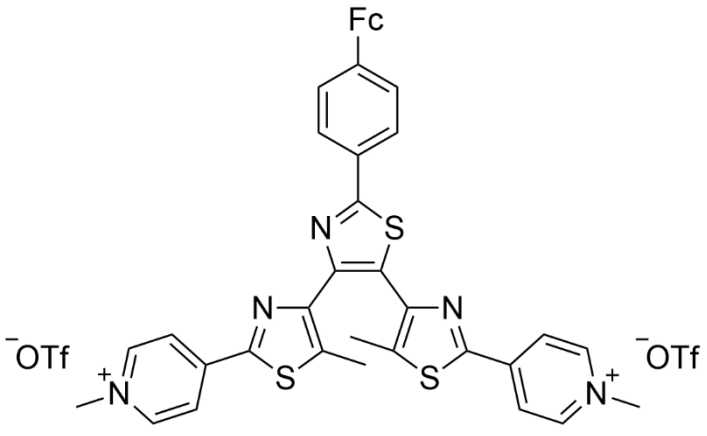

Red2^{2+}

Step 1: terthiazole **42** (140 mg, 0.20 mmol) has been dissolved in a mixture of dichloromethane (10 mL) and acetonitrile (5 mL). Iodomethane (454 mg, 0.200 mL, 3.2 mmol) has been added to the resulting red solution before stirring it at 45°C for ~20 h. The mixture has been concentrated under reduced pressure and the residue has been dispersed in methanol (10 mL) and stirred for ~30 min. The resulting red solid has been collected by suction, washed with methanol (5 mL) and dried under vacuum to give **Red2^{2+}2I^{-}** (140 mg, 0.14 mmol, 71%). *Step 2:* **Red2^{2+}2I^{-}** (135 mg, 0.138 mmol) has been largely solubilized a mixture of dichloromethane (10 mL) and methanol (25 mL). AgOTf (71 mg, 0.276 mmol in 5 mL of methanol) has been added to this solution and the stirring has been continued for 2-3 h at room temperature. The solid precipitate has been filtered off and washed with methanol. The orange-red filtrate has been evaporated to dryness and the residue has been taken in THF (20 mL). After stirring for ~30 min at room temperature, **Red2^{2+}** (117 mg, 0.114 mmol, 83%) has been obtained as a red microcrystalline solid that has been collected by suction, washed with THF and dried under vacuum.

^{1}H-NMR (DMSO-d_6, 360 MHz): δ (ppm) 9.03 (d, *J* = 6.8 Hz, 2H), 8.94 (d, *J* = 6.4 Hz, 2H), 8.52 (d, *J* = 6.4 Hz, 2H), 8.22 (d, *J* = 6.8 Hz, 2H), 8.00 (d, *J* = 8.2 Hz, 2H), 7.74 (d, *J* = 8.2 Hz, 2H), 4.93 (s, 2H), 4.47 (s, 2H), 4.36 (s, 3H), 4.29 (s, 3H), 4.07 (s, 5H), 2.84 (s, 3H), 2.24 (s, 3H).
^{13}C-NMR (DMSO-d_6, 101 MHz): δ (ppm) 167.49, 157.36, 156.75, 148.28, 147.29, 146.93, 146.85, 146.17, 145.81, 145.77, 143.33, 141.47, 140.58, 130.09, 127.89, 126.96, 126.87, 123.46, 123.04, 122.75, 119.55, 83.57, 70.17, 70.07, 67.12, 48.06, 47.98, 13.69, 12.96.
HRMS (ESI): calcd. for $C_{39}H_{33}FeN_5S_3$ $[M/2]^{2+}$ 361.5619, found $[M/2]^{2+}$ 361.5590.

Terthiazole **44**

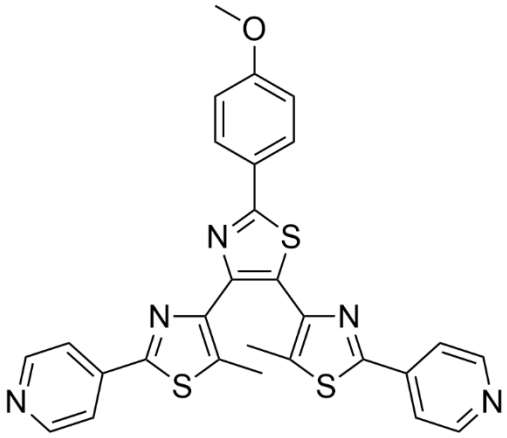

44

The same procedure used for the synthesis of terthiazole **38** has been followed by replacing **37** with 2-(4-methoxyphenyl)-4-bromo-5-iodothiazole, **43** (198 mg, 0.50 mmol) to obtain terthiazole **44** (219 mg, 0.405 mmol, 81%) as an off-white crystalline solid.

^{1}H-NMR ($CDCl_3$, 300 MHz): δ (ppm) 8.70 (d, *J* = 6.2 Hz, 2H), 8.59 (d, *J* = 6.3 Hz, 2H), 7.99 (d, *J* = 8.8 Hz, 2H), 7.81 (d, *J* = 6.3 Hz, 2H), 7.60 (d, *J* = 6.3 Hz, 2H), 7.00 (d, *J* = 8.9 Hz, 2H), 3.89 (s, 3H), 2.69 (s, 3H), 2.20 (s, 3H).

Terthiazole **Red3^{2+}**

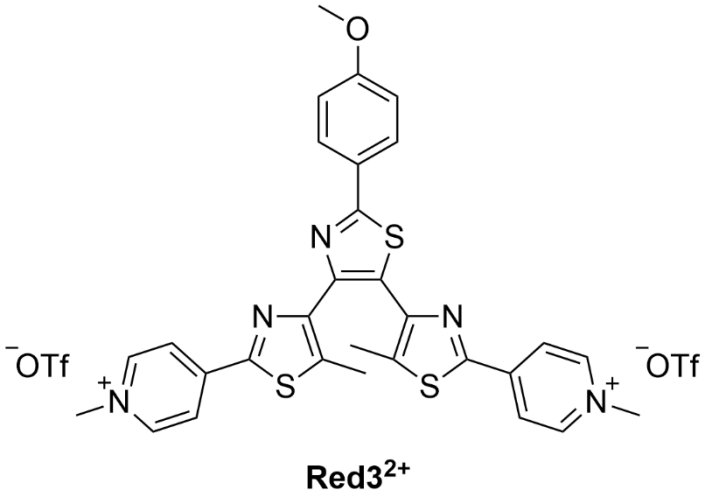

Red3^{2+}

Step 1: terthiazole **44** (120 mg, 0.22 mmol) has been dissolved in dichloromethane (10 mL). Iodomethane (341 mg, 0.150 mL, 2.4 mmol) has been added to the resulting solution before stirring it at 45°C for 24 h. Once cooled to room temperature, **Red3^{2+}2I^{-}** (143 mg, 0.17 mmol, 78%) has been recovered by filtration as a yellow solid. *Step 2:* **Red3^{2+}2I^{-}** (142 mg, 0.17 mmol) has been solubilized a mixture of methanol (10 mL) and acetonitrile (10 mL). AgOTf (88 mg, 0.34 mmol in 5 mL of methanol) has been added to this solution and the stirring has been continued for 1 h at room temperature. The solid precipitate has been filtered off and washed with methanol and acetonitrile. The yellow filtrate has been evaporated to dryness and the residue has been taken in methanol (5 mL). After stirring for ~15 min at room temperature, **Red3^{2+}** (75 mg, 0.09 mmol, 50%) has been obtained as a yellow solid that has been collected by filtration and dried under vacuum.

^{1}H-NMR ($CDCl_3$, 250 MHz): δ (ppm) 8.70 (m, 4H), 8.35 (d, *J* = 6.2 Hz, 2H), 7.98 (d, *J* = 8.7 Hz, 2H), 7.80 (d, *J* = 6.1 Hz, 2H), 7.02 (d, *J* = 8.8 Hz, 2H), 4.38 (s, 3H), 4.30 (s, 3H), 3.90 (s, 3H), 3.01 (s, 3H), 2.48 (s, 3H).

Photochrome **46**

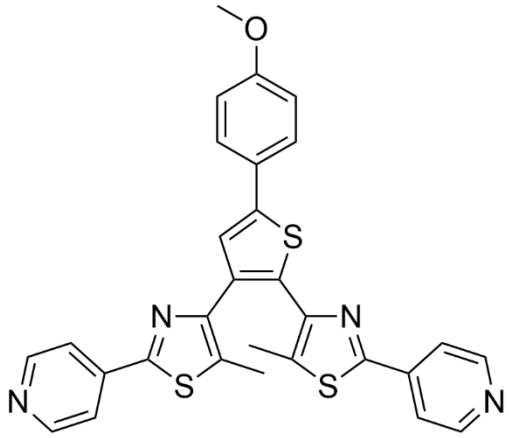

46

The same procedure used for the synthesis of terthiazole **38** has been followed by replacing **37** with 2,3-dibromo-5-(4-methoxyphenyl)thiophene, **45** (70 mg, 0.20 mmol) to obtain terthiazole **46** (82 mg, 0.15 mmol, 76%) as light greenish solid.

^{1}H-NMR ($CDCl_3$, 300 MHz): δ (ppm) 8.68 (d, *J* = 5.8 Hz, 4H), 7.81 (m, 4H), 7.63 (d, *J* = 8.8 Hz, 2H), 7.42 (s, 1H), 6.97 (d, *J* = 8.8 Hz, 2H), 3.87 (s, 3H), 2.17 (s, 3H), 2.14 (s, 3H).

Photochrome **Red4^{2+}**

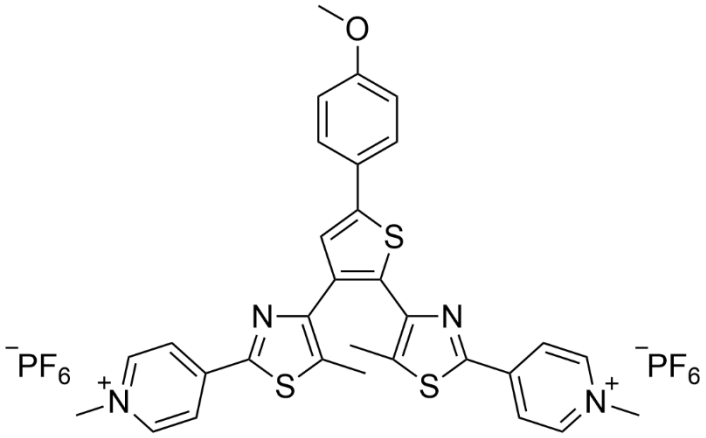

Red4^{2+}

Step 1: terthiazole **46** (80 mg, 0.15 mmol) has been dissolved in dichloromethane (10 mL). Iodomethane (341 mg, 0.150 mL, 2.4 mmol) has been added to the resulting solution before stirring it at 45°C for 24 h. The mixture has been concentrated under reduced pressure and the residue has been partially dissolved in methanol (3-4 mL) and water (20 mL). It has been filtered and methanol has been removed under reduced pressure. *Step 2:* KPF_6 (440 mg, 2.4 mmol in 5 mL of water) has been added to the orange solution to induce the immediate precipitation of an orange solid. The mixture has been stirred for 30 min at room temperature. The solid precipitate has been recovered by filtration and re-dissolved in acetone. The solution has been concentrated and diethyl ether has been slowly added. The solution has been kept in the fridge until the observation of the precipitation of an orange solid. After stirring for ~30 min at room temperature, **Red4^{2+}** (106 mg, 0.12 mmol, 82%) has been obtained as a yellow solid that has been collected by filtration and dried under vacuum.

^{1}H-NMR (DMSO-d_6, 300 MHz): δ (ppm) 9.06 – 8.95 (m, 4H), 8.52 – 8.39 (m, 4H), 7.74 (d, *J* = 8.8 Hz, 2H), 7.72 (s, 1H), 7.06 (d, *J* = 8.9 Hz, 2H), 4.35 (s, 3H), 4.32 (s, 3H), 3.83 (s, 3H), 2.33 (s, 3H), 2.13 (s, 3H).

Photochromes **Ox1** and **Ox3**

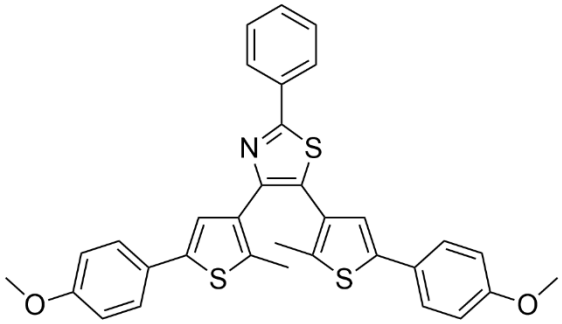

Ox1

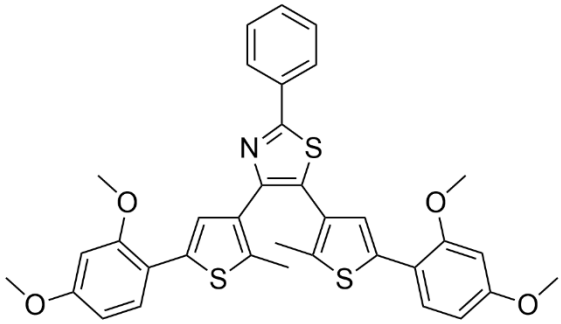

Ox3

2-(5-(4-methoxyphenyl)-2-methylthiophen-3-yl)-4,4,5,5-tetramethyl-1,3,2-dioxaborolane, **59** (380 mg, 1.15 mmol), 2-phenyl-4,5-dibromothiazole, **37** (160 mg, 0.50 mmol), CsF (380 mg, 2.50 mmol) and $Pd(PPh_3)_4$ (52 mg, 0.045 mmol) have been partially solubilized in dry 1,4-dioxane (15 mL) and the obtained mixture has been stirred at reflux under argon for 24 h. The reaction has been quenched with water (20 mL) and extracted with chloroform. The combined organic phase has been washed with brine, dried over anhydrous Na_2SO_4 and filtered. The solvents have been removed under vacuum and the obtained residue has been purified by silica gel column chromatography (eluent: initially dichloromethane / petroleum ether 6:4, then dichloromethane / petroleum ether 8:2) to give photochrome Ox1 (108 mg, 0.19 mmol, 38%) as a light blue solid.

^{1}H-NMR ($CDCl_3$, 300 MHz): δ (ppm) 8.07 – 8.00 (m, 2H), 7.50 – 7.38 (m, 7H), 7.11 (s, 1H), 7.02 (s, 1H), 6.93 – 6.83 (m, 4H), 3.83 (s, 3H), 3.81 (s, 3H), 2.33 (s, 3H), 2.20 (s, 3H).
^{13}C-NMR ($CDCl_3$, 91 MHz): δ (ppm) 165.66, 159.29, 159.01, 148.57, 140.67, 139.96, 136.76, 136.39, 133.75, 133.00, 130.11, 129.15, 129.04, 128.07, 127.41, 126.88, 126.81, 126.48, 124.22, 123.80, 114.41, 114.31, 114.31, 55.45, 14.69, 14.35.
HRMS (ESI): calcd. for $C_{33}H_{28}NO_2S_3^+$ $[M+H]^+$ 566.1277, found $[M+H]^+$ 566.1258.

The same procedure has been followed by replacing **59** with 2-(5-(2,4-dimethoxyphenyl)-2-methylthiophen-3-yl)-4,4,5,5-tetramethyl-1,3,2-dioxaborolane, **60** (432 mg, 1.2 mmol) to obtain photochrome **Ox3** (178 mg, 0.285 mmol, 57%) as an almost colorless solid.

^{1}H-NMR ($CDCl_3$, 360 MHz): δ (ppm) 8.08 – 8.00 (m, 2H), 7.49 – 7.40 (m, 5H), 7.29 (s, 1H), 7.22 (s, 1H), 6.54 – 6.43 (m, 4H), 3.85 (s, 3H), 3.83 (s, 3H), 3.81 (s, 3H), 3.805 (s, 3H), 2.37 (s, 3H), 2.20 (s, 3H).
^{13}C-NMR ($CDCl_3$, 91 MHz): δ (ppm) 165.21, 160.18, 159.86, 156.80, 156.77, 148.79, 136.87, 136.55, 135.98, 135.26, 133.93, 131.93, 129.91, 128.97, 128.89, 128.79, 128.23, 128.17, 126.71, 126.43, 126.15, 116.79, 116.23, 105.05, 99.07, 55.50, 14.50, 14.11.
HRMS (ESI): calcd. for $C_{35}H_{32}NO_4S_3^+$ $[M+H]^+$ 626.1488, found $[M+H]^+$ 626.1460.

Photochromes **Ox2**, **Ox4**, **Ox5** and **Ox6**

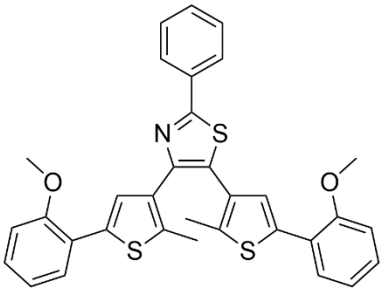

Ox2

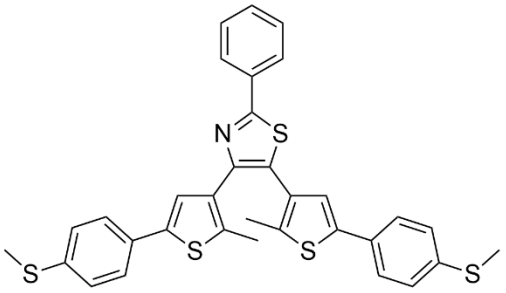

Ox4

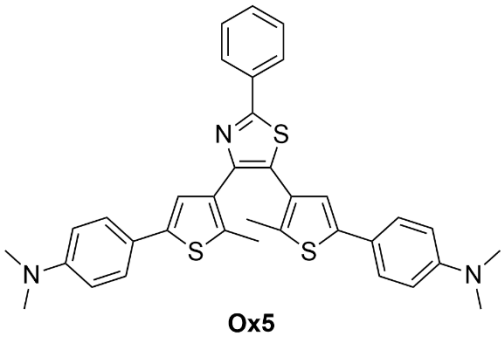

Ox5

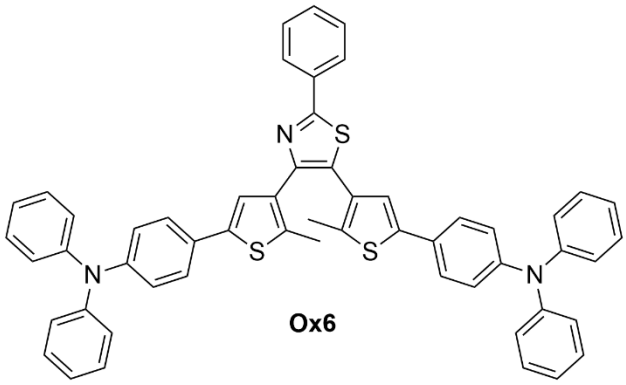

Ox6

4-(5-(2-methoxyphenyl)-2-methylthiophen-3-yl)-2-phenylthiazole, **61** (92 mg, 0.25 mmol), 3-bromo-5-(2-methoxyphenyl)-2-methylthiophene, **54** (72 mg, 0.25 mmol), $P(tBu)_2MeHBF_4$ (12 mg, 0.05 mmol), Cs_2CO_3 (166 mg, 0.51 mmol), pivalic acid (10 mg, 0.10 mmol) and $Pd(OAc)_2$ (6 mg, 0.03 mmol) have been partially solubilized in dry xylenes (3 mL) and the obtained mixture has been stirred at reflux for 24 hours. The reaction has been diluted with chloroform and filtered through a Celite pad. The obtained solution has been washed with water, dried over anhydrous Na_2SO_4 and filtered. The filtrate has been concentrated under vacuum and silica gel column chromatography (eluent: dichloromethane / petroleum ether 1:1) of the residue afforded pure photochrome **Ox2** (107 mg, 0.19 mmol, 76%) as a pale green solid thanks to a re-precipitation from ethanol.

^{1}H-NMR ($CDCl_3$, 360 MHz): δ (ppm) 8.09 – 8.02 (m, 2H), 7.56 (d, *J* = 1.8 Hz, 1H), 7.53 (d, *J* = 1.6 Hz, 1H), 7.48 – 7.43 (m, 4H), 7.42 (s, 1H), 7.35 (s, 1H), 7.24 – 7.16 (m, 2H), 7.03 – 6.88 (m, 4H), 3.89 (s, 3H), 3.84 (s, 3H), 2.38 (s, 3H), 2.22 (s, 3H).
^{13}C-NMR ($CDCl_3$, 91 MHz): δ (ppm) 165.39, 155.66, 148.77, 138.12, 137.79, 135.90, 135.18, 133.91, 132.01, 129.98, 129.01, 128.39, 128.25, 128.18, 128.10, 128.02, 127.93, 127.86, 127.30, 126.46, 123.51, 123.00, 121.04, 120.94, 111.70, 55.56, 55.53, 14.55, 14.17.
HRMS (ESI): calcd. for $C_{33}H_{28}NOS_3^+$ $[M+H]^+$ 566.1277, found $[M+H]^+$ 566.1248.

The same procedure has been followed by replacing **61** and **54** with 4-(2-methyl-5-(4-(methylthio)phenyl)thiophen-3-yl)-2-phenylthiazole, **62** (132 mg, 0.35 mmol) and 3-bromo-2-methyl-5-(4-(methylthio)phenyl)thiophene, **56** (105 mg, 0.35 mmol), respectively, to obtain photochrome **Ox4** (130 mg, 0.22 mmol, 62%) as cream white solid.

^{1}H-NMR ($CDCl_3$, 360 MHz): δ (ppm) 8.14 – 8.06 (m, 2H), 7.49 (m, 3H), 7.45 – 7.40 (m, 4H), 7.25 – 7.18 (m, 5H), 7.09 (s, 1H), 2.50 (s, 3H), 2.49 (s, 3H), 2.32 (s, 3H), 2.21 (s, 3H).
^{13}C-NMR ($CDCl_3$ + drops of methanol-d_4, 91 MHz): δ (ppm) 166.04, 148.30, 140.25, 139.57, 137.87, 137.51, 137.30, 137.09, 133.44, 132.92, 131.29, 130.74, 130.18, 129.06, 129.02, 128.01, 126.97, 126.91, 126.41, 125.79, 125.75, 124.75, 124.41, 15.87, 15.77, 14.55, 14.27.
HRMS (ESI): calcd. for $C_{33}H_{28}NS_5^+$ $[M+H]^+$ 598.0820, found $[M+H]^+$ 598.0778.

The same procedure has been followed by replacing **61** and **54** with N,N-dimethyl-4-(5-methyl-4-(2-phenylthiazol-4-yl)thiophen-2-yl)aniline, **63** (150 mg, 0.40 mmol) and 4-(4-bromo-5-methylthiophen-2-yl)-N,N-dimethylaniline, **57** (127 mg, 0.43 mmol), respectively, to obtain photochrome **Ox5** (146 mg, 0.25 mmol, 62%) as pale cream white solid.

^{1}H-NMR ($CDCl_3$, 360 MHz): δ (ppm) 8.06 – 8.00 (m, 2H), 7.51 – 7.36 (m, 7H), 7.08 (s, 1H), 6.99 (s, 1H), 6.70 (m, 4H), 2.98 (s, 6H), 2.96 (s, 6H), 2.30 (s, 3H), 2.16 (s, 3H).
^{13}C-NMR ($CDCl_3$, 91 MHz): δ (ppm) 165.40, 150.05, 149.84, 148.67, 141.50, 140.78, 135.62, 135.23, 133.87, 132.92, 129.99, 129.01, 128.29, 126.55, 126.49, 123.23, 123.01, 122.62, 122.56, 112.72, 112.66, 40.65, 40.58, 14.66, 14.31.
HRMS (ESI): calcd. for $C_{35}H_{34}N_3S_3^+$ $[M+H]^+$ 592.1909, found $[M+H]^+$ 592.1885.

The same procedure has been followed by replacing **61** and **54** with 4-(5-methyl-4-(2-phenylthiazol-4-yl)thiophen-2-yl)-N,N-diphenylaniline, **64** (150 mg, 0.30 mmol) and 4-(4-bromo-5-methylthiophen-2-yl)-N,N-diphenylaniline, **58** (126 mg, 0.30 mmol), respectively, to obtain photochrome **Ox6** (164 mg, 0.195 mmol, 65%) as greenish solid.

^{1}H-NMR ($CDCl_3$, 300 MHz): δ (ppm) 8.02 (m, 2H), 7.54 – 7.41 (m, 3H), 7.41 – 7.31 (m, 5H), 7.30 – 7.20 (m, 7H), 7.12 (m, 6H), 7.09 (m, 3H), 7.07 – 6.99 (m, 9H), 2.34 (s, 3H), 2.19 (s, 3H).
^{13}C-NMR ($CDCl_3$, 91 MHz): δ (ppm) 165.73, 148.54, 147.66, 147.57, 147.39, 147.00, 140.70, 139.96, 137.03, 136.58, 133.76, 133.11, 130.14, 129.44, 129.40, 129.25, 129.07, 128.76, 128.09, 128.05, 126.51, 126.43, 126.39, 124.62, 124.50, 124.40, 124.02, 123.96, 123.80, 123.23, 123.07, 14.79, 14.44.

Terthiazoles **Ox7, Ox8** and **Ox9**

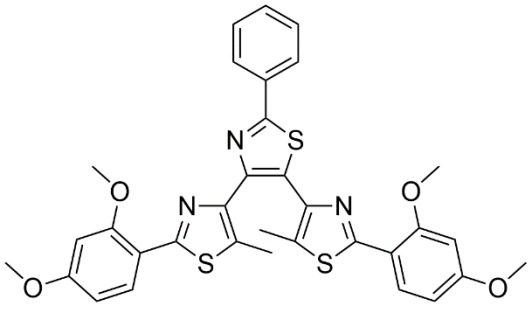

Ox7

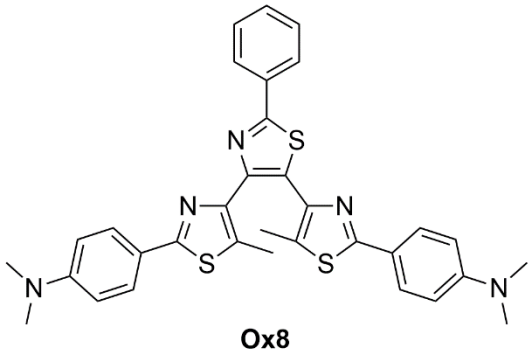

Ox8

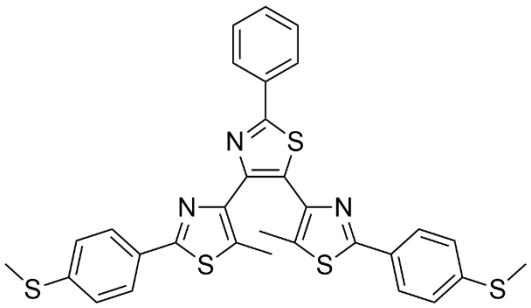

Ox9

2-(2,4-dimethoxyphenyl)-5-methyl-4-(4,4,5,5-tetramethyl-1,3,2-dioxaborolan-2-yl)thiazole, **73** (470 mg, 1.30 mmol), 2-phenyl-4,5-dibromothiazole, **37** (191 mg, 0.60 mmol), CsF (497 mg, 3.27 mmol) and $Pd(PPh_3)_4$ (46 mg, 0.04 mmol) have been partially solubilized in dry 1,4-dioxane (20 mL) and the obtained mixture has been stirred at reflux under argon for 24 h. The reaction has been quenched with water (20 mL) and extracted with chloroform. The combined organic phase has been washed with brine, dried over anhydrous Na_2SO_4 and filtered. The solvents have been removed under vacuum and the obtained residue has been purified by silica gel column chromatography (eluent: initially dichloromethane, then dichloromethane / diethyl ether 95:5). The fractions have been evaporated to dryness and the obtained solid has been re-dissolved in a mixture of hexane and diethyl ether. Removal of the solvent under reduced pressure allowed to obtain terthiazole **Ox7** (232 mg, 0.37 mmol, 61%) as a greenish solid.

^{1}H-NMR ($CDCl_3$, 300 MHz): δ (ppm) 8.34 (d, *J* = 8.7 Hz, 1H), 8.17 (d, *J* = 8.7 Hz, 1H), 8.11 – 8.04 (m, 2H), 7.49 – 7.41 (m, 3H), 6.65 – 6.44 (m, 4H), 3.99 (s, 3H), 3.97 (s, 3H), 3.87 (s, 3H), 3.83 (s, 3H), 2.34 (s, 3H), 1.98 (s, 3H).
^{13}C-NMR ($CDCl_3$, 91 MHz): δ (ppm) 166.95, 161.91, 161.68, 158.84, 158.65, 157.55, 157.44, 147.79, 144.53, 141.65, 133.93, 131.96, 131.35, 130.38, 130.02, 129.68, 129.51, 128.91, 126.72, 116.11, 115.90, 105.71, 105.51, 98.41, 98.28, 55.63, 55.59, 55.55, 12.11, 11.84.
HRMS (ESI): calcd. for $C_{33}H_{30}N_3O_4S_3^+$ $[M+H]^+$ 628.1393, found $[M+H]^+$ 628.1362.

The same procedure has been followed by replacing **73** with N,N-dimethyl-4-(5-methyl-4-(4,4,5,5-tetramethyl-1,3,2-dioxaborolan-2-yl)thiazol-2-yl)aniline, **74** (330 mg, 0.72 mmol) to obtain terthiazole **Ox8** (80 mg, 0.135 mmol, 45%) as a greenish solid.

^{1}H-NMR ($CDCl_3$, 300 MHz): δ (ppm) 8.07 (m, 2H), 7.81 (d, *J* = 8.9 Hz, 2H), 7.74 (d, *J* = 8.8 Hz, 2H), 7.44 (m, 3H), 6.72 (d, *J* = 9.0 Hz, 2H), 6.66 (d, *J* = 8.9 Hz, 2H), 3.03 (s, 6H), 3.00 (s, 6H), 2.35 (s, 3H), 2.01 (s, 3H).
^{13}C-NMR ($CDCl_3$, 91 MHz): δ (ppm) 167.04, 165.22, 165.11, 151.56, 151.40, 147.60, 145.99, 142.98, 133.86, 130.70, 130.24, 130.07, 130.04, 128.92, 127.67, 127.42, 126.77, 122.25, 121.93, 111.92, 111.85, 40.37, 12.50, 12.28.
HRMS (ESI): calcd. for $C_{33}H_{32}N_5S_3^+$ $[M+H]^+$ 594.1814, found $[M+H]^+$ 594.1794.

The same procedure has been followed by replacing **73** with 5-methyl-2-(4-(methylthio)phenyl)-4-(4,4,5,5-tetramethyl-1,3,2-dioxaborolan-2-yl)thiazole, **75** (416 mg, 1.20 mmol) to obtain terthiazole **Ox9** (265 mg, 0.44 mmol, 88%) as a light blue solid.

^{1}H-NMR ($CDCl_3$, 360 MHz): δ (ppm) 8.06 (m, 2H), 7.85 (d, *J* = 8.1 Hz, 2H), 7.70 (d, *J* = 8.1 Hz, 2H), 7.47 (m, 3H), 7.29 (d but partially covered by $CHCl_3$ peak, , *J* = 8.1 Hz, 2H), 7.18 (d, *J* = 8.1 Hz, 2H), 2.52 (s, 6H), 2.49 (s, 3H), 2.11 (s, 3H).
^{13}C-NMR ($CDCl_3$, 91 MHz): δ (ppm) 167.16, 163.79, 163.44, 147.77, 146.33, 143.70, 141.23, 140.82, 133.65, 132.70, 131.98, 130.47, 130.27, 130.23, 129.41, 129.00, 126.71, 126.68, 126.63, 126.22, 126.13, 15.44, 12.79, 12.39.
HRMS (ESI): calcd. for $C_{31}H_{26}N_3S_5^+$ $[M+H]^+$ 600.0725, found $[M+H]^+$ 600.0695.

Terthiazole **Ox10**

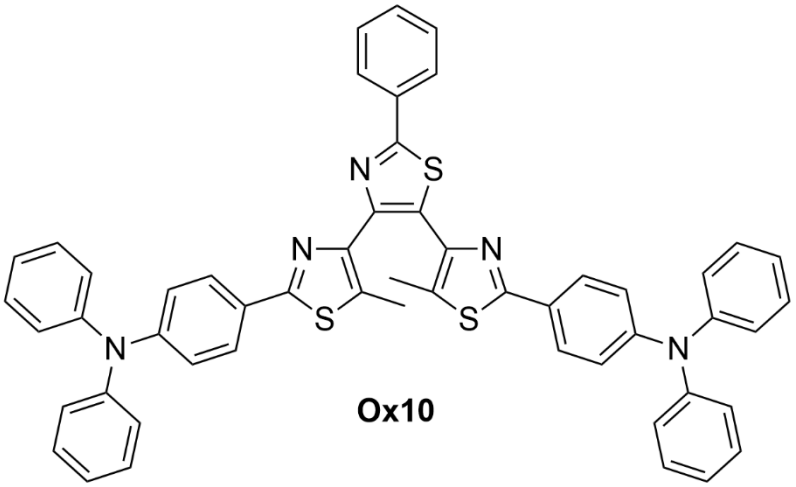

Ox10

4-(5-methyl-2'-phenyl-[4,4'-bithiazol]-2-yl)-N,N-diphenylaniline, **77** (136 mg, 0.271 mmol), 4-(4-bromo-5-methylthiazol-2-yl)-N,N-diphenylaniline, **76** (115 mg, 0.273 mmol), $P(tBu)_2MeHBF_4$ (7 mg, 0.03 mmol), Cs_2CO_3 (176 mg, 0.54 mmol), pivalic acid (8.80 mg, 0.09 mmol) and $Pd(OAc)_2$ (5 mg, 0.02 mmol) have been partially solubilized in dry xylenes (3 mL) and the obtained mixture has been stirred at reflux for 24 hours. The reaction has been diluted with dichloromethane and filtered through a Celite pad. The obtained solution has been washed with water, dried over anhydrous Na_2SO_4 and filtered. The filtrate has been concentrated under vacuum and silica gel column chromatography (eluent: dichloromethane) of the residue afforded pure photochrome **Ox10** (188 mg, 0.222 mmol, 82%) as a pale green solid thanks to a re-precipitation from a mixture of diethyl ether and ethanol 96%.

^{1}H-NMR ($CDCl_3$, 360 MHz): δ (ppm) 8.05 (dd, *J* = 7.4, 2.2 Hz, 2H), 7.75 (d, *J* = 8.7 Hz, 2H), 7.66 (d, *J* = 8.7 Hz, 2H), 7.45 (m, 2H), 7.33 – 7.24 (m, 9H), 7.19 – 6.94 (m, 16H), 2.46 (s, 3H), 2.08 (s, 3H).
^{13}C-NMR ($CDCl_3$, 91 MHz): δ (ppm) 167.08, 164.19, 163.91, 149.48, 149.24, 147.64, 147.29, 147.24, 146.33, 143.51, 133.74, 132.08, 131.34, 130.20, 129.77, 129.51, 128.98, 127.48, 127.44, 127.39, 127.12, 126.72, 125.13, 125.09, 123.74, 123.65, 122.54, 122.51, 12.75, 12.45.

Photochrome **Ox11**

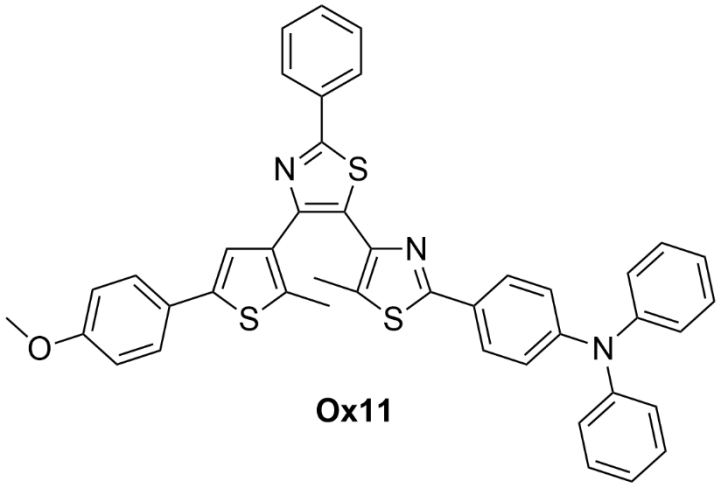

Ox11

44-(5-(4-methoxyphenyl)-2-methylthiophen-3-yl)-2-phenylthiazole, **78** (128 mg, 0.35 mmol), 4-(4-bromo-5-methylthiazol-2-yl)-N,N-diphenylaniline, **76** (149 mg, 0.35 mmol), $P(tBu)_2MeHBF_4$ (9 mg, 0.04 mmol), Cs_2CO_3 (230 mg, 0.70 mmol), pivalic acid (11 mg, 0.11 mmol) and $Pd(OAc)_2$ (6.40 mg, 0.03 mmol) have been partially solubilized in dry xylenes (3 mL) and the obtained mixture has been stirred at reflux for 24 hours. The reaction has been diluted with chloroform (15 mL) and water (15 mL). The organic layer has been extracted with chloroform. The obtained solution has been washed with water, dried over anhydrous Na_2SO_4 and filtered. The filtrate has been concentrated under vacuum and silica gel column chromatography (eluent: dichloromethane) of the residue afforded pure photochrome **Ox10** (188 mg, 0.222 mmol, 82%) as a pale green solid thanks to a precipitation from a dichloromethane solution induced by methanol.

^{1}H-NMR ($CDCl_3$, 360 MHz): δ (ppm) 8.08 – 8.01 (m, 2H), 7.78 (d, *J* = 8.7 Hz, 2H), 7.51 – 7.39 (m, 5H), 7.34 – 7.27 (m, 4H), 7.18 – 7.12 (m, 5H), 7.11 – 7.04 (m, 4H), 6.87 (d, *J* = 8.8 Hz, 2H), 3.82 (s, 3H), 2.36 (s, 3H), 2.01 (s, 3H).
^{13}C-NMR ($CDCl_3$, 91 MHz): δ (ppm) 166.93, 164.69, 159.04, 149.64, 149.09, 147.20, 143.41, 140.16, 136.78, 133.75, 133.28, 131.11, 130.22, 129.56, 129.04, 127.83, 127.40, 127.34, 126.91, 126.80, 126.59, 125.17, 123.82, 122.53, 114.32, 55.47, 14.58, 12.30.
HRMS (ESI): calcd. for $C_{43}H_{34}N_3OS_3^+$ $[M+H]^+$ 704.1858, found $[M+H]^+$ 704.1836.

Annexes

Nicolò Baggi

Complementary characterizations

5.4 Chapter 2

*5.4.1 Kinetic profiles of **1** – **4**, **6** and **7** in acetonitrile*

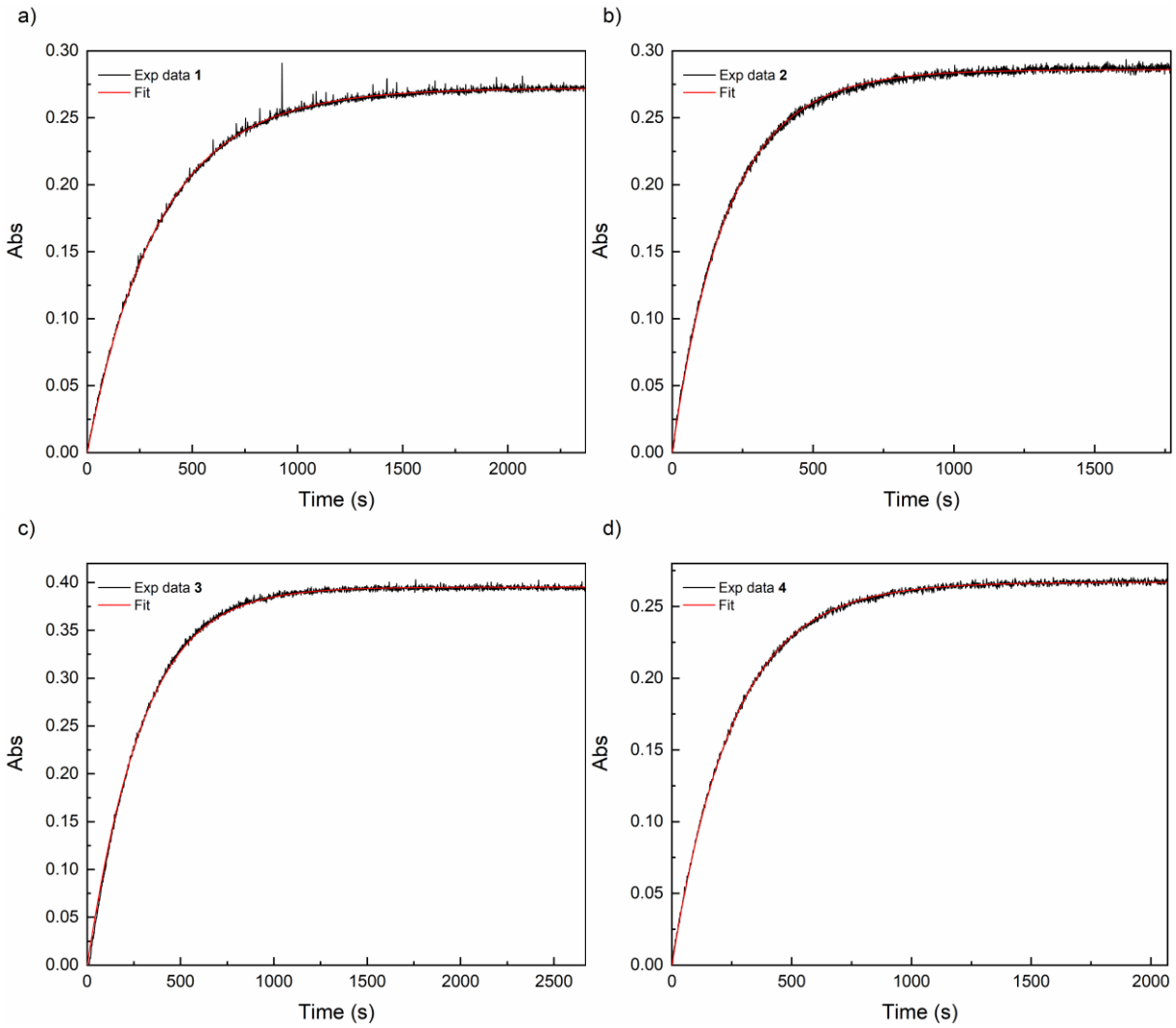

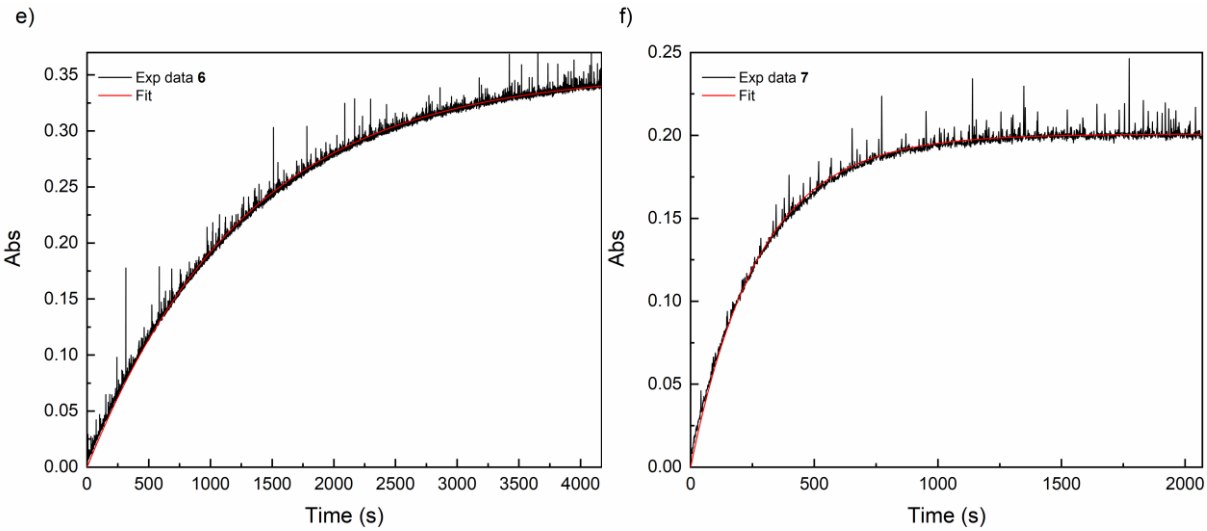

Figure A1: Kinetic profiles for the photocyclization in acetonitrile under irradiation at 335 nm of a) **1** (592 nm), b) **2** (586 nm), c) **3** (603 nm), d) **4** (607 nm), e) **6** (664 nm) and f) **7** (634 nm). Red line: fit. The observation wavelengths are indicated between the brackets.

5.5 Chapter 3

*5.5.1 Emission spectrum of **SWIST1** in acetonitrile*

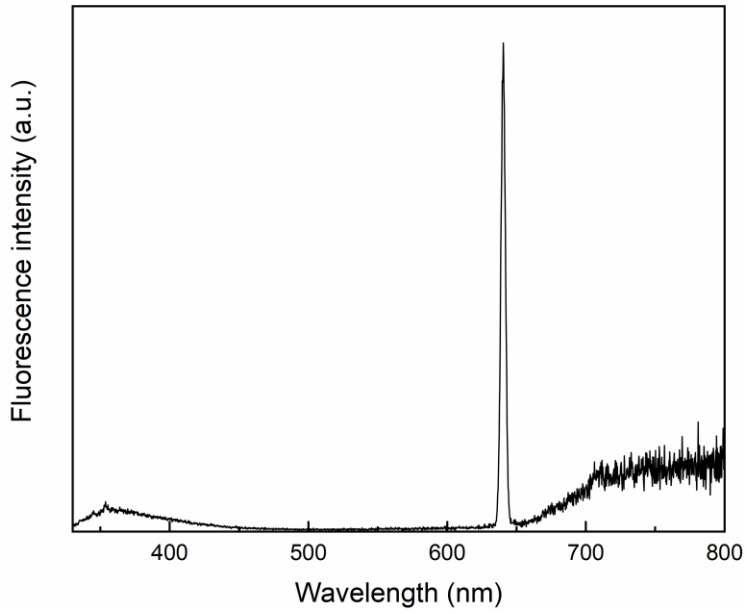

Figure A2: Fluorescence spectrum of **SWIST1** (λ_{exc} = 320 nm) in acetonitrile.

*5.5.2 X-ray structure of **SWIST1***

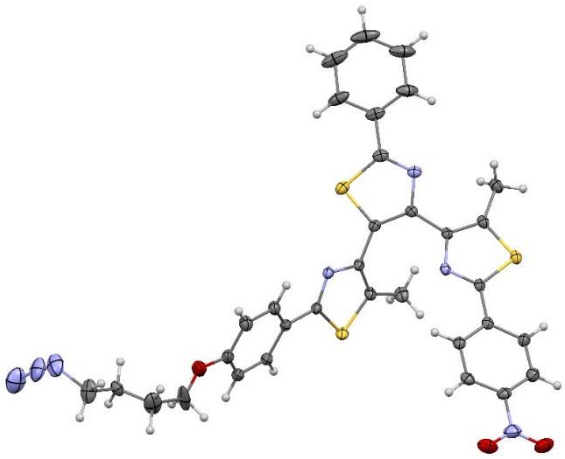

Figure A3: ORTEP drawing of **SWIST1**.

5.6 Chapter 4

*5.6.1 Emission spectra of **Red1**$^{2+}$ in acetonitrile*

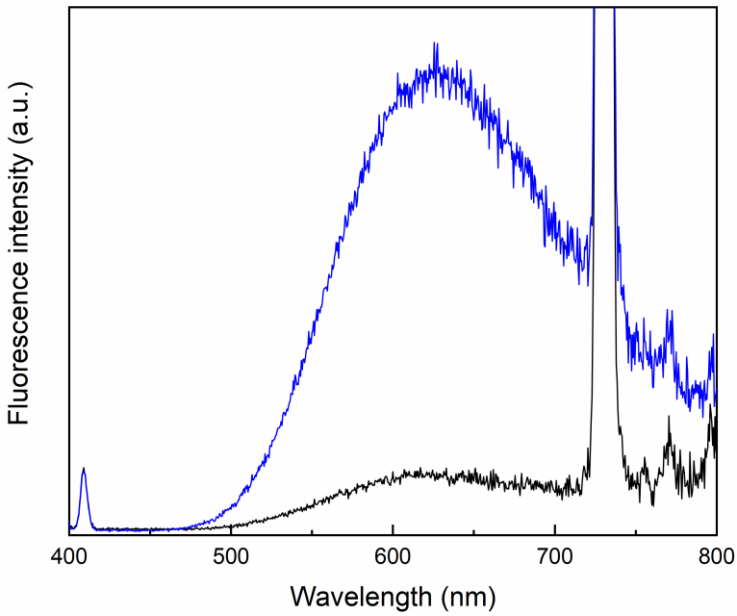

Figure A4: Emission spectra in acetonitrile of **Red1**$^{2+}$ (λ_{exc} = 365 nm); (blue solid line) emission of the OF and (black solid line) residual emission at the PSS (reached by irradiation at 340 nm).

*5.6.2 UV-vis spectra of **42** and **Red2**$^{2+}$ in acetonitrile after oxidation with Cu(OTf)$_2$*

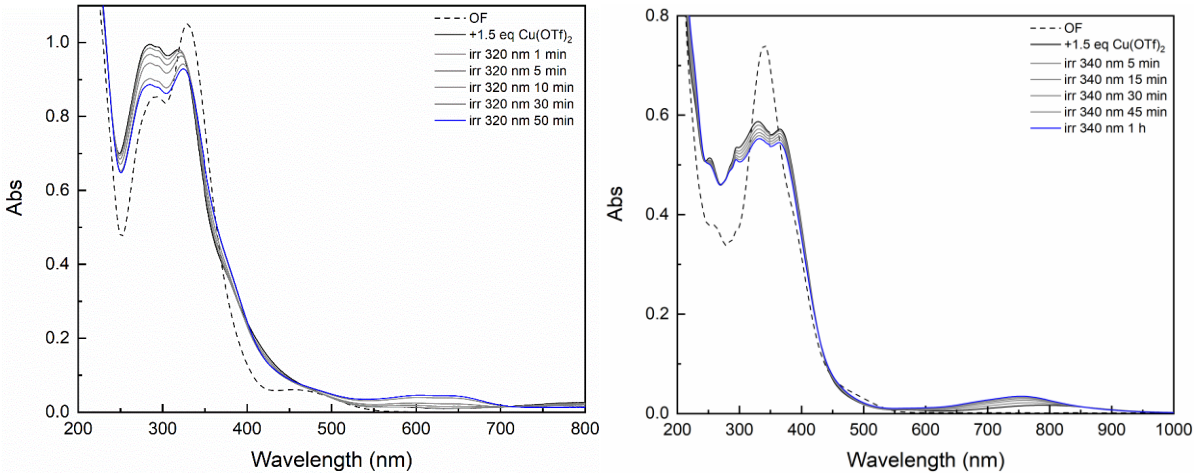

Figure A5: left) Absorption spectra of **42** in CH_3CN, (black dashed line) OF before the oxidation of Fc, (black solid line) OF after the oxidation to Fc^+ and (blue solid line) PSS reached by irradiating at 320 nm; right) Absorption spectra of **Red2**$^{2+}$ in CH_3CN; (black dashed line) OF before the oxidation of Fc, (black solid line) OF after the oxidation to Fc^+ and (blue solid line) PSS reached by irradiating at 340 nm. Optical path of the cuvette: 1 cm.

*5.6.3 X-ray structure of **Red1**$^{2+}$*

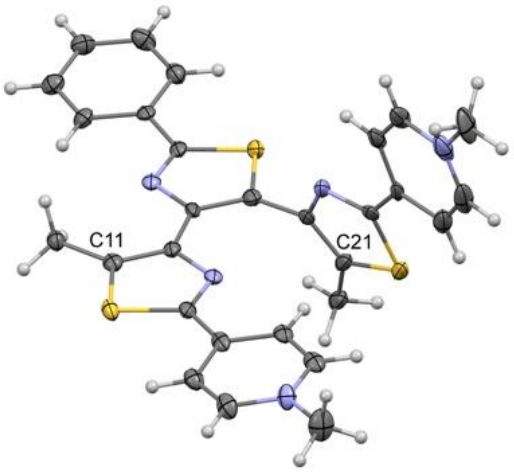

Figure A6: ORTEP drawing of **Red1**$^{2+}$, as published in ref. [212]. Thermal ellipsoids are shown at the 30 % level. Anions and solvent molecules have been omitted for clarity.

*5.6.4 CV of **Red2^{2+}** with oxidation up to 0.75 V vs SCE*

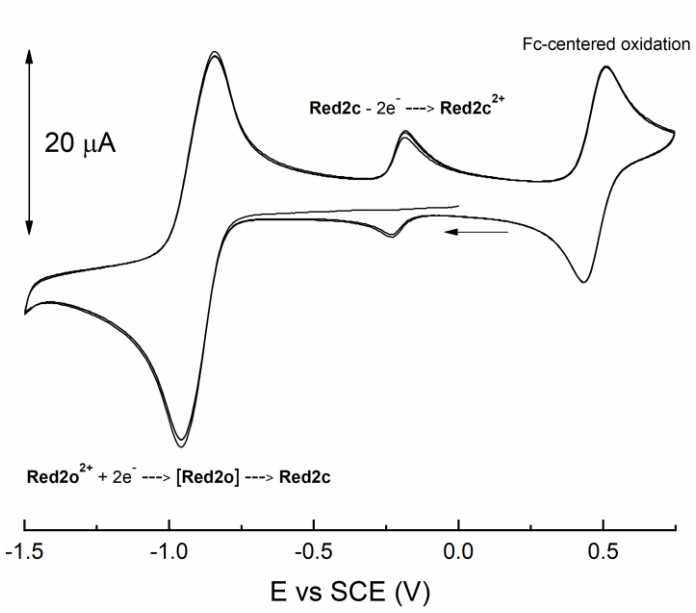

Figure A7: CV of **Red2o^{2+}** (1 mM) in CH_3CN / $TBAPF_6$ 0.1 M showing the reductive cyclization and the oxidative ring-opening induced by the generation of Fc^+. ν = 100 mV/s.

5.6.5 Thermodynamic cycle to model redox potentials

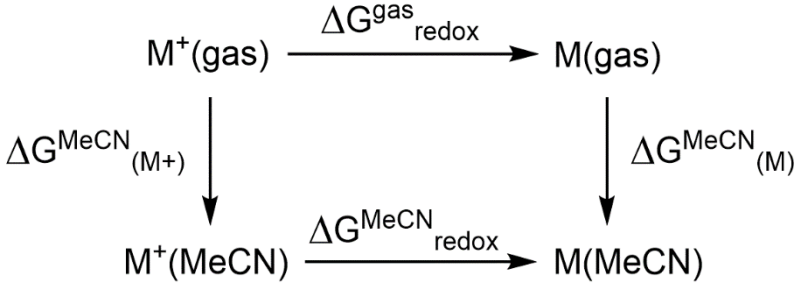

Figure A8: Thermodynamic cycle for the modelling of the redox properties, adapted from ref. [212].

Where:

$$\Delta G_{redox}^{MeCN} = \Delta G_{redox}^{gas} + \Delta G_{(M+)}^{MeCN} + \Delta G_{(M)}^{MeCN}$$

And:

$$\Delta G_{redox}^{gas} = G_{(M)}^{gas} - G_{(M+)}^{gas}$$

Finally, the redox potential is related to Gibbs free energy through:

$$\Delta G_{redox}^{MeCN} = -FE_{redox}^{0}$$

Where F is the Faraday constant (23.06 kcal·mol^{-1}V^{-1}) and the standard hydrogen electrode potential, V_{SHE}, is 4.43 eV [249].

*5.6.6 Isocontour plots of **Red1**'s MOs in the different redox states*

Table A1: Isocontour plots involved in the main transitions of the dicationic and neutral open and closed form isomers of **Red1**, adapted from the Supporting Information of ref. [212]

Red1o^{2+}		
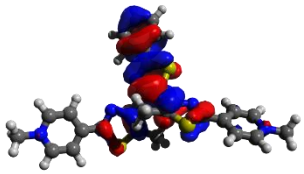	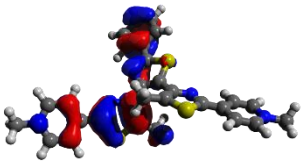	
HOMO	HOMO-1	
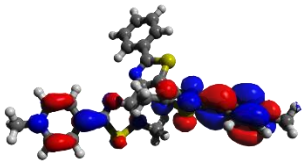	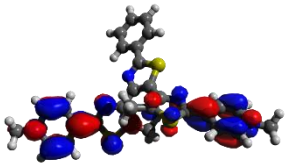	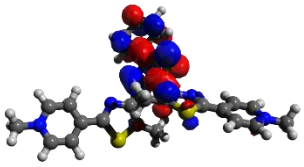
LUMO	LUMO+1	LUMO+2
Red1c^{2+}		
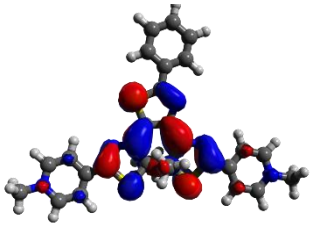	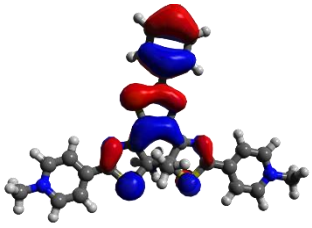	
HOMO	HOMO-1	
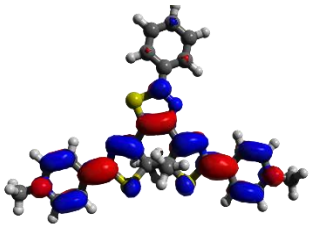	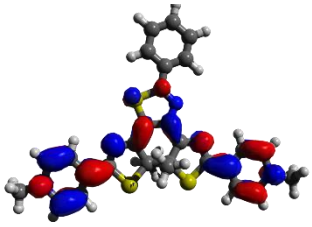	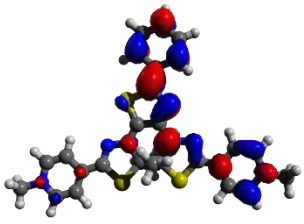
LUMO	LUMO+1	LUMO+2

Red1o

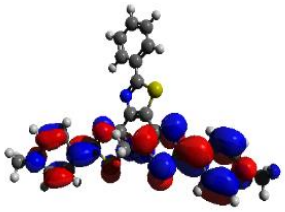

HOMO

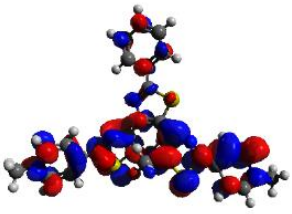

LUMO+6

Red1c

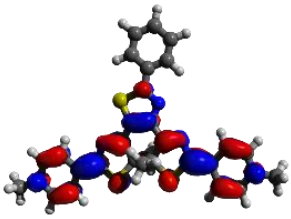

HOMO

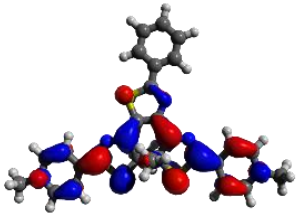

HOMO-1

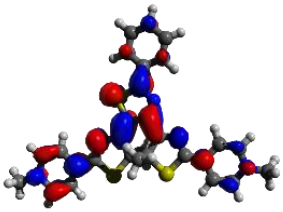

LUMO

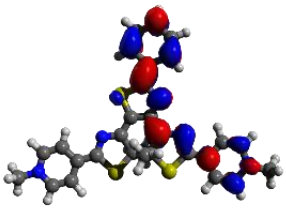

LUMO+1

*5.6.7 Theoretical UV-vis spectra of **Red2o**$^{2+}$ and **Red2c**$^{2+}$*

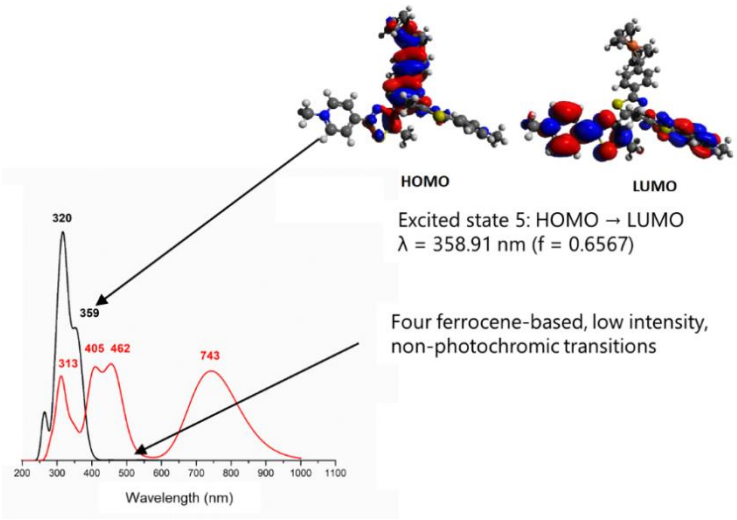

Figure A9: Theoretical UV-vis spectra of **Red2o**$^{2+}$ and **Red2c**$^{2+}$, adapted from the Supporting Information of ref. [212]

*5.6.8 Emission spectra of **Red4**$^{2+}$ in acetonitrile*

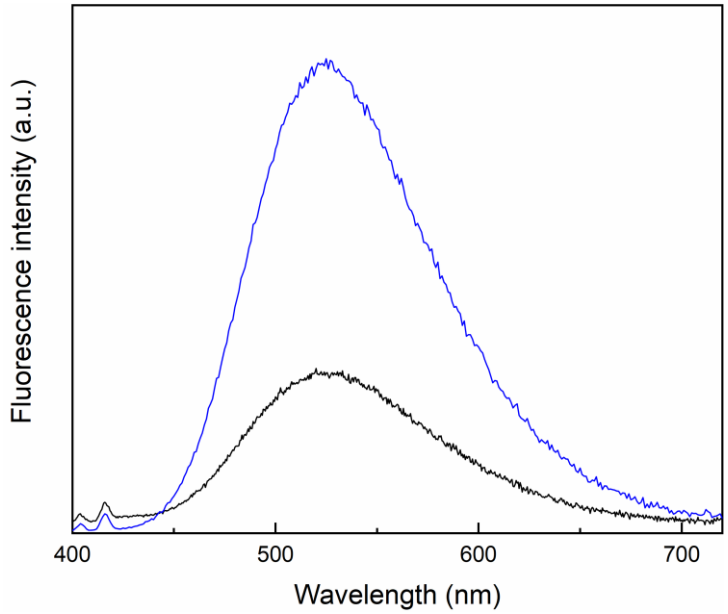

Figure A10: Emission spectra of **Red4**$^{2+}$in acetonitrile under Ar (λ_{exc} = 370 nm); (blue solid line) emission of the OF and (black solid line) residual emission at the PSS (reached by irradiation at 405 nm).

*5.6.9 Emission spectrum of **76** in dichloromethane*

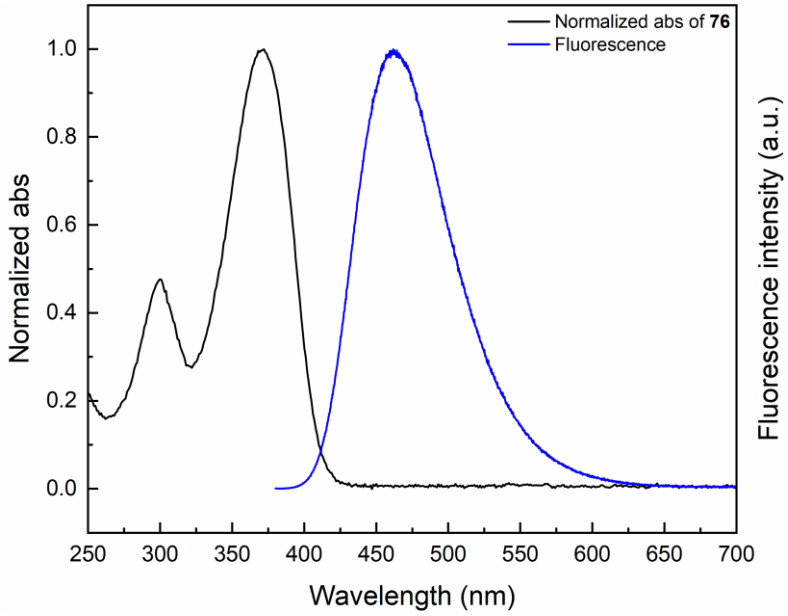

Figure A11: (black solid line) normalized UV-vis spectrum of **76** in dichloromethane; (blue solid line) emission spectrum of **76** in dichloromethane (λ_{exc} = 370 nm).

*5.6.10 Emission spectrum of **Ox10o** in dichloromethane*

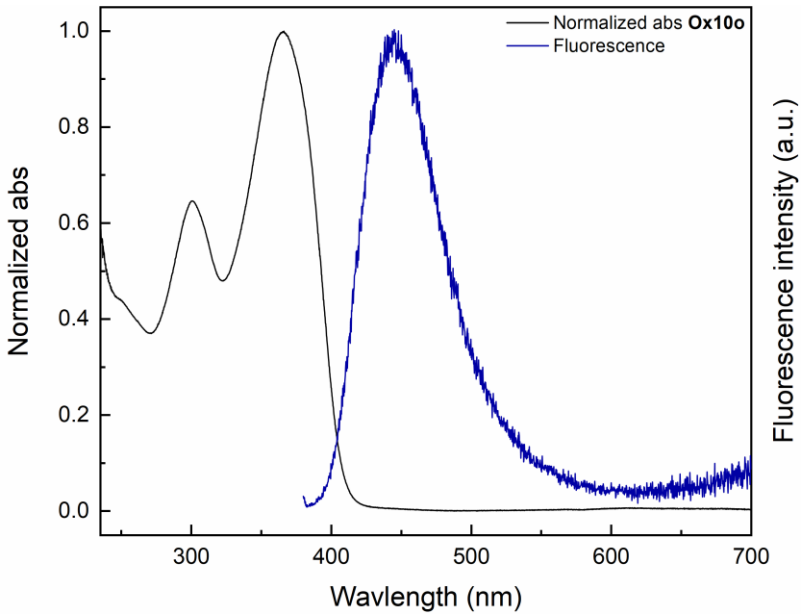

Figure A12: (black solid line) normalized UV-vis spectrum of **Ox10o** in dichloromethane; (navy blue solid line) emission spectrum of **Ox10o** in dichloromethane (λ_{exc} = 370 nm).

*5.6.11 UV-Vis spectra of **Ox11** in acetonitrile + minimum amount of dichloromethane*

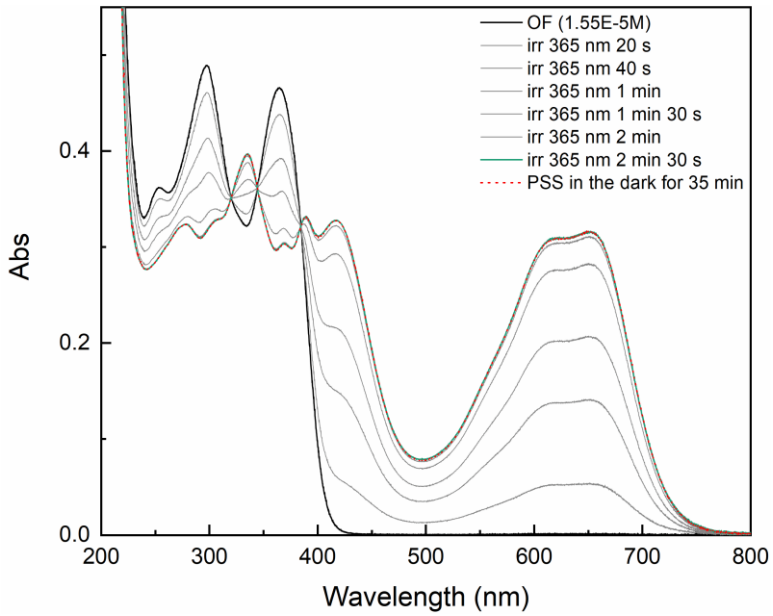

Figure A13: Absorption spectrum in acetonitrile + minimum amount of dichloromethane of **Ox11** (1.55 x 10^{-5} M), showing the evolution under UV light irradiation at 365 nm from the black line for the OF to the green solid line at the PSS. Thermal stability is confirmed by the red dotted line. Optical path of the cuvette: 1 cm.

*5.6.12 Emission spectrum of **Ox11o** in dichloromethane*

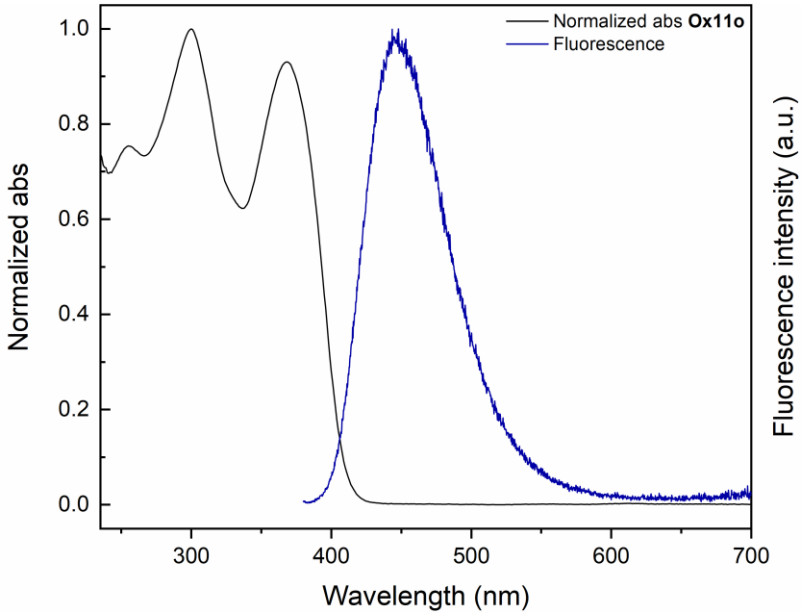

Figure A14: (black solid line) normalized UV-vis spectrum of **Ox11o** in dichloromethane; (navy blue solid line) emission spectrum of **Ox11o** in dichloromethane (λ_{exc} = 370 nm).

*5.6.13 Disproportionation of **Ox11c**$^{+\cdot}$*

As stated by Feringa and co-workers in they work about the oxidative switching of DTEs [137], the comproportionation reaction and its equilibrium constant can provide an indication about the stability of the monocationic closed form.

The comproportionation reaction is:

$$\mathbf{Ox11c} + \mathbf{Ox11c^{2+}} \rightleftarrows 2\ \mathbf{Ox11c^{+\cdot}}$$

And the comproportionation constant is defined as:

$$K_C = \frac{[\mathbf{Ox11c^{+\cdot}}]^2}{[\mathbf{Ox11c}][\mathbf{Ox11c^{2+}}]} = e^{\frac{\Delta E}{25.69}}$$

Since ΔE = 160 mV (as reported in Table 15) for the two waves related to the redox reactions occurring on the closed form isomer of **Ox11**, K_C results ~510. This means that the disproportionation is thermodynamically unfavorable. Nevertheless, it might be supposed that its impact, if any, is bigger at slower scan rates.

*5.6.14 CV of **Ox11o** at ν = 1 V/s*

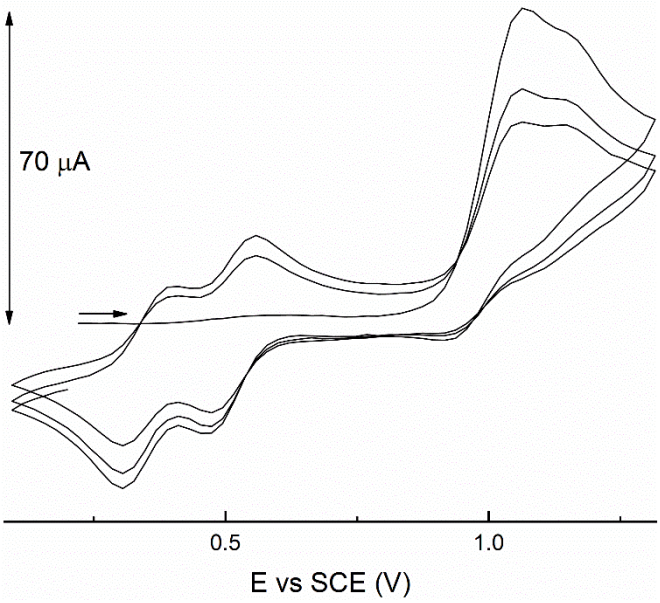

Figure A15: CV of **Ox11** (1 mM) in CH_2Cl_2 / $TBAPF_6$ 0.1 M. ν = 1 V/s.

Nicolò Baggi

List of References

1. Fritzsche, J. Notes sur les carbures d'hydrogène solides, tirés du goudron de houille. *Comptes Rendus Acad. Sci.* **64**, 1035–1037 (1867).
2. Meer, E. Ter. Ueber Dinitroverbindungen der Fettreihe. *Berichte der Dtsch. Chem. Gesellschaft* **8**, 1080–1088 (1875).
3. Markwald, W. Über Phototropie. *Zeitschrift für Phys. Chemie* **30U**, 140–145 (1899).
4. Hirshberg, Y. *Comptes Rendus Acad. Sci.* **231**, 903–904 (1950).
5. Irie, M., Fukaminato, T., Matsuda, K. & Kobatake, S. Photochromism of diarylethene molecules and crystals: Memories, switches, and actuators. *Chem. Rev.* **114**, 12174–12277 (2014).
6. Barachevsky, V. A. Negative photochromism in organic systems. *Rev. J. Chem.* **7**, 334–371 (2017).
7. Aiken, S., Edgar, R. J. L., Gabbutt, C. D., Heron, B. M. & Hobson, P. A. Negatively photochromic organic compounds: Exploring the dark side. *Dye. Pigment.* **149**, 92–121 (2018).
8. Irie, M. Photoswitchable Molecular Systems Based on Diarylethenes. in *Molecular Switches* 37–62 (Wiley, 2001). doi:10.1002/3527600329.ch2
9. Boelke, J. & Hecht, S. Designing Molecular Photoswitches for Soft Materials Applications. *Adv. Opt. Mater.* **7**, 1–14 (2019).
10. Hartley, G. S. *The Cis-form of Azobenzene*. *Nature* **216**, (1937).
11. Bandara, H. M. D. & Burdette, S. C. Photoisomerization in different classes of azobenzene. *Chem. Soc. Rev.* **41**, 1809–1825 (2012).
12. Lerch, M. M., Hansen, M. J., van Dam, G. M., Szymanski, W. & Feringa, B. L. Emerging Targets in Photopharmacology. *Angew. Chemie - Int. Ed.* **55**, 10978–10999 (2016).
13. Welleman, I. M., Hoorens, M. W. H., Feringa, B. L., Boersma, H. H. & Szymański, W. Photoresponsive molecular tools for emerging applications of light in medicine. *Chem. Sci.* **11**, 11672–11691 (2020).
14. Pianowski, Z. L. Recent Implementations of Molecular Photoswitches into Smart Materials and Biological Systems. *Chem. - A Eur. J.* **25**, 5128–5144 (2019).
15. Jerca, F. A., Jerca, V. V. & Hoogenboom, R. Advances and opportunities in the exciting world of azobenzenes. *Nat. Rev. Chem.* **6**, 51–69 (2022).
16. Riefolo, F. *et al.* Rational Design of Photochromic Analogues of Tricyclic Drugs. *J. Med. Chem.* **64**, 9259–9270 (2021).
17. Prischich, D. *et al.* Adrenergic Modulation With Photochromic Ligands. *Angew. Chemie - Int. Ed.* **60**, 3625–3631 (2021).
18. Eleya, N., Ghosh, S., Lork, E. & Staubitz, A. A new photo switchable azobenzene macrocycle without thermal relaxation at ambient temperature. *J. Mater. Chem. C* **9**, 82–87 (2021).
19. Hirshberg, Y. & Fischer, E. Photochromism and Reversible Multiple Internal Transitions in Some spiroPyrans at Low Temperatures. Part I. *Order A J. Theory Ordered Sets Its Appl.* 297–303 (1951).
20. Hirshberg, Y. & Fischer, E. Low-temperature photochromism and its relation to thermochromism. *J. Chem. Soc.* 629–636 (1953). doi:10.1039/jr9530000629
21. Hirshberg, Y. & Fischer, E. Photochromism and reversible multiple internal transitions in some spiropyrans at low temperatures. Part II. *J. Chem. Soc.* 3129–3137 (1954).

doi:10.1039/JR9540003129
22. Hirshberg, Y. Reversible Formation and Eradication of Colors by Irradiation at Low Temperatures. A Photochemical Memory Model. *J. Am. Chem. Soc.* **78**, 2304–2312 (1956).
23. Heiligman-Rim, R., Hirshberg, Y. & Fischer, E. *photochromism in some spiropyrans. part iii.* **297**, (1956).
24. Minkin, V. I. Photo-, thermo-, solvato-, and electrochromic spiroheterocyclic compounds. *Chem. Rev.* **104**, 2751–2776 (2004).
25. Kortekaas, L. & Browne, W. R. The evolution of spiropyran: Fundamentals and progress of an extraordinarily versatile photochrome. *Chem. Soc. Rev.* **48**, 3406–3424 (2019).
26. Zhou, J. *et al.* Detailed investigation on a negative photochromic spiropyran. *J. Photochem. Photobiol. A Chem.* **90**, 117–123 (1995).
27. Funasako, Y., Miyazaki, H., Sasaki, T., Goshima, K. & Inokuchi, M. Synthesis, Photochromic Properties, and Crystal Structures of Salts Containing a Pyridinium-Fused Spiropyran: Positive and Negative Photochromism in the Solution and Solid State. *J. Phys. Chem. B* **124**, 7251–7257 (2020).
28. Bertelson, R. C. Reminiscences about Organic Photochromics. *Mol. Cryst. Liq. Cryst. Sci. Technol. Sect. A. Mol. Cryst. Liq. Cryst.* **246**, 1–8 (1994).
29. Maeda, S. Spirooxazines. in *Organic Photochromic and Thermochromic Compounds* (eds. Crano, J. C. & Guglielmetti, R. J.) 85–109 (Kluwer Academic Publishers, 2002). doi:10.1007/0-306-46911-1_3
30. Xia, H., Xie, K. & Zou, G. Advances in spiropyrans/spirooxazines and applications based on fluorescence resonance energy transfer (FRET) with fluorescent materials. *Molecules* **22**, (2017).
31. Becker, R. S. & Michl, J. Photochromism of Synthetic and Naturally Occurring 2H-Chromenes and 2H-Pyrans. *J. Am. Chem. Soc.* **88**, 5931–5933 (1966).
32. Van Gemert, B. Benzo and Naphthopyrans (Chromenes). *Org. Photochromic Thermochromic Compd.* **1**, 111–140 (2002).
33. Paramonov, S. V., Lokshin, V. & Fedorova, O. A. Spiropyran, chromene or spirooxazine ligands: Insights into mutual relations between complexing and photochromic properties. *J. Photochem. Photobiol. C Photochem. Rev.* **12**, 209–236 (2011).
34. Natali, M. & Giordani, S. Molecular switches as photocontrollable "smart" receptors. *Chem. Soc. Rev.* **41**, 4010–4029 (2012).
35. Bohne, C. & Mitchell, R. H. Characterization of the photochromism of dihydropyrenes with photophysical techniques. *J. Photochem. Photobiol. C Photochem. Rev.* **12**, 126–137 (2011).
36. Mitchell, R. H. *et al.* Synthesis and photochromic properties of molecules containing [e]-annelated dihydropyrenes. Two and three way π-switches based on the dimethyldihydropyrene-metacyclophanediene valence isomerization. *J. Am. Chem. Soc.* **125**, 2974–2988 (2003).
37. Garmshausen, Y., Klaue, K. & Hecht, S. Dihydropyrene as an Aromaticity Probe for Partially Quinoid Push–Pull Systems. *Chempluschem* **82**, 1025–1029 (2017).
38. Huang, X. & Li, T. Recent progress in the development of molecular-scale electronics based on photoswitchable molecules. *J. Mater. Chem. C* **8**, 821–848 (2020).
39. Klaue, K., Garmshausen, Y. & Hecht, S. Taking Photochromism beyond Visible: Direct One-Photon NIR Photoswitches Operating in the Biological Window. *Angew. Chemie - Int. Ed.* **57**, 1414–1417 (2018).
40. Cobo, S. *et al.* Reactivity of a pyridinium-substituted dimethyldihydropyrene switch

under aerobic conditions: Self-sensitized photo-oxygenation and thermal release of singlet oxygen. *Chem. Commun.* **51**, 13886–13889 (2015).
41. Bakkar, A., Cobo, S., Lafolet, F., Saint-Aman, E. & Royal, G. A new surface-bound molecular switch based on the photochromic dimethyldihydropyrene with light-driven release of singlet oxygen properties. *J. Mater. Chem. C* **3**, 12014–12017 (2015).
42. Stobbe, H. Die farbigen Anhydride der Butadiën-β,γ-dicarbonsäuren; ihr Verhalten gegen Licht und Wärme. (II. Abhandlung über Butadiënverbindungen.). *Berichte der Dtsch. Chem. Gesellschaft* **37**, 2236–2240 (1904).
43. Yokoyama, Y. Fulgides for Memories and Switches. *Chem. Rev.* **100**, 1717–1739 (2000).
44. Eichler, C. *et al.* Paving the Way to the First Functional Fulgide@MOF Hybrid Materials. *Chem. Mater.* **33**, 3757–3766 (2021).
45. Irie, M. Diarylethenes for Memories and Switches. *Chem. Rev.* **100**, 1685−1716 (2000).
46. Helmy, S. *et al.* Photoswitching using visible light: A new class of organic photochromic molecules. *J. Am. Chem. Soc.* **136**, 8169–8172 (2014).
47. Stenhouse, J. Ueber die Oele, die bei der Einwirkung der Schwefelsäure auf verschiedene Vegetabilien entstehen. *Justus Liebigs Ann. Chem.* **74**, 278–297 (1850).
48. Lerch, M. M., Wezenberg, S. J., Szymanski, W. & Feringa, B. L. Unraveling the Photoswitching Mechanism in Donor-Acceptor Stenhouse Adducts. *J. Am. Chem. Soc.* **138**, 6344–6347 (2016).
49. Hemmer, J. R. *et al.* Tunable Visible and Near Infrared Photoswitches. *J. Am. Chem. Soc.* **138**, 13960–13966 (2016).
50. Hemmer, J. R. *et al.* Controlling Dark Equilibria and Enhancing Donor-Acceptor Stenhouse Adduct Photoswitching Properties through Carbon Acid Design. *J. Am. Chem. Soc.* **140**, 10425–10429 (2018).
51. Mallo, N. *et al.* Structure-function relationships of donor-acceptor Stenhouse adduct photochromic switches. *Chem. Sci.* **9**, 8242–8252 (2018).
52. Sroda, M. M., Stricker, F., Peterson, J. A., Bernal, A. & Read de Alaniz, J. Donor–Acceptor Stenhouse Adducts: Exploring the Effects of Ionic Character. *Chem. - A Eur. J.* **27**, 4183–4190 (2021).
53. Berraud-Pache, R. *et al.* Redesigning donor-acceptor Stenhouse adduct photoswitches through a joint experimental and computational study. *Chem. Sci.* **12**, 2916–2924 (2021).
54. Gomes, R. F. A., Coelho, J. A. S. & Afonso, C. A. M. Synthesis and Applications of Stenhouse Salts and Derivatives. *Chem. - A Eur. J.* **24**, 9170–9186 (2018).
55. Baeyer, A. Ueber die Verbindungen der Indigogruppe. *Berichte der Dtsch. Chem. Gesellschaft* **16**, 2188–2204 (1883).
56. Petermayer, C., Thumser, S., Kink, F., Mayer, P. & Dube, H. Hemiindigo: Highly Bistable Photoswitching at the Biooptical Window. *J. Am. Chem. Soc.* **139**, 15060–15067 (2017).
57. Wiedbrauk, S. & Dube, H. Hemithioindigo-An emerging photoswitch. *Tetrahedron Lett.* **56**, 4266–4274 (2015).
58. Kink, F., Collado, M. P., Wiedbrauk, S., Mayer, P. & Dube, H. Bistable Photoswitching of Hemithioindigo with Green and Red Light: Entry Point to Advanced Molecular Digital Information Processing. *Chem. - A Eur. J.* **23**, 6237–6243 (2017).
59. Sailer, A. *et al.* Pyrrole Hemithioindigo Antimitotics with Near-Quantitative Bidirectional Photoswitching that Photocontrol Cellular Microtubule Dynamics with Single-Cell Precision**. *Angew. Chemie - Int. Ed.* **60**, 23695–23704 (2021).
60. Hatano, S., Horino, T., Tokita, A., Oshima, T. & Abe, J. Unusual negative photochromism via a short-lived imidazolyl radical of 1,1′-binaphthyl-bridged imidazole dimer. *J. Am.*

Chem. Soc. **135**, 3164–3172 (2013).
61. Hayashi, T. & Maeda, K. Preparation of a New Phototropic Substance. *Bull. Chem. Soc. Jpn.* **33**, 565–566 (1960).
62. Kishimoto, Y. & Abe, J. A fast photochromic molecule that colors only under UV light. *J. Am. Chem. Soc.* **131**, 4227–4229 (2009).
63. Mutoh, K., Kobayashi, Y., Hirao, Y., Kubo, T. & Abe, J. Stealth fast photoswitching of negative photochromic naphthalene-bridged phenoxyl-imidazolyl radical complexes. *Chem. Commun.* **52**, 6797–6800 (2016).
64. Yamaguchi, T., Kobayashi, Y. & Abe, J. Fast Negative Photochromism of 1,1′-Binaphthyl-Bridged Phenoxyl-Imidazolyl Radical Complex. *J. Am. Chem. Soc.* **138**, 906–913 (2016).
65. Mutoh, K., Miyashita, N., Arai, K. & Abe, J. Turn-On Mode Fluorescence Switch by Using Negative Photochromic Imidazole Dimer. *J. Am. Chem. Soc.* **141**, 5650–5654 (2019).
66. Kometani, A., Inagaki, Y., Mutoh, K. & Abe, J. Red or near-infrared light operating negative photochromism of a binaphthyl-bridged imidazole dimer. *J. Am. Chem. Soc.* **142**, 7995–8005 (2020).
67. Kobayashi, Y. & Abe, J. Real-Time Dynamic Hologram of a 3D Object with Fast Photochromic Molecules. *Adv. Opt. Mater.* **4**, 1354–1357 (2016).
68. Irie, M. & Mohri, M. Thermally irreversible photochromic systems. Reversible photocyclization of 1,2-bis (2-methylbenzo[b]thiophen-3-yl)perfluorocyclocoalkene derivatives. *J. Org. Chem.* **53**, 803–808 (1988).
69. Uchida, K. *et al.* Thermally reversible photochromic systems. Photochromism of a dipyrrolylperfluorocyclopentene. *Chemistry Letters* 835–836 (1999). doi:10.1246/cl.1999.835
70. Kawai, S. *et al.* Novel photochromic molecules based on 4,5-dithienyl thiazole with fast thermal bleaching rate. *Chem. Mater.* **19**, 3479–3483 (2007).
71. Inaba, K., Iwai, R., Morimoto, M. & Irie, M. Thermally reversible photochromism of dipyrrolylethenes. *Photochem. Photobiol. Sci.* **18**, 2136–2141 (2019).
72. Nakahama, T., Kitagawa, D. & Kobatake, S. Tuning of Optical Properties and Thermal Cycloreversion Reactivity of Photochromic Diarylbenzene by Introducing Electron-Donating Substituents. *J. Phys. Chem. C* **123**, 31212–31218 (2019).
73. Nakatani, K., Piard, J., Yu, P. & Métivier, R. Introduction: Organic Photochromic Molecules. *Photochromic Mater. Prep. Prop. Appl.* 1–45 (2016). doi:10.1002/9783527683734.ch1
74. Shibata, K., Kuroki, L., Fukaminato, T. & Irie, M. Fluorescence switching of a diarylethene derivative having oxazole rings. *Chem. Lett.* **37**, 832–833 (2008).
75. Kawai, T., Iseda, T. & Irie, M. Photochromism of triangle terthiophene derivatives as molecular re-router. *Chem. Commun.* **4**, 72–73 (2004).
76. Li, X. & Tian, H. One-step synthesis and photochromic properties of a stable triangle terthiophene. *Tetrahedron Lett.* **46**, 5409–5412 (2005).
77. Nakashima, T. *et al.* Photochromism of Thiazole-Containing Triangle Terarylenes. *European J. Org. Chem.* **2007**, 3212–3218 (2007).
78. Kobatake, S., Uchida, K., Tsuchida, E. & Irie, M. Single-crystalline photochromism of diarylethenes: reactivity–structure relationship. *Chem. Commun.* **2**, 2804–2805 (2002).
79. Irie, M. Photochromism of diarylethene single molecules and single crystals. *Photochem. Photobiol. Sci.* **9**, 1535–1542 (2010).
80. Morimoto, M. & Irie, M. A diarylethene cocrystal that converts light into mechanical work. *J. Am. Chem. Soc.* **132**, 14172–14178 (2010).
81. Zou, Y. *et al.* Amphiphilic diarylethene as a photoswitchable probe for imaging living

cells. *J. Am. Chem. Soc.* **130**, 15750–15751 (2008).
82. Roubinet, B. *et al.* Carboxylated Photoswitchable Diarylethenes for Biolabeling and Super-Resolution RESOLFT Microscopy. *Angew. Chemie - Int. Ed.* **55**, 15429–15433 (2016).
83. Orgiu, E. *et al.* Optically switchable transistor via energy-level phototuning in a bicomponent organic semiconductor. *Nat. Chem.* **4**, 675–679 (2012).
84. Hou, L. *et al.* Optically switchable organic light-emitting transistors. *Nat. Nanotechnol.* **14**, 347–353 (2019).
85. Leydecker, T. *et al.* Flexible non-volatile optical memory thin-film transistor device with over 256 distinct levels based on an organic bicomponent blend. *Nat. Nanotechnol.* **11**, 769–775 (2016).
86. Jia, C. *et al.* Covalently bonded single-molecule junctions with stable and reversible photoswitched conductivity. *Science (80-.).* **352**, 1443–1446 (2016).
87. Zhang, J. & Tian, H. The Endeavor of Diarylethenes: New Structures, High Performance, and Bright Future. *Adv. Opt. Mater.* **6**, 1–30 (2018).
88. Woodward, R. B. & Hoffmann, R. The Conservation of Orbital Symmetry. *Angew. Chemie Int. Ed. English* **8**, 781–853 (1969).
89. Irie, M., Sakemura, K., Okinaka, M. & Uchida, K. Photochromism of Dithienylethenes with Electron-Donating Substituents. *J. Org. Chem.* **60**, 8305–8309 (1995).
90. Miyasaka, H. *et al.* Picosecond laser photolysis studies on photochromic reactions anhydride in solutions. *Chem. Phys. Lett.* **230**, 249–254 (1994).
91. Tamai, N., Saika, T., Shimidzu, T. & Irie, M. Femtosecond Dynamics of a Thiophene Oligomer with a Photoswitch by Transient Absorption Spectroscopy. *J. Phys. Chem.* **100**, 4689–4692 (1996).
92. Miyasaka, H., Nobuto, T., Itaya, A., Tamai, N. & Irie, M. *Picosecond laser photolysis studies on a photochromic dithienylethene in solution and in crystalline phases*. *Chemical Physics Letters* **269**, (1997).
93. Hamdi, I. *et al.* Cyclization Dynamics and Competitive Processes of Photochromic Perfluorocyclopentene Dithienylethylene in Solution. *ChemPhysChem* **21**, 2223–2229 (2020).
94. Boggio-Pasqua, M., Ravaglia, M., Bearpark, M. J., Garavelli, M. & Robb, M. A. Can Diarylethene Photochromism be Explained by a Reaction Path Alone? A CASSCF Study with Model MMVB Dynamics. *J. Phys. Chem. A* **107**, 11139–11152 (2003).
95. Levine, B. G., Ko, C., Quenneville, J. & Martínez, T. J. Conical intersections and double excitations in time-dependent density functional theory. *Mol. Phys.* **104**, 1039–1051 (2006).
96. Fihey, A., Perrier, A. & Maurel, F. Tuning the optical properties of dithienylethenes: Theoretical insights. *J. Photochem. Photobiol. A Chem.* **247**, 30–41 (2012).
97. Uchida, K., Tsuchida, E., Aoi, Y., Nakamura, S. & Irie, M. Substitution effect on the coloration quantum yield of a photochromic bisbenzothienylethene. *Chem. Lett.* 63–64 (1999). doi:10.1246/cl.1999.63
98. Li, W. *et al.* Separation of photoactive conformers based on hindered diarylethenes: Efficient modulation in photocyclization quantum yields. *Angew. Chemie - Int. Ed.* **53**, 4603–4607 (2014).
99. Zhu, W. *et al.* Unprecedented stability of a photochromic bisthienylethene based on benzobisthiadiazole as an ethene bridge. *Angew. Chemie - Int. Ed.* **50**, 10986–10990 (2011).

100. Morinaka, K., Ubukata, T. & Yokoyama, Y. Structurally versatile novel photochromic bisarylindenone and its acetal: Achievement of large cyclization quantum yield. *Org. Lett.* **11**, 3890–3893 (2009).
101. Fukumoto, S., Nakashima, T. & Kawai, T. Photon-Quantitative Reaction of a Dithiazolylarylene in Solution. *Angew. Chemie Int. Ed.* **50**, 1565–1568 (2011).
102. Li, R. *et al.* Photon-Quantitative 6π-Electrocyclization of a Diarylbenzo[b]thiophene in Polar Medium. *Chem. - An Asian J.* **10**, 1725–1730 (2015).
103. Ferreira, P. *et al.* A Visible–Near-Infrared Light-Responsive Host–Guest Pair with Nanomolar Affinity in Water. *Chem. - A Eur. J.* **25**, 3477–3482 (2019).
104. Stellacci, F. *et al.* High quantum yield diarylethene-backbone photochromic polymer. *Adv. Mater.* **11**, 292–295 (1999).
105. Meng, S. & Ma, J. Solvent effects on isomerization and spectral properties of photochromic-switching diarythene derivatives in polar and apolar solutions. *J. Phys. Chem. A* **116**, 913–923 (2012).
106. Okuno, K., Shigeta, Y., Kishi, R. & Nakano, M. Theoretical design of solvatochromism switching by photochromic reactions using donor-acceptor disubstituted diarylethene derivatives with oxidized thiophene rings. *Phys. Chem. Chem. Phys.* **17**, 6484–6494 (2015).
107. Takeuchi, S., Nakagawa, T. & Yokoyama, Y. A photon-working on/off switch for intramolecular donor-acceptor interactions and invisible modulation of the fluorescence. *Photochem. Photobiol. Sci.* **15**, 325–328 (2016).
108. Takeuchi, S., Nakagawa, T. & Yokoyama, Y. A thermoresponsive fluorophore based on a photochromic diarylethene having donor-acceptor moieties. *Chem. Commun.* **56**, 6492–6494 (2020).
109. Kanazawa, R., Nakashima, T. & Kawai, T. Photophysical Properties of a Terarylene Photoswitch with a Donor-Acceptor Conjugated Bridging Unit. *J. Phys. Chem. A* **121**, 1638–1646 (2017).
110. Li, Z. *et al.* Solvent-dependent and visible light-activated NIR photochromic dithienylethene modified by difluoroboron β-diketonates as fluorescent turn-on pH sensor. *Dye. Pigment.* **162**, 339–347 (2019).
111. Li, Z. *et al.* Multi-modulated photochromic behavior of a D-A type dithienylethene. *Dye. Pigment.* **162**, 712–720 (2019).
112. Li, Z. *et al.* Blue-/NIR Light-Excited Fluorescence Switch Based on a Carbazole-Dithienylethene-BF2bdk Triad. *J. Org. Chem.* **84**, 13364–13373 (2019).
113. Li, Z. *et al.* Dithienylethene-functionalized difluoroboron β-diketonate complexes: Synthesis, photophysical properties and NIR photochromism. *Opt. Mater. (Amst).* **94**, 257–265 (2019).
114. Wan, H. *et al.* Electron donor and acceptor functionalized dithienylethenes: Effects of charge density on photochromic properties. *Phys. Chem. Chem. Phys.* **20**, 14348–14356 (2018).
115. Park, J. M., Jung, C. Y., Jang, W. D. & Jaung, J. Y. Effect of donor-π-acceptor structure on photochromism of dithienylethene-based dyes. *Dye. Pigment.* **177**, 108315 (2020).
116. Grabowski, Z. R., Rotkiewicz, K. & Rettig, W. Structural Changes Accompanying Intramolecular Electron Transfer: Focus on Twisted Intramolecular Charge-Transfer States and Structures. *Chem. Rev.* **103**, 3899–4031 (2003).
117. Irie, M. & Sayo, K. Solvent effects on the photochromic reactions of diarylethene derivatives. *J. Phys. Chem.* **96**, 7671–7674 (1992).
118. Herder, M. *et al.* Switching with orthogonal stimuli: Electrochemical ring-closure and

photochemical ring-opening of bis(thiazolyl)maleimides. *Chem. Sci.* **4**, 1028–1040 (2013).
119. Thomas Bens, A. *et al.* Coupling of Chromophores: Carotenoids and Photoactive Diarylethenes – Photoreactivity versus Radiationless Deactivation. *European J. Org. Chem.* **1998**, 2333–2338 (1998).
120. Matsuda, K. *et al.* Very High Cyclization Quantum Yields of Diarylethene Having Two N-Methylpyridinium Ions. *Chem. Lett.* **32**, 1178–1179 (2003).
121. Léaustic, A. *et al.* Photochromic and reductive electrochemical switching of a dithiazolylethene with large redox modulation. *Chem. - A Eur. J.* **17**, 2246–2255 (2011).
122. Irie, M., Eriguchi, T., Takada, T. & Uchida, K. Photochromism of diarylethenes having thiophene oligomers as the aryl groups. *Tetrahedron* **53**, 12263–12271 (1997).
123. Sumi, T., Takagi, Y., Yagi, A., Morimoto, M. & Irie, M. Photoirradiation wavelength dependence of cycloreversion quantum yields of diarylethenes. *Chem. Commun.* **50**, 3928–3930 (2014).
124. Ishibashi, Y., Umesato, T., Kobatake, S., Irie, M. & Miyasaka, H. Femtosecond laser photolysis studies on temperature dependence of cyclization and cycloreversion reactions of a photochromic diarylethene derivative. *J. Phys. Chem. C* **116**, 4862–4869 (2012).
125. Honick, C. R., Peters, G. M., Young, J. D., Tovar, J. D. & Bragg, A. E. Core structure dependence of cycloreversion dynamics in diarylethene analogs. *Phys. Chem. Chem. Phys.* **22**, 3314–3328 (2020).
126. Deng, X. & Liebeskind, L. S. A Contribution to the Design of Molecular Switches: Novel Acid-Mediated Ring-Closing−Photochemical Ring-Opening of 2,3-Bis(heteroaryl)quinones (Heteroaryl = Thienyl, Furanyl, Pyrrolyl). *J. Am. Chem. Soc.* **123**, 7703–7704 (2001).
127. Nakashima, T., Miyamura, K., Sakai, T. & Kawai, T. Photo-, solvent-, and ion-controlled multichromism of imidazolium- substituted diarylethenes. *Chem. - A Eur. J.* **15**, 1977–1984 (2009).
128. Kutsunugi, Y., Coudret, C., Micheau, J. C. & Kawai, T. Photomodulation of the proton affinity and acid gated photochromism of a novel dimethylaminophenyl thiazole diarylethene. *Dye. Pigment.* **92**, 838–846 (2012).
129. Pu, S. Z., Sun, Q., Fan, C. Bin, Wang, R. J. & Liu, G. Recent advances in diarylethene-based multi-responsive molecular switches. *J. Mater. Chem. C* **4**, 3075–3093 (2016).
130. Koshido, T., Kawai, T. & Yoshino, K. Optical and electrochemical properties of cis-1,2-dicyano-1,2-bis(2,4,5-trimethyl-3-thienyl)ethene. *J. Phys. Chem.* **99**, 6110–6114 (1995).
131. Peters, A. & Branda, N. R. Electrochromism in Photochromic Dithienylcyclopentenes. *J. Am. Chem. Soc.* **125**, 3404–3405 (2003).
132. Moriyama, Y., Matsuda, K., Tanifuji, N., Irie, S. & Irie, M. Electrochemical cyclization/cycloreversion reactions of diarylethenes. *Org. Lett.* **7**, 3315–3318 (2005).
133. Nakashima, T. *et al.* Efficient oxidative cycloreversion reaction of photochromic dithiazolythiazole. *J. Am. Chem. Soc.* **134**, 19877–19883 (2012).
134. Calupitan, J. P., Nakashima, T., Hashimoto, Y. & Kawai, T. Fast and Efficient Oxidative Cycloreversion Reaction of a π-Extended Photochromic Terarylene. *Chem. - A Eur. J.* **22**, 10002–10008 (2016).
135. Peters, A. & Branda, N. R. Electrochemically induced ring-closing of photochromic electrochromism is observed for two 1 , 2-bis (dithienyl) cyclo-. *Chem. Commun.* 954–955 (2003).
136. Guirado, G., Coudret, C., Hliwa, M. & Launay, J. P. Understanding electrochromic

processes initiated by dithienylcyclopentene cation-radicals. *J. Phys. Chem. B* **109**, 17445–17459 (2005).
137. Browne, W. R. *et al.* Oxidative electrochemical switching in dithienylcyclopentenes, part 1: Effect of electronic perturbation on the efficiency and direction of molecular switching. *Chem. - A Eur. J.* **11**, 6414–6429 (2005).
138. Browne, W. R. *et al.* Oxidative electrochemical switching in dithienylcyclopentenes, part 2: Effect of substitution and asymmetry on the efficiency and direction of molecular switching and redox stability. *Chem. - A Eur. J.* **11**, 6430–6441 (2005).
139. Herder, M. *et al.* Improving the fatigue resistance of diarylethene switches. *J. Am. Chem. Soc.* **137**, 2738–2747 (2015).
140. Logtenberg, H. *et al.* Electrochemical switching of conductance with diarylethene-based redox-active polymers. *J. Phys. Chem. C* **116**, 24136–24142 (2012).
141. Areephong, J., Browne, W. R., Katsonis, N. & Feringa, B. L. Photo- and electro-chromism of diarylethene modified ITO electrodes - Towards molecular based read-write-erase information storage. *Chem. Commun.* 3930–3932 (2006). doi:10.1039/b608502d
142. Hnid, I., Frath, D., Lafolet, F., Sun, X. & Lacroix, J. C. Highly Efficient Photoswitch in Diarylethene-Based Molecular Junctions. *J. Am. Chem. Soc.* **142**, 7732–7736 (2020).
143. Hnid, I. *et al.* Combining Photomodulation and Rectification in Coordination Molecular Wires Based on Dithienylethene Molecular Junctions. *J. Phys. Chem. C* **124**, 26304–26309 (2020).
144. Hnid, I. *et al.* Unprecedented ON/OFF Ratios in Photoactive Diarylethene-Bisthienylbenzene Molecular Junctions. *Nano Lett.* (2021). doi:10.1021/acs.nanolett.1c01983
145. Berberich, M. & Würthner, F. Tuning the redox properties of photochromic diarylethenes by introducing electron-withdrawing substituents. *Asian J. Org. Chem.* **2**, 250–256 (2013).
146. Gorodetsky, B., Samachetty, H. D., Donkers, R. L., Workentin, M. S. & Branda, N. R. Reductive electrochemical cyclization of a photochromic 1,2-dithienylcyclopentene dication. *Angew. Chemie - Int. Ed.* **43**, 2812–2815 (2004).
147. Gorodetsky, B. & Branda, N. R. Bidirectional ring-opening and ring-closing of cationic 1,2-dithienylcyclopentene molecular switches triggered with light or electricity. *Adv. Funct. Mater.* **17**, 786–796 (2007).
148. Kleinwächter, M., Teichmann, E., Grubert, L., Herder, M. & Hecht, S. Oxidative and reductive cyclization in stiff dithienylethenes. *Beilstein J. Org. Chem.* **14**, 2812–2821 (2018).
149. Gilat, S. L., Kawai, S. H. & Lehn, J. M. Light-triggered electrical and optical switching devices. *J. Chem. Soc. Chem. Commun.* 1439–1442 (1993). doi:10.1039/C39930001439
150. Chatir, E. *et al.* Synthesis of Redox-Active Photochromic Phenanthrene Derivatives. *Chem. - A Eur. J.* **28**, (2022).
151. Quinton, C. *et al.* Redox-controlled fluorescence modulation (electrofluorochromism) in triphenylamine derivatives. *RSC Adv.* **4**, 34332–34342 (2014).
152. Lin, H. T., Huang, C. L. & Liou, G. S. Design, Synthesis, and Electrofluorochromism of New Triphenylamine Derivatives with AIE-Active Pendent Groups. *ACS Appl. Mater. Interfaces* **11**, 11684–11690 (2019).
153. Capodilupo, A. L. *et al.* Arylamino-fluorene derivatives: Optically induced electron transfer investigation, redox-controlled modulation of absorption and fluorescence. *Dye. Pigment.* **177**, (2020).
154. Al Sabea, H. *et al.* Dual Light and Redox Control of NIR Luminescence with

Complementary Photochromic and Organometallic Antennae. *J. Am. Chem. Soc.* **141**, 20026–20030 (2019).
155. Ouhenia-Ouadahi, K. *et al.* Photochromic–fluorescent–plasmonic nanomaterials: towards integrated three-component photoactive hybrid nanosystems. *Chem. Commun.* **50**, 7299–7302 (2014).
156. Hantzsch, A. & Weber, J. H. Ueber Verbindungen des Thiazols (Pyridins der Thiophenreihe). *Berichte der Dtsch. Chem. Gesellschaft* **20**, 3118–3132 (1887).
157. Erlenmeyer, H., Becker, C., Sorkin, E., Bloch, H. & Suter, E. Über den Einfluss primärer Amine zweikerniger, nichtkondensierter Ringverbindungen auf das Wachstum von Tuberkelbazillen. *Helv. Chim. Acta* **30**, 2058–2062 (1947).
158. Manaka, A. & Sato, M. Synthesis of aromatic thioamide from nitrile without handling of gaseous hydrogen sulfide. *Synth. Commun.* **35**, 761–764 (2005).
159. Schnürch, M., Spina, M., Khan, A. F., Mihovilovic, M. D. & Stanetty, P. Halogen dance reactions—A review. *Chem. Soc. Rev.* **36**, 1046–1057 (2007).
160. Jia, C., Kitamura, T. & Fujiwara, Y. Catalytic functionalization of arenes and alkanes via C-H bond activation. *Acc. Chem. Res.* **34**, 633–639 (2001).
161. Mc Glacken, G. P. & Bateman, L. M. Recent advances in aryl–aryl bond formation by direct arylation. *Chem. Soc. Rev.* **38**, 2447–2464 (2009).
162. Liégault, B., Petrov, I., Gorelsky, S. I. & Fagnou, K. Modulating reactivity and diverting selectivity in palladium-catalyzed heteroaromatic direct arylation through the use of a chloride activating/blocking group. *J. Org. Chem.* **75**, 1047–1060 (2010).
163. Galangau, O., Nakashima, T., Maurel, F. & Kawai, T. Substituent effects on the photochromic properties of benzothiophene-based derivatives. *Chem. - A Eur. J.* **21**, 8471–8482 (2015).
164. Hashimoto, Y., Nakashima, T., Shimizu, D. & Kawai, T. Photoswitching of an intramolecular chiral stack in a helical tetrathiazole. *Chem. Commun.* **52**, 5171–5174 (2016).
165. Strotman, N. A. *et al.* Catalyst-controlled regioselective suzuki couplings at both positions of dihaloimidazoles, dihalooxazoles, and dihalothiazoles. *J. Org. Chem.* **75**, 1733–1739 (2010).
166. Stranius, K. & Börjesson, K. Determining the photoisomerization quantum yield of photoswitchable molecules in solution and in the solid state. *Sci. Rep.* **7**, 1–9 (2017).
167. Hurley, R. & Testa, A. C. Triplet-state yield of aromatic nitro compounds. *J. Am. Chem. Soc.* **90**, 1949–1952 (1968).
168. Ohtani, H., Kobayashi, T., Suzuki, K. & Nagakura, S. Picosecond Spectroscopy Studies of the Intersystem Crossing of Aromatic Carbonyl and Nitro Compounds in Solution. *Bull. Chem. Soc. Jpn.* **53**, 43–47 (1980).
169. Zobel, J. P., Nogueira, J. J. & González, L. Mechanism of Ultrafast Intersystem Crossing in 2-Nitronaphthalene. *Chem. – A Eur. J.* **24**, 5379–5387 (2018).
170. Grewer, C. & Brauer, H.-D. Mechanism of the Triplet-State Quenching by Molecular Oxygen in Solution. *J. Phys. Chem.* **98**, 4230–4235 (1994).
171. Liu, G., Pu, S. & Wang, R. Photochromism of asymmetrical diarylethenes with a pyrrole unit: Effects of aromatic stabilization energies of aryl rings. *Org. Lett.* **15**, 980–983 (2013).
172. Raymo, F. M. & Tomasulo, M. Electron and energy transfer modulation with photochromic switches. *Chem. Soc. Rev.* **34**, 327–336 (2005).
173. Cusido, J., Deniz, E. & Raymo, F. M. Fluorescent switches based on photochromic compounds. *European J. Org. Chem.* 2031–2045 (2009). doi:10.1002/ejoc.200801244

174. Fukaminato, T., Ishida, S. & Métivier, R. Photochromic fluorophores at the molecular and nanoparticle levels: fundamentals and applications of diarylethenes. *NPG Asia Mater.* **10**, 859–881 (2018).
175. Yamaguchi, T. & Irie, M. Photochromic and fluorescent properties of bisfurylethene derivatives. *J. Mater. Chem.* **16**, 4690–4694 (2006).
176. Elsaesser, T. & Bakker, H. *Ultrafast Hydrogen Bonding Dynamics and Proton Transfer Prosesses in the Condensed Phase*. (Springer Netherlands, 2002). doi:10.1007/978-94-017-0059-7
177. Guérin, J. *et al.* A multifunctional photoswitch: 6π electrocyclization versus esipt and metalation. *Chem. - A Eur. J.* **20**, 12279–12288 (2014).
178. Uno, K. *et al.* In situ preparation of highly fluorescent dyes upon photoirradiation. *J. Am. Chem. Soc.* **133**, 13558–13564 (2011).
179. Takagi, Y. *et al.* Turn-on mode fluorescent diarylethenes: Control of the cycloreversion quantum yield. *Tetrahedron* **73**, 4918–4924 (2017).
180. Iwai, R., Morimoto, M. & Irie, M. Turn-on mode fluorescent diarylethenes: Effect of electron-donating and electron-withdrawing substituents on photoswitching performance. *Photochem. Photobiol. Sci.* **19**, 783–789 (2020).
181. Irie, M. & Morimoto, M. Photoswitchable Turn-on Mode Fluorescent Diarylethenes: Strategies for Controlling the Switching Response. *Bull. Chem. Soc. Jpn.* **91**, 237–250 (2018).
182. Nevskyi, O. *et al.* Fluorescent Diarylethene Photoswitches—A Universal Tool for Super-Resolution Microscopy in Nanostructured Materials. *Small* **14**, 1–12 (2018).
183. Fernández-Acebes, A. & Lehn, J. M. Optical switching and fluorescence modulation in photochromic metal complexes. *Adv. Mater.* **10**, 1519–1522 (1998).
184. Endtner, J. M., Effenberger, F., Hartschuh, A. & Port, H. Optical ON/OFF switching of intramolecular photoinduced charge separation in a donor-bridge-acceptor system containing dithienylethene. *J. Am. Chem. Soc.* **122**, 3037–3046 (2000).
185. Liddell, P. A., Kodis, G., Moore, A. L., Moore, T. A. & Gust, D. Photonic switching of photoinduced electron transfer in a dithienylethene-porphyrin-fullerene triad molecule. *J. Am. Chem. Soc.* **124**, 7668–7669 (2002).
186. Fukaminato, T. *et al.* Fluorescence photoswitching of a diarylethene-perylenebisimide dyad based on intramolecular electron transfer. *Photochem. Photobiol. Sci.* **9**, 181–187 (2010).
187. Berberich, M. *et al.* Nondestructive Photoluminescence Read-Out by Intramolecular Electron Transfer in a Perylene Bisimide-Diarylethene Dyad. *Chem. – A Eur. J.* **18**, 13651–13664 (2012).
188. Irie, M., Fukaminato, T., Sasaki, T., Tamai, N. & Kawai, T. A digital fluorescent molecular photoswitch. *Nature* **420**, 759–760 (2002).
189. Tian, H. & Yang, S. Recent progresses on diarylethene based photochromic switches. *Chem. Soc. Rev.* **33**, 85–97 (2004).
190. Tian, H. & Wang, S. Photochromic bisthienylethene as multi-function switches. *Chem. Commun.* 781–792 (2007). doi:10.1039/b610004j
191. Ouhenia-Ouadahi, K. *et al.* Fluorescence photoswitching and photoreversible two-way energy transfer in a photochrome-fluorophore dyad. *Photochem. Photobiol. Sci.* **11**, 1705–1714 (2012).
192. Valeur, B. & Berberan-Santos, M. N. Characteristics of Fluorescence Emission. in *Molecular Fluorescence* **8**, 53–74 (Wiley-VCH Verlag GmbH & Co. KGaA, 2012).

193. Métivier, R. *et al.* Fluorescence photoswitching in polymer matrix: Mutual influence between photochromic and fluorescent molecules by energy transfer processes. *J. Phys. Chem. C* **113**, 11916–11926 (2009).
194. Fölling, J. *et al.* Synthesis and characterization of photoswitchable fluorescent silica nanoparticles. *Small* **4**, 134–142 (2008).
195. Jung, H. Y., You, S., Lee, C., You, S. & Kim, Y. One-pot synthesis of monodispersed silica nanoparticles for diarylethene-based reversible fluorescence photoswitching in living cells. *Chem. Commun.* **49**, 7528–7530 (2013).
196. Ishida, S., Fukaminato, T., Kim, S., Ogata, T. & Kurihara, S. Sequential Red-Green-Blue (RGB) fluorescence color photoswitching in multicomponent photochromic fluorescent nanoparticles. *Chem. Lett.* **46**, 1182–1185 (2017).
197. Nakahama, T. *et al.* Fluorescence On/Off Switching in Nanoparticles Consisting of Two Types of Diarylethenes. *ACS Omega* **3**, 2374–2382 (2018).
198. Ikariko, I. *et al.* Highly-stable red-emissive photochromic nanoparticles based on a diarylethene-perylenebisimide dyad. *Dye. Pigment.* **180**, (2020).
199. Watanabe, K., Hayasaka, H., Miyashita, T., Ueda, K. & Akagi, K. Dynamic control of full-colored emission and quenching of photoresponsive conjugated polymers by photostimuli. *Adv. Funct. Mater.* **25**, 2794–2806 (2015).
200. Nakahama, T. *et al.* Fluorescence On/Off Switching in Polymers Bearing Diarylethene and Fluorene in Their Side Chains. *J. Phys. Chem. C* **121**, 6272–6281 (2017).
201. Hong, Y., Lam, J. W. Y. & Tang, B. Z. Aggregation-induced emission. *Chem. Soc. Rev.* **40**, 5361–5388 (2011).
202. Mei, J., Leung, N. L. C., Kwok, R. T. K., Lam, J. W. Y. & Tang, B. Z. Aggregation-Induced Emission: Together We Shine, United We Soar! *Chem. Rev.* **115**, 11718–11940 (2015).
203. Shi, J. *et al.* Solid State Luminescence Enhancement in π-Conjugated Materials: Unraveling the Mechanism beyond the Framework of AIE/AIEE. *J. Phys. Chem. C* **121**, 23166–23183 (2017).
204. Yamasaki, S. *et al.* Efficient NIR-I fluorescence photoswitching based on giant fluorescence quenching in photochromic nanoparticles. *Chem. Commun.* **57**, 5422–5425 (2021).
205. Shimizu, K., Métivier, R. & Kobatake, S. Synthesis and fluorescence on/off switching of hyperbranched polymers having diarylethene at the branching point. *J. Photochem. Photobiol. A Chem.* **390**, 112341 (2020).
206. Meldal, M. & Tomøe, C. W. Cu-catalyzed azide - Alkyne cycloaddition. *Chem. Rev.* **108**, 2952–3015 (2008).
207. Zengerle, M. *et al.* Highly efficient cyclosarin degradation mediated by a β-cyclodextrin derivative containing an oxime-derived substituent. *Beilstein J. Org. Chem.* **7**, 1543–1554 (2011).
208. Singh, M. S., Chowdhury, S. & Koley, S. Advances of azide-alkyne cycloaddition-click chemistry over the recent decade. *Tetrahedron* **72**, 5257–5283 (2016).
209. Maisonneuve, S. Synthèse et études photophysiques de nouvelles molécules multichromophoriques photochromes et fluorescentes pour la photocommutation de fluorescence. (2016).
210. Casimiro, L. *et al.* Photophysical Properties of 4-Dicyanomethylene-2-methyl-6-(p-dimethylamino-styryl)-4H-pyran Revisited: Fluorescence versus Photoisomerization. *Chem. – A Eur. J.* **26**, 14341–14350 (2020).
211. Zhou, Y. *et al.* Photoisomerization of a 4-dicyanomethylene-2-methyl-6-(p-

dimethylaminostyryl)-4H-pyran analog dye: a combined photophysical and theoretical investigation. *Phys. Chem. Chem. Phys.* (2022). doi:10.1039/D1CP05170A
212. Baggi, N. *et al.* A Photo- and Redox-Driven Two-Directional Terthiazole-Based Switch: A Combined Experimental and Computational Investigation. *Chem. – A Eur. J.* **27**, 12866–12876 (2021).
213. Guirado, G., Coudret, C. & Launay, J.-P. Electrochemical Remote Control for Dithienylethene-Ferrocene Switches. *J. Phys. Chem. C* **111**, 2770–2776 (2007).
214. Katritzky, A. R., Karelson, M., Sild, S., Krygowski, T. M. & Jug, K. Aromaticity as a Quantitative Concept. 7. Aromaticity Reaffirmed as a Multidimensional Characteristic. *J. Org. Chem.* **63**, 5228–5231 (1998).
215. Boys, M. L. & Downs, V. L. Preparation of primary thioamides from nitriles using sodium hydrogen sulfide and diethylamine hydrochloride. *Synth. Commun.* **36**, 295–298 (2006).
216. Irie, M. & Takami, S. Photochromism of dithiazolylethenes having pyridyl and N-methylpyridinium groups. *J. Phys. Org. Chem.* **20**, 894–899 (2007).
217. Milde, B., Schaarschmidt, D., Rüffer, T. & Lang, H. Phosphino imidazoles and imidazolium salts for Suzuki C-C coupling reactions. *Dalt. Trans.* **41**, 5377–5390 (2012).
218. Taylor, N. J. *et al.* Derisking the Cu-Mediated 18F-Fluorination of Heterocyclic Positron Emission Tomography Radioligands. *J. Am. Chem. Soc.* **139**, 8267–8276 (2017).
219. Kobayashi, K., Sugie, A., Takahashi, M., Masui, K. & Mori, A. Palladium-catalyzed coupling reactions of bromothiophenes at the C-H bond adjacent to the sulfur atom with a new activator system, AgNO3/KF. *Org. Lett.* **7**, 5083–5085 (2005).
220. Cai, Y. *et al.* Ferrocene-Grafted Photochromic Triads Based on a Sterically Hindered Ethene Bridge: Redox-Switchable Fluorescence and Gated Photochromism. *Adv. Opt. Mater.* **4**, 1410–1416 (2016).
221. Savéant, J.-M. *Elements of Molecular and Biomolecular Electrochemistry*. *Elements of Molecular and Biomolecular Electrochemistry* (John Wiley & Sons, Inc., 2006). doi:10.1002/0471758078
222. Connelly, N. G. & Geiger, W. E. Chemical redox agents for organometallic chemistry. *Chem. Rev.* **96**, 877–910 (1996).
223. Bard, A. J. & Faulkner, L. R. *Electrochemical Methods: Fundamentals and Applications, 2nd Edition*. (John Wiley & Sons, Incorporated, 2000).
224. Aki, S., Fujioka, T., Ishigami, M. & Minamikawa, J. ichi. A Practical Synthesis of 3,4-Diethoxybenzthioamide Based on Friedel–Crafts Reaction with Potassium Thiocyanate in Methanesulfonic Acid. *Bioorg. Med. Chem. Lett.* **12**, 2317–2320 (2002).
225. Sreenath, K., Suneesh, C. V., Ratheesh Kumar, V. K. & Gopidas, K. R. Cu(II)-mediated generation of triarylamine radical cations and their dimerization. An easy route to tetraarylbenzidines. *J. Org. Chem.* **73**, 3245–3251 (2008).
226. Blanchard, P., Malacrida, C., Cabanetos, C., Roncali, J. & Ludwigs, S. Triphenylamine and some of its derivatives as versatile building blocks for organic electronic applications. *Polym. Int.* **68**, 589–606 (2019).
227. Zhou, M. *et al.* Triphenylamines consisting of bulky 3,5-di-tert-butyl-4-anisyl group: Synthesis, redox properties and their radical cation species. *Chinese Chem. Lett.* (2021). doi:10.1016/j.cclet.2021.11.054
228. Lacroix, J. C., Trippe-Allard, G., Ghilane, J. & Martin, P. Electrografting of conductive oligomers and polymers using diazonium electroreduction. *Adv. Nat. Sci. Nanosci. Nanotechnol.* **5**, 6 (2014).
229. Liu, M. *et al.* Nanometer-Thick Bilayers by Stepwise Electrochemical Reduction of

Diazonium Compounds for Molecular Junctions. *ACS Appl. Nano Mater.* **4**, 13861–13870 (2021).
230. Yurchenko, O. *et al.* Electrochemically Induced Reversible and Irreversible Coupling of Triarylamines. *J. Phys. Chem. B* **116**, 30–39 (2012).
231. Han, W., Mayer, P. & Ofial, A. R. Palladium-Catalyzed Direct Arylations of Azoles with Aryl Silicon and Tin Reagents. *Chem. – A Eur. J.* **17**, 6904–6908 (2011).
232. Ouhenia-Ouadahi, K. *et al.* Photochromic–fluorescent–plasmonic nanomaterials: Towards integrated three-component photoactive hybrid nanosystems. *Chem. Commun.* **50**, 7299–7302 (2014).
233. Cho, D., Ahn, J., De Castro, K. A., Ahn, H. & Rhee, H. P4S10/dimethicone tandem: Efficient reagent for thionation of various aromatic amides and esters. *Tetrahedron* **66**, 5583–5588 (2010).
234. Kutsunugi, Y., Coudret, C., Micheau, J. C. & Kawai, T. Photomodulation of the proton affinity and acid gated photochromism of a novel dimethylaminophenyl thiazole diarylethene. *Dye. Pigment.* **92**, 838–846 (2012).
235. Miller, R. D., Lee, V. Y. & Moylan, C. R. Substituted Azole Derivatives as Nonlinear Optical Chromophores. *Chem. Mater.* **6**, 1023–1032 (1994).
236. Mori, A. *et al.* Facile Synthesis of 2,5-Diarylthiazoles via Palladium-Catalyzed Tandem C−H Substitutions. Design of Tunable Light Emission and Liquid Crystalline Characteristics. *J. Am. Chem. Soc.* **125**, 1700–1701 (2003).
237. Strotman, N. A. *et al.* Catalyst-Controlled Regioselective Suzuki Couplings at Both Positions of Dihaloimidazoles, Dihalooxazoles, and Dihalothiazoles. *J. Org. Chem.* **75**, 1733–1739 (2010).
238. Castellanos, S., Grubert, L., Stößer, R. & Hecht, S. Diarylethene Photoswitches Featuring Tetrathiafulvalene-Containing Aryl Units. *J. Phys. Chem. C* **117**, 23529–23538 (2013).
239. Oggioni, L. *et al.* Photochromic Polyurethanes Showing a Strong Change of Transparency and Refractive Index. *Polymers (Basel).* **9**, 462 (2017).
240. Hashimoto, Y., Nakashima, T., Shimizu, D. & Kawai, T. Photoswitching of an intramolecular chiral stack in a helical tetrathiazole. *Chem. Commun.* **52**, 5171–5174 (2016).
241. Schnürch, M., Hämmerle, J., Mihovilovic, M. D. & Stanetty, P. A Systematic Study of Suzuki-Miyaura Cross-Coupling Reactions on Thiazoleboronic Esters in the 4- and 5-Position. *Synthesis (Stuttg).* **2010**, 837–843 (2010).
242. Huang, Z.-B. *et al.* Selectively Oxidative Thiolysis of Nitriles into Primary Thioamides and Insecticidal Application. *Asian J. Org. Chem.* **9**, 1243–1248 (2020).
243. Rasmussen, P. B. & Bøwadt, S. Ketene Chemistry 2.1 A General Procedure for the Synthesis of 2-Alkoxycyclopropane-carboxylic Esters and Acids Starting from Aldehydes and Ketene. *Synthesis (Stuttg).* **1989**, 114–117 (1989).
244. Begtrup, M. *et al.* New Methods for the Introduction of Substituents into Thiazoles. *Acta Chemica Scandinavica* **46**, 372–383 (1992).
245. Liu, G., Pu, S. & Wang, X. Synthesis and the effect of substituent position upon unsymmetrical isomeric diarylethenes bearing a pyrrole unit. *J. Photochem. Photobiol. A Chem.* **214**, 230–240 (2010).
246. Sevez, G. & Pozzo, J. L. Toward multi-addressable molecular systems: Efficient synthesis and photochromic performance of unsymmetrical bisthienylethenes. in *Dyes and Pigments* **89**, 246–253 (Elsevier, 2011).
247. Ordronneau, L. *et al.* Photochromic Metal Complexes: Photoregulation of both the

Nonlinear Optical and Luminescent Properties. *Inorg. Chem.* **51**, 5627–5636 (2012).
248. Miwatashi, S. *et al.* Synthesis and Biological Activities of 4-Phenyl-5-pyridyl-1,3-thiazole Derivatives as p38 MAP Kinase Inhibitors. *Chem. Pharm. Bull.* **53**, 410–418 (2005).
249. Reiss, H. & Heller, A. The absolute potential of the standard hydrogen electrode: a new estimate. *J. Phys. Chem.* **89**, 4207–4213 (1985).

Résumé en langue française

Au cours des dernières années, de nombreuses molécules photochromiques ont été largement étudiées en tant que commutateurs moléculaires en vue d'une large gamme d'applications potentielles.

Le **premier chapitre** de cette thèse est une présentation générale des différentes familles de photocommutateurs regroupés selon mécanisme d'isomérisation et les photochromes plus récemment développés sont évoqués. Les diaryléthènes (DAEs), photocommutateurs très étudiés pour leurs propriétés et faisant l'objet de ce travail de recherche, ont été décrits de manière plus détaillée avec un accent mis sur l'importance du rendement quantique et sa modulation, qui reste toujours un défi.

Dans le cadre du **deuxième chapitre**, une famille homogène de huit terthiazoles présentant un caractère de transfert de charge progressivement croissant a été synthétisée et caractérisée afin de rationaliser l'impact des groupes fonctionnels donneurs et accepteurs d'électrons sur le rendement quantique de la photocyclisation, paramètre indiquant l'efficacité de l'isomérisation et donc important à contrôler. En combinant les données expérimentales déterminées par photolyse continue avec la modélisation théorique de l'état fondamental (S_0) et du premier état excité singlet (S_1), il a été possible de proposer un modèle permettant d'ajuster le rendement quantique de la photocyclisation grâce au caractère de transfert de charge. Une corrélation presque linéaire entre ce paramètre et la charge transférée pendant la transition S_0 vers S_1 a été observée.

Ce modèle permettant d'anticiper la modulation du rendement quantique a été exploité afin de synthétiser un dérivé approprié pour la préparation d'un système multichromophore photocommutable et présentant une hystérésis de fluorescence induite par la lumière. Ce travail fait l'objet du **troisième chapitre**. Dans un projet conjoint avec l'ENS Paris-Saclay, des architectures moléculaires composées de multiples unités fluorescentes et photochromiques (i.e. *dicyanométhylènes, DCM)* et le terarylène synthétisé ont été obtenues par chimie click en vue de permettre d'induire des processus de transfert d'énergie entre eux. Comme l'importance de l'hystérésis dépend de la différence de vitesse d'isomérisation entre celle de l'espèce DCM et celle de l'unité terarylène, des propriétés photochromiques limitées du terthiazole étaient requises. Des études préliminaires ont confirmé que la différence entre la cinétique de photoisomérisation de notre photochrome et celle de l'autre unité fluorescente photo-active conduit à une hystérésis de fluorescence sous irradiation UV ou visible.

Une autre caractéristique intéressante des diaryléthènes est d'être facilement fonctionnalisable et de permettre ainsi d'envisager la possibilité de développer un système présentant un comportement à double réponse (un autre stimulus en plus des photons peut induire l'isomérisation). En particulier, dans le cadre de ce projet de thèse, une étude a été menée sur des terarylènes photochromes et présentant une isomérisation induite par réduction ou oxydation selon la fonctionnalisation choisie. Les résultats font l'objet du **quatrième chapitre** de cette thèse.

Les résultats obtenus par voltamperométrie cyclique et spectroélectrochimie à basse

température concernant une famille de quatre terarylènes fonctionnalisés par des groupements bis-N-méthylpyridinium ont montré qu'une cyclisation par réduction peut être obtenue de manière similaire à celle des diaryléthènes à pont éthène précédemment rapportés. Des calculs DFT et TD-DFT ont été menés et permettent de rationaliser les résultats expérimentaux. De plus, ces dérivés montrent également la possibilité d'une cycloréversion oxydative, ce qui en fait les premiers terarylènes caractérisés par une commutation photo- et redox- bidirectionnelle.

D'autre part, onze terarylènes ont été développés pour la cyclisation oxydative (six dérivés à base de thiophène, quatre terthiazoles et un système mixte) en les fonctionnalisant avec différents substituants donneurs d'électrons et tous ont montré un comportement électrochimique différent de celui rapporté dans la littérature pour les diaryléthènes avec des ponts cyclopentène ou perfluorocyclopentène.

Concernant les molécules contenant du thiophène, aucune forme fermée neutre n'a été obtenue par électrolyse et un mécanisme différent a été proposé en combinant la voltampérométrie cyclique, la spectroélectrochimie, la RPE et la modélisation théorique. Globalement, ces dérivés photochromiques ont montré une isomérisation classique « forme ouverte neutre – forme fermée neutre » induite par la lumière et une isomérisation « forme ouverte neutre – forme fermée dicationique » induite par voie électrochimique.

L'étude des quatre terthiazoles a montré que la formation de l'espèce de forme fermée ne pouvait pas être observée par voltampérométrie cyclique et, grâce au système mixte (thiophène – thiazole), il a été confirmé que la présence d'un bras thiophène riche en électrons et réactif est nécessaire pour observer une cyclisation oxydative par voltampérométrie cyclique. Néanmoins, comme pour la série thiényle, aucune forme fermée neutre n'a pu être obtenue par électrolyse.

En conclusion, les travaux présentés dans cette thèse concernent deux axes distincts de recherche sur les terarylènes. Dans une première partie (i.e. chapitres 2 et 3), une étude destinée à développer un modèle pour la modulation du rendement quantique liée à l'influence du caractère de transfert de charge au sein du photochrome et son exploitation dans un système multichromophore a été présentée. Dans la deuxième partie (i.e. chapitre 4), le travail de recherche présenté concerne la synthèse et l'étude de plusieurs terarylènes photo- et électro-actifs. Contrairement au comportement à double réponse des diaryléthènes connus dans la littérature, celui des terarylènes a été beaucoup moins étudié et il a été possible au cours de cette étude de montrer que certains d'entre eux présentaient également ce comportement double et une interprétation des résultats est proposée.